

UCSF

UC San Francisco Electronic Theses and Dissertations

Title

Activation of Apoptotic Procaspases

Permalink

<https://escholarship.org/uc/item/14q613v5>

Author

Zorn, Julie Anne

Publication Date

2012

Peer reviewed|Thesis/dissertation

Activation of Apoptotic Procaspases

by

Julie Anne Zorn

DISSERTATION

Submitted in partial satisfaction of the requirements for the degree of

DOCTOR OF PHILOSOPHY

in

Chemistry and Chemical Biology

in the

GRADUATE DIVISION

of the

UNIVERSITY OF CALIFORNIA, SAN FRANCISCO

To my family.

Acknowledgements

My interest in pursuing a scientific career started at my undergraduate institution, New York University. Tamar Schlick and Edward McNelis provided unique experiences for me in computational biology and synthetic chemistry, respectively. I value the knowledge that I gained in both labs, and the guidance that both individuals gave me. While I tended toward the experimental sciences, I appreciated the information that could be gained from computational insights. I initially came to UCSF as a research technician in the lab of Fred Cohen, which combined aspects of both. Barney May was an amazing mentor for me in this lab. I built upon my synthetic background, while being exposed to different aspects of drug discovery. I enjoyed the research in the Cohen lab, and was encouraged to continue on to graduate school.

I could not imagine a better place to do research than UCSF. UCSF provides a unique setting to nurture the development of young scientists, such as myself. The rich collaborative environment and the emphasis on research related to human health and disease are appealing attributes that sparked by interest in this particular graduate institution.

I was fortunate enough to start graduate school when my advisor, James Wells, was recruited to UCSF. I would not be the scientist I am today without my experiences in the Wells lab. Jim promotes an atmosphere where scientific ideas are rich and creativity is not only encouraged, but also an incredible asset. He is adept at identifying important questions in science and finding unique and clever ways to address them. I hope one day to possess the amazing scientific innovation that Jim clearly has.

Many other faculty members at UCSF have also contributed to my development as a scientist. My experience has been that their doors are always open. One of the more difficult processes to go through in graduate school was my qualifying oral exam.

My orals committee (Jim McKerrow, Michael Marletta, Pam England, and Kevan Shokat) was helpful in preparing me for the exam. I was more equipped to critically assess my proposal as a result of the exam and my committee members. My chair, Kevan, was also crucial in guiding me through the exam. Kevan and Charly Craik have continued to help guide my research on my thesis committee. They both have provided constructive criticism throughout the years, which has definitely made me a more thoughtful and effective scientist. Finally, Sue Miller and Brian Shoichet have been amazing mentors to me on various aspects of my project. They have been very supportive, helped to build my confidence, and provided valuable insight into various aspects of my project.

I would not have made it through graduate school without the amazing mentorship of the postdoctoral scholars and other students around me. Dennis Wolan took on the hefty responsibility for my training in the Wells lab. He taught me how to execute experiments and how to interpret results. Without his support and guidance, I would not have developed as much as I have. Sami Mahrus challenged me to think critically about the experiments that I performed. He encouraged me to stick with graduate school, and made me feel like I belonged here. I am indebted to both Sami and Dennis, and I hope one day to be as effective a scientist as either one of them.

The Wells lab (and its affiliated members) has changed tremendously over the years but the caliber of the scientists in it has not. It has been a pleasure to see all these amazingly talented scientists evolve over the years and to be mentored by each and every one of them. I will miss all of them: Nick Agard, Emily Crawford, Jon Choy, Deb Datta, Juan Diaz, Junjun Gao, Dan Gray, Zach Hill, Gerald Hsu, Olivier Julien, JT Koerber, Sami Mahrus, Paul Marinec, Chris McClendon, Charlie Morgan, Huy Nguyen, Jason Porter, Justin Rettenmeir, Jack Sadowsky, Justin Scheer, Julia Seaman, Kazu Shimbo, Ashley Smart, Nathan Thomsen, Hai Tran, Arun Wiita, Pete Wildes, Dennis Wolan, Hikari Yoshihara, and Min Zhuang. Hikari Yoshihara, Jack Sadowsky, and Deb

Datta provided much needed distractions from the day-to-day failures in the lab. They are not only amazing scientists, but also know just how to cheer me up. From generating plasma, to igniting nitrocellulose, to tossing a football, to Internet nonsense, their diversions were always appreciated. Nick Agard, Junjun Gao, and Pete Wildes provided much needed mentorship and general scientific knowledge to me in my early days. Min Zhuang has been an amazing scientific role model and a great friend over the years. Her diligence, intelligence, and talent are something to aspire to. JT Koerber and Sarah Gilmore provided mentorship and guidance to me at a time when finishing graduate school seemed almost unattainable. Kazu Shimbo is the hardest working, most incredibly thoughtful scientist I have ever met. I enjoyed being around him my last year. Finally, it has been a pleasure to work directly with Olivier Julien. He has amazing ideas, and a general excitement about science. He values my contribution to the project and has given me confidence in myself. I look forward to seeing how his research progresses.

I have been blessed with amazing collaborations over the years. Holger Wille in Stan Prusiner's lab was instrumental in elucidating the mechanism of 1541 activation. He has been a fantastic collaborator with extensive skill and knowledge. Allison Doak in Brian Shoichet's lab has been extremely accommodating with use of their instruments, and she has provided valuable insights into small molecule aggregates. Dan Hostetter and Cheryl Tajon from Charly Craik's lab have been amazing to work with on projects and incredibly generous with their granzyme B. I could not have executed many of my experiments without them. It has been a pleasure to work with Brian Hearn and Adam Renslo on projects. They are incredibly knowledgeable and patient. I have enjoyed learning from them and interacting with them. The Small Molecule Discovery Center is filled with incredible scientists who are always eager to help. My interactions with them over the years has always progressed my science forward.

The administrative staffs in both the Wells lab and the Chemistry and Chemical Biology (CCB) program have also provided much needed support and guidance. Mary Betlach helped me apply for and receive fellowships during my graduate career. Marja Tarr has kept the Wells lab running. Christine Olson has been an amazing source of encouragement for me in the CCB program. Julia Molla and Nicole Takesono Flowers have helped me maneuver my way through the final stages of graduate school. Without their wonderful organization and tenacity, life would have been much more difficult.

Fellowships have not come easy to me, but persistence allowed me to receive two awards for my efforts. The Achievement Rewards for College Scientists Foundation and the Evnin-Wright Scleroderma Research Foundation provided generous funding to me during my graduate career. These incredible foundations bolstered my self-confidence and allowed me to attend great conferences. I am grateful for their support.

I would like to thank my family for all of their encouragement. I would not have made it through graduate school without them. My mom has instilled in me a strong work ethic and moral compass. Without them, I would be a much different scientist and person. My mom's trips to the city have always been welcome and a nice distraction from lab work. My dad and his wife Fera have also provided much needed diversions that range from barbeques to Les Miserables. I always enjoy our outings. My parents have managed to raise five successful children. I am very proud of all my siblings. My sister and her husband Lex Nadeau have given me a social life throughout my graduate career. They took me on a cruise, let me join them in Tahoe, and took me to Las Vegas, among many other trips. I am amazed, and grateful, at how much they tolerated me, although I do think that they are trying to kill me. My brothers, Doug, Wyatt, and Josh, are always a source of laughter, whether it is intentional or not. I am incredibly proud of my niece Sabrina and my nephew Charlie. I can only hope that they learn from my mistakes.

Finally, I cannot finish this section without thanking Nick Agard. Your love, patience, and skepticism have always been appreciated, even if I am not always the best at expressing it. You constantly challenge me and make me want to become not only a better scientist, but also a better person. I would not have been able to finish graduate school without your support throughout the difficult times. Your family has been amazing to me as well: Matt, Mary, Alicia, Marnie, and Irv. I do not think that I have ever met such a nice, warm, and friendly group. I can see how you ended up being such a wonderful person.

Statement concerning co-authorships of previously published materials

The material in Chapter 1 was originally published as a review in *Nature Chemical Biology* (2010) 6: 179-188. Julie Zorn gathered research from the literature. James Wells and Julie Zorn wrote the manuscript.

The material in Chapter 2 was originally published as a report in *Science* (2009) 326: 853-858. Julie Zorn was the second author in this report. As part of her thesis, Julie Zorn contributed significantly to the published material in Chapter 2. Dennis Wolan designed and performed most of the experiments described in Chapter 2. In collaboration with Dennis Wolan, Julie Zorn prepared recombinant procaspases and caspases. Julie Zorn assisted with compound synthesis and purification. She characterized 1541 and related analogs by ^1H and ^{13}C NMR. Julie Zorn determined EC_{50} values of 1541 analogs for procaspase-3, procaspase-6, and procaspase-7 activation. Julie performed tests of 1541C and 1541D in BT549 cells to determine cellular viability and caspase activity over time. Finally, she developed and performed proteolytic susceptibility assays against procaspase-3 using granzyme B as the upstream protease. Dan Gray provided guidance and help with cellular assays. Dan Gray generated stably transfected MCF7 cell lines with wild-type and S198A procaspase-3. Dennis Wolan and

James Wells wrote the manuscript. Julie Zorn and Dan Gray edited the manuscript. James Wells supervised the research.

The material in Chapter 3 was originally published as a communication in the *Journal of the American Chemical Society* (2011) 133: 19630-19633. Julie Zorn performed most of the work described in this chapter with exceptions listed below. Holger Wille prepared and acquired transmission electron microscopy images of 1541 and related analogs. Dennis Wolan helped with recombinant procaspase and caspase expression. Dennis Wolan performed initial tests for small molecule aggregates. Julie Zorn and James Wells wrote the manuscript. Dennis Wolan and Holger Wille edited the manuscript. James Wells supervised the research.

The material in Chapter 4 has been submitted for publication. Julie Zorn performed most of the work described in this chapter with exceptions listed below. Dennis Wolan cloned procaspase and caspase constructs and helped with the preparation of recombinant procaspases and caspases. Dennis Wolan advised research. Nicholas Agard performed computational analysis of the rates of procaspase activation. Julie Zorn and James Wells wrote the manuscript. Dennis Wolan and Nicholas Agard edited the manuscript. James Wells supervised the research.

The material in Chapter 5 has not yet been submitted for publication. Julie Zorn performed most of the work described in this chapter with exceptions listed below. Dennis Wolan helped with the preparation of recombinant procaspases and caspases. Dennis Wolan also aided in compound synthesis. Holger Wille prepared and acquired transmission electron microscopy images of 1541 analogs. James Wells supervised the research.

Abstract

Activation of Apoptotic Procaspases

Julie Anne Zorn

Most proteases are expressed as inactive precursors, known as zymogens. Studies to explore zymogen activation can further elucidate biological regulatory mechanisms and lead to novel chemical biology tools to trigger them. Caspases, or cysteine aspartyl proteases, are expressed as such inactive precursors, or procaspases, which become activated in fate-determining transformations, such as apoptosis. Procaspases are naturally activated upon binding to scaffolding complexes or as a result of cleavage by upstream proteases in response to extrinsic or intrinsic cellular signals. Removal of an N-terminal prodomain and an additional cleavage to yield a large and small subunit generates the mature enzyme.

A small molecule, termed 1541, was identified from a high-throughput screen to facilitate procaspase-3 maturation. Unexpectedly, 1541 assembles into nanofibrils that bind procaspase-3, however, the proenzyme alone cannot auto-process. A trace amount of mature caspase-3 contaminant dominates procaspase-3 activity measurements. Thus, 1541 acts as a scaffolding moiety to promote induced proximity of procaspase-3 with caspase-3 to enhance autocatalytic maturation of the proenzyme. Similar to known signaling complexes, proteogenic fibrils may serve as a platform for procaspase maturation. These studies suggest that increasing the activity of an upstream protease or promoting colocalization of the proenzyme with an active protease are reasonable approaches to facilitate procaspase-3 activation.

1541 represents a first-in-class, self-assembling, small-molecule nanofibril, which catalyzes procaspase-3 activation. A focused library of 1541-analogs was generated to evaluate the structural requirements for procaspase binding and activation. An initial

screen of the library against procaspase-3, -6, and -7 identified compounds that can selectively activate each procaspase. These active molecules also form fibrils, yet demonstrate selective interactions with the zymogen and mature caspases. Thus, procaspase binding and activation can be tuned based on the substituents of the small molecule.

Surprisingly, 1541 also induces apoptosis in a manner dependent upon the fibrils. While 1541 promotes cell death and caspase activity in most cell lines tested, additional fibril-forming analogs appear to have more selective toxicity profiles. Cell death induced by the fibrils is independent of both the intrinsic and extrinsic cellular pathways. Nevertheless, the cellular activity of these fibrils is unlikely due to direct binding of procaspases.

Table of Contents

	Page
Chapter 1	1
Introduction – Turning enzymes on with small molecules	
Chapter 2	33
Small-molecule activators of a proenzyme	
Chapter 3	80
Self-assembling small molecules form nanofibrils that bind and activate procaspase-3	
Chapter 4	120
Fibrils colocalize caspase-3 with procaspase-3 to foster maturation	
Chapter 5	180
Small molecule nanofibrils selectively activate executioner procaspases-3, -6, and -7	
Chapter 6	225
Conclusions and Future Directions	
References	234

List of Tables

	Page
Table 1-1. Chemical structures of some of the prominent non-natural, synthetic activators	25
Table 3-1. Unique Properties of 1541 and Related Analogues Compared with Standard Aggregators	99
Table 4-1. 1541 fibrils increase the catalytic efficiency of upstream proteases	152
Table 4-2. Decreased catalytic efficiency of caspase-3 resistance mutations	153
Table 4-3. Mature caspase-3 present with procaspase-3 dominates activity measurements	154
Table 4-4. Summary of zymogenicity values	155
Table 5-1. Modifications to the substituents on the 1541 coumarin core	202
Table 5-2. Distinct meta substituents on the central ring of 1541	204
Table 5-3. Different heterocycles in place of the coumarin on 1541	214

List of Charts

	Page
Chart 3-1. Compound 1541 and Analogues	100

List of Schemes

	Page
Scheme 5-1. Synthetic route for 1541 analogues	215

List of Figures

	Page
Figure 1-1. Mechanisms of small-molecule-induced enzyme activation	27
Figure 1-2. Small-molecule activators of a proenzyme	28
Figure 1-3. Allosteric activation of glucokinase	29
Figure 1-4. Allosteric activation of PDK1	30
Figure 1-5. Small-molecule binding to regulatory subunits leads to enzyme activation	31
Figure 2-1. HTS scatter plot identifies 1541 as a procaspase-3 activator	59
Figure 2-2. Specificity of small-molecule activators for executioner procaspases	60
Figure 2-3. Specificity of 1541 and time course	62
Figure 2-4. Procaspase-1 is insensitive to 1541 activation	64
Figure 2-5. Schematic of general chemical synthesis of 1541 derivatives	65
Figure 2-6. In vitro characterization of apoptotic procaspase small-molecule activators	66
Figure 2-7. Initial activity constants of procaspase-3 in presence of 1541B	68
Figure 2-8. Procaspase-3 self-cleavage in the presence of 1541	70
Figure 2-9. Michaelis-Menten analysis shows competitive inhibition of executioner caspases-3 and -6 by 1541	71
Figure 2-10. Induction of apoptosis in a p53-deficient breast cancer cell line by 1541	72

	Page
Figure 2-11. Mechanisms of small-molecule-induced enzyme activation.	74
Figure 2-12. Small-molecule activators of a proenzyme	75
Figure 2-13. Allosteric activation of glucokinase	76
Figure 2-14. Allosteric activation of PDK1	77
Figure 2-15. Cellular viability time course with normal and cancerous B cells	79
Figure 3-1. 1541 promotes procaspase-3 activation in the presence of detergents	101
Figure 3-2. 1541 does not inhibit β -lactamase	102
Figure 3-3. BSA prevents activation of procaspase-3 by 1541	103
Figure 3-4. 1541 forms particles that are required for binding and activation of procaspase-3	104
Figure 3-5. Analogues of 1541 form particles that interact with procaspase-3	105
Figure 3-6. Co-sedimentation of procaspase-3 (C163A) with varying concentrations of 1541 and analogues	106
Figure 3-7. Lack of procaspase-3 processing when isolated from 1541 or 1541B by a dialysis membrane	107
Figure 3-8. 1541 and 1541B particles have different affinities for procaspase-3 that correlate to distinct rates of activation	108
Figure 3-9. Cosedimentation of varying concentrations of procaspase-3 with 20 μ M 1541, 1541B, and 1541D	109

	Page
Figure 3-10. Standard aggregators do not activate procaspase-3	110
Figure 3-11. Autocorrelation curves from DLS analysis	111
Figure 3-12. Particles of 1541 analogs and standard aggregators analyzed by particle flow cytometry	112
Figure 3-13. Analogues of 1541 pellet at 37°C	113
Figure 3-14. Transmission electron micrographs of fibrils, particles, and procaspase-3 (C163A)	114
Figure 3-15. TEM images of 1541 nanofibrils with and without procaspase-3	115
Figure 3-16. Rate of 1541 particle sedimentation by centrifugation at room temperature and at 37°C	116
Figure 3-17. Model of procaspase-3 activation by 1541 nanofibrils	117
Figure 3-18. A β fibrils activate procaspase-3	118
Figure 3-19. Procaspace-3 activation by 1541 and analogs at room temperature and at 37°C	119
Figure 4-1. Possible models of procaspase-3 processing on 1541 fibrils	156
Figure 4-2. Enhanced susceptibility of procaspase-3 to processing by mature caspase-3 in the presence of 1541 fibrils	157
Figure 4-3. No processing of the inactive procaspase-3 (C163A) by the uncleavable procaspase-3 (D9A/D28A/D175A)	158
Figure 4-4. Wild-type procaspase-3 can auto-activate at high concentrations	159
Figure 4-5. Activity-based probe for mature caspase-3	160

	Page
Figure 4-6. Catalytic efficiency of caspase-3, caspase-8, and granzyme B is similar with or without 1541	161
Figure 4-7. Mature caspase-3 drives activation of procaspase-3 in the presence of 1541	162
Figure 4-8. K_m approximation for caspase-3 and caspase-8 against the procaspase-3 substrate	163
Figure 4-9. Effective change in catalytic efficiency of upstream proteases due to 1541 fibrils	164
Figure 4-10. Rate of procaspase-3 cleavage by an active protease depends on its catalytic efficiency and the extent of binding to fibrils	165
Figure 4-11. Resistance mutations in procaspase-3 are susceptible to processing by caspase-3	167
Figure 4-12. Amyloid- β (1-40) fibrils bind and enhance procaspase-3 activation	168
Figure 4-13. Caspase-8 binds but does not process procaspase-3 on amyloid- β (1-40) fibrils	169
Figure 4-14. Variable times to autocatalytic maturation of wild-type procaspase-3 by different batches of amyloid- β (1-40)	170
Figure 4-15. Multiple caspase-3 cleavage products identified by active site titration with Ac-DEVD-cmk	171
Figure 4-16. Low concentrations of Ac-DEVD-cmk do not completely quench the mature caspase-3 contaminant	172
Figure 4-17. Dithiothreitol quenches Ac-DEVD-cmk at low concentrations, and Ac-VAD-fmk slowly inactivates trace caspase-3 contaminants	173
Figure 4-18. Multiple active caspase-3 variants with distinct kinetics in procaspase-3 batches	174
Figure 4-19. Wild-type procaspase-3 and uncleavable procaspase-3 (D9A/D28A/D175A) lack large impurities	176

	Page
Figure 4-20. Multiple, trace caspase-3 cleavage products detected in the uncleavable procaspase-3 (D9A/D28A/D175A)	177
Figure 4-21. Activity of 50 μ M uncleavable procaspase-3 (D9A/D28A/D175A) after thorough purification	178
Figure 4-22. Minimum detectable concentration of mature caspase-3	179
Figure 5-1. Modifications tolerated on 1541 for procaspase-3 activation	216
Figure 5-2. 1541 analogues exhibit unique profiles for procaspase-3 activation	217
Figure 5-3. Processing of procaspase-3 by 1541 analogues	218
Figure 5-4. 1541 analogues show selective activation of executioner procaspases-3, -6, and -7	219
Figure 5-5. Transmission electron micrographs of 1541 analogues	220
Figure 5-6. Selective activation of procaspase-7	222
Figure 5-7. Analogues exhibit selective cell death and caspase activation profiles	223
Figure 5-8. 1541 analogues induce cell death independent of direct procaspase activation	224

Chapter 1:
Introduction- Turning Enzymes On With Small Molecules

Julie A. Zorn[†] and James A. Wells^{†‡}

[†]Department of Pharmaceutical Chemistry, University of California, San Francisco,
California

[‡]Department of Cellular and Molecular Pharmacology, University of California, San
Francisco, California

This work was published in *Nature Chemical Biology* (2010) 6: 179-188.

Abstract

Drug discovery and chemical genetic efforts typically focus on the identification and design of inhibitors or loss-of-function probes as a means to perturb enzyme function. These tools are effective in determining the physiological consequence of ablating the activity of a specific enzyme. Remarkably, nearly a dozen examples of non-natural small molecules that activate enzyme catalysis have been identified within the past decade. In aggregate, these studies delineate four unique activation mechanisms that the small molecules exploit. These complementary gain-of-function probes offer a way to address the sufficiency of an enzyme to drive a particular cellular phenotype, and they also provide new opportunities for drug discovery. This review covers the identification and characterization of these unique small-molecule activators.

Most chemical biology and drug discovery efforts are focused on identifying small-molecule tools or drugs that inhibit enzyme function (1). It is rare to encounter small-molecule enzyme activators, yet there are significant advantages to finding them. Importantly, activators provide a means to better understand the endogenous methods of enzyme activation and the allosteric mechanisms that underlie them. Many enzymes such as proteases, kinases and phosphatases are stored in dormant forms that await activation by post-translational modifications, including proteolysis and phosphorylation, or by interactions with other proteins or metabolites (2). Such mechanisms typically stabilize an active enzyme conformation. Synthetic small-molecule activators can often promote similar transitions.

We learn new information by igniting a signaling pathway from a particular point as opposed to inhibiting it—in other words, by facilitating a gain of function in a specific enzyme instead of a loss of function (3). In contrast to inhibitors that reveal the necessity of the target for a phenotype, activators probe the sufficiency of the target for the phenotype. Further, to block such phenotypic effects using an inhibitor often requires reaching an IC_{90} or even IC_{95} (inhibitor concentration at 90% to 95% enzyme inhibition). This is because in many cases small amounts of active enzyme are sufficient to trigger a signaling cascade and drive biological responses (4-6). By the same token, the concentration of an allosteric activator may only need to reach an AC_{10} (activator concentration at 10% maximal activation level). Such small-molecule activators expand the target landscape for drug discovery.

There are almost a dozen examples of mechanistically well-characterized small-molecule activators for enzymes, which include regulators of proteases, kinases, deacetylases, dehydrogenases, phosphatases and nucleases. Here we review their discovery and the four means of inducing enzyme activity that these activators exploit (**Fig. 1-1**). These mechanisms are binding of a small molecule to an allosteric site

directly on the catalytic domain to promote an active conformation (type A1); binding to an allosteric site to facilitate an irreversible, activating post-translational modification (type A2); binding to a regulatory subunit to indirectly promote activity at the catalytic domain (type B1); and binding to a regulatory subunit to promote an activating oligomerization (type B2). Further research in this area may elaborate additional activation mechanisms. Though previous reports have highlighted protein-engineering approaches to activate enzymes (7), some clear patterns emerge from the small-molecule cases described here.

Allosteric binding site on the catalytic domain

One of the simplest means to activate an enzyme with a small molecule is to bind to an allosteric site directly on the catalytic domain of a dormant enzyme and induce a conformational change, which can occur cooperatively with substrate (**Fig. 1-1**, mechanism A1).

Glucokinase activators- Glucokinase (GK) catalyzes the phosphorylation of glucose to generate glucose-6-phosphate (8). Interest in regulating GK activity originates from its association with initiating glucose metabolism in liver hepatocytes and with insulin secretion in pancreatic beta cells (9-11). The appeal of GK as a possible therapeutic target intensified with the discovery of activating mutations that are associated with hypoglycemia and inactivating mutations linked to hyperglycemic conditions, such as maturity onset diabetes of the young, type 2 (9,12).

Initial efforts to modulate GK activity focused on identifying small molecules that could indirectly promote its activation by altering its cellular localization. GK is both inhibited and restricted to the nucleus, away from its cytosolic substrate, by GKRP (GK regulatory protein) (13). The affinity of GK for GKRP is affected by metabolites, such as fructose-6-phosphate or fructose-1-phosphate, which bind to GKRP and either bolster or

weaken GK binding, respectively (14,15). Thus, Grimsby *et al.* set up an *in vitro* HTS (high-throughput screen) of 120,000 compounds and assayed for an increase in GK activity in the presence of GKRP (16). Serendipitously, they identified the first direct GK activator (GKA), which bound to a novel allosteric site on GK. This small-molecule activator not only reversed GKRP inhibition, but also directly impacted GK catalytic activity by decreasing its $K_{0.5}$ for glucose by fourfold and increasing its V_{max} by 1.5-fold (16).

In addition to impacting GK catalytic activity *in vitro*, a chemically optimized GKA, RO-28-1675 (**Table 1-1**), also influenced glucose homeostasis in cells and in animal models of diabetes (16). These promising results inspired several pharmaceutical companies to discover dozens of new GKA scaffolds. These exhibit a similar decrease in the $K_{0.5}$ of GK for glucose but with varying effects on V_{max} (9,10,17,18).

The crystal structure for the unbound GK as well as the complex of GK with glucose and a novel GKA, compound A (**Table 1-1**), provided a rationale for the activating effects (**Fig. 1-2**) (19). GK is a monomeric enzyme that contains a large and a small domain bridged by a prominent cleft that shapes the active site. The cleft is accessible to substrate in the super-open, inactive form of the enzyme, but the catalytic residues are not properly oriented. Glucose binding induces a large rotation of the small domain to a more compact, closed active structure. This conformational change properly orients catalytic residues and exposes the allosteric binding site of compound A (**Fig. 1-2A, Fig. 1-2B**). Thus both glucose and compound A bind to GK to stabilize the active form (19). Interestingly, activating mutations in GK associated with hypoglycemia localize to the same allosteric cavity that binds the GKAs. This suggests that the mutations could similarly stabilize an active conformation (**Fig. 1-2C**) (9). GKAs have not only opened the door to new therapeutic strategies for diabetes, but have also expanded our understanding of the possible mechanisms for enhancing enzyme activities by a

small molecule.

Sirtuin activators- Following on the heels of the discovery of GKAs, researchers began to explore direct activation of a class of deacetylases known as the sirtuins as a new strategy for treating age-related diseases, such as type 2 diabetes (20,21). The founding member of the sirtuin family, yeast Sir2p (silent information regulator protein 2), was identified as an important determinant of yeast longevity (22). Specifically, Sir2p activation is associated with enhanced longevity in response to calorie restriction (23,24). Although this correlation is still debated, small molecules were quickly discovered that could mimic the beneficial effects of calorie restriction through direct activation of SIRT1, the human ortholog of Sir2p (25-27).

SIRT1 catalyzes the NAD⁺-dependent deacetylation of acetyllysine residues. Several natural effectors, including metabolites such as nicotinamide and proteins such as AROS and DBC1, directly impact sirtuin activity (28-32). To identify small molecules that could similarly influence SIRT1 activity, Howitz *et al.* screened focused libraries of compounds that included relevant metabolites. In a fluorescence-based assay detecting deacetylation of an acetyllysine residue in a fluorophore-labeled peptide substrate, they identified two polyphenolic compounds that weakly activated SIRT1 (33). In a secondary screen against structurally related plant metabolites, resveratrol was identified as the most potent SIRT1 activator (**Table 1-1**). These initial compounds have micromolar AC₅₀ values for activation of SIRT1 and decrease the K_m for acetylated substrate with little effect on the V_{max} . Despite their modest potencies, these sirtuin activators show beneficial effects on yeast lifespan, which is dependent on the expression of Sir2p.

Despite these promising observations associating *in vitro* activity with cellular activity, the mechanism of SIRT1 activation by resveratrol and related analogs remained elusive (34). To address this, Milne *et al.* identified 127 unique activators of SIRT1 from a HTS of 290,000 compounds (35). One series of compounds with an imidazo[2,1-

b]thiazole core scaffold decreased the K_m for acetylated substrate, which correlates well with the AC_{50} values for activation (**Table 1-1**). Notably, this series of activators show varying effects on the maximal level of activation attained, A_{max} ; yet, the determinants of A_{max} for a particular small molecule remain unclear.

Milne *et al.* used isothermal titration calorimetry (ITC) to demonstrate a binding interaction between their small-molecule activator and SIRT1, which required the presence of the acetylated substrate (35). Yet recent reports have suggested that the SIRT1 activators, including resveratrol, do not promote deacetylation of full-length substrates or of peptides lacking the fluorophore (34,36). However, in the presence of the fluorophore-labeled peptide, activation of SIRT1 is observed in multiple different biochemical assays (36). This is reminiscent of the activation of GK by GKAs where substrate and activator collaborate to stabilize the active conformer. Unfortunately, in contrast to GK, the HTS for SIRT1 was not carried out in the presence of a native substrate, and the fluorophore tag seems to contribute to small-molecule-induced activation.

Intriguingly, in cell-based assays, Milne *et al.* suggested that SIRT1 is the direct target of the activators by showing deacetylation of a SIRT1 substrate upon addition of compound (35). Furthermore, the activators were able to mimic the phenotype associated with calorie restriction and to decrease plasma glucose levels in several different mouse models for type 2 diabetes. Conflicting results have also called into question the *in vivo* efficacy of the compounds (36). Future studies and analyses would help to address these discrepancies.

PDK1 activators- HTS efforts drove the discovery of novel small-molecule activators for SIRT1 and GK, but exploring activation by mimicking endogenous interactions has also proven to be a beneficial strategy. For AGC kinases, intermolecular interactions are promoted by phosphorylation of a serine or threonine residue in a region

C-terminal to the catalytic domain, termed the HM (hydrophobic motif) (37,38). One member of the AGC kinase family, PDK1 (phosphoinositide-dependent protein kinase 1), lacks an HM but contains an HM binding pocket in its catalytic domain, or more specifically a PIF (PDK1 interacting fragment) pocket. The PIF pocket facilitates recruitment of substrates, and binding at this allosteric site also increases the catalytic activity of PDK1 (39,40). A peptide derived from the HM of a downstream substrate (“PIFtide”) activates PDK1 4.5-fold with an AC₅₀ of 110 nM (41,42).

Engel *et al.* performed an *in silico* screen of 60,000 compounds to identify small molecules that would interact with the HM binding site on the catalytic domain and promote activation (42). One compound, 3-((*p*-chlorophenyl)-3-oxo-1-phenyl)-propylsulfanylacetic acid, called compound 1, was identified as a hit from the computational screen (**Table 1-1**). Compound 1 resulted in a fivefold activation of PDK1 with an AC₅₀ of 34 μM. Engel *et al.* further demonstrated a specific interaction between their activator and the PIF pocket by identifying mutations in the PIF pocket that rendered PDK1 resistant to compound activation (**Fig. 1-3A**) (42). They also showed that compound 1 selectively activates PDK1 over other AGC kinases, and that subtle modifications to the chloro substitutions on the scaffold demonstrate structure-activity relationships (SAR) suggestive of specific binding to a single site.

SAR studies around the original compound generated a new lead compound, (Z)-5-(4-chlorophenyl)-3-phenylpent-2-enoic acid (PS48, **Table 1-1**), with an AC₅₀ of 8 μM and an A_{max} of fourfold over basal PDK1 activity levels (43). The AC₅₀ values of the compounds against PDK1 ranged from 2.8 to 41.3 μM, and exhibited a strong correlation to binding affinities determined by ITC, demonstrating that tighter binding in the allosteric site was coupled with more potent activation. Interestingly, the A_{max}, which ranged from 1.4-fold to 4.4-fold over basal levels of PDK1 activity for the analogs, did not exhibit a strong trend with binding affinity.

To elucidate the mechanism of activation, Hindie *et al.* determined the crystal structure for PDK1 bound to their activator in the presence of ATP (44). Modest differences between the two structures included a shift of residues in the PIF pocket where the compound is bound, small changes in a glycine-rich loop at the top of the ATP binding site, movement of the active site lysine residue, and ordering of the activation loop (**Fig. 1-3B**) (44). Further structural analysis of PDK1 in the presence and absence of nucleotide would help to elucidate the structural transitions between the active and inactive kinase.

Exploring the biological impact of these compounds is complicated by unique mechanisms of activation for various downstream substrates (45). For example, these new small molecules inhibit PDK1 phosphorylation of S6K (70 S6 kinase) and SGK (serum- and glucocorticoid-induced protein kinase), which require the PIF pocket for docking of their HMs (42). The opposite effect might be expected for substrates that do not require the PIF pocket for activation. These studies have demonstrated that targeting the HM site on other AGC kinases is a relevant strategy for identifying kinase activators as well as inhibitors (46).

Analogous to the discovery of activators that bind to the PIF pocket in PDK1, Tappan *et al.* designed a small-molecule activator for PP1 (protein phosphatase 1) that binds at a known regulatory site and increases enzyme activity (47). This designed activator mimics an interaction between PP1 and its endogenous protein regulator, glycogen binding protein. Whereas peptidomimetics and HTS have stimulated the discovery of several direct enzyme activators, an SAR study around an inhibitor of histone acetyltransferase p300 serendipitously led to the discovery of an activator believed to act by directly altering the enzyme's conformation (48).

PTM induced by binding to the catalytic domain

Proteases are typically expressed as inactive precursors, or zymogens, that need to be processed by an upstream protease, or autoprocessed, to form the active, mature enzyme. Small molecules have been identified that can interact directly with the catalytic domain of a protease and enhance this activating, irreversible post-translational modification (PTM; **Fig. 1-1**, mechanism A2).

MARTX_{Vc} toxin activator- The MARTX (multifunctional autoprocessing repeats-in-toxins) toxin is one of the virulence factors released by *Vibrio cholerae* during an infection of the gastrointestinal tract. Similar to other bacterial toxins, such as toxin A and toxin B from *Clostridium difficile*, an essential cysteine protease domain (CPD) on MARTX_{Vc} mediates autoproteolysis of the full-length toxin to release the effector domains within a target cell (49-51). Induced proteolysis of the MARTX_{Vc} toxin by natural small molecules, such as inositol hexakisphosphate (InsP₆), that bind directly to the CPD is thought to lead to proteolysis and disintegration of the host cytoskeleton.

A structure of the mature form of the CPD of the MARTX_{Vc} toxin in a cocomplex with InsP₆ provides visual evidence that InsP₆ interacts directly with a cluster of basic residues at an allosteric site on the enzyme (**Fig. 1-4A**) (52,53). This site includes residues previously shown to be important for InsP₆-promoted autocatalysis through mutational analysis of residues that are highly conserved among 24 other known CPDs of bacterial proteins (54). Lupardus *et al.* identified residues that bridge the allosteric and active sites and allow the binding affinity of InsP₆ to become uncoupled from induced processing. This suggests that binding of InsP₆ facilitates either access to or ordering of the active site through a conformational change (52).

Prochazkova *et al.* determined the structure of the zymogen CPD bound to InsP₆, demonstrating the presence of the N-terminal cleavage site in the active site of the proenzyme (55). They also showed increased stability of the proenzyme in the presence of InsP₆ through thermal shift and trypsin resistance assays. They proposed that InsP₆

binding locks the site to be processed in the active site, allowing for autoproteolysis to occur. Once cleaved, the mature enzyme has a 500-fold decrease in affinity for InsP₆ compared to the zymogen form. Though InsP₆ binds to the mature enzyme much more weakly, labeling of the active site with an irreversible active site inhibitor restores high affinity for InsP₆ (55). This suggests that InsP₆ and substrate bind cooperatively to promote catalysis. InsP₆ activation of the CPD provides the first example of a natural metabolite activator of a proprotease.

Procaspase activators- Caspases, similar to MARTX_{Vc} toxin, belong to the CD clan of cysteine proteases. These enzymes are expressed as inactive zymogens; some as single-chain monomers (such as procaspase-1, procaspase-4, procaspase-5, procaspase-8 and procaspase-9) and others as preformed dimers (such as procaspase-3, procaspase-6 and procaspase-7) (56). These proteases are best characterized for their central role in the induction and execution of apoptosis (57,58). In contrast to the MARTX_{Vc} toxin, where self-processing is induced upon binding of a metabolite, procaspase activation is regulated via a signaling cascade (59).

Apoptotic caspase activation can occur via two distinct signaling networks: an extrinsic pathway initiated by extracellular ligands or an intrinsic pathway initiated by intracellular damage (60). Initiator procaspases (including procaspase-8, procaspase-9 and procaspase-10) are recruited to scaffolding complexes in response to these signals to facilitate oligomerization and activate autoproteolysis. Once processed, initiator caspases target downstream executioner procaspase-3, procaspase-6 and procaspase-7, which become activated upon removal of an N-terminal prodomain in addition to processing within each monomer to generate a large and small subunit (61). The mature, active executioner caspases then cleave a plethora of vital cellular proteins, resulting in apoptosis. Endogenous protein inhibitors, such as XIAP and cFLIP, ensure that spurious caspase activation within these cascades does not result in inadvertent cell

death (56). Further, although self-processing is limited, these enzymes are known to be dynamic, and auto-activation can occur (62-67).

Putt *et al.* screened a library of 20,500 small molecules to discover a compound, PAC-1, that enhances the auto-activation of procaspase-3 by about threefold (68). Although others have reported difficulty replicating this, further reports from Denault *et al.* and Peterson *et al.* suggest that PAC-1 acts indirectly to chelate an inhibitory zinc ion from the active site (69,70).

In a separate effort, our lab screened a library of 62,000 compounds and identified a dozen hits that could dramatically stimulate autoproteolysis of procaspase-3 *in vitro* by up to 1,000-fold (71). The most potent compound, 1541 (**Table 1-1**), induces proteolysis of both procaspase-3 and procaspase-6, but not procaspase-7. After an initial slow phase, 1541 stimulates an accelerated activation of procaspase-3. This is consistent with 1541 promoting activation of a small population of procaspase-3 to the mature form, which can cleave additional procaspase-3 molecules in a positive feedback mechanism (**Fig. 1-4B**). During the lag phase before any appreciable procaspase-3 is cleaved, kinetic analysis shows that the procaspase exists in an intermediate state. This is 57-fold more active, in terms of catalytic efficiency, than the proenzyme alone, yet 40-fold less active than the mature enzyme. In addition to this enhanced catalytic activity in the presence of 1541, procaspase-3 is also more accessible to processing by an upstream protease.

Interestingly, the dose-response curve for 1541 against procaspase-3 is bell-shaped, rather than the typical monotonic sigmoid. It shows an AC_{50} for activation of 2.4 μ M, which plateaus at ~ 10 μ M, and decreases to about 25% maximal activity with an IC_{50} of 34 μ M. Despite the inhibition observed at higher concentrations, procaspase-3 is completely cleaved in the presence of 1541. Furthermore, 1541 inhibits mature caspase-3 with an IC_{50} virtually identical to that seen against procaspase-3. This suggests that

1541 not only activates the zymogen, but also inhibits the processed enzyme. We propose that 1541 binds near one active site of the dimeric proenzyme to induce an active conformation. This enhances proteolysis at the other active site. At higher concentrations, 1541 is able to bind both active sites, leading to partial inhibition (**Fig. 1-4B**).

Compound 1541 not only induces zymogen maturation *in vitro*, but also promotes rapid procaspase activation and apoptosis in a variety of cancer cell lines. Cell lines that are deficient in the intrinsic or extrinsic pathways upstream of the executioner caspases are still sensitive to apoptosis induced by 1541, which is consistent with procaspase-3 being a target in cells. These results demonstrate that it is possible to identify activators of dynamic protease zymogens.

Pro-caspase activation is also of potential interest to the oncology community as a new strategy for the development of chemotherapeutic agents. Initial results as well as previous observations suggest that 1541 might be selective for inducing cell death in cancer cells versus normal cells (62,68,71,72).

Allosteric binding site on regulatory subunits

Interactions with regulatory subunits can either activate or inactivate enzymes. Here we review small molecules that promote an active conformation of an enzyme through binding interactions with regulatory subunits (**Fig. 1-1**, mechanism B1).

AMPK activators- Many current therapeutic agents for type 2 diabetes, including metformin and rosiglitazone, indirectly activate AMPK (AMP-activated protein kinase), an enzyme involved in regulating cellular metabolism (73). Researchers began to target direct activation of AMPK to treat such metabolic diseases and possibly avoid the side effects associated with current drugs (74,75).

AMPK is a serine/threonine kinase that assembles into a heterotrimeric complex

composed of a catalytic α -subunit and two regulatory β - and γ -subunits (**Fig. 1-5A**) (76). The α -subunit (residues 1–548) contains the catalytic kinase domain, an AID (autoinhibitory domain), and a scaffolding domain that facilitates association of the β - and γ -subunits (77). The full-length α -subunit exhibits little activity due to interactions between the kinase domain (residues 1–312) and the AID (residues 313–335), which keep the kinase in an open, inactive conformation (78). Structural evidence suggests that the regulatory subunits, which bind endogenous ligands, signal through interactions with the AID of the α -subunit to modulate activity (78). For example, the γ -subunit contains four CBS (cystathio-nine β -synthase) domains that bind either ATP, which inhibits activity, or AMP, which enhances activity (79). The importance of AMP binding for AMPK activation is further demonstrated by mutations that localize to the CBS domains of the γ -subunit in AMPK in Wolff-Parkinson-White Syndrome (**Fig. 1-5B**) (80,81).

Thus, small molecules that mimic AMP binding to the γ -subunit could directly activate AMPK. For example, AICAR (5-aminoimidazole-4-carboxamide-1- β -D-ribofuranoside) becomes converted in cells by adenosine kinase into ZMP (5-aminoimidazole-4-carboxamide-1- β -D-ribofuranoside monophosphate), an AMP analog (82,83). ZMP binds to the same site on the γ -subunit of AMPK as AMP, and similarly activates the enzyme, but with a 50-fold less potent AC_{50} (**Fig. 1-5A**). Since ZMP influences the activity of other enzymes, some of the effects observed when cells are treated with AICAR could be mediated through off-target effects.

Cool *et al.* identified a new AMPK small-molecule activator, A592017, in a HTS of 700,000 compounds against the full-length complex by monitoring for increased phosphorylation of the AMPK substrate SAMS peptide (84,85). In these assays, AMP exhibits an AC_{50} of 56 μ M, while A592017 exhibits a comparable AC_{50} of 38 μ M. This non-nucleoside, thienopyridone compound was further optimized to generate a more

potent activator, A769662, with an AC_{50} of 0.8 μM (**Table 1-1**). As seen with AMP, A769662 acts by promoting catalytic activity and by inhibiting dephosphorylation of a residue critical for activity in the activation loop of the kinase. Remarkably, A769662 does not compete with AMP for binding to the CBS domains of the γ -subunit and does not activate the isolated α -subunit (85). Mutational analyses guided by computational docking suggest that A769662 stabilizes an interaction between the β - and γ -subunits, although additional studies are needed to determine the exact binding surface (**Fig. 1-5A**) (85-87).

Though a binding site has yet to be identified, confirmation of direct activation of AMPK is supported by the increase in phosphorylation of a downstream substrate, ACC (acetyl-CoA carboxylase), in the presence of A769662 in primary rat hepatocytes (85). Furthermore, a panel of 170 analogs of A769662 exhibit a correlation between the AC_{50} for AMPK activation and the extent of ACC phosphorylation, measured as inhibition of fatty acid synthesis (85,88). Remarkably, AICAR and A769662 behave somewhat differently in cells; AICAR has a larger impact on AMPK phosphorylation, yet the two compounds similarly affect the phosphorylation of ACC (85). This observation implies that maximal phosphorylation of a downstream substrate might occur even when only a small proportion of AMPK is activated.

Although A769662 interaction with the regulatory subunits enhances catalytic activity, Pang *et al.* explored new mechanisms for small-molecule activation of AMPK. They reasoned that a small molecule could directly disrupt the interaction between the AID and the catalytic domain on the α -subunit to stabilize an active conformation, even in the absence of the regulatory domains. In a screen of 3,600 randomly selected compounds from a diverse compound library, they monitored the activation of a truncated version of the α -subunit (residues 1–394) that included the catalytic domain and the AID. A novel activator, PT1 (**Table 1-1**), was identified that exhibits an AC_{50} of 8

μM with an A_{max} eightfold over the unstimulated α -subunit (89). The full-length AMPK $\alpha\beta\gamma$ complex is also activated by PT1, and shows a more potent AC_{50} of $0.3 \mu\text{M}$, but has a weaker A_{max} of 1.5-fold over basal activity levels for the full-length complex (89). PT1 is hypothesized to directly disrupt the AID–catalytic domain interaction to relieve auto-inhibition (**Fig. 1-5A**). Despite the need for greater mechanistic understanding, both PT1 and A769662 should prove invaluable in the elucidation of downstream AMPK substrates and as potential treatments for metabolic diseases.

Protein kinase activators- Similar to AMPK, PKA (protein kinase A) contains regulatory subunits known to bind intracellular metabolites, such as cAMP, resulting in activation of the kinase (90-92). Saldanha *et al.* have developed an HTS assay called LiReC (ligand-regulated competition) to identify small-molecule modulators of PKA (93). LiReC is a fluorescence polarization assay that uses a fluorescently labeled peptide probe that competes with the regulatory subunit for binding to the catalytic domain. A small-molecule activator would bind to and sequester the regulatory subunits. This would promote a binding interaction between the probe and the catalytic domain, thus leading to an increased fluorescence polarization signal. These studies highlight a technology that can be applied to other regulated enzyme complexes to similarly identify small-molecule activators.

Budas *et al.* have explored a similar strategy of disrupting a protein-protein interaction within the subunits of PKC (protein kinase C) to facilitate activation. Initial studies focused on developing short peptides derived from proteins known to bind to PKC to enhance activity (94). RACKs (receptors for activated C kinases) act to anchor PKCs to specific subcellular locations, and relieve auto-inhibition of PKC through a direct binding interaction (95). Peptides derived from RACK bind to an auto-inhibitory regulatory domain of PKC to promote activation (96). A small molecule could behave in a similar manner.

Binding to regulatory subunits leads to oligomerization

Oligomerization of some enzymes can promote activation. Thus, small molecules that facilitate oligomerization, either by binding to an allosteric site on the catalytic domain or by interacting with a regulatory subunit, can enhance activity (**Fig. 1-1**, mechanism B2).

RNase L activators- During a viral infection, the presence of large quantities of dsRNA (double-stranded RNA) signals enhanced expression of several enzymes involved in mounting an antiviral response, including RNase L and OAS (2'-5'-oligoadenylate synthetase), both of which are translated in an inactive form (97). Upon binding of dsRNA, OAS generates short, atypical 2-5As (2'-5'-phosphodiester-linked oligoadenylates). The 2-5A trimer subsequently binds to a regulatory subunit on RNase L, promoting activation of hydrolysis of single-stranded RNA, including the viral RNA genome (98).

RNase L consists of three domains: an N-terminal ankyrin-repeat domain, a protein-kinase domain, and the RNase domain. Tanaka *et al.* and Nakanishi *et al.* show both structurally and biochemically that trimeric 2-5As bind to the ankyrin-repeat domain (99-102). This interaction with a regulatory subunit induces a conformational change, which promotes dimerization by exposing previously occluded residues in the nuclease domain.

Thakur *et al.* envisioned RNase L activation as a general strategy to combat viral infection. To identify small-molecule mimetics of 2-5A, they developed an HTS using a FRET (fluorescence resonance energy transfer) oligoribonucleotide probe that consisted of several RNase L cleavage sites, thereby monitoring for a direct increase in the hydrolytic activity of the enzyme induced by the compounds (103). They identified 7 hits out of a library of 32,000 compounds that resulted in increased RNase L activity (**Table**

1-1).

The activators exhibit ~40,000× higher AC₅₀ values for activation in comparison to the 2-5A trimer in the *in vitro* FRET assay (20 to 100 μM versus 0.5 nM, respectively) (103). The weaker AC₅₀ values of the hits in the biochemical assays are reflected by their 10,000× weaker binding affinities (K_d values) and slower rate of RNase L activation. Although the compounds are not potent mimetics of 2-5A, a competition binding assay demonstrates that 2-5A and the new compounds have an overlapping binding site, or at the very least their binding is mutually exclusive (**Fig. 1-5C**) (103). Cross-linking studies additionally demonstrate that the compounds induce dimerization of the nuclease, similar to 2-5A (103).

Despite their modest affinities, two of the small molecules identified in the HTS have antiviral activity dependent on RNase L expression in cells (103). These compounds limit the growth of five different viral strains in cells with no associated cytotoxicity. Although these activators are at an early stage, Thakur *et al.* have identified an exciting strategy to combat viral infections through small molecules that mimic 2-5A activation of RNase L, whose expression is limited to virally infected cells.

Other enzyme complexes are also amenable to activation using a small molecule to promote oligomerization through interactions with regulatory domains. For example, Papa *et al.* discovered a novel mechanism of activation of Ire1 (inositol-requiring enzyme 1), an endoplasmic reticulum stress sensor that consists of an endoplasmic reticulum luminal domain, a kinase domain and an RNase domain. Binding of an ATP-competitive active site inhibitor to the kinase domain leads to a conformational change and promotes oligomerization and activation of the RNase domain (104).

Summary and future perspective

There are roughly 30,000 genes in the human genome, and approximately 30% encode enzymes (105,106). Recent advancements in chemical biology have brought to the forefront at least four mechanisms whereby non-natural small molecules can activate enzyme function (**Fig. 1-1**). Initial discoveries of such activating ligands were driven by the search for new approaches to treat diseases and often occurred serendipitously. In addition to their potential therapeutic applications, these compounds are valuable tools in understanding both the conformational changes linked to enzyme activation and the biological consequences of enzyme activation within a specific signaling pathway.

Properties of candidate enzymes- Small-molecule activators often require different approaches than inhibitors for target validation. For example, gene knockout and siRNA coupled with phenotypic analysis are popular strategies to 'validate' drug targets for inhibitor design. There are no equivalent approaches for enzyme activators. Adjusting gene dosage via transfection is not a general surrogate for enzyme activation, since it does not guarantee that the enzyme is indeed activated (2). A comprehensive understanding of the common properties of enzymes that have been successfully targeted by small-molecule activators can help to identify future enzyme candidates.

First and foremost, it is important to consider the natural processes used to promote enzyme activation. We highlight four unique mechanisms that synthetic small molecules can exploit to enhance activity (**Fig. 1-1**). Understanding these characteristics is not only important in identifying potential targets, but it can also aid later discovery efforts by focusing assay development efforts, defining specific sites to target and identifying potential small-molecule leads.

Second, we rarely invent what nature has not. Thus, insight into endogenous regulators of enzyme function can help to identify new small-molecule activators. Targeting known protein-protein interaction surfaces, as in PDK1 and PP1, led to the

discovery of small molecules that promote activation. Additionally, in the cases of AMPK, PKA and RNase L, metabolites are known to interact with either the catalytic domain or the regulatory domains to promote enzymatic activity. Targeting these metabolite-binding sites with synthetic small molecules proved to be a successful strategy for identifying activators. Thus, known mechanisms for activating an enzyme, either by a post-translational modification or by binding of a natural effector protein or small molecule, suggest promising targets.

Third, proteins that are known to be dynamic are good potential targets. Even in the absence of known regulatory mechanisms, a protein that can exist in multiple states offers the possibility of stabilizing an 'on state' by binding to a site present only in an active conformation, as was found for the procaspases. Similarly, though structural evidence for the dynamics of GK before the discovery of GKAs was not well known, this intrinsic property of the enzyme proved to be important for the identification of these small-molecule activators.

Fourth, if there are known mutations (either natural or induced) that result in a more active enzyme, a small molecule might be able to induce the same transition. For both GK and AMPK, the binding site for the small-molecule activators mapped to the same site as activating mutations associated with disease states.

Finally, the best guess as to which enzymes will make the best therapeutic targets for generating activators may come from analyses of metabolic or signaling pathways, as was the case for GK and AMPK. A recent report describing the discovery of small-molecule activators of mitochondrial ALDH2 (aldehyde dehydrogenase 2) stemmed from a motivation to treat cardiac ischemia (107). Targeted inhibition is no longer the default approach to identify pharmaceutical agents; direct activation of an enzyme provides an alternative method, which researchers are beginning to recognize.

Challenges and opportunities- Once a target enzyme is identified and validated,

there are a number of important considerations for discovering and characterizing small-molecule activators.

In terms of discovery, HTS remains the most widely used approach for finding small molecules that modulate protein function, as demonstrated by GK, SIRT1, procaspase-3, AMPK and RNase L. Notably, the hit rates tend to be lower in the small-molecule activator screens presented above in comparison to traditional inhibitor screens. In addition to HTS, focused screens centered around natural metabolites and precursors as well as randomly picked compounds from diverse libraries have led to the discovery of synthetic small-molecule activators, as seen with SIRT1 and AMPK, respectively. Rational approaches to activator design that mimic known interactions have also been successful, as seen with PDK1, PKC, PP1 and AMPK. So, although HTS is the most predominant method thus far for finding activators, other approaches have been effective.

In terms of *in vitro* characterization, classic Michaelis-Menten kinetic analysis, used to describe the basis for enzyme inhibition, does not easily apply to activators. One can assess the AC_{50} to get a sense of the affinity of the compound for the target. Indeed, the AC_{50} correlates well with a binding affinity for GK, SIRT1 and PDK1. However, determining affinities this way would not apply well to the 'hit and run' activators that induce an irreversible transition in the enzyme, such as the procaspase activators. Further, an understanding of the varying A_{max} values that are associated with small molecules in a chemical series, as seen with PDK1 and SIRT1, is still lacking. It is possible that the fluctuating A_{max} values are reminiscent of partial agonists of receptors, such as GPCRs (G protein-coupled receptors). These well-known partial agonists can trap intermediate conformers of GPCRs. If this also applied to enzymes, it should be possible to tune their activation level, thus allowing for greater pharmacological control. Structural information on a series of activating compounds with varying A_{max} values

bound to an enzyme might help to elucidate the relationship between chemical structure and activation levels.

Very few structures of enzymes bound to small-molecule activators have been determined so far. Inhibitors usually stabilize an inactive conformation, making them somewhat more amenable to crystallographic analysis. In the case of GK, the small-molecule activators seemed to similarly stabilize an active conformation with the substrate bound. Interestingly, the affinity of a number of activators is cooperative with substrate, such as for GK, SIRT1 and MARTX_{Vc} toxin. However, binding of the small-molecule activators could enhance enzyme dynamics, making structural determination more difficult.

One advantage of small-molecule activators versus inhibitors is that the former typically act through an allosteric mechanism. It is less likely that these binding pockets will be as conserved as the enzyme's active site. This offers better opportunities to generate more specific compounds. Interestingly, though agonists and antagonists of GPCRs bind to the same site, they induce contrasting signaling effects. This has long suggested that binding at the small-molecule site can elicit different conformational effects at the G protein interface, dependent on the structural components of the allosteric compound. This analogy would suggest that it might be possible to generate an allosteric enzyme activator from an allosteric inhibitor and vice versa. This is further supported by the discovery that a synthetic derivative of a p300 inhibitor functions as an activator.

Another advantage of activators is that weak potencies seem to be sufficient to elicit a phenotypic response. Natural effectors often demonstrate more potent AC₅₀ values than their synthetic small-molecule counterparts, as seen for the initial activator hits for PDK1, AMPK and RNase L. Yet modest activation of an enzyme pool within a cell leads to amplification of that signal within a pathway (4-6). In contrast, to completely

block pathway signaling, an inhibitor needs to saturably impede the enzyme active site.

It is important to consider the mechanism of action when characterizing direct enzyme activators in cells. A compound that acts to increase enzyme activity *in vitro* against purified enzyme might actually behave as an inhibitor in cells. For example, small molecules that bind to a regulatory pocket in PDK1 increase catalytic activity but disrupt recruitment of protein substrates to that site. This causes inhibition of phosphorylation of downstream substrates that require this site for docking. Similarly, compounds characterized as inhibitors in enzyme assays can act as activators in cells. This was recently shown to occur through two unique mechanisms. In one case, an active site inhibitor of AKT stabilized an active conformation to promote phosphorylation by an upstream kinase, yet AKT catalytic activity was still blocked (108). In the second case, an inhibitor of HER (human epidermal growth factor receptor)-family kinases resulted in transient inhibition followed by increased membrane localization and phosphorylation of HER3 due to negative-feedback signaling (109).

There has been impressive progress in identifying and characterizing direct small-molecule enzyme activators. Although we are only beginning to scratch the surface of this new field, these studies provide a proof of concept that activators can be found for numerous classes of enzymes. These compounds offer exciting new opportunities for drug discovery and novel gain-of-function probes for the chemical biologist.

Acknowledgements

We thank J. Sadowsky, S. Mahrus and D. Wolan for helpful discussions and N. Agard, J. Diaz, D. Wildes and D. Wolan for critically reviewing the manuscript.

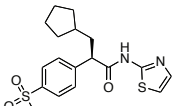
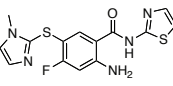
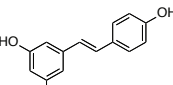
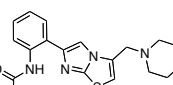
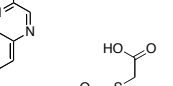
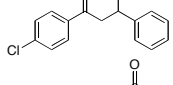
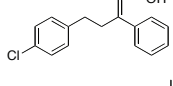
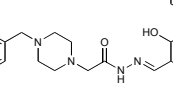
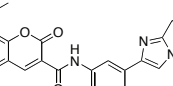
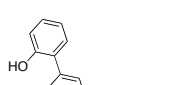
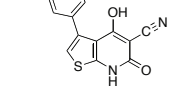
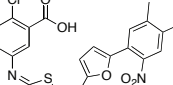
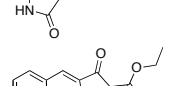
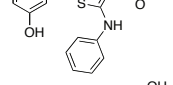
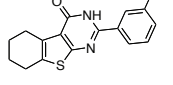
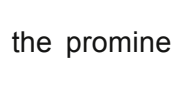
Class	Example	Activator	Natural Regulators
A1	Glucokinase (GK)		GKRP (Glucokinase Regulatory Protein); Substrate (glucose)
	RO281675		
	Compound A		
SIRT1	Resveratrol		Nicotinamide; DBC1 (Delected in Breast Cancer 1); AROS (Active Regulator of SIRT1)
	SRT1720		
	Compound 1		Substrate (RSK; S6K; SGK)
PDK1	Compound 1		
	PS48		
	Compound 1		
A2	Procaspase-3/ Caspase-3		XIAP (X-linked Inhibitor of Apoptosis); p35/p49; Initiator Caspases; Granzyme B
	1541		
B1	AMPK		AMP; ATP; glycogen
	A769662		
	PT1		
B2	RNase L		2-5A (2'-5'-Phosphodiester-linked Oligoadenylate) Trimer
	C1		

Table 1-1. The structures of some of the prominent non-natural, synthetic activators, which represent each of the four mechanistic classes, are described. For all cases, the cell has evolved natural mechanisms to regulate enzyme activity. The natural binding

partners, which include small molecules, nucleic acids and proteins, mediate either activation or inhibition.

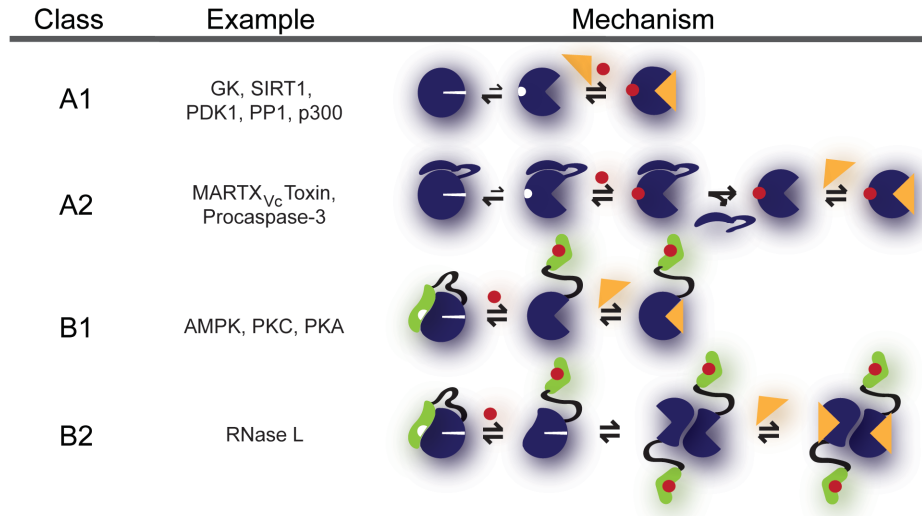


Figure 1-1. Mechanisms of small-molecule-induced enzyme activation. Four general mechanisms have been identified for small-molecule activation of an enzyme (blue circles). A closed enzyme active site indicates an inactive conformation, whereas an open active site, which binds substrate (orange triangle), indicates an active conformation. Type A mechanisms are defined by a direct binding interaction between the small-molecule activator (red dot) and an allosteric site on the enzyme's catalytic domain. Type A1 involves a direct binding interaction to stabilize an active conformation; this often requires the presence of substrate. Type A2 is a direct binding interaction that results in an irreversible, activating post-translational modification, such as proteolysis. Type B mechanisms are defined by the activator binding to a regulatory subunit (green subunit), which can either be covalently linked to the catalytic domain (as depicted) or an isolated subunit of the complex. Type B1 involves an activating conformational change in the catalytic domain as a result of binding to the regulatory subunit. Type B2 requires additional oligomerization of the catalytic domain to generate the active enzyme. For simplicity, many potential conformational states of the enzymes are not shown in the figure.

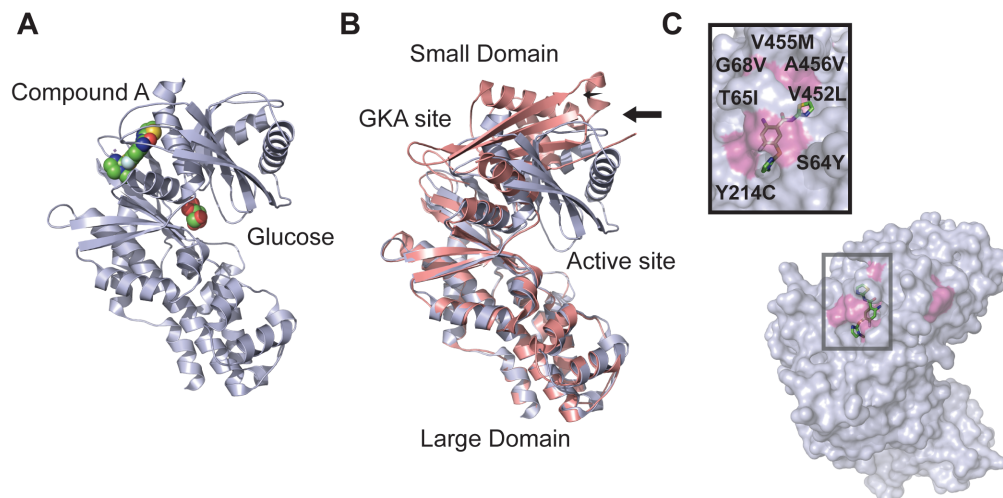


Figure 1-2. Allosteric activation of glucokinase. The discovery of GKAs set the stage for understanding the large structural transitions that enzymes can undergo from an inactive to an active conformation with unnatural small molecules. (a) GK bound to the GKA, compound A, and glucose (blue, Protein Data Bank (PDB) ID 1V4S). Compound A binds at a site distal from the active site, which is highlighted by the presence of the substrate, glucose. (b) Structural overlay of GK in the presence of compound A and glucose with an unliganded, inactive GK (pink, PDB ID 1V4T). In the unbound GK, the GKA binding site is occluded. A large shift in the small subunit of GK occurs from the unbound to bound structures (black arrow). Glucose promotes the active conformation, which is hindered from shifting back to the inactive conformation in the presence of compound A. (c) 7 mutations (out of 13) (9) identified in GK (pink) that are associated with disease map to the GKA binding site. These mutations highlight an important regulatory site within GK, and could similarly stabilize a closed, active conformation.

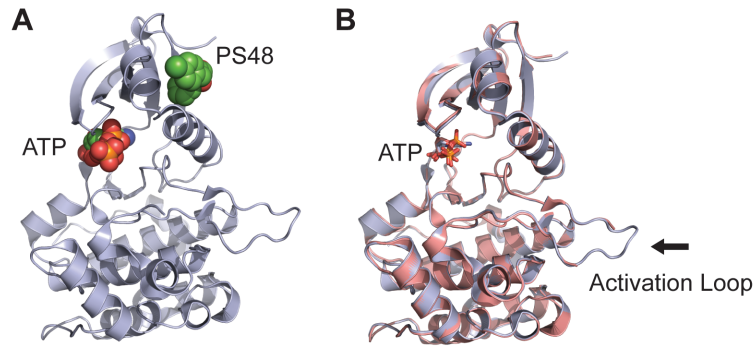


Figure 1-3. Allosteric activation of PDK1. In contrast to GK, PDK1 undergoes modest structural changes in the presence of an activator, PS48. (a) PDK1 bound to PS48 and ATP (blue, PDB ID 3HRF). PS48 binds at an allosteric site. (b) Structural overlay of PDK1 bound to ATP and PS48 versus ATP alone (pink, PDB ID 3HRC) shows modest changes in PDK1. The activation loop (black arrow) becomes more ordered in the presence of PS48. The structure of PDK1 in the absence of ATP has not been determined. Because ATP could strongly influence the conformation of PDK1, such a structure might more accurately depict the influence of PS48 on the conformation of PDK1.

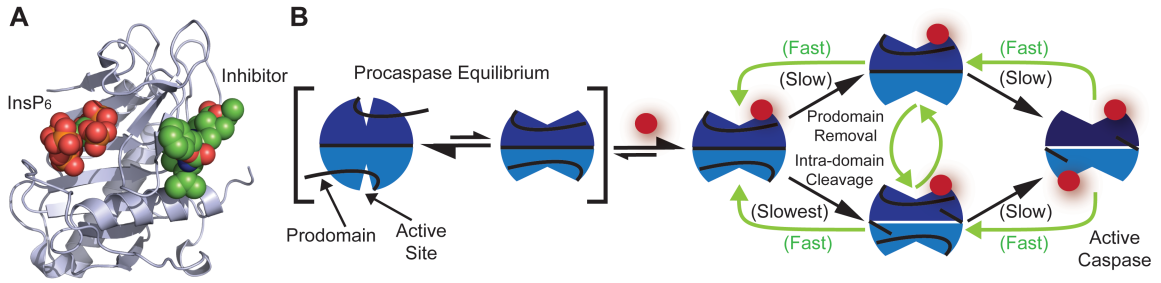


Figure 1-4. Small-molecule-induced activation of proproteases. (a) MARTX_{Vc} toxin is bound to inositol hexaphosphate (InsP₆) and an aza-peptide epoxide inhibitor (blue, PDB ID 3GCD). The endogenous ligand binds at an allosteric site to promote processing at the active site. (b) The procaspase-3 activator, 1541 (red dot), is proposed to stabilize an active conformation of the enzyme. Active, cleaved caspases exist in a dynamic equilibrium between active and inactive conformations. Procaspsases could similarly exist in an equilibrium that strongly favors an inactive conformation (left), limiting auto-proteolysis. Upon binding to the procaspase, 1541 induces a more active conformation and promotes self-processing to remove an N-terminal prodomain and generate a large and small subunit (black arrows) within each monomer of the homodimer. Active enzyme can cleave additional procaspase molecules (green arrows) in a positive feedback mechanism. At saturating concentrations of 1541, both active sites are occupied, leading to partial inhibition.

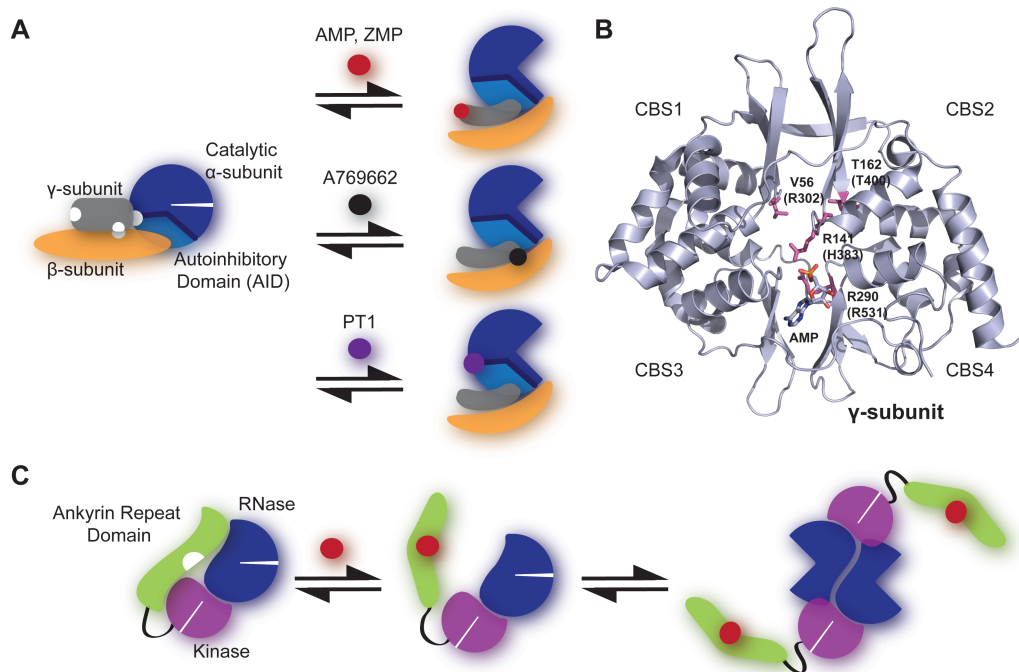


Figure 1-5. Small-molecule binding to regulatory subunits leads to enzyme activation. (a) AMPK is composed of a catalytic α -subunit (blue circle) with an AID and two regulatory β - and γ -subunits (orange and gray subunits, respectively). In addition to the endogenous activator, AMP, three different synthetic small-molecule activators for AMPK have been identified. Each activator is proposed to have a unique binding site, but all three similarly activate catalysis (73). AMP and ZMP (red dot) interact with the CBS domains on the γ -subunit. Although one binding site is depicted, multiple binding sites for AMP on the γ -subunit are known. A769662 (black dot) is proposed to stabilize an interaction between the β - and γ -subunits. PT1 (purple dot) is proposed to interact with the AID of the catalytic domain. (b) The crystal structure for one molecule of AMP bound to the regulatory γ -subunit of yeast AMPK is shown (blue, PDB ID 2O0X) (80). Functional mutations in AMPK localize to the γ -subunit (pink). These impair AMP binding yet increase AMPK activity. The corresponding residues in the γ 2-subunit of human AMPK are shown in parentheses. (c) The proposed mechanism for RNase L activation by the novel small-molecule activators (red dot) is illustrated (101,103). The endogenous

regulator 2-5A and the small-molecule activators are proposed to bind to the same site on the ankyrin repeat domain (green subunit). The regulator binds, induces a conformational change in the ankyrin repeat domain and exposes previously occluded residues in the RNase domain (blue circles). The RNase then dimerizes to generate an active enzyme conformation.

Chapter 2:
Small-Molecule Activators of a Proenzyme

Dennis W. Wolan[†], Julie A. Zorn[†], Daniel C. Gray[†], and James A. Wells^{†‡}

[†]Department of Pharmaceutical Chemistry, University of California, San Francisco,
California

[‡]Department of Cellular and Molecular Pharmacology, University of California, San
Francisco, California

This work was published in *Science* (2009) 326: 853-858.

Abstract

Virtually all of the 560 human proteases are stored as inactive proenzymes and are strictly regulated. We report the identification and characterization of the first small molecules that directly activate proenzymes, the apoptotic procaspases-3 and -6. It is surprising that these compounds induce autoproteolytic activation by stabilizing a conformation that is both more active and more susceptible to intermolecular proteolysis. These procaspase activators bypass the normal upstream proapoptotic signaling cascades and induce rapid apoptosis in a variety of cell lines. Systematic biochemical and biophysical analyses identified a cluster of mutations in procaspase-3 that resist small-molecule activation both *in vitro* and in cells. Compounds that induce gain of function are rare, and the activators reported here will enable direct control of the executioner caspases in apoptosis and in cellular differentiation. More generally, these studies presage the discovery of other proenzyme activators to explore fundamental processes of proenzyme activation and their fate-determining roles in biology.

Activation of proteases triggers a myriad of biological events, such as apoptosis and blood clotting, both inside and outside of the cell (110). Proteases are generally stored as inactive proenzymes that are usually activated by upstream proteases or by themselves. These activation events may sometimes involve binding a protein partner or, in rare instances, interaction with a natural small molecule (52) or peptide (111). In the case of autoproteolysis, the proenzyme must achieve not only an active state, but also one in which the sites of proteolysis are exposed. In situ activation of specific proproteases with synthetic small molecules could uncover new molecular principles in zymogen activation and would facilitate direct control of these important processes in biology.

The executioner procaspases, consisting of procaspases-3, -6 and -7, represent excellent initial candidates for discovery of small-molecule protease activators. Caspases are a family of homodimeric cysteine proteases responsible for many of the fate-determining processes in cell biology, including apoptosis, innate immune signaling, early stages of stem cell differentiation, and cellular remodeling (58,60,112). As with most proteases, caspases are synthesized as inactive procaspases, or zymogens, and are activated by upstream proteolysis or autoproteolysis. Previous studies have shown that the mature active caspases are intrinsically dynamic (113,114) and sample both an “on state” and an “off state” that structurally resemble the zymogen-like conformation (65,115). Small molecules have been found to trap these two forms of the mature enzyme (63,64). We reasoned that if the procaspases existed in a similar dynamic equilibrium of off and on states, it might be possible to find small molecules that promote autoproteolytic activation via stabilization of an on-state conformation. Executioner procaspases are particularly good targets as they are susceptible to rapid activation by both upstream proteases and self-proteolysis. Thus, any activation would be accentuated in trans by autocatalytic activation. Moreover, these particular caspases are

essential for executing the final processes of apoptosis, and specific activation by a small molecule would elicit robust and precise phenotypic responses within cells.

High-throughput screening was employed to identify compounds that could promote autoproteolytic activation of procaspase-3 at physiological concentrations. A dozen compounds out of 62,000 promoted >20-fold activation of procaspase-3 (**Fig. 2-1**) and were resynthesized to validate their chemical composition. To warrant further analysis, dynamic light-scattering was used to select compounds with solubilities greater than 100 μ M, and a β -lactamase inhibition assay was performed to discard promiscuous aggregators (116). The most robust procaspase activator fulfilling these criteria was compound 1541, a substituted phenyl-imidazopyridine-methoxy coumarin with a median effective concentration (EC_{50}) for activation of 2.4 μ M (**Fig. 2-2A**). Mass spectrometry revealed that the compound did not covalently label either the mature or proenzyme forms of caspase-3, nor was 1541 modified by enzyme hydrolysis.

We compared the rate of 1541 activation and specificity for the executioner procaspases-3, -6, and -7, which share 40 to 50% sequence identity. Granzyme B, a natural proteolytic activator of procaspase-3, rapidly and fully activates the zymogen within 90 min. In contrast, after an initial slow phase that lasts ~30 min, 1541 induces accelerated activation of caspase-3 to a level that is finally ~70% that of granzyme B within 2.5 hours (**Fig. 2-2B**). Granzyme B and 1541 both induce full proteolytic processing of procaspase-3, as evidenced by production of the large (17-kD) and small (12-kD) subunits of caspase-3 (**Fig. 2-3**). Procaspase-7 is robustly activated and fully processed by granzyme B, but not by 1541 (**Fig. 2-2C**). The compound 1541 does induce ~10% self cleavage of its prodomain (residues 1 to 23) (**Fig. 2-3**), but prodomain removal by itself does not elicit caspase-7 activation (117). Procaspase-6 is resistant to granzyme B (118,119), but 1541 promotes activation and complete self-processing similar to procaspase-3 (**Fig. 2-2D**). Furthermore, 1541 does not activate or induce self-

cleavage of inflammatory procaspase-1 (**Fig. 2-4**). We also tested PAC-1, a compound previously reported to induce a slight activation of procaspase-3 (68), but found no detectable increase in activity or self-proteolysis among the executioner procaspases (**Fig. 2-2, B to D**). Others have reported a similar inability to activate procaspase-3 with PAC-1 (69,70). Thus, 1541 is a highly specific and robust activator of executioner procaspases-3 and -6, and does not activate procaspases-1 or -7.

To further validate activity and specificity, several 1541 analogs with modifications on the coumarin ring were tested (**Fig. 2-2A**, and **Fig. 2-5**). Substitution of the 8-methoxy with an 8-hydroxy (1541B) improves the EC_{50} by about twofold for activation of procaspase-3, but dramatically reduces activity toward procaspase-6. A 6-bromo substitution (1541C) reduces potency for procaspase-3 and for procaspase-6 by factors of 15 and 35, respectively. Deletion of the imidazopyridine substituent meta to the coumarin on the phenyl ring (1541D) eliminates activation of procaspases-3 and -6 (**Fig. 2-2A**). Thus, relatively modest modifications to 1541 can alter efficacy and selectivity, which suggests that 1541 has high specificity to the site of interaction.

A series of in vitro biochemical and kinetic analyses was performed to assess the activation mechanism of procaspase-3 by 1541 and to test our initial hypothesis of autoproteolysis through stabilization of an on-state conformation (**Fig. 2-2E**). Mature caspase-3 has a catalytic efficiency (k_{cat}/K_m) of $2.5 \text{ min}^{-1}\mu\text{M}^{-1}$ for hydrolyzing a fluorogenic peptide substrate Ac-IETD-AFC that mimics the activating cleavage site (residues 172 to 175) between the large and small subunits (**Fig. 2-6A**). Procaspase-3 is substantially less active (by a factor of 2100), with a corresponding k_{cat}/K_m of $0.0012 \text{ min}^{-1}\mu\text{M}^{-1}$. We titrated procaspase-3 with compound 1541B (from 0 to 50 μM) and measured the kinetic parameters for Ac-IETD-AFC by Michaelis-Menten analysis within 15 min, where no detectable processing or self-activation of procaspase-3 occurred that would contribute to substrate recognition and cleavage. As 1541B is increased, a dose-

dependent decrease is observed in K_m (101 to 14 μM , a factor of seven) and an increase in k_{cat} (0.12 to 0.93 min^{-1} , a factor of eight) (**Fig. 2-6A**). Compound 1541B, therefore, induces an immediate kinetic state where the catalytic efficiency is increased 57-fold (k_{cat}/K_m of 0.068 $\text{min}^{-1}\mu\text{M}^{-1}$) over unstimulated procaspase-3. Note that the K_m value for procaspase-3 improves to 14 μM in the presence of 1541B, compared with 212 μM and 101 μM for the mature enzyme and unstimulated proenzyme, respectively. These data strongly imply that the initial catalytic activity of 1541B-stimulated procaspase-3 results from a different on-state conformation than that of mature caspase-3 and represents the first intermediate of the activator-bound procaspase-3 (**Fig. 2-2E**). For hydrolyzing amide substrates, K_m is a reasonable estimate of the K_D (120,121). Thus, the 1541B-activated procaspase-3 binds Ac-IETD-AFC about 15 times as tightly as the mature enzyme, albeit with a k_{cat} value substantially lower than that of the mature enzyme (**Fig. 2-6A** and **Fig. 2-7**). Small amounts of mature caspase-3 that are generated in the presence of 1541 eventually overtake the activation process and account for the subsequent rapid increase in activity.

As activation of caspase zymogens requires cleavage of the junction between the large and small subunits, we tested whether these compounds could also enhance the proteolytic susceptibility of the proenzyme itself. We generated an inactive procaspase-3 by mutating the catalytic cysteine, C163A (in which Cys¹⁶³ is replaced by Ala), and then tested whether 1541 enhances C163A processing by granzyme B. Incubation with granzyme B alone resulted in ~10% cleavage of C163A after 30 min and 20% after 60 min. Addition of 1541 significantly increased the rate of processing to 40% after 30 min, and 80% after 60 min (**Fig. 2-6B**). Coincubation with a nonactivating analog 1541D (**Fig. 2-2A**) did not enhance proteolysis by granzyme B. Thus, these activating compounds increase both the catalytic efficiency of unprocessed procaspase-3 (**Fig. 2-6A**) and its susceptibility to proteolysis (**Fig. 2-6B**). The ability to induce autoproteolytic

activation was then evaluated by titrating 1541 (0.1 to 100 μM) with wild-type procaspase-3 and measuring activation as a function of time (**Fig. 2-6C**). As the incubation times increase, the EC_{50} values of the activation curves shift to lower values, and the slopes dramatically increase, which are indicative of a highly cooperative activation process consistent with the feedback activation proposed in **Fig. 2-2E** (122).

We next investigated why the maximal autoproteolytic activation of procaspase-3 was only about 70% of that induced by granzyme B (**Fig. 2-2B**), even though procaspase-3 was fully processed (**Fig. 2-3**). Titration of procaspase-3 with 1541 (from 0.1 to 100 μM) assayed after 4 hours shows a biphasic dose-response (**Fig. 2-6D**). At low concentrations, the enzyme is activated (EC_{50} of 2.4 μM) whereas, at high concentrations, it is partially inhibited [median inhibitory concentration (IC_{50}) of 34 μM]. The proenzyme becomes fully processed over the time course of the dose-response study (EC_{50} of ~ 2 μM) (**Fig. 2-8**). To understand the basis for this inhibition, we directly tested 1541 on mature caspase-3. Indeed, caspase-3 is inhibited by 1541 with a virtually identical IC_{50} of 35 μM (**Fig. 2-6E**). A similar biphasic dose-response curve was observed for procaspase-6 (EC_{50} of 2.8 μM and IC_{50} of 38 μM). Michaelis-Menten analyses revealed that 1541 acts as a competitive or mixed noncompetitive inhibitor of caspases-3 and -6 (**Fig. 2-9**). Overall, these results are consistent with a mechanism whereby, at low concentration, a single 1541 molecule binds near one active site of the dimer as an inhibitor and stabilizes an on-state conformation that promotes self-cleavage at the unoccupied subunit (**Fig. 2-2E**). At very high concentrations, 1541 can inhibit both active sites.

On the basis of kinetic inhibition data of caspase-3 by 1541 (**Fig. 2-9**) and conservation with caspase-6, we used alanine-scanning mutagenesis on residues near the active site to probe for resistance mutations (**Fig. 2-6F**). Three procaspase-3 mutants (S198A, T199A, and S205A) rendered the proenzyme insensitive to 1541

activation. Each of the three variants were efficiently activated by granzyme B, which showed that these were fully functional enzymes (**Fig. 2-6G**). These mutational studies indicate specific residues near the active site that alter binding of 1541 and/or susceptibility to autoproteolysis of wild-type procaspase-3.

We next tested the ability of 1541 to induce apoptosis in a p53-deficient breast cancer cell line, BT549. Cells were treated with 1541 (25 μ M), as well as with traditional inducers, such as staurosporine (STS) [a nonspecific kinase inhibitor (123)] and etoposide [a topoisomerase II inhibitor (124-126)]. Cells were probed every two hours for cellular viability and executioner caspase activity (DEVDase). After 4 hours, 1541 and STS induce comparable and near-complete apoptosis of BT549 cells (**Fig. 2-10A**). Etoposide induced much slower apoptosis because of dependence on p53 for activity. The decrease in cellular viability in presence of STS and 1541 is accompanied by a reciprocal increase in DEVDase activity, characteristic of caspase-3, which peaks after 8 hours (**Fig. 2-10B**). DEVDase activity is significantly higher with STS than with 1541. Western blots confirmed production of active caspases-3, -6, and -7 and the hallmark apoptotic cleavage of poly(adenosine diphosphate-ribose) polymerase (PARP); however, more extensive cleavage is observed with STS (**Fig. 2-11**). Procaspase-7 is also cleaved in cells treated with 1541, which likely reflects the ability of mature caspases-3 and/or -6 to activate procaspase-7, as previously reported (117) (**Fig. 2-11**).

Two other cell lines were tested: MDA-MB361, a p53-proficient breast cancer cell line; and HEK293, a transformed human embryonic kidney cell line (**Fig. 2-12**). A similar pattern of cell viability and DEVDase activity was observed in MDA-MB361, as for BT549 cells. In HEK293 cells, 1541 was the most potent apoptotic inducer, compared with STS and etoposide, and generated the highest level of DEVDase activity. These data suggest that 1541 is as potent an inducer of cell death as STS and functions independently of p53. The fact that STS and 1541 induce comparable apoptotic rates,

despite the higher caspase activity associated with STS, suggests that activation of only a fraction of the pool of executioner procaspases in these cells is required to induce cell death. Compounds 1541C and D, respectively, induce limited to no apoptosis or DEVDase activity in these three cell lines (**Fig. 2-10A** and **Fig. 2-12**). Significantly, the cellular results for these 1541 analogs correlate with their in vitro activity against procaspase-3 (**Fig. 2-6A**). Preincubation of cells with irreversible cell-permeable caspase inhibitors [carbobenzoxy-valyl-alanyl-aspartyl-[O-methyl]-fluoromethylketone (VAD-FMK) or carbobenzoxy-aspartyl-(O-methyl)-glutamyl-(O-methyl)-valyl-aspartyl-(O-methyl)-fluoromethylketone (DEVD-FMK)] completely blocked apoptosis with 1541, which indicated that the caspase activity is responsible for the observed apoptosis (**Fig. 2-10C**).

The breadth of 1541 induction of apoptosis was then assessed in a variety of cancerous and transformed cell lines including BT549, MDA-MB361, HEK293, HeLa, and HCC1954. Cells were incubated with increasing concentrations of 1541 and assayed for cell death after 24 hours (**Fig. 2-13**). All cell lines underwent apoptosis, with EC_{50} values ranging between 4 and 9 μM , similar to those measured in vitro for procaspases-3 and -6 (EC_{50} of 2 to 3 μM). Compound 1541B, which is comparably active toward procaspase-3, but inactive against procaspase-6, exhibited virtually the same EC_{50} for inducing apoptosis (**Fig. 2-13**). These results imply that direct activation of procaspase-3 alone is sufficient to induce rapid apoptosis.

We assessed the effects of 1541-induced apoptosis on apoptotic hallmarks and signaling pathways. Typical inducers of the intrinsic apoptosis pathway, such as STS, operate indirectly to activate executioner procaspases by releasing mitochondrial cytochrome c into the cytoplasm, which leads to activation of procaspase-9, which in turn targets executioner procaspases. Direct activation of procaspase-3 by 1541 should be independent of cytochrome c in the cytoplasm. BT549 cells were incubated with

either 1541 or STS and harvested every 3 hours, and cytoplasmic extracts were probed by Western blot to establish levels of activated caspase-3 and cytochrome c (**Fig. 2-10D**). Indeed, STS induced much greater and more rapid mitochondrial cytochrome c release than did 1541. As expected, small amounts of cytochrome c appeared in the cytosol at later time points with 1541, because positive-feedback loops from activated caspase-3 are known to produce mitochondrial damage eventually, as well as subsequent cytochrome c release (127).

We next evaluated if 1541 induces apoptosis directly through the executioner caspases or if the compound requires an intact extrinsic or intrinsic pathway. To test the requirement for the extrinsic cell death pathway, wild-type (A3) and caspase-8–deficient human Jurkat cells (19.2) (128) were treated with 1541, STS, and FasL, a specific inducer of the extrinsic pathway (**Fig. 2-14A**). Compound 1541 produced rapid and comparable rates of apoptosis in both wild-type and caspase-8–deficient Jurkat cells. As expected, FasL was active in wild-type Jurkats, but not in caspase-8–deficient cells. STS induction was comparable to 1541 in wild-type Jurkats, and somewhat slower in caspase-8–deficient cells, which suggested that the extrinsic pathway augments some of its activity. Thus, cells with genetic lesions within either the intrinsic (p53) or extrinsic (caspase-8) pathways are resistant to traditional intrinsic or extrinsic inducers, respectively, but both are susceptible to cell death by 1541.

To determine whether 1541 targets are downstream of the mitochondria within the intrinsic pathway, we compared induction of apoptosis in wild-type murine embryonic fibroblasts (MEFs) and MEFs that lack the proapoptotic proteins Bak and Bax (129,130). Deletion of Bak and Bax prevents release of mitochondrial cytochrome c and blocks the apoptotic response of intrinsic apoptotic inducers STS and etoposide. Wild-type MEFs and Bak^{-/-}/Bax^{-/-} double-knockout (DKO) MEFs were incubated with STS or 1541 and then assayed for apoptosis by using a histone enzyme-linked immunosorbent assay

(ELISA) that measures solubilization of histones caused by DNA fragmentation, a hallmark of apoptosis. As expected, wild-type MEFs were susceptible to apoptosis by either 1541 or STS (**Fig. 2-14B**). However, DKO MEFs retained sensitivity to 1541, but were completely resistant to STS. Western blots probed for active caspase-3 and PARP confirmed cleavage of these markers in 1541-induced DKO MEF lysates, but not in STS-treated cells (**Fig. 2-14C**). Thus, 1541 can bypass the lesion of Bak and Bax, which is consistent with direct activation of procaspase-3.

To decide whether the compounds act specifically through procaspase-3 in cells, we tested the ability of 1541 to induce apoptosis in human MCF-7 cells that lack a functional caspase-3 gene (131,132). Indeed, MCF-7 cells were far less susceptible to 1541-induced apoptosis, which could be restored upon stable transfection with wild-type procaspase-3 (**Fig. 2-14D**). Cells transfected with the S198A procaspase-3 mutant, previously determined *in vitro* to resist 1541-induced activation, also largely resisted apoptosis in cells. This mutant did exhibit some apoptosis after a 24-hour incubation, which may arise from leaky activation of S198A procaspase-3. Overall, these data provide strong support that procaspase-3 is the primary intracellular target of 1541 and a major mediator of 1541-induced apoptosis *in vivo*. To begin to explore a therapeutic window for procaspase activators, we tested the effects of 1541B on a cancerous B cell line (DB) in comparison with Epstein-Barr virus transformed immortalized normal B cells (EBV). We found the cancerous cell line to be more sensitive to apoptosis induced by 1541B (**Fig. 2-15**). Further experiments will be needed to explore these compounds as selective chemotherapeutic agents that bypass typical proapoptotic lesions.

In conclusion, our studies reveal a unique mechanism for activation of executioner procaspases by synthetic small molecules. Remarkably, the compounds both reorganize the active site for catalysis and render their internal cleavage sites more accessible to proteolysis, which may reflect aspects of the natural zymogen-activation

process. These compounds could either stabilize the on state of procaspase-3 or destabilize the off state and enhance susceptibility to proteolysis through a more flexible on-state conformation. The small-molecule analogs exhibit selectivity toward procaspase-3 in vitro and in cells. Selective small-molecule activators of procaspases will have great utility for in-depth studies of caspase-dependent apoptotic and nonapoptotic processes, such as stem cell differentiation (112) and cellular remodeling (58). Finally, our results, together with the recently characterized allosteric activation of the monomeric *Vibrio cholerae* RTX cysteine protease by a natural small-molecule metabolite (52), suggest that it may be possible to discover synthetic small-molecule activators for other proenzymes to facilitate functional and mechanistic studies and further to enhance their utility in biology and disease.

Materials and Methods

Protein expression and purification

Full-length human procaspase clones (residues 1-277 (procaspase-3), 1-293 (procaspase-6) and 1-303 (procaspase-7)) were generated with standard PCR based cloning and verified with double-stranded plasmid sequencing. Procaspases-3, -6 and -7 were expressed with a C-terminal His₆-affinity tag from a pET-23b vector (Novagen) in *E. coli* BL21(DE3)pLysS cells (Stratagene). Cells were grown in 2xYT media supplemented with 200 µg/mL ampicillin and 50 µg/mL chloramphenicol at 37°C to an OD_{600nm} of 0.8-1.0. Overexpression of procaspase was induced with 0.2 mM IPTG at 30°C for 20 minutes to limit autolysis. Cells were immediately harvested and resuspended in ice cold 100 mM Tris, pH 8.0, 100 mM NaCl (buffer A) and subjected to 3 cycles of lysis by microfluidization (Microfluidics). The cell lysate was clarified by centrifugation at 45,000xg for 30 minutes at 4 °C and soluble fractions were loaded onto a 1 mL HisTrap HP Ni-NTA affinity column (GE Amersham) pre-equilibrated with buffer A and eluted with buffer A containing 200 mM Imidazole. The eluted protein was immediately diluted two-fold with buffer B (20 mM Tris, pH 8.0) and purified by anion-exchange chromatography (HiTrap Q HP, GE Amersham) with a 30-column volume gradient to 50% of buffer B containing 1 M NaCl. The protein was injected over a Superdex 200 16/60 gel filtration column (GE Amersham) in 20 mM Tris, pH 8.0, 50 mM NaCl to buffer exchange and to remove any remaining contaminants. Fractions corresponding to purified homodimeric procaspase-3, -6 or -7 were pulled and concentrated to approximately 1 mg/mL using Millipore Ultrafree-15 devices with a MWCO of 10,000 Da. All fast protein liquid chromatography (FPLC) procaspase purification steps were performed within 5 hours on an AKTA FPLC (GE Amersham) at 4°C and immediately frozen and stored at -70°C to eliminate potential spontaneous self-activation. Purified procaspase concentrations were measured using both Bio-Rad colorimetric assay and A280 absorbance in denaturing

conditions (133). Protein purity was assayed by electrospray ionization mass spectrometry on an LCT Premier Mass Spectrometer (Waters) and SDS-PAGE under reducing conditions. All procaspases are >98% pure and have <0.1% the activity of fully-processed caspase. Active caspases- 3 and -7 are produced using the same plasmids and purification protocols as the procaspases, except that overexpression is extended to 4 and 24 hours, respectively, in order to promote autocatalysis. Active caspase-6 clones were made by incorporation of the large subunit (residues 24-179) into pET-24b (Novagen) and the small subunit (residues 194-293 with a C-terminal His6-affinity tag) into pET-23b. Both plasmids were co-transformed into *E. coli* BL21(DE3) cells and colonies were selected for resistance against 200 µg/mL ampicillin and 50 µg/mL kanamycin. Soluble active caspase-6 was overexpressed by induction with 0.2 mM IPTG in 2xYT media supplemented with 200 µg/mL ampicillin and 50 µg/mL kanamycin overnight at 16°C. Active caspase-6 was purified as described for procaspase.

High throughput screen for procaspase-3 activators

A total of 62,000 compounds were screened for their ability to activate procaspase-3 in a 384-well plate assay. Procaspase-3 was incubated at a physiologically-relevant concentration of 100 nM (72,134) with 30 µM HTS compounds in a total volume of 50 µl consisting of a reaction buffer of 50 mM HEPES, pH 7.4, 50 mM KCl, 0.1 mM EDTA, 1 mM DTT and 0.1% CHAPS (to reduce false positive hits due to compound aggregation). The procaspase-3/small molecule incubations were then agitated for 3 hours at 37 °C. A fluorogenic peptide substrate rhodamine 110, bis-(*N*-CBZ-DEVD) (Z-DEVD-R110) was subsequently added to a final concentration of 10 µM by a MultiMex bulk liquid dispenser (Beckman) and incubated for an additional 30 minutes at room temperature. The reaction was quenched with a final concentration of 40 mM HCl and the endpoint fluorescence was measured on an Analyst HT Assay Detection System (LJL Biosystem).

The final concentration of DMSO in each well was 3% and had no effect on enzyme stability or activity. In order to obtain a large endpoint disparateness between the proenzyme and activated caspase species for Z', procaspase-3 was proteolytically cleaved with granzyme B to attain maximal activity. Granzyme B was added at a concentration 1:1000 of procaspase-3 and, thus, did not contribute to observable activity of substrate cleavage. The granzyme B-activated caspase-3 fluorescence averaged 100-fold greater than the background fluorescence by procaspase-3. A Z' ranging from 0.85 to 0.95 was conserved over the course of the HTS assays. Any compounds from the high throughput screens with an increased activity of 20% or more over the inherent activity of procaspase-3 were considered potential "hits". All components of the assay including protein, substrate and inhibitor were stored as frozen aliquots and thawed immediately prior to the assay.

Elimination of promiscuous and aggregating HTS hits

All potential procaspase-3 small molecule HTS activators were re-synthesized and analyzed to identify false-positives with potential for aggregation or promiscuity. All compounds were subjected to dynamic light scattering at concentrations ranging from 0.1 to 100 μ M in a buffer consisting of 50 mM HEPES, pH 7.4, 50 mM KCl, 0.1 mM EDTA and 1 mM DTT to determine aggregation potential. Any compounds that exhibited a propensity towards aggregation or insolubility in the absence of detergent were eliminated from further analysis. Similarly, the functional effects of all HTS hits were analyzed for inhibition of β -lactamase, which is extremely sensitive to promiscuous inhibition, as previously described (135,136). Briefly, 1 nM β -lactamase was incubated in the presence of various concentrations of HTS procaspase activators (25 to 100 μ M) in a buffer consisting of 50 mM sodium cacodylate, pH 6.5 in the presence or absence of 0.01% Triton-X100 for 1 hour at 37 °C. A kinetic assay was initiated by addition of 40 μ M

CENTATM (CalBiochem) and monitored for 10 minutes on a SpectraMax M5 microplate reader (Molecular Devices) at an absorbance of 405 nm. Any compounds that inhibited β -lactamase in the presence or absence of 0.01% Triton-X100 were determined to be promiscuous and/or aggregating compounds and eliminated from further studies.

***In vitro* procaspase activator characterization**

Time course assays of procaspase activation: Compounds were assayed for activation potential against 100 nM of each executioner procaspases-3, -6 and -7 with either 25 μ M 1541, 1 nM granzyme B, DMSO or 100 μ M PAC1 (TimTec) in an optimized reaction buffer (50 mM HEPES, pH 7.4, 0.01% Triton-X100, 50 mM KCl, 0.1 mM EDTA, 1 mM DTT for procaspase-3; 100 mM HEPES, pH 7.4, 0.01% Triton-X100, 10 mM DTT for procaspase-6; 100 mM HEPES, 5 mM CaCl₂, 0.01% Triton-X100, 1 mM DTT for procaspase-7) (59,68,137-141). Kinetic assays were initiated after incubation at 37°C by addition of the fluorogenic peptide Ac-DEVD-AFC (-3 and -7) or Ac-VEID-AFC (-6) to 25 μ M. All sample incubations were harvested after 4 hours and subjected to SDS-PAGE to determine the extent of proteolysis of the procaspases.

Initial activity rates of procaspase-3 in presence of 1541B: Procaspase-3 was incubated at 100 nM in the presence of various amounts of compound 1541B (0.78 to 50 μ M) in a buffer consisting of 50 mM HEPES, pH 7.4, 50 mM KCl, 0.1 mM EDTA, 1 mM DTT and 0.1% CHAPS in a total volume of 100 μ l. The kinetic activity of the mixtures were immediately assayed by addition of Ac-IETD-7-amino-4-trifluoromethylcoumarin (Ac-IETD-AFC) (1.2 to 300 μ M) for approximately 15 minutes at 37°C by monitoring the emission at 495 nm on excitation at 365 nm every 45 seconds. Ac-IETD-AFC was chosen as the cleavage reporter as it is the self-cleavage intradomain sequence in procaspase-3.

Granzyme B cleavage of procaspase-3 C163A: C163A procaspase-3 was incubated at 250 nM with 500 pM granzyme B in the presence of DMSO or 25 μ M 1541. The reaction buffer consisted of 50 mM HEPES, pH7.4, 50 mM KCl, 0.1 mM EDTA, 1 mM DTT and 0.1% CHAPS and mixtures were agitated at 37°C with aliquots removed after 30 and 60 minutes. Aliquots were immediately quenched with addition of 1% SDS reducing gel loading buffer and boiled. Samples were subjected to silver stain gel electrophoresis to determine extent of granzyme B cleavage.

1541 EC₅₀ (activation) and IC₅₀ (inhibition) for procaspase-3 and active caspase-3: Procaspase-3, or active caspase-3, was incubated at 100 nM and 25 nM, respectively, in the presence of increasing amounts of compound 1541 (0.1 to 100 μ M) in a reaction buffer consisted of 50 mM HEPES, pH7.4, 50 mM KCl, 0.1 mM EDTA, 1 mM DTT and 0.1% CHAPS. The mixtures were assayed for kinetic activity by incubation with 20 μ M Ac-DEVD-AFC for 5 minutes after 4 hours of incubation at 37 °C (procaspase-3) or 10 minutes (active caspase-3).

Time course activation of procaspase-3 with 1541: Procaspase-3 was incubated at 100 nM in the presence of 1541 (0.1 to 100 μ M) to assess speed of self-activation. The mixtures were agitated at 37°C and assayed for kinetic activity every hour for 18 hours by incubation with 20 μ M Ac-DEVD-AFC for 5 minutes.

Competitive vs. non-competitive inhibition of active caspases-3, -6 and -7 with 1541: Active caspases-3, -6 or -7 were incubated at 10 nM (caspase-3 or -7) or 50 nM (caspase-6) in the presence of compound 1541 (6.25 to 200 μ M) in their optimal buffers in a total volume of 50 μ l. The kinetic inhibition of the mixtures was immediately assayed

by addition of Ac-DEVD-AFC (-3 and -7) or Ac-VEID-AFC (-6) (1.2 to 300 μM) for 10 minutes at room temperature.

Procaspase-1 incubation with 1541: Procaspase-1 (purified as described for procaspase-3) was incubated at 1 μM with 25 μM 1541 in an optimal reaction buffer consisting of 50 mM HEPES, pH 7.4, 0.01% Triton-X100, 200 mM NaCl, 50 mM KCl, 0.1 mM EDTA, 10 mM DTT overnight at 37°C. The mixtures were agitated for 24 hours and aliquots were quenched with addition of 1% SDS reducing gel loading buffer and boiled. Samples were subjected to silver stain gel electrophoresis to determine extent of potential of procaspase-1 self-cleavage in the presence of 1541. All *in vitro* kinetic experiments were performed in 96-well plates with fluorescence read on a SpectraMax M5 microplate reader (Molecular Devices). Michaelis-Menten values (K_m and k_{cat}), Hill slopes, EC_{50} , IC_{50} , values were determined using GraphPad Prism software (GraphPad, Inc.).

Chemical Synthesis

General procedure: 6-bromo-3-carboxy-coumarin was purchased from Alfa Aesar; O-(7-azabenzotriazole-1-yl)-N,N,N,N'-tetramethyluronium hexafluorophosphate was purchased from Applied Biosystems; 3-imidazo[1,2-a]pyridin-2-yl-phenylamine was purchased from Matrix Scientific; 8-methoxy-2-oxo-2H-chromene-3-carboxylic acid was purchased from Maybridge; 2,2-dimethyl-1,3-dioxane-4,6-dione (Meldrum's acid), 2,3-dihydroxybenzaldehyde, aniline, dimethylformamide and all other solvents and reagents were purchased from Sigma-Aldrich. The 3-carboxycoumarin ring was constructed from commercially available salicylaldehydes. The salicylaldehyde was reacted with Meldrum's acid in an aqueous solution (50-100°C) to afford the 3-carboxycoumarin, as previously described (142). The resulting carboxylic acid was then converted to various

amide derivatives using well-known coupling reactions, including direct coupling of the acid with amines using carbodiimide reagents. The products that precipitated out of solution were collected by filtration and dried under vacuum. ^1H and ^{13}C NMR data were collected on a Varian 400 MHz spectrometer in $\text{DMSO-}d_6$. LCMS data was acquired on a Waters Micromass ZQ in ESI+ mode, equipped with a Waters 2996 photodiode array detector and Waters Alliance 2795 separations module. The LCMS protocol consisted of sample elution through an analytical Xterra C-18 column (2.1 mm x 50 mm x 3.5 μm) at a gradient of 5-95% methanol (0.2% formic acid)/water (0.2% formic acid) over 6 minutes at a flow rate of 1.0 mL/min.

8-Methoxy-2-oxo-2H-chromene-3-carboxylic acid (3-imidazo[1,2-a]pyridin-2-yl-phenyl)-amide (1541): Diisopropylethylamine (DIEA, 0.044 mL, 0.25 mmol) was added to 8-methoxy-2-oxo-2H-chromene-3-carboxylic acid (0.05 g, 0.23 mmol) and O-(7-Azabenzotriazole-1-yl)-N,N,N,N'-tetramethyluronium hexafluorophosphate (HATU, 0.096 g, 0.25 mmol) in 2 mL of dimethylformamide (DMF) with constant stirring at room temperature until a clear solution resulted. 3-Imidazo[1,2-a]pyridin-2-yl-phenylamine (0.048 g, 0.023 mmol) was then added and allowed to react for approximately 30 minutes. A yellow solid precipitated out of solution, was filtered and dried under suction and *in vacuo* to give 1541: ^1H NMR (400 MHz, $\text{DMSO-}d_6$) δ 10.76 (s, 1H), 8.91 (s, 1H), 8.54 (ddd, $J = 6.8, 1.1, 1.1$ Hz, 1H), 8.44 (d, $J = 0.6$ Hz, 1H), 8.31 (dd, $J = 1.8, 1.9$ Hz, 1H), 7.73 (m, 2H), 7.60 (dd, $J = 8.9, 0.7$ Hz, 1H), 7.56 (dd, $J = 7.7, 1.3$ Hz, 1H), 7.44 (m, 3H), 7.26 (ddd, $J = 8.9, 6.8, 1.2$ Hz, 1H), 6.90 (ddd, $J = 6.8, 6.8, 1.1$ Hz, 1H), 3.96 (s, 3H); ^{13}C NMR (400 MHz, $\text{DMSO-}d_6$) δ 160.20, 159.87, 147.61, 146.33, 144.79, 143.87, 143.19, 142.36, 138.35, 134.72, 129.42, 126.92, 125.23, 125.04, 121.54, 121.19, 120.09, 119.05, 116.95, 116.66, 116.25, 112.33, 109.39, 56.24; LCMS (ESI) m/z 412 (MH+).

8-Hydroxy-2-oxo-2H-chromene-3-carboxylic acid (3-imidazo[1,2-a]pyridin-2-yl-phenyl)-amide (1541B): 2,3-dihydroxybenzaldehyde (0.096 g, 0.69 mmol) and Meldrum's acid (0.100 g, 0.69 mmol) were combined in H₂O (1 mL). The solution was stirred at 75°C for 2 hr. After cooling to room temperature, the precipitate was filtered and dried at suction to give 0.123 g of 8-hydroxy-3-carboxy-coumarin in an 85% yield: LCMS (ESI) *m/z* 207 (MH⁺). DIEA (0.046 mL, 0.27 mmol) was added to 8-hydroxy-3-carboxycoumarin (0.050 g, 0.24 mmol) and HATU (0.101 g, 0.27 mmol) in 1 mL of DMF with constant stirring at room temperature until a clear solution resulted. 3-imidazo[1,2-a]pyridin-2-yl-phenylamine (0.051 g, 0.24 mmol) was then added and allowed to react overnight with a resulting yellow solid precipitation. The precipitate was filtered and dried under suction and *in vacuo* to give 0.021 g of 1541B in a 22% yield: ¹H NMR (400 MHz, DMSO-*d*₆) δ 10.80 (s, 1H), 10.50 (s, 1H), 8.88 (s, 1H), 8.54 (ddd, *J* = 6.8, 1.1, 1.1 Hz, 1H), 8.44 (s, 1H), 8.31 (dd, *J* = 1.8, 1.7 Hz, 1H), 7.73 (m, 2H), 7.61 (d, *J* = 9.9 Hz, 1H), 7.45 (dd, *J* = 7.9, 7.8 Hz, 1H), 7.43 (dd, *J* = 6.6, 2.7 Hz, 1H), 7.25 (m, 3H), 6.90 (ddd, *J* = 6.8, 6.6, 1.2 Hz, 1H); ¹³C NMR (400 MHz, DMSO-*d*₆) δ 160.43, 159.96, 147.87, 144.77, 144.52, 143.85, 142.54, 138.38, 134.69, 129.42, 126.92, 125.25, 125.06, 121.50, 120.33, 120.11, 119.68, 119.43, 119.10, 116.93, 116.64, 112.33, 109.39; LCMS (ESI) *m/z* 412 (MH⁺).

Synthesis of 6-Bromo-2-oxo-2H-chromene-3-carboxylic acid (3-imidazo[1,2-a]pyridin-2-yl-phenyl)-amide (1541C): DIEA (35.6 μL, 0.2 mmol) was added to 6-bromo-3-carboxy-coumarin (50.0 mg, 0.19 mmol) and HATU (77.7 mg, 0.2 mmol) in 2 mL of DMF with constant stirring at room temperature until a clear solution resulted. 3-Imidazo[1,2-a]pyridin-2-yl-phenylamine (38.9 mg, 0.19 mmol) was then added and allowed to react overnight with a resulting solid precipitation. The precipitate was filtered, dried under

suction and *in vacuo* to give 0.061 g of product in 68 % yield: ^1H NMR (400 MHz, DMSO-*d*6) δ 10.71 (s, 1H), 8.87 (s, 1H), 8.54 (d, J = 6.6 Hz, 1H), 8.43 (s, 1H), 8.32 (dd, J = 1.7, 1.8 Hz, 1H), 8.30 (d, J = 2.3 Hz, 1H), 7.93 (dd, J = 8.8, 2.1 Hz, 1H), 7.72 (m, 2H), 7.59 (d, J = 9.2 Hz, 1H), 7.54 (d, J = 8.8 Hz, 1H), 7.45 (dd, J = 7.9, 7.9 Hz, 1H), 7.25 (ddd, J = 8.1, 6.7, 0.8 Hz, 1H), 6.90 (dd, J = 6.7, 6.8 Hz, 1H); ^{13}C NMR (400 MHz, DMSO-*d*6) δ 159.91, 159.64, 152.90, 145.89, 144.79, 143.86, 138.29, 136.38, 134.72, 132.10, 129.42, 126.91, 125.04, 121.60, 121.29, 120.34, 119.12, 118.54, 116.96, 116.77, 116.66, 112.32, 109.39; LCMS (ESI) m/z 461 (MH⁺).

8-Methoxy-2-oxo-2H-chromene-3-carboxylic acid phenylamide (1541D): DIEA (0.044 mL, 0.25 mmol) was added to 8-methoxy-2-oxo-2H-chromene-3-carboxylic acid (0.050 g, 0.23 mmol) and HATU (0.095 g, 0.25 mmol) in 1 mL of DMF with constant stirring at room temperature until a clear solution resulted. Aniline (0.021 g, 0.23 mmol) was then added and allowed to react overnight with a resulting yellow solid precipitation. The precipitate was filtered and dried under suction and *in vacuo* to give 0.055 g of 1541D in an 82% yield: ^1H NMR (400 MHz, DMSO-*d*6) δ 10.65 (s, 1H), 8.88 (s, 1H), 7.72 (m, 2H), 7.54 (dd, J = 7.7, 1.5 Hz, 1H), 7.46 (dd, J = 8.2, 1.5 Hz, 1H), 7.39 (m, 3H), 7.14 (ddd, J = 7.4, 7.3, 1.0 Hz, 1H), 3.95 (s, 3H); ^{13}C NMR (400 MHz, DMSO-*d*6) δ 160.13, 159.80, 147.58, 146.30, 143.16, 137.89, 129.00, 125.20, 124.29, 121.16, 120.06, 119.87, 119.03, 116.21, 56.23; LCMS (ESI) m/z 296 (MH⁺).

Cellular procaspase activator characterization

All cells were maintained in the optimal media as suggested by ATCC.

1541 and 1541B EC₅₀ determination with panel of cancer cell lines: 2,000 BT549, MDA-MB361, HeLa, HCC1954, 600MPE and HEK293 cells were incubated with 1541 or

1541B (0.39 to 50 μM) or DMSO (final DMSO 0.5%) for 24 hours in a final volume of 50 μL . Incubations were assayed for cell viability by addition of 50 μL of the CellTiter-Glo® (Promega).

Caspase activation and cell death time course: 2,000 BT549, MDA-MB361 or HEK293 cells were plated in 96-well plates for incubation with 25 μM 1541, 25 μM 1541C, 25 μM 1541D, 1 μM staurosporine (STS, Cayman Chemicals), 100 μM Etoposide (Sigma), or DMSO (final DMSO 0.5%). Plates were assayed for executioner caspase activity and cell viability with Caspase-Glo® 3/7 and CellTiter-Glo® Luminescence Assay Kits (Promega), respectively, at 2, 4, 6, 8, 12 and 24 hours according to manufacturer's protocol.

Protection against apoptosis by 1541 with irreversible caspase peptide inhibitors: 2,500 BT549 cells were plated in 96-well plates and incubated overnight with Biotin-DEVD-FMK or Biotin-VAD-FMK (0.78 to 100 μM). Cells were exchanged into new media containing 25 μM 1541 and respective concentration of peptide inhibitor. Cells were incubated for 24 hours in a final volume of 50 μL . Incubations were assayed for cell viability by addition of 50 μL of the CellTiter-Glo® with luminescence read on an Analyst HT plate reader.

Whole cell lysate western blot analysis of apoptotic BT549 cells: One million BT549 cells were plated in 75 cm^2 T flasks for incubation with 25 μM 1541, 1 μM STS, 100 μM Etoposide or DMSO (final DMSO 0.5%) for 8 hours. In all cases, medium from individual wells, which might contain floating dead cells, was collected and mixed with the cell pellet from the same well. Cells were resuspended in 200 μL of PBS containing 1% SDS for cellular lysis and subjected to sonication. Whole cell lysates were quantified with BCA

Protein Assay reagent (Pierce) to standardize protein levels, boiled for 5 minutes in the presence of reducing SDS-PAGE loading buffer and subjected to Western blot analysis probing for the presence of active caspase-3 (Cell Signaling 9664), caspase-6 (AbCam 32366), caspase-7 (Cell Signaling 9492) and PARP (Cell Signaling 9542). Western blots were stripped with methanol and reprobbed for GAPDH (Cell Signaling 2118) as a loading control. For BT549 cytoplasmic extracts, cells were treated as described, harvested into PBS containing 0.025% digitonin, incubated for 30 minutes on ice and clarified by centrifugation at 4°C. Western blots were probed for presence of active caspase-3 and cytochrome C (Cell Signaling 4272).

1541-induced cellular death of wild type and caspase-8 deficient human Jurkat: 100,000 wild type A3 or caspase-8 deficient I9.2 human Jurkat cells (128) were incubated with 25 µM 1541, 1 µM STS or 100 ng/mL Super FasL (Axorra) in 100 µL of optimal media. Incubations were assayed for cell viability every 2 hours by addition of 100 µl of CellTiter-Glo®.

Apoptosis of wild type and Bak^{-/-}/Bax^{-/-} MEFs: 5,000 wild-type and Bak^{-/-}/Bax^{-/-} double knockout MEFs (kind gift from Dr. Scott Oaks, UCSF) were incubated with 1 µM STS, 25 µM 1541 or DMSO (final DMSO 0.5%) at 37°C for 12 hours and assessed for apoptosis with the Cell Death Detection Elisa kit (Roche) according to manufacturer's protocol. The histone ELISA was used instead of the simpler CellTiter-Glo® viability assay to measure ATP levels because the mitochondria, and hence ATP levels, are preserved in the DKO MEFs.

Whole cell lysate western blot analysis of apoptotic wild type and Bak^{-/-}/Bax^{-/-} MEFs: One million cells of both wild type and Bak^{-/-}/Bax^{-/-} DKO MEFs were plated and

incubated with 1 μ M STS, 25 μ M 1541 or DMSO (final DMSO 0.5%) at 37°C for 12 hours. After harvesting both cells and media, cell pellets were resuspended in 200 μ L of PBS containing 1% SDS for cellular lysis and subjected to sonication. Whole cell lysates were treated quantified and probed as described for the presence of active caspase-3 and PARP cleavage. For all cellular experiments, assays were performed in 96-well plates with luminescence read on an Analyst HT plate reader. IC50 values were determined using GraphPad Prism software.

Cell death comparison among cancerous and immortalized normal B cells: 25,000 normal (Epstein Barr Virus (EBV)-transformed B cells and cancerous large B cell lymphoma (DB) cells were incubated with 12.5 μ M 1541B (final DMSO 0.5%). Plates were assayed for cell viability with CellTiter-Glo® at 2, 4, 6, 8, 12 and 30 hours according to manufacturer's protocol.

Mutations of procaspase-3 that confer resistance to activation by 1541

Sequence alignment of procaspase-3, -6 and -7 revealed residue conservation in areas near the active site with large conformational rearrangement upon procaspase activation (66) and were subjected to point mutational analysis. Point mutations of procaspase-3 were performed using QuickChange (Qiagen) mutagenesis. Procaspase-3 mutants were constructed using forward primer 5'-CGA CTT CTT GTA TGC ATA CGC CAC AGC ACC TGG-3' and complement for S198A, forward primer 5'-CGA CTT CTT GTA TGC ATA CTC CGC AGC ACC TGG-3' and complement for T199A and forward primer 5'-CCT GGT TAT TAT GCT TGG CGA AAT TCA AAG GAT GGC-3' and complement for S205A. Purification was performed exactly as described for procaspases-3, -6 and -7. Procaspase-3 mutants were incubated at 100 nM with 25 μ M 1541 in 50 μ L of 50 mM HEPES, pH 7.4, 0.01% Triton-X100, 50 mM KCl, 0.1 mM EDTA, 1 mM DTT at 37 °C and

sampled for activation via kinetic analysis after 5 hours. Kinetic assays were initiated by addition of substrate Ac-DEVD-AFC to a final concentration of 50 μ M. The activity was measured for 20 minutes in 96-well plates on a SpectraMax M5 microplate reader.

Preparation of stable MCF-7 transfections with wild type and mutant procaspase-3: Wild-type and 1541-resistant (S198A) procaspase-3 variants were PCR subcloned from the corresponding pET23b vectors into the NotI and EcoRI sites of the bicistronic retroviral expression vector pQCXIP (Clontech) using forward primer 5'-AAA GGG AAA GCG GCC GCC ACC ATG GAG AAC ACT GAA AAC TCA GTG-3' and reverse primer 5'-AAA GGG AAA GAA TTC TCA TTT GTC GTC GTC ATC TTT GTA ATC GTG ATG GTG GTG ATG ATG GTG ATA AAA ATA GAG TTC TTT TGT GAG CAT-3'. A 6x-His-FLAG was appended in-frame to the C-terminus of procaspase-3 to facilitate detection by Western blotting. Expression clones were sequence-verified and transfected into the GPG retroviral producer cell line (a kind gift from Orion Weiner, UCSF) using Lipofectamine 2000 (Invitrogen) to generate retroviral supernatants, which were clarified by centrifugation, supplemented with 8 μ g/mL polybrene and used to transduce early-passage MCF-7 cells for 12 hours. Infections were repeated three times over the course of 72 hours and stable pools of procaspase-3-expressing MCF-7 cells were selected in 0.5 μ g/mL puromycin (Invivogen) for 12 days. *MCF-7 transfection cell viability assays:* Stable procaspase-3 variant transfection MCF-7 cell lines (wild type, S198A, empty pQCXIP vector) were plated at 6,000 cells per well in a 96-well plate and incubated in the presence of 2 μ M STS or 7.5 μ M 1541 at 37°C for 24 hours. Incubations were assayed for cell viability by addition of CellTiter-Glo® Luminescence Assay. Plates were analyzed for luminescence on an Analyst HT plate reader.

Acknowledgements

We thank J. Williams, B. Wolff and the University of California, San Francisco (UCSF) Small Molecule Discovery Center for assistance in the HTS of procaspase-3 activators; S. Mahrus, H. Yoshihara, A. Renslo, M. Burlingame, and J. Sadowsky for critical suggestions; I. Wilson, J. Taunton, and Z. Gartner for critical reading of the manuscript, J. Gao for procaspase-1; J. Gray for cell lines; and C. Craik and D. Hostetter for granzyme B. This research was supported by grants from the National Institutes of Health (R21 N5057022, R01 CA136779), National Cancer Institute Postdoctoral Fellowship (F32 CA119641-03) (to D.W.W.), UC Cancer Research Committee Fellowship (to D.C.G.) and the Hartwell Foundation.

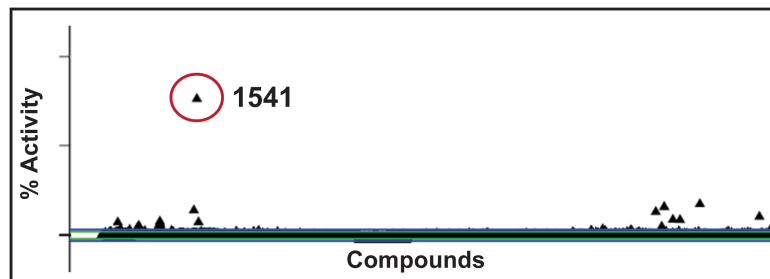


Figure 2-1. HTS scatter plot identifies 1541 as a procaspase-3 activator. A total of 62,000 compounds were screened for their ability to activate procaspase-3 after a 3-hour incubation at 37°C. Granzyme B activated caspase-3 fluorescence averaged 100-fold greater than the background procaspase-3 fluorescence. The assay was very reproducible with Z' ranging from 0.85 to 0.95. Blue lines indicate 3 standard deviations above or below the mean. All compounds that induced procaspase-3 activity above 3 standard deviations were considered potential “hits”. Compound 1541 is circled in red.

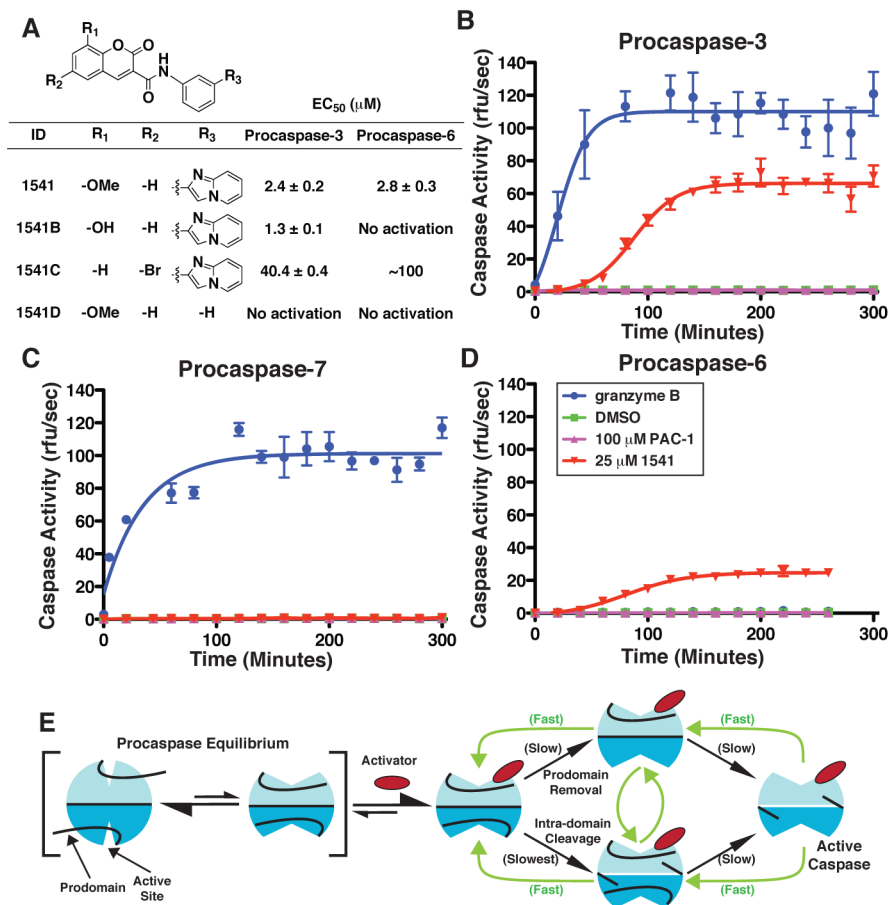


Figure 2-2. Specificity of small-molecule activators for executioner procaspases. **(A)** Chemical analogs of 1541 and EC₅₀ values of procaspases-3 and -6 activation. Small-molecule activators require the imidazopyridine moiety and prefer a heteroatom substituent at the 8-position on the coumarin ring. Substitution of the 8-methoxy with an 8-hydroxy (1541B) improves the EC₅₀ and specificity for activation of procaspase-3 over procaspase-6. Addition of a 6-bromo (1541C) reduces potency of activation of both procaspases. Complete removal of the imidazopyridine substituent (1541D) ablates activation of procaspases-3 and -6. **(B to D)** Time course of executioner procaspase activation by 1541 facilitates full self-cleavage of procaspases-3 and -6. Procaspases-3 (B), -7 (C), and -6 (D) were incubated at 100 nM with granzyme B, DMSO (green on

baseline), PAC-1, or 1541 at 37°C and assayed every 20 min for activity by addition of fluorogenic peptide substrates Ac-DEVD-AFC (caspases-3 and -7) or Ac-VEID-AFC (caspase-6). Rfu, relative fluorescence units. (E) Proposed model for small molecule–assisted procaspase self-activation. We hypothesize that procaspases are in a dynamic equilibrium between an off state (left) and on state (right), similar to mature caspases. Unlike mature caspases, the population favors the off-state conformation. On binding a small-molecule activator, the equilibrium shifts to an on state (center). This complex slowly undergoes autoproteolytic activation (black arrows) that accelerates with increasing production of mature caspase (green arrows). This model also accounts for activation, at low concentrations, of small molecule where the on state is preferred and one active site is available in the dimer for processing and, at high concentrations, where both sites are saturated and can lead to inhibition.

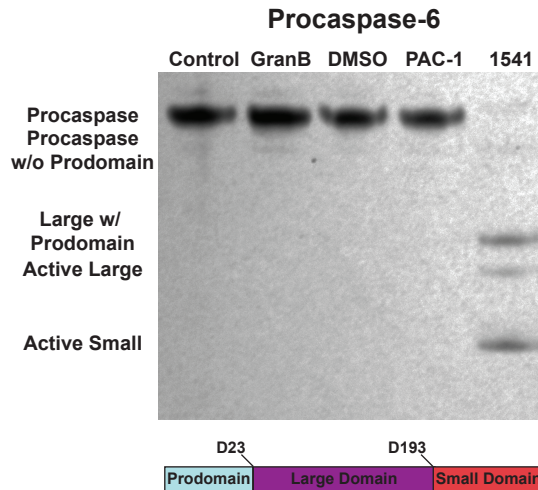
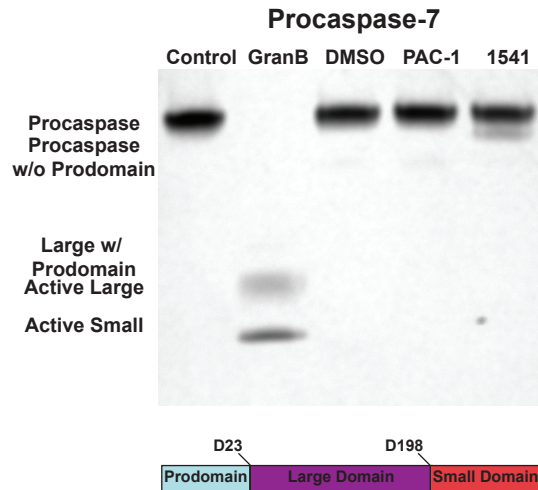
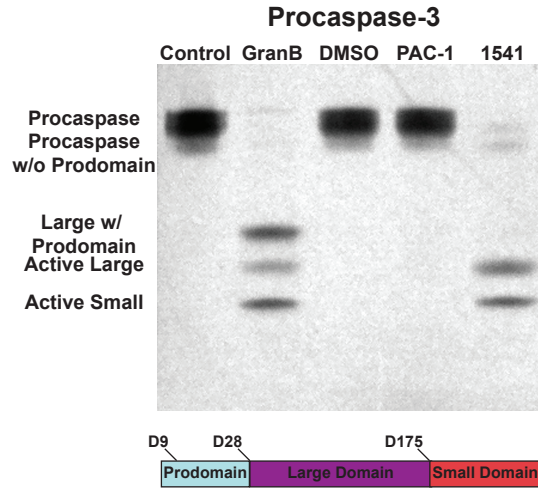


Figure 2-3. Specificity of 1541 and time course. Time course of executioner procaspase

activation by 1541 facilitates full self-cleavage of procaspases-3 and -6. Procaspases-3, -6 and -7 were incubated at 100 nM with 1 nM granzyme B, DMSO, 100 μ M PAC-1 or 25 μ M 1541 at 37°C. All procaspase incubations were harvested at 4 hours and subjected to silver-stain SDS-PAGE to determine the extent of autocleavage to the mature, active caspases. Schematic representations of the executioner procaspases-3, -6 and -7 sequences depict aspartic acid residues cleaved during activation. At 4 hours, 1541 induces full processing of procaspases-3 and -6 as seen by cleavage of both the prodomain and the intradomain junction between the large (17 kDa) and small (12 kDa) subunits. Procaspase-7 is robustly activated by granzyme B, but not by 1541 as indicated by only ~10% auto-proteolysis of the prodomain (residues 1-23). Previous studies show removal of the prodomain alone does not activate caspase-7 (117). Under our assay conditions, PAC-1 does not detectably increase the activity nor promote self-proteolysis of any of the executioner procaspases.

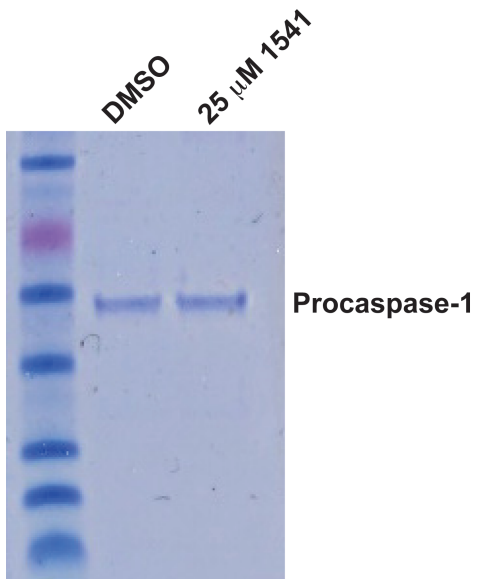


Figure 2-4. Procaspase-1 is insensitive to 1541 activation. Procaspase-1 (expressed and purified in the absence of the N-terminal prodomain residues 1-120) was incubated at 1 μ M for 24 hours at 37°C with 25 μ M 1541 in an optimal reaction buffer. SDS-PAGE reveals procaspase-1 does not self-activate in the presence of 1541.

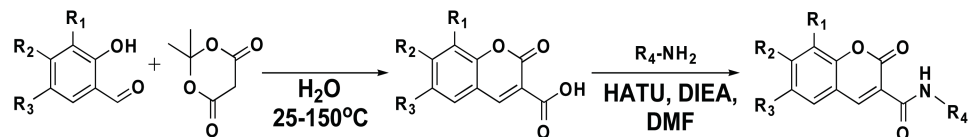


Figure 2-5. Schematic of general chemical synthesis of 1541 derivatives. The 3-carboxycoumarin ring is constructed from commercially available salicylaldehydes. The salicylaldehyde is reacted with Meldrum's acid in an aqueous solution (50-100°C) to assemble the 3-carboxycoumarin (142). The carboxylic acid substituent on the coumarin scaffold is subsequently converted to amide derivatives using well-known coupling reactions with the final products collected by filtration and dried under vacuum.

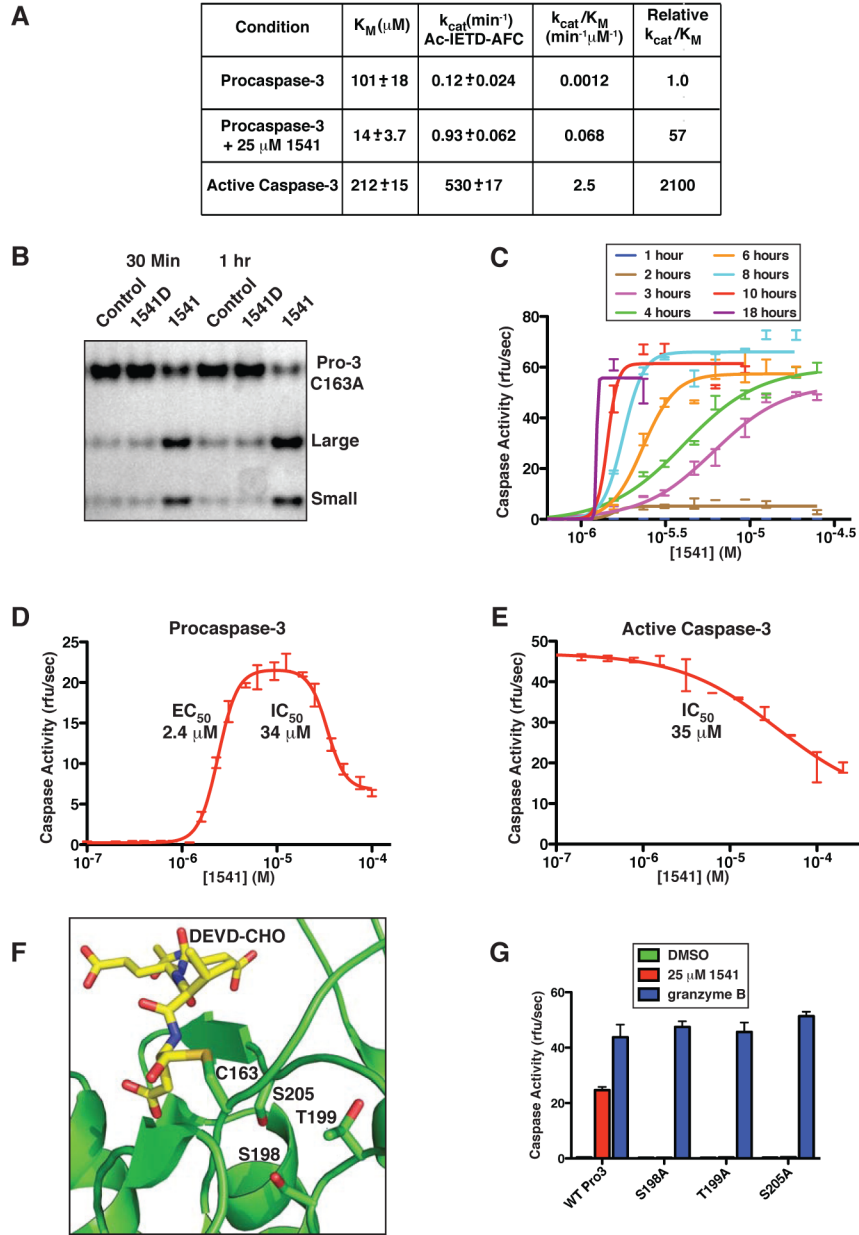


Figure 2-6. *In vitro* characterization of apoptotic procaspase small-molecule activators.

(A) Initial rates of activation of procaspase-3 in presence of 1541B, as measured by Ac-IETD-AFC compared with unstimulated zymogen and mature caspase-3. Procaspase-3 (100 nM) was incubated with 1541B (0.78 to 50 μM), and initial rates of activity were measured over \sim 15 min by addition of Ac-IETD-AFC (1.2 to 300 μM) at 37°C. Presence of 1541 improves the k_{cat}/K_M of procaspase-3 by 57-fold and stimulates autocatalytic

processing. **(B)** Silver-stained SDS–polyacrylamide gel electrophoresis (SDS-PAGE) gel of inactive C163A procaspase-3 (250 nM) incubated with granzyme B (0.5 nM), with and without 1541 (25 μ M), shows increased cleavage susceptibility by granzyme B with 1541, but not with the inactive analog 1541D. **(C)** Procaspase-3 was incubated at 100 nM with 1541 (0.1 to 100 μ M) to assess the rate of self-activation. Kinetic activity of the mixtures was determined every hour for 18 hours by incubation with 20 μ M Ac-DEVD-AFC. Once procaspase-3 is activated by 1541, the zymogen rapidly self-activates. The effective concentration of 1541 is \sim 1.5 μ M, with no activation below this concentration despite extended incubation periods. **(D)** Procaspase-3 at 100 nM was incubated with 1541 (100 nM to 100 μ M). After a 4-hour incubation at 37°C, the samples were assayed for caspase activity by addition of Ac-DEVD-AFC. Low concentrations of 1541 induce activity of procaspase-3 with an EC_{50} of 2.4 μ M, and, at high concentrations, inhibit with an IC_{50} of 34.0 μ M. **(E)** Compound 1541 exerts a similar inhibitory effect on active caspase-3 (IC_{50} = 35 μ M), as seen for procaspase-3. Mature caspase-3 was incubated at 25 nM in various concentrations of 1541 for 10 min and assayed with Ac-DEVD-AFC. **(F)** Structural model of the active site of procaspase-3 showing the residues targeted for mutation. The location of the DEVD substrate is shown and modeled from caspase-3 in complex with tetrapeptide aldehyde inhibitor Ac-DEVD-CHO (Protein Data Bank structure 2DKO). **(G)** Identification of mutations in procaspase-3 that confer resistance to activation by 1541. Wild-type and mutant (S198A, T199A, and S205A) procaspases were incubated for 5 hours with 25 μ M 1541 (red), 1 nM granzyme B (blue), or DMSO (green on baseline) at 37°C and sampled for activation via kinetic assays initiated by addition of substrate Ac-DEVD-AFC. The procaspase-3 variants S198A, T199A, and S205A displayed wild-type activity when activated by granzyme B, but were unable to self-activate in the presence of 1541.

A.

1541B (μM)	K_M (μM)	k_{cat} (min^{-1}) Ac-IETD-AFC	k_{cat}/K_M ($\text{min}^{-1}\mu\text{M}^{-1}$)
50.00	19.4	1.22	6.28E-02
25.00	13.7	0.93	6.80E-02
12.50	14.9	0.79	5.26E-02
6.25	14.8	0.58	3.94E-02
3.13	22.6	0.96	4.28E-02
1.56	54.1	0.65	1.19E-02
0.78	91.8	0.43	4.66E-03
0	100.5	0.12	1.21E-03
Active Casp-3 Alone	~215	~500	~2.3
Active Casp-3 50 μM 1541B	~140	~300	~2.1

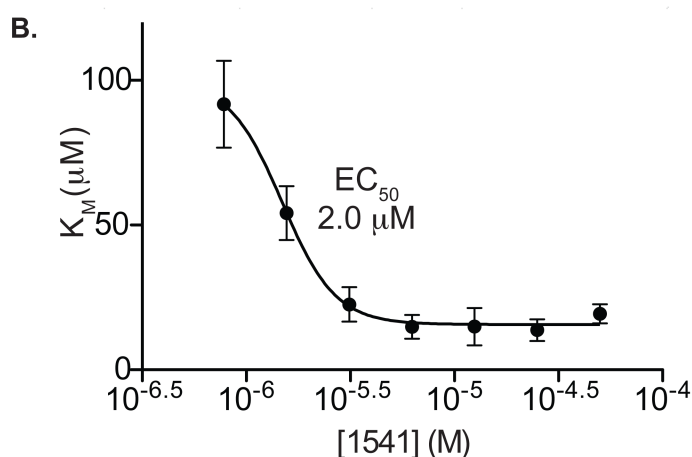


Figure 2-7. Initial activity constants of procaspase-3 in presence of 1541B. **(A)** Procaspase-3 was incubated at 100 nM in the presence of 1541B (0.78 to 50 μM) and immediately assessed for kinetic activity by addition of Ac-IETD-AFC (1.2 to 300 μM) at 37°C. Ac-IETD-AFC represents the intradomain sequence procaspase-3 recognizes and cleaves to become active. Incubation with 1541 increases the catalytic efficiency of procaspase-3 by 57-fold over the unstimulated protein in the absence of selfproteolysis. Importantly, the K_m for Ac-IETD-AFC of mature caspase-3 is 10-fold greater (~215 μM) and, even in the presence of 50 μM 1541B, remains nearly unchanged (~140 μM). For amide bond hydrolysis by serine and cysteine proteases, K_m is a reasonable approximation of K_d (120,121). Therefore, the Ac-IETD-AFC substrate binds more tightly

to the 1541B-stimulated procaspase-3 than to mature caspase-3. **(B)** Plot of $k_{\text{cat}}/K_{\text{m}}$ of procaspase-3 versus the concentration of 1541B. Procaspase-3 (100 nM) was incubated with 1541B (0.78 to 50 μM) and initial rates of activity were measured over ~10 min by addition of Ac-IETD-AFC (1.2 to 300 μM) at 37 °C. The $k_{\text{cat}}/K_{\text{M}}$ inflection point matches the EC_{50} of 1541-induced autoproteolysis of procaspase-3 (Fig. 1A).

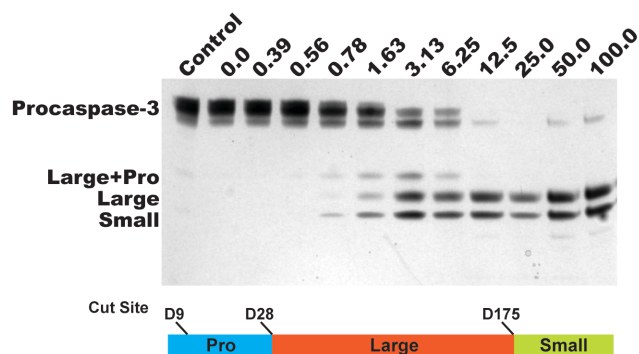
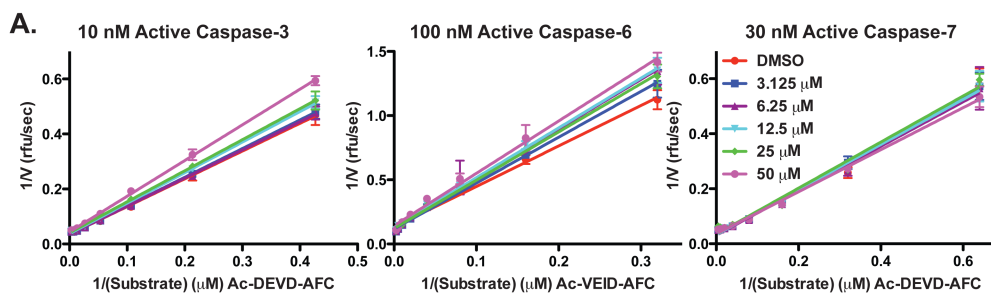


Figure 2-8. Procaspase-3 self-cleavage in the presence of 1541. Procaspase-3 was incubated at 100 nM with increasing concentrations of 1541 (0-100 μ M) for 4 hours at 37°C. Aliquots were quenched with addition of 1% SDS reducing gel loading buffer and boiled. Samples were subjected to silver stain SDS-PAGE electrophoresis to determine extent of autocatalysis. A diagram of the procaspase-3 protein with cleavage sites is indicated. At intermediate concentrations, mixed populations of all possible cleaved species are present. Procaspase-3 becomes fully activated at higher 1541 concentrations, despite a reduced activity, suggesting 1541 inhibits the activated caspase species.



B.

Protein Species	K_m (μM)	k_{cat} (s^{-1})	k_{cat}/K_m ($\mu\text{M}^{-1}\text{s}^{-1}$)	Decrease in Catalytic Efficiency
10 nM Active Caspase-3 Alone	19.0	11.4	0.6	1.5
10 nM Active Caspase-3 50 μM 1541	27.0	10.7	0.4	
100 nM Active Caspase-6 Alone	38.4	0.4	1.1×10^{-2}	1.6
100 nM Active Caspase-6 50 μM 1541	68.8	0.5	7.0×10^{-3}	
30 nM Active Caspase-7 Alone	11.9	3.3	0.28	0.9
30 nM Active Caspase-7 50 μM 1541	11.4	3.3	0.29	

Figure 2-9. Michaelis-Menten analysis shows competitive inhibition of executioner caspases-3 and -6 by 1541. **(A)** Caspases-3, -6 and -7 were incubated with increasing concentrations of 1541 (0 μM – red, 3.125 – blue, 6.25 – purple, 12.5 – light blue, 25 – green and 50 – magenta) and assayed for 10 minutes at room temperature by addition of various concentrations of fluorogenic peptides Ac-DEVD-AFC (caspases-3 and -7) or Ac-VEID-AFC (caspase-6). **(B)** In the presence of 50 μM 1541, the strongest effect by the compound is reflected in binding affinity of the substrate as K_m decreases by up to 30% for active caspase-3 and k_{cat} decreases by only a marginal amount of 8% (apparent K_i is ~ 98 μM). A similar effect occurs with active caspase-6, as the majority of 1541 influence is exerted on K_m (decrease $\sim 50\%$) as k_{cat} decreases by only 7% (apparent K_i is ~ 63 μM). Unlike the other two executioner caspases, caspase-7 remains essentially unaffected with 1541 incubation.

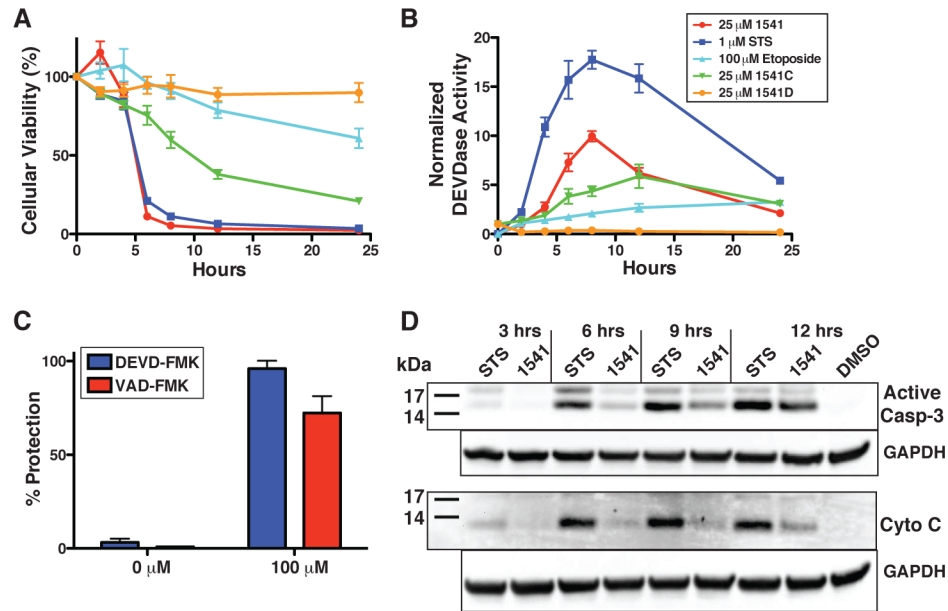


Figure 2-10. Induction of apoptosis in a p53-deficient breast cancer cell line by 1541. **(A)** Time course of cell viability in BT549 cells. BT549 cells ($n = 2000$) were incubated with compounds as shown in the key or DMSO (final 0.5%) and assayed for cell viability at 2, 4, 6, 8, 12, and 24 hours. Analogs 1541C and D induce limited to no cellular death, respectively, with correlation to the in vitro effects on procaspase-3 self-activation. **(B)** Time course of DEVDase activity in BT549 cells. All concentrations and variables are as in (A). 1541 induces less DEVDase activity in comparison with STS, but results in similar rates of apoptosis. **(C)** Protection against 1541-induced apoptosis with caspase inhibitors. BT549 cells ($n = 2500$) were incubated overnight with the caspase-3 and -7 inhibitor biotin-DEVD-FMK or the general caspase inhibitor biotin-VAD-FMK from 0.78 to 100 μ M. Cells were exchanged into new media containing 25 μ M 1541 and respective concentrations of peptide inhibitor. After 24 hours of incubation at 37°C with 1541, the cells were assayed for cell viability. Caspase inhibitors prevented cellular apoptosis induced by 1541. **(D)** Cytoplasmic extracts of BT549 cells reveal limited cytochrome c release from mitochondria during 1541-induced apoptosis. One million BT549 cells were

incubated with 25 μ M 1541, 1 μ M STS, or DMSO (0.5% final) and harvested every 3 hours. Cytoplasmic supernatants were subjected to Western blot analysis for presence of active caspase-3 or cytochrome c. Compared with STS, 1541 induced far less release of cytochrome c during apoptosis.

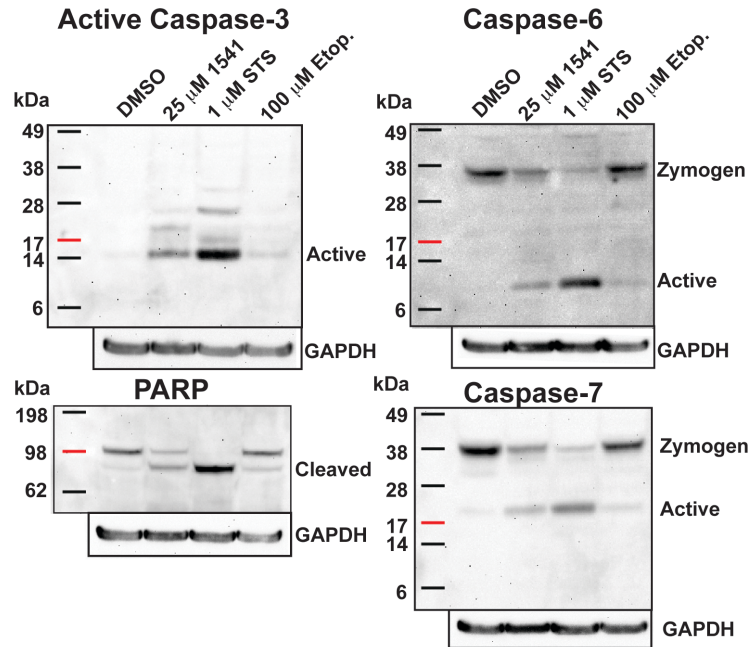


Figure 2-11. Traditional apoptotic hallmarks. One million BT549 cells were incubated for 8 hours in the presence of 25 μM 1541, 1 μM STS, 100 μM etoposide or DMSO (final 0.5%). Whole cell lysates were subjected to Western blot analysis probing for presence of active caspases-3, -6 and -7 and PARP cleavage. Large subunits of active caspases-3, -6 and -7 are clearly observable for the cells incubated with compound 1541; however, cleavage is more pronounced when incubated with 1 μM STS and is consistent with the higher overall DEVDase activity, as shown in **Fig. 3B**.

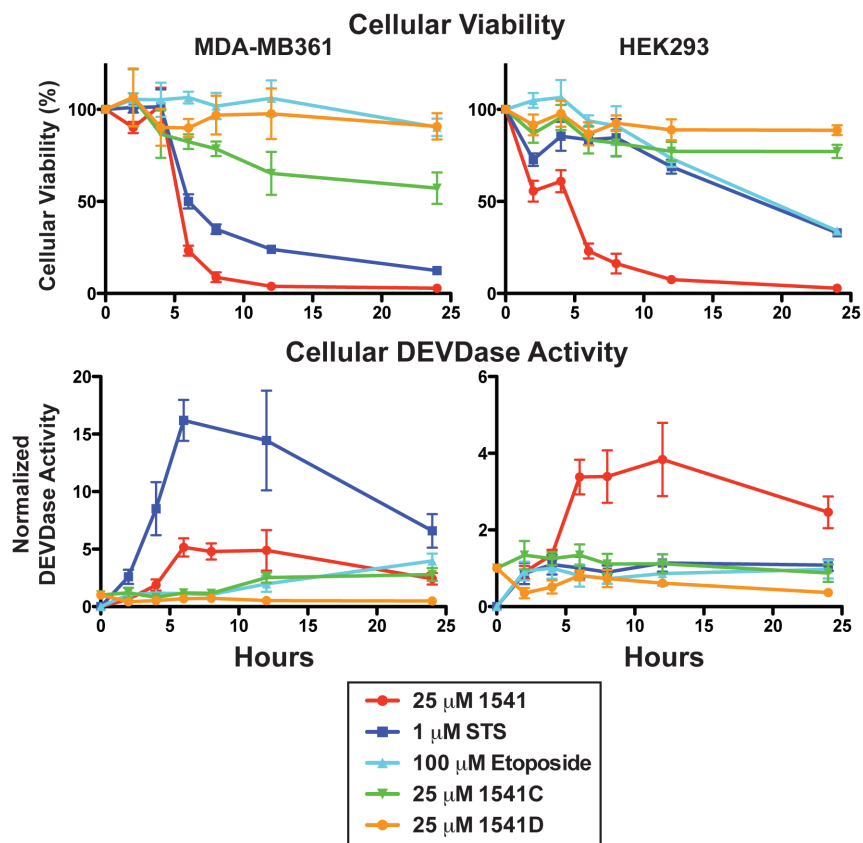


Figure 2-12. DEVDase activity and cellular viability time courses with HEK293 and MDA-MB361. 2,500 cells were incubated with 25 μ M 1541 (red), 25 μ M 1541C (green), 25 μ M 1541D (orange), 1 μ M STS (blue), 100 μ M etoposide (light blue), or DMSO (final 0.5%) and assayed for executioner caspase DEVDase activity and cell viability at 2, 4, 6, 8, 12 and 24 hours. Similar to BT549, cell death was achieved rapidly for both cell lines despite having an overall lower executioner caspase activity in the presence of 1541 compared to STS. Compounds 1541C and D, respectively, induce limited to no apoptosis or DEVDase activity in these cell lines. The cellular results for these 1541 analogs correlate with their *in vitro* activity against procaspase-3.

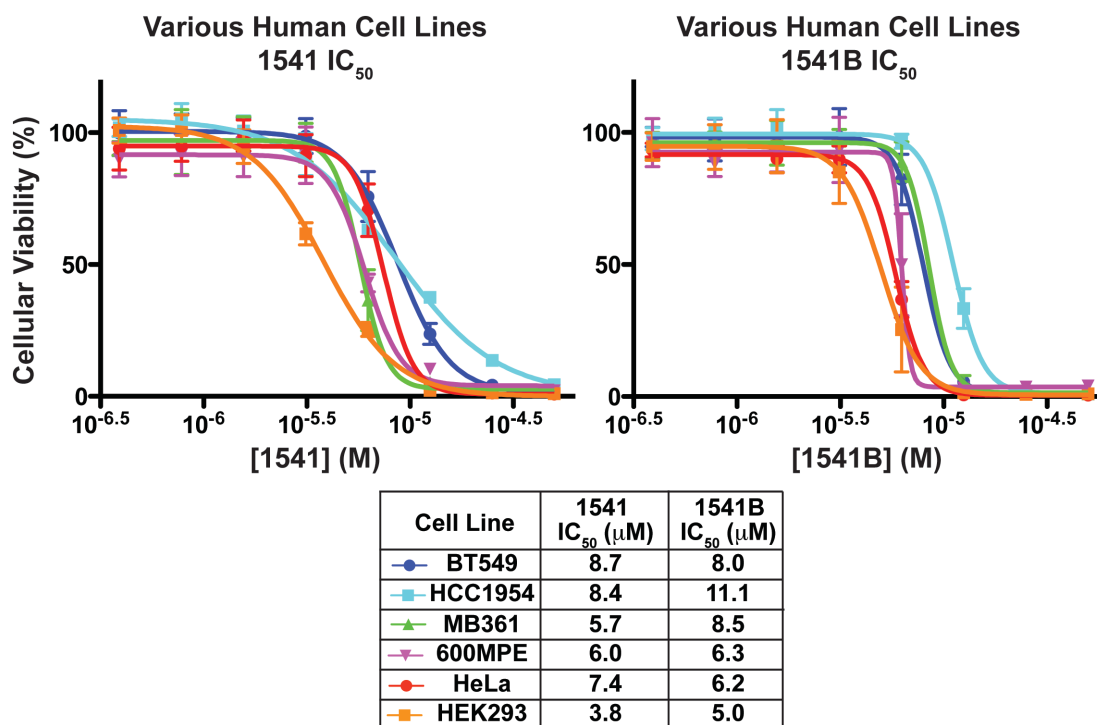


Figure 2-13. Induction of apoptosis by 1541 in cancer cell lines. 2,000 cells from BT549 (blue), MDAMB361 (green), HeLa (red), HCC1954 (light blue), 600MPE (magenta) and HEK293 (orange) were incubated with 1541 or 1541B (0.39 to 50 μM) (final DMSO 0.5%) for 24 hours. Cell viability was determined by the reduction in ATP levels using CellTiter-Glo®. The EC₅₀ values range between 4 and 9 μM and are consistent with the *in vitro* EC₅₀ of 1541 and 1541B for procaspases-3 and -6 activation. Compound 1541B, which is comparably active toward procaspase-3, but inactive against procaspase-6, shows virtually the same EC₅₀ for inducing apoptosis. This implies that procaspase-3 activation is much more important for driving cellular apoptosis than procaspase-6.

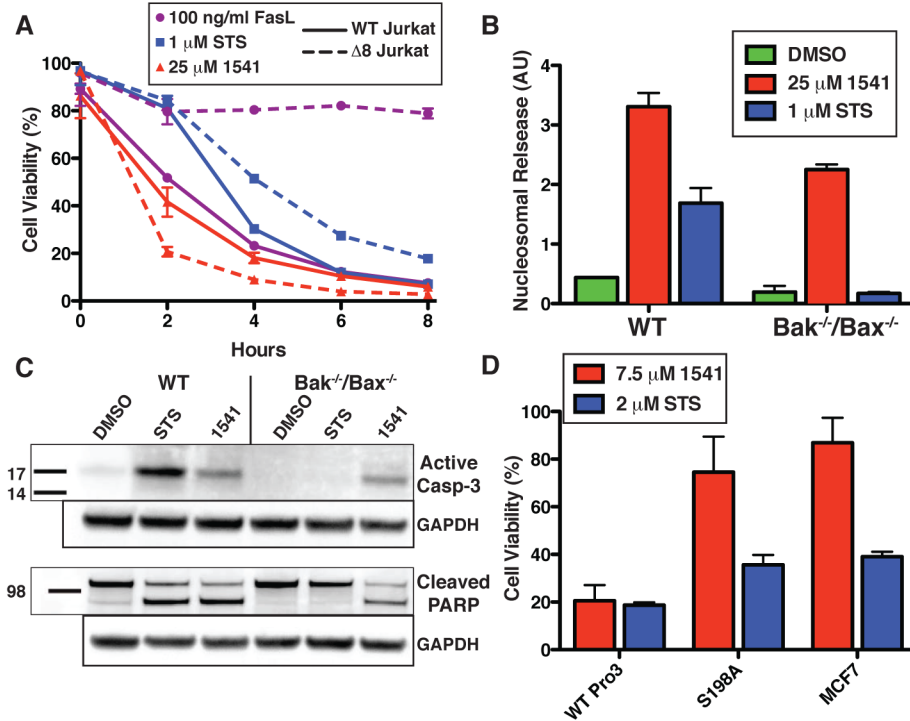


Figure 2-14. Validation of executioner procaspases as cellular target of 1541. **(A)** Wild-type (A3) (solid line) or caspase-8–deficient (I9.2) (dotted line) Jurkat cells (100,000 cells) were incubated with 1541, STS, or FasL and assayed for cellular viability every 2 hours. 1541 induces cell death independent of the extrinsic pathway. **(B)** Cells (n = 5000) derived from either wild-type or Bak^{-/-}/Bax^{-/-} DKO MEFs were incubated with STS, 1541, or DMSO (final 0.5%) at 37°C. A histone sandwich ELISA (Roche) was performed on the lysates to determine the extent of apoptosis after 12 hours. Induction of cell death by 1541, in the absence of Bak and Bax, supports direct activation of the executioner procaspases. **(C)** For Western blot analysis, one million cells of both wild-type and Bak^{-/-}/Bax^{-/-} DKO MEFs were plated and incubated as in (B) for 12 hours. Western blots of whole-cell lysates were probed for the presence of active caspase-3 and cleavage of PARP. **(D)** Transfection of MCF-7 cells with wild-type procaspase-3 and 1541-resistant S198A procaspase-3 supports ablation of 1541-induced procaspase-3

activation in cells. Cells (n = 6000) from stably transfected MCF-7 cell lines were incubated for 24 hours with 1541, STS, or DMSO (final concentration 0.5%) and assayed for cell viability. S198A procaspase-3 MCF-7 cells resisted apoptosis similarly to the parental MCF-7 cell line; wild-type procaspase-3 transfection of MCF-7 cells had increased apoptotic susceptibility to 1541.

Cellular Viability of Normal (EBV) vs. Cancerous (DB) B Cells

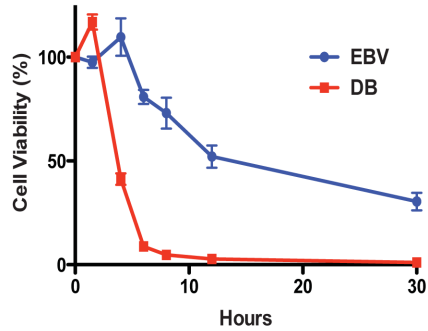


Figure 2-15. Cellular viability time course with normal and cancerous B cells. 25,000 normal EBV-transformed B cells (blue) and large B cell lymphoma (DB) cells (red) were incubated with 12.5 μ M 1541B and assayed for cell viability at 2, 4, 6, 8, 12 and 30 hours. Preferential cell death was rapidly achieved for the B cell lymphoma in comparison to the immortalized normal B cell line. These preliminary results suggest that the cancerous cells were more sensitive to apoptosis induced by 1541.

Chapter 3:
Self-Assembling Small Molecules Form Nanofibrils That Bind Procaspase-3 To
Promote Activation

Julie A. Zorn[†], Holger Wille^{||,¶}, Dennis W. Wolan[†], and James A. Wells^{†,‡}

[†]Department of Pharmaceutical Chemistry, University of California, San Francisco,
California

^{||}Institute for Neurodegenerative Disease, University of California, San Francisco,
California

[¶]Department of Neurology, University of California, San Francisco, California

[‡]Department of Cellular and Molecular Pharmacology, University of California, San
Francisco, California

This work was published in the *Journal of the American Chemical Society* (2011) 133:
19630-19633.

Abstract

Modulating enzyme function with small-molecule activators, as opposed to inhibitors, offers new opportunities for drug discovery and allosteric regulation. We previously identified a compound, called 1541, from a high-throughput screen (HTS) that stimulates activation of a proenzyme, procaspase-3, to generate mature caspase-3. Here we further investigate the mechanism of activation and report the surprising finding that 1541 self-assembles into nanofibrils exceeding 1 μm in length. These particles are an unanticipated outcome from an HTS that have properties distinct from standard globular protein aggregators. Moreover, 1541 nanofibrils function as a unique biocatalytic material that activates procaspase-3 via induced proximity. These studies demonstrate a novel approach for proenzyme activation through binding to fibrils, which may mimic how procaspases are naturally processed on protein scaffolds.

Many proteases are expressed in dormant forms, known as zymogens, that are activated in response to diverse stimuli. Activation of these latent enzymes is often catalyzed by processing from upstream proteases and, in some cases, via autoproteolysis (143). These transitions can be promoted by binding cofactors, sequestering cellular inhibitors, or interacting with signaling complexes (144). Cysteine aspartyl proteases (caspases) are expressed as such inactive precursors, or procaspases, which become activated in fate-determining transformations as diverse as cell death, innate immune responses, and differentiation (145). Further mechanistic insight into the processes that facilitate procaspase activation will foster the design of novel chemical probes to study the sufficiency of caspases for these phenotypes (146,147).

Procaspases are typically activated upon cleavage by upstream proteases or binding to protein scaffolds in response to intrinsic or extrinsic cellular signals (61). For example, the apoptosome recruits procaspase-9, the death-inducing signaling complex (DISC) interacts with procaspase-8, and the various inflammasome complexes associate with procaspase-1 to stimulate activity (145,148). Procaspases bind to these signaling platforms, which triggers clustering, oligomerization and/or a conformation change, and proteolytic processing. Removal of an N-terminal prodomain and an additional cleavage to yield a large and small subunit generate the mature enzyme (149). While procaspase-3 self-activation is normally restricted under physiological conditions, autoproteolysis can occur (62).

In an earlier investigation, we identified a synthetic small molecule, termed 1541 (**Chart 3-1**), that promotes autoactivation of procaspase-3 (71). After a lag phase, the compound induces a burst in activity due to the formation of processed caspase-3. These results plus additional characterization suggest that the compounds work through an allosteric mechanism to promote autoproteolysis. In this study, we show that 1541

and related analogues spontaneously assemble into highly ordered nanofibrils. Procaspase-3 becomes immobilized on the surface of the fibrils and generates active caspase-3. It is conceivable that these “amyloid-like” fibrils mimic natural protein scaffolds for activating procaspases.

Globular aggregates of small molecules that inhibit enzyme activity have been described previously (150-152). These aggregates are readily identified by diagnostic experiments, including detergent sensitivity, β -lactamase inhibition, and sensitivity to bovine serum albumin (BSA) (116,153,154). Furthermore, others have reported that detergent-sensitive molecules in screening libraries can also promote enzyme activity (155). We performed these diagnostic tests on 1541 with mixed results. For example, common detergents such as Triton or CHAPS did not disrupt procaspase-3 activation, and 1541 did not inhibit β -lactamase (**Fig. 3-1 and 3-2**). Unexpectedly, the addition of BSA protected against procaspase-3 activation (**Fig. 3-3**). This result alone is not definitive, since BSA contains hydrophobic patches that can bind soluble small molecules.

Because of these inconclusive results, we investigated the solubility of 1541 by centrifugation (156). Surprisingly, 1541 pelleted from solution at 16100g with a solubility constant (K_{sp}) of 1–2 μ M, concentrations close to the concentration of half-maximal activation (AC_{50}) of procaspase-3 by 1541 (**Fig. 3-1 and 3-4A**). Interestingly, both active and inactive analogues pelleted upon centrifugation, suggesting that the particles may not necessarily be responsible for the observed activity (**Fig. 3-5**).

We next evaluated whether procaspase-3 could directly interact with the particulates. We used procaspase-3 (C163A), an inactive/catalytically dead variant, to analyze the binding directly without the complication of processing. Varying concentrations of 1541 and 1541B were added to 200 nM procaspase-3 (C163A). The

solutions were immediately centrifuged, and the amounts of procaspase-3 in the pellet were assayed by gel electrophoresis and quantified by densitometry (**Fig. 3-5**). We observed cosedimentation of the C163A enzyme for both 1541 and 1541B at concentrations that correlated to their AC_{50} values (**Fig. 3-4B and 3-6**). Furthermore, enzyme sedimentation was not observed with the inactive analogue 1541D, even though compound sedimentation occurred. These data provide evidence that procaspase-3 binds to the high-molecular-weight particulates of the active compounds. While the data suggest a mechanism dependent on particles, both soluble small molecules and larger particles were present in the activation assay.

We performed a dialysis experiment to establish the relevant activating species. Procaspase-3 was placed inside a dialysis chamber with a 12–14 kDa molecular weight cutoff (~ 2 nm radius of gyration), and 10 μ M 1541 or 1541B was placed in buffer outside the membrane. After a 12-h incubation, no activation or processing of the proenzyme was observed (**Fig. 3-4C and 3-7**). In contrast, when the compounds were placed both inside and outside of the dialysis membrane, we saw dramatic activation and complete processing of procaspase-3. This suggests that particulates larger than roughly 4 nm are responsible for the activation effects.

We subsequently analyzed if 1541 and 1541B particles exhibit saturation behavior to assess whether the compounds provide a fixed number of binding sites to accommodate the enzyme or promote nonspecific aggregation of procaspase-3. We set the concentration of the active analogues at 20 μ M, 10-fold above their K_{sp} values, and titrated them with procaspase-3 (C163A) to investigate binding saturation directly. The mixtures were centrifuged, and the amounts of enzyme in the pellets were measured. The particulates from both compounds showed clear saturation behavior, yet with varying affinities for procaspase-3 (**Fig. 3-8A and 3-9**). Furthermore, when monitoring

the rates of procaspase-3 activation by 1541 and 1541B, we found that the binding affinity and activation rate were coincident (**Fig. 3-8B**). This suggests that procaspase-3 is immobilized by the particles with specific and saturable sites of interaction that impact the activity.

While the particles of 1541 and 1541B seemed to account for procaspase-3 activation, they were resistant to standard tests of small-molecule aggregation. Thus, we determined whether compounds that are known to form aggregates could activate procaspase-3 (150,154). Six aggregators that are well-known for promiscuous enzyme inhibition were incapable of activating procaspase-3 (**Fig. 3-10**). We did see that one of the promiscuous compounds, Congo red, inhibited mature caspase-3. As expected, the inhibition of caspase-3 by the aggregator was detergent-sensitive (**Fig. 3-10**). This demonstrated a functional interaction between Congo red and caspase-3, but no activation of procaspase-3 was observed. In contrast, 1541 particles appear to be responsible for procaspase-3 activation and behave differently from standard aggregators. Because of the discrepancies in behavior, we sought to characterize further the physical properties of 1541 to establish whether it exhibits novel properties of known colloidal aggregators or assembles into unique particles that promote procaspase-3 activity.

As with the centrifugation experiments, dynamic light scattering (DLS) studies demonstrated the presence of particles at room temperature for 10 μ M 1541 and 1541B. Remarkably, these particles showed characteristics distinct from standard aggregators (**Table 3-1 and Fig. 3-11**). Common properties of aggregators have been previously published, with 3',3'',5',5''-tetraiodophenolphthalein (TIPT) repeated here for direct comparison (153,157). The intensities of scattered light (I_{DLS}) for 1541 and 1541B were 10–20-fold lower than for TIPT [270.2, 170.1, and 3903.5 kilocounts/s (kcps),

respectively]. Conversely, the radii determined by DLS (r_{DLS}) for 1541 and 1541B particles (1112.8 and 910.7 nm) were >10-fold greater than that of TIPT (71.1 nm). The inactive analogue 1541D had properties similar to TIPT ($I_{\text{DLS}} = 3317.0$ kcps, $r_{\text{DLS}} = 164.1$ nm). These results suggest that 1541 and 1541B form particles that are different from 1541D and other standard colloidal aggregates.

The distinct properties of 1541 and 1541B were further characterized by particle flow cytometry (156). Notably, the K_{sp} values determined for 1541 and 1541B closely matched the AC_{50} values for self-activation of procaspase-3 (**Table 3-1**). The particle counts increased linearly with concentration until reaching maximum values at 4 μM for 1541 and 5 μM for 1541B (**Fig. 3-12**). Increasing the concentration beyond this point generated only larger particle sizes and not larger numbers of particles. Once nucleated, 1541 and 1541B particles appear to favor recruitment of additional small molecules to grow in size. Conversely, TIPT and 1541D appear to maintain a constant size but increase the particle count with increasing concentration (**Fig. 3-12**). These results further depict unique features of 1541 and 1541B in comparison with standard aggregators.

Since procaspase-3 self-activation assays are performed at 37 °C, we studied the properties of 1541 and 1541B particles after agitation at this temperature. Interestingly, the I_{DLS} and r_{DLS} values for 1541 and 1541B particles decreased to buffer values for these conditions (**Table 3-1**). Because the particle flow cytometer also uses light scattering to detect particles, shifts in K_{sp} to 10 and 20 μM at 37 °C were similarly observed for both 1541 and 1541B, respectively. Nonetheless, incubation and centrifugation of 1541 and 1541B at 37 °C still resulted in pelleting of the compound (**Fig. 3-13**). These results indicate that the particles were still present at increased temperatures but were significantly altered and became undetectable by light scattering.

Notably, temperature had minimal impact on the properties of both TIPT and 1541D.

Given the strong evidence that the particles of 1541 and 1541B are distinct from promiscuous inhibitors, we investigated the molecular structure of 1541 relative to a colloidal aggregator, TIPT, by transmission electron microscopy (TEM). TEM images of TIPT showed the typical globular structures of known aggregators (**Fig. 3-14**). In dramatic contrast, 1541 produced long thin fibrils extending to over 1 μm in length (**Fig. 3-15**). The fibrils tended to cluster into braided bundles, but individual strands were as thin as 2.6 nm, perhaps only a few molecules thick (**Fig. 3-14**). At 37 °C, 1541 tended to form thicker fibrils and typically appeared as single strands rather than the larger tangles observed at room temperature. Consistent with the tangles breaking apart at higher temperatures, we observed delayed centrifugation of 1541 particles after a 1 h incubation at 37 °C (compared with room temperature) (**Fig. 3-16**). Disrupting the clusters at 37 °C may allow a greater extent of the fibril surface to be accessible to the procaspase to facilitate activation. However, additional experiments are necessary to elucidate the temperature effects.

We subsequently examined whether binding of procaspase-3 to 1541 fibrils could be observed by TEM. We incubated 50 μM 1541 with 500 nM procaspase-3 (C163A) at 37 °C and also at 25 °C. At both temperatures, the edges of the nanofibrils no longer looked crisp but appeared to be decorated with protein particles, suggesting that procaspase-3 lined the length of the fibrils (**Fig. 3-14 and 3-15**). The nanofibrils also appeared to be wider, consistent with the enzyme being bound to the surface.

Our results show that 1541 and 1541B spontaneously assemble into nanofibrils that can activate procaspase-3. These particles have properties distinct from those of standard aggregators identified in high-throughput screening, which typically lead to enzyme inhibition (150). We propose that these fibrils act as a scaffold to concentrate procaspase-3 where it can be processed by other enzymes in close proximity (**Fig. 3-**

17). In this regard, these synthetic fibrils mimic signaling platforms, such as the inflammasomes, the apoptosome, and the DISC, which facilitate procaspase activation (145,148,158). Alternatively, the fibrils may alter the conformation of the proenzyme to promote intramolecular processing. Further studies are underway to distinguish between cis versus trans activation promoted by the fibrils.

Intriguingly, 1541 particles appear structurally similar to the fibrous β -sheet aggregates formed by amyloid- β proteins (A β). A β proteins have been shown to facilitate proenzyme activation, such as the conversion of prekallikrein to kallikrein of the plasma kinin-forming cascade as well as the conversion of plasminogen into the active protease plasmin by the tissue-type plasminogen activator (tPA) (159,160). Furthermore, several cellular proteins assemble into an amyloid fold, such as fibrin and Pmel17, to facilitate natural processes, including proenzyme activation (161-163). Filamentous structures within the cell have even been shown to associate directly with caspase-3 (164). In this regard, 1541 fibrils appear to mimic endogenous and possibly disease-related fibrous structures on which the procaspases can become concentrated and activated.

To evaluate whether such physiologically relevant fibrils can interact with procaspase-3, we generated fibrils from A β (1–40) by agitation of the peptide at 37 °C in a caspase activity buffer (**Fig. 3-18A**). The A β fibrils were subsequently serially diluted and incubated with procaspase-3. Similar to our small-molecule fibrils, addition of these peptide fibrils to procaspase-3 stimulated activation (**Fig. 3-18B**). This result has potential implications for Alzheimer's disease, where A β aggregates have been linked to caspase-dependent neurotoxicity (165). Moreover, we previously described the apoptotic activity induced by 1541 and 1541B (71). We are now exploring how these nanofibrils promote cell death. Such a mechanism is certainly intriguing and nonstandard from a drug discovery perspective.

For bioprocessing applications, enzyme immobilization on nanostructures offers

an exciting alternative to traditional approaches for manipulating enzyme functionality, such as genetic and chemical engineering (166,167). 1541 represents a first-in-class, self-assembling, small-molecule nanofibril that acts as a catalyst for procaspase-3 activation. Future studies aim to elucidate the specific structural properties of the molecule that drive fibril assembly as well as those that facilitate procaspase-3 activation. It may be possible to use this scaffold for the design of other proenzyme activators or to discover novel fibril-forming small molecules that activate proenzymes.

Materials and Methods

Synthesis of 1541: Synthesis, purification, and characterization of 1541 and related analogs were previously described (71).

Procaspase-3 (wild type and C163A) expression and purification: Full-length human procaspase-3 clone (residues 1-277) was generated as previously described (71,168). Briefly, procaspases-3 was expressed with a C-terminal His₆-affinity tag. Cells were grown at 37°C to an OD_{600nm} of ~0.6. Overexpression of procaspase-3 was induced at 30°C for only 20 min with 0.2 mM IPTG. Cells were immediately placed on ice, harvested, suspended in lysis buffer (100 mM Tris, pH 8.0 and 100 mM NaCl), and lysed. The cell lysate was clarified and purified by Ni-NTA affinity column, followed by anion-exchange chromatography. Fractions corresponding to purified procaspase-3 were collected and stored at -80°C.

We used QuickChange (Qiagen) mutagenesis to generate catalytically dead procaspase-3 (C163A) with the active site cysteine mutated to alanine. Procaspase-3 (C163A) was generated using the same expression and purification protocols as wildtype procaspase-3, except that overexpression was extended to 15 hours.

Procaspase-3 activation assays: Under standard assay conditions, 1541, 1541B, 1541D, DMSO, or a standard aggregator was pre-incubated for 1 h at 37°C with agitation in activity assay buffer that contained 50 mM HEPES, pH 7.4, 50 mM KCl, 0.1 mM EDTA, 1 mM DTT and 0.1% CHAPS. In some assays, either no detergent or different detergents, such as 0.1% Triton or 0.01% Triton, were used in place of 0.1% CHAPS. After compound pre-incubation, 100 nM procaspase-3 was added to each sample. 4 nM granzyme B (a kind gift from the Craik lab at UCSF) was added to procaspase-3 as a

positive control. Samples were agitated at 37°C for the times indicated, the mixtures were assayed for kinetic activity by the addition of 50 μ M Ac-DEVD-AFC (SM Biochemicals LLC), a fluorogenic caspase-3 substrate, over 10 minutes on a SpectraMax M5 (Molecular Devices).

Time course assays of procaspase-3 activation: 5 μ M 1541 and 1541B were pre-incubated at 37°C for 1 h, and subsequently 100 nM procaspase-3 was added. Compounds were assayed for activation potential against procaspases-3 over 220 minutes at 37°C. Kinetic assays were initiated after incubation at 37°C by addition of Ac-DEVD-AFC.

β -lactamase inhibition assays: β -lactamase (a kind gift from the Shoichet lab at UCSF) has previously been described as being sensitive to inhibition by non-specific aggregating small molecules (116). 1 nM β -lactamase was added to a buffer containing 50 mM sodium cacodylate, pH 6.5 and 0.01% Triton-X100. 50 μ M 1541, 1541B, 1541D, DMSO, or Congo red (Sigma-Aldrich) was added to the enzyme and incubated at 37°C for either 5 or 60 minutes to assess time-dependent inhibition. Following compound incubation, 40 μ M CENTATM (CalBiochem) was added to each sample and the absorbance was monitored at 405 nm to determine the activity of β -lactamase. 1541 and 1541B were further tested in a full dose-response for β -lactamase inhibition in a buffer consisting of 50 mM sodium cacodylate, pH 6.5 and 0.1% CHAPS, which is the standard buffer for monitoring β -lactamase activity with the detergent typically used for our procaspase-3 activation assays. Compound impact on β -lactamase activity was also determined in a buffer containing 20 mM HEPES, pH 7.4, 10 mM KCl, 1.5 mM MgCl₂, 1.5% Sucrose, 1 mM DTT and 0.1% CHAPS, which is a caspase activity buffer.

Procaspase-3 activation assays with BSA: Bovine Serum Albumin (BSA, Equitech Bio, Inc.) was added to caspase-3 activity buffer (50 mM HEPES, pH 7.4, 50 mM KCl, 0.1 mM EDTA, 1 mM DTT and 0.1% CHAPS) to 1 mg/mL, 0.1 mg/mL, 0.01 mg/mL, and 0.001 mg/mL concentrations. Buffer containing BSA was aliquoted in 96-well black-bottom plates. A dilution series of 1541, 1541B, or 1541D was added to the wells. 100 nM procaspase-3 was added to each well, and 4 nM granzyme B with 100 nM procaspase-3 was included on each plate as the positive control. Samples were agitated at 37°C for 5 hrs. The mixtures were assayed for kinetic activity by the addition of 50 µM Ac-DEVD-AFC, and fluorescence intensity was monitored over 10 minutes.

Caspase activity assays with aggregators: Miconazole, TIPT (3',3'',5',5''-Tetraiodophenolphthalein), clotrimazole, rottlerin, 4BPAP, and Congo red were previously characterized as standard aggregators (150,154). These small molecules were a kind gift from the Shoichet lab at UCSF. A 2-fold dilution series of each aggregator starting at 100 µM in our standard caspase-3 activity assay buffer was incubated with 100 nM procaspase-3 for 4 hrs. 1541 was used as a positive control. 50 µM Ac-DEVD-AFC was added to each sample, and fluorescence intensity was monitored over 10 minutes.

10 nM mature caspase-3 was added to assay buffer with 0.1% CHAPS and without 0.1% CHAPS. A dilution series of Congo red, starting at 2 mM, was added to caspase-3. After a 5-minute incubation, 50 µM Ac-DEVD-AFC was added to each sample, and fluorescence intensity was monitored over 10 minutes.

A dilution series of Congo red, starting at 1 mM, was added to 100 nM procaspase-3. The concentration range was chosen over which inhibition of cleaved caspase-3 is observed. 1541 was used as the positive control. Samples were incubated for 6 hrs at

37°C. 50 μ M Ac-DEVD-AFC was added, and fluorescence intensity was monitored over 10 minutes.

Activation assay under dialysis conditions: 500 mL of 10 μ M 1541, 500 mL of 10 μ M 1541B, and 500 mL of 2% DMSO in activity assay buffer were incubated for 1 h at 37°C. For control samples, 200 nM procaspase-3 was added to 1 mL 10 μ M 1541 (A), to 1 mL 10 μ M 1541B (B), and to 1 mL buffer alone (C). For 3 additional test samples, 200 nM procaspase-3 was added to 1 mL assay buffer alone (D-F). 250 μ L of each sample was placed in a D-Tube™ Mini Dialyzer (Novagen) with a MWCO 12-14 kDa, for a total of six dialysis samples. Samples A and D were inserted into one floating rack. The rack was placed in the remaining 500 mL of 10 μ M 1541 in an Erlenmeyer flask. Similarly, samples B and E were placed in another floating rack. This rack was placed in a flask containing the remaining 500 mL of 1541B. The final two dialysis chambers, C and F, were inserted into a rack and placed in 500 mL of 2% DMSO in assay buffer. All three flasks were then sealed with parafilm and gently agitated overnight at 37°C. 50 μ L (in duplicate) of each sample was placed in an 96 well black bottom plate, and 50 μ M Ac-DEVD-AFC was added to each well. Fluorescence intensity was monitored over 10 minutes, and initial rates were measured to determine activities of each sample. LDS sample buffer (Invitrogen) was added to the remaining samples, and they were analyzed by SDS-PAGE (Invitrogen). The gel was silver stained to determine amounts of procaspase-3 auto-processing.

Compound centrifugation assays (169): DMSO stocks of 1541, 1541B, and 1541D were created at 2.5, 1.0, 0.5, 0.25, 0.2, 0.1, 0.05, 0.025, and 0 mM concentrations. 20 μ L of each stock was added to 980 μ L of activity assay buffer in an Eppendorf tube to create samples at 50, 20, 10, 5, 4, 3, 2, 1, 0.5, and 0 μ M compound. A standard curve was

created by monitoring absorbance of both the DMSO stocks and the mixtures in buffer at 320 nm. A standard curve was also created for compounds in buffer after 1 h incubation at 37°C.

Two additional dilution series were prepared for each compound in buffer, as described above. One set of samples was immediately centrifuged at 16,100-x g in an Eppendorf Centrifuge 5415D for 10 minutes. Another set was incubated at 37°C for 1 h, followed by centrifugation. After centrifugation of each set, 2 x 200 µL samples of the supernatant were added to a 96-well clear bottom plate. The remaining supernatant was removed by aspiration. 250 µL of DMSO was added to each tube, and 200 µL was transferred to a 96 well plate. Absorbance at 320 nm was determined for each sample, and concentration was determined based on a standard curve. Each sample was repeated in triplicate.

Procaspase-3 co-sedimentation assays: 50, 20, 15, 10, 7.5, 5, 4, 3, 2, 1, 0.5, and 0 µM 1541, 1541B, and 1541D was added to 200 nM procaspase-3 (C163A) in 1 mL activity assay buffer. Samples were agitated at 37°C for 1 h to mimic assay conditions, followed by centrifugation. The supernatant was aspirated, and 100 µL of assay buffer was added to each tube. After the addition of LDS sample buffer, samples were analyzed by SDS-PAGE, coomassie (Bio-Rad) stained, and imaged on a LI-COR Odessey Infrared Imaging System. The concentration of procaspase-3 in each pellet was determined relative to standards included in each gel and quantified using ImageJ.

To determine if the particles become saturated and to further define affinities, 20 µM 1541, 1541B, or 1541D was added to 1 mL 8, 4, 2, 1, 0.5, 0.25, 0.125, 0.0625, 0.03125, or 0 µM procaspase-3 (C163A) in 1 mL of activity assay buffer. After vortexing, each

sample was immediately centrifuged for 10 minutes at 16,100-x g. Again, the supernatant was aspirated, and 100 μ L of assay buffer was added to each tube. Concentrations of procaspase-3 were determined as described above. The amount of procaspase-3 in the pellet was plotted versus the log of the initial concentration of procaspase-3 in prism and fitted to a log scale with variable slope equation to determine an EC₅₀. Approximately 70% saturation was reached with 1541.

Particle flow cytometry assays (169): To characterize the particles formed by 1541 and related analogs, we used a BD Gentest Solubility Scanner, a flow cytometer intended for particle detection. The flow cytometer has a 3 mW laser at 635 nm with the detector angle at 90°. Photon signatures of samples were collected with a PMT setting of 99 and the threshold channel set to 25. Compound mixtures were prepared in the standard assay buffer unless otherwise noted. The buffer (50 mM HEPES, pH 7.4, 50 mM KCl, 0.1 mM EDTA, 1 mM DTT, and 0.1% CHAPS) was filtered through a 0.22 μ m filter unit to remove any particulates. 1541, 1541B, and 1541D were diluted in filtered assay buffer from concentrated DMSO stocks for a final concentration of 2% DMSO in 1.5 mL eppendorfs. 2% DMSO in assay buffer alone was included in each run to evaluate the background. 3', 3'', 5', 5''-tetraiodophenolphthalein (TIPT; a kind gift from the Shoichet lab at UCSF) dilutions were added to caspase buffer without CHAPS and with a final concentration of 1% DMSO. Mixtures were either analyzed immediately or agitated at 37°C for 1 h. 200 μ L of each sample was added to a 96 well plate (in duplicate), and injected for 3 s at a flow rate of 0.5 μ L/s. The particle flow cytometer was first calibrated using Nile Red calibration beads at 2.49 μ m. All samples were repeated in triplicate.

Dynamic Light Scattering (DLS) Assays (150): Particles of 1541 were detected by DLS (Wyatt Technology DynaPro MS/X). The instrument has a 55 mW laser at 826.6 nm, and

the laser power was set to 100%, unless otherwise noted. The intensity of scattered light was monitored at an angle of 90°. Again, compound mixtures were prepared in standard assay buffer (50 mM HEPES, pH 7.4, 50 mM KCl, 0.1 mM EDTA, 1 mM DTT, and 0.1% CHAPS). 1541, 1541B, 1541D, and TIPT were diluted in the buffer from concentrated DMSO stocks for a final concentration of 2% DMSO. 2% DMSO in assay buffer alone was used as a control sample to determine the background. Mixtures were either analyzed immediately or incubated at 37°C for 1 h. Each measurement was repeated in triplicate.

Transmission Electron Microscopy: Compound samples were generated by diluting DMSO stocks in standard assay buffer (50 mM HEPES, pH 7.4, 50 mM KCl, 0.1 mM EDTA, 1 mM DTT, and 0.1% CHAPS) for a final concentration of 2% DMSO. 10 µM 1541, 100 µM 1541, 50 µM TIPT, and 50 µM 1541 with 500 nM procaspase-3 solutions were immediately placed on the grids after mixing at room temperature or after agitation at 37°C for approximately 1 h. Prior to sample addition, formvar/carbon coated 200 mesh copper grids (Ted Pella, Inc.) were first glow discharged. 5 µL of each sample was next adsorbed onto the grids followed by negative staining in 50 µL drops (x2) of filtered 2% sodium phosphotungstate, pH 7.4. The grids were viewed in a FEI Tecnai F20 electron microscope (Eindhoven, The Netherlands) at 80 kV. A Gatan Ultrascan CCD camera recorded the images.

Beta-Amyloid (1-40) assays: Fibrils were formed from solid peptide stocks, as previously described (170). Briefly, solid beta-amyloid (1-40) (AnaSpec Inc.) stocks were diluted to 25 µM in 1,1,1,3,3,3-hexafluoroisopropanol (HFIP; Sigma-Aldrich) and sonicated for 2 h to remove impurities. 500 µL aliquots were stored at -80°C for later use. As samples were needed, aliquots were lyophilized for approximately 1 h, and 250 µL of a caspase

activity buffer (20 mM HEPES, pH 7.4, 10 mM KCl, 1.5 mM MgCl₂, 1.5% Sucrose, 10 mM DTT, 0.1% CHAPS) was added to the solid to generate a 50- μ M mixture. The samples were agitated at 37°C, and fibril formation was monitored over time by the addition of 15 μ L of sample to 250 μ L 5 μ M Thioflavin T (Sigma-Aldrich). Fluorescence intensity was monitored at an excitation wavelength of 440 nm and an emission wavelength of 490 nm. At maximum fluorescence intensity, samples were serially diluted, and 200 nM procaspase-3 was added. 4 nM granzyme B was incubated with procaspase-3 alone as a positive control. Samples were incubated for 6 h at 37°C. 50 μ M Ac-DEVD-AFC was added to each well and activity was monitored over time. Notably, the extent of activation observed is dependent upon the purity of the beta-amyloid (1-40) preparation.

Acknowledgment

We thank S. Mahrus, N. Agard, and J. Porter for invaluable advice, guidance, and support. We acknowledge M. Bennett and H. Rodriguez at Calithera for advice and discussions. We thank A. Doak, B. Feng, S. Prusiner, and B. Shoichet for helpful discussions on promiscuous enzyme inhibitors and for use of their instruments. We thank D. Hostetter for providing granzyme B. We thank the Wells lab, the Small Molecule Discovery Center at UCSF, and W. F. DeGrado for suggestions. This research was supported by grants from the National Institutes of Health (R01 CA136779, P01 AG02132), a National Cancer Institute Postdoctoral Fellowship (F32 CA119641-03 to D.W.W.), an ARCS Foundation Award (to J.A.Z.), and a Schleroderma Research Foundation Evnin-Wright Fellowship (to J.A.Z.).

sample ^a	T(°C)	I_{DLS} (kcps)	r_{DLS} (nm)	K_{sp} (μM) ^b	AC ₅₀ (μM) ^c
control	25	19.7 ± 1.3	1.0 ± 0.3	no particles	NA
control	37	20.8 ± 1.2	1.3 ± 0.3	no particles	NA
1541	25	270.2 ± 77.9	1112.8 ± 86.6	1.3 ± 0.3	>50
1541	37	17.5 ± 1.4	0.5 ± 0.1	10 ± 5	3.0 ± 0.6
1541B	25	170.1 ± 44.7	910.7 ± 66.7	1.6 ± 0.4	3.1 ± 0.5 ^d
1541B	37	15.8 ± 0.9	0.4 ± 0.1	20 ± 5	1.8 ± 0.1
1541D	25	3317.0 ± 854.0 ^e	164.1 ± 7.7	7.5 ± 0.5	NA
1541D	37	3071.9 ± 465.1 ^e	186.4 ± 21.6	7.5 ± 0.5	NA
TIPT	25	3903.5 ± 1423.0	71.1 ± 8.6	–	NA
TIPT	37	3933.2 ± 1369.0	76.7 ± 7.8	–	NA

a Control samples contained no aggregator. The concentrations of 1541, 1541B, and 1541D in DLS measurements were 10 μM. The concentration of TIPT was 50 μM.

b Determined using particle flow cytometry.

c Activity measurements were performed at $t = 8$ h. NA = no activation.

d The maximum percent activation for 1541B was 8% at 25 °C vs 60% at 37 °C.

e 1541D samples were run at 25% laser power.

Table 3-1. Unique Properties of 1541 and Related Analogues Compared with Standard Aggregators



Chart 3-1. Compound 1541 and Analogues

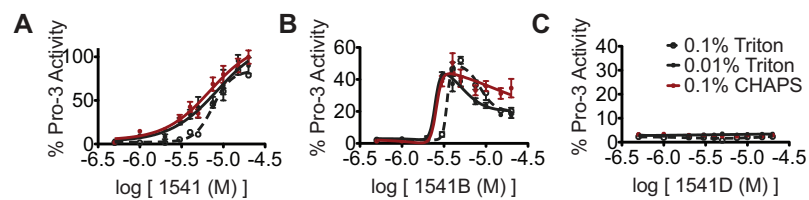


Figure 3-1. 1541 promotes procaspase-3 activation in the presence of detergents. Compounds were pre-incubated with agitation in assay buffer for 1 h at 37°C with 0.1% CHAPS (red circles), 0.01% Triton (black closed circles), or 0.1% Triton (black open circles). Compounds in each buffer were plated, followed by the addition of 100 nM procaspase-3. 4 nM granzyme B was added to 100 nM procaspase-3 alone as a positive control, and used to establish 100% proenzyme activation. Activity was measured after a 4 h incubation at 37°C with Ac-DEVD-AFC. (A) Percent activation of procaspase-3 with 1541 dilution series in different detergents. (B) Percent activation of procaspase-3 with 1541B dilution series. (C) Percent activation of procaspase-3 with 1541D dilution series.

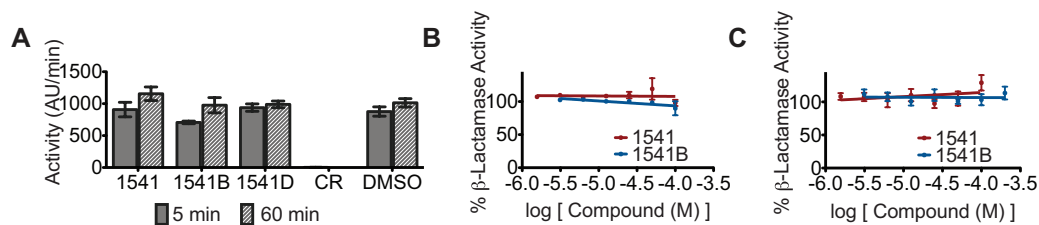


Figure 3-2. 1541 does not inhibit β -lactamase. 1541 and related analogs were tested for inhibition of β -lactamase. (A) 50 μ M 1541, 1541B, 1541D, or congo red was incubated for 5 min and 60 min at 37°C with 1 nM β -lactamase in a buffer consisting of 50 mM sodium cacodylate, pH 6.5 in the presence of 0.01% Triton-X100. Activity of the enzyme was determined after the incubation times. (B) A full dose-response for 1541 and 1541B was determined against β -lactamase in 50 mM sodium cacodylate, pH 6.5 with 0.1% CHAPS. (C) A full dose-response for 1541 and 1541B was determined against β -lactamase in a standard caspase activity buffer (20 mM HEPES, pH 7.4, 10 mM KCl, 1.5 mM MgCl₂, 1.5% sucrose, and 1 mM DTT) with 0.1% CHAPS.

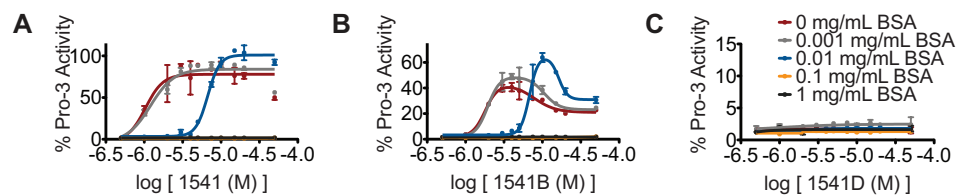


Figure 3-3. BSA prevents activation of procaspase-3 by 1541. Under standard procaspase-3 activation assay conditions, various concentrations of BSA (0, 0.001 mg/mL, 0.01 mg/mL, 0.1 mg/mL and 1 mg/mL) were included to determine the effect on procaspase-3 activation by 1541 and related analogs. (A) The AC_{50} of activation by 1541 is shifted by the inclusion of 0.01 mg/mL BSA in the buffer. At 0.1 mg/mL BSA and 1 mg/mL BSA, no activation is observed. (B) A similar trend for 1541B activation of procaspase-3 in the presence of BSA is observed. (C) No activation is observed for 1541D under any of the conditions.

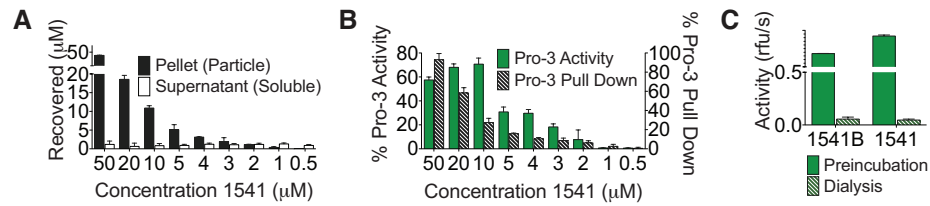


Figure 3-4. 1541 forms particles that are required for binding and activation of procaspase-3. (A) The amounts of 1541 in the pellet (solid black bars) and the supernatant (open bars) were analyzed after centrifugation. (B) (i) Samples of procaspase-3 (C163A) with varying concentrations of 1541 were centrifuged, and the amount of procaspase-3 in the pellet was determined (hatched bars). (ii) The activity of wild-type procaspase-3 with 1541 was determined (filled green bars). (C) In a preincubation control sample, procaspase-3 was added to 10 μM 1541 (or 1541B) inside a dialysis membrane (filled green bars). In the test sample, only procaspase-3 was inside the dialysis chamber, with 1541 (or 1541B) outside the chamber (hatched green bars). After 12 h at 37 $^{\circ}\text{C}$, the activity of each sample was measured.

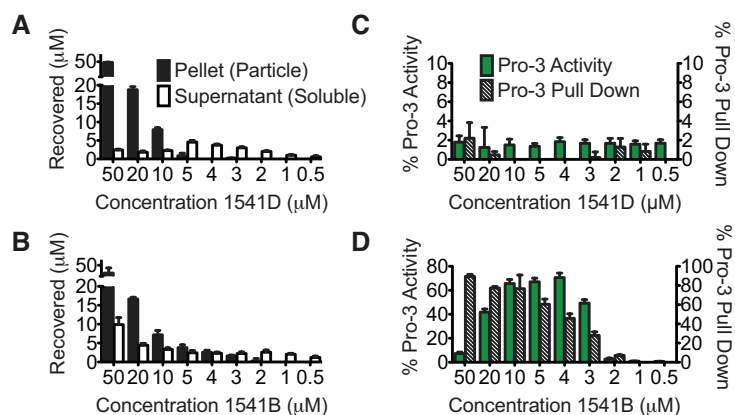


Figure 3-5. Analogs of 1541 form particles that interact with procaspase-3. (A) Varying concentrations of 1541D were vortexed in 1 mL of assay buffer and then pelleted in a centrifuge. Absorbance of the supernatant was monitored at 320 nm. After removal of the remaining supernatant, 250 μL of DMSO was added and the concentration of compound in the pellet was determined. (B) Similarly, amounts of 1541B in the pellet and the supernatant were determined after centrifugation. (C) (i) 200 nM procaspase-3 (C163A) was added to 1 mL of assay buffer followed by 1541D. After 1 h incubation at 37°C, the samples were centrifuged, the supernatant was removed, and the pelleted material was re-suspended in 100 μL of assay buffer followed by dilution in LDS loading buffer. Samples were analyzed by SDS-PAGE to assess the concentration of enzyme in the pellet. (ii) 100 nM procaspase-3 was incubated with 1541D for 2 h at 37°C. Percent activity was determined relative to 100% activation by the upstream protease, granzyme B. (D) (i) Co-sedimentation of procaspase-3 with 1541B was evaluated. (ii) 100 nM procaspase-3 was incubated with a dilution series of 1541B for 2 h at 37°C. Plots show that activity correlates with procaspase-3 pull down for both 1541D and 1541B.

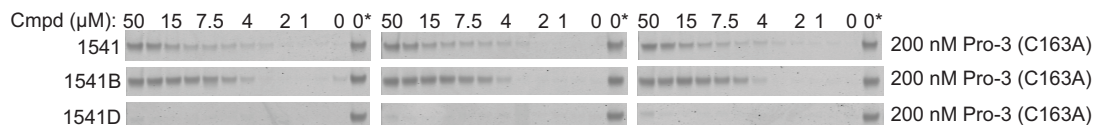


Figure 3-6. Co-sedimentation of procaspase-3 (C163A) with varying concentrations of 1541 and analogs. 200 nM procaspase-3 (C163A) was added to 1 mL of assay buffer followed by a dilution series of 1541, 1541B, or 1541D. After 1 h incubation at 37°C, the samples were centrifuged, the supernatant was removed, and the pelleted material was re-suspended in 100 μL of assay buffer followed by dilution in LDS sample buffer. Samples were run by SDS-PAGE and coomassie stained. Gels were imaged using the LI-COR Odessey Infrared Imaging System. Band intensities were quantified using ImageJ. Replicates are shown above.

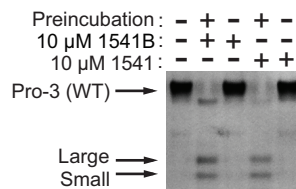


Figure 3-7. Lack of procaspase-3 processing when isolated from 1541 or 1541B by a dialysis membrane. 200 nM procaspase-3 was either co-incubated with 10 μ M 1541 or 1541B, or the enzyme was isolated from the compounds by a MWCO 12-14 kDa dialysis membrane and allowed to equilibrate with 500 mL of compound in buffer. After 12 h incubation, the samples inside the dialysis chamber were added to LDS sample buffer, and after SDS-PAGE and silver stain analysis, the presence of the cleaved or proenzyme was assessed. Only control samples that were co-incubated with 1541 or 1541B showed processing.

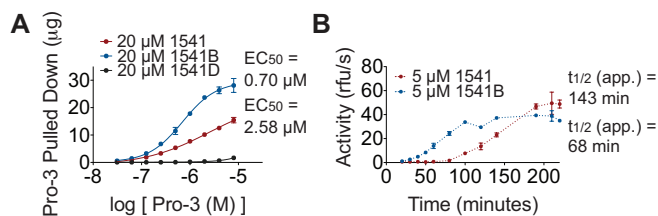


Figure 3-8. 1541 and 1541B particles have different affinities for procaspase-3 that correlate to distinct rates of activation. (A) 1541, 1541B, or 1541D (20 μ M) was incubated with a dilution series of procaspase-3 (C163A). After centrifugation, the pellet was examined for procaspase-3. (B) 1541 or 1541B (5 μ M) was added to wild-type procaspase-3, and activities were plotted versus time. An apparent $t_{1/2}$ value incorporating the lag phase and the actual $t_{1/2}$ value were calculated for each compound. Notably, the distinct lag phases drive the difference in the apparent $t_{1/2}$ values.

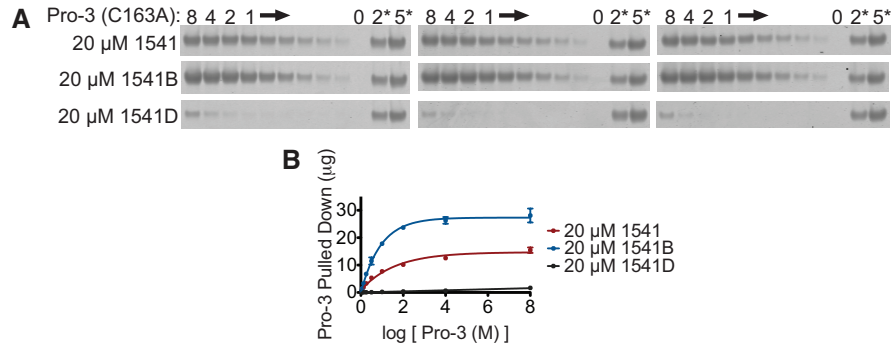


Figure 3-9. Cosedimentation of varying concentrations of procaspase-3 with 20 μ M 1541, 1541B, and 1541D. (A) A dilution series of procaspase-3 (C163A) starting at 8 μ M was added to 1 mL of assay buffer. Subsequently, 20 μ M 1541, 1541B, or 1541D was added to each sample. After vortexing, the samples were centrifuged for 10 min, and the supernatant was removed. The pelleted material was re-suspended in 100 μ L of assay buffer followed by dilution in LDS sample buffer. Samples were run by SDS-PAGE and coomassie stained. Gels were imaged using the LI-COR Odessey Infrared Imaging System. Band intensities were quantified using ImageJ. Replicates are shown above. (B) Quantification of band intensities plotted along a linear scale in Prism.

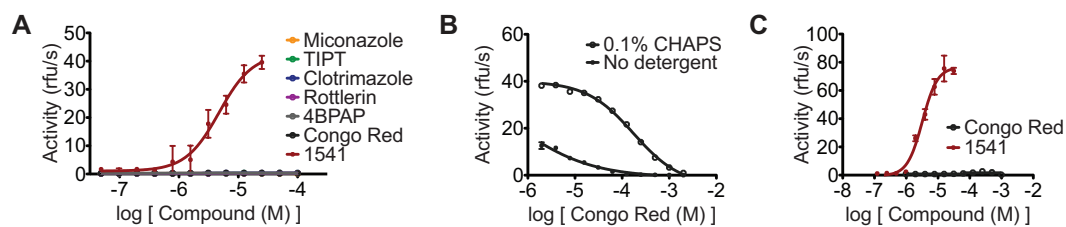


Figure 3-10. Standard aggregators do not activate procaspase-3. A panel of aggregators was tested for activation of procaspase-3 under standard assay conditions. 1541 was used as a positive control. (A) At 4 h, common aggregators did not activate procaspase-3. (B) Congo red inhibits caspase-3 both with and without detergent. Inhibition is more potent in the absence of detergent, which is characteristic of a small molecule colloidal aggregator. (C) At 6 h, higher concentrations of Congo red do not activate procaspase-3. There is a functional interaction between Congo red and caspase-3 that results in inhibition of the enzyme, but no activation of procaspase-3 is observed.

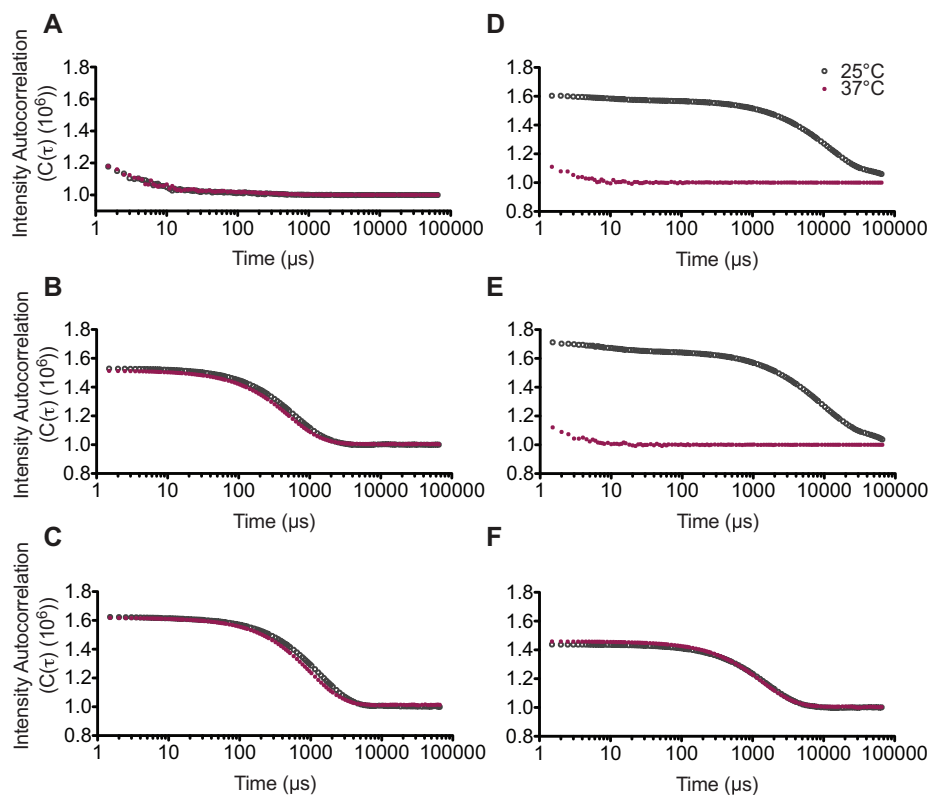


Figure 3-11. Autocorrelation curves from DLS analysis. Compound mixtures were prepared in standard assay buffer. Mixtures were either analyzed immediately or incubated at 37°C for 1 h prior to analysis. Each trace is a single experiment. (A) 2% DMSO in assay buffer alone. (B) A characteristic autocorrelation curve for a standard small molecule aggregator, 50 μM TIPT, at 25°C and at 37°C. (C) 200 nm beads in our standard assay buffer with 2% DMSO. Autocorrelation curves for (D) 10 μM 1541 and (E) 10 μM 1541B indicated a unique behavior for these particles. (F) 10 μM 1541D behaves more like colloidal particles or known aggregators.

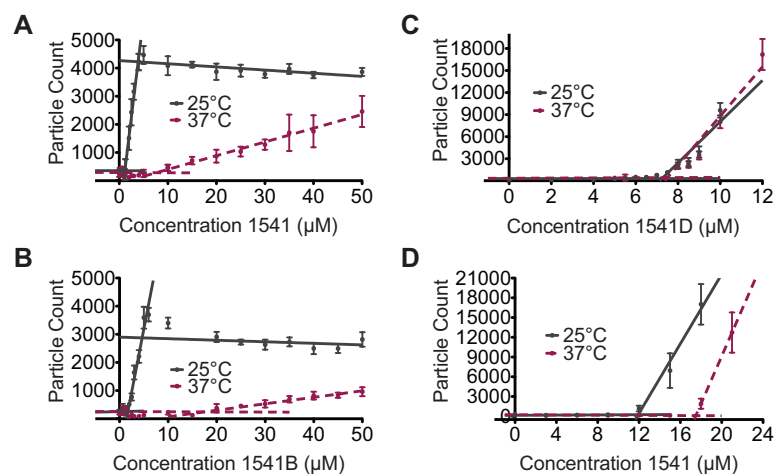


Figure 3-12. Particles of 1541 analogs and standard aggregators analyzed by particle flow cytometry. A dilution series of each compound was added to 1 mL standard assay buffer to a final concentration of 2% DMSO. 2 x 200 μ L of each sample was added to a 96-well plate and analyzed by particle flow cytometry. The remaining 600 μ L of sample was incubated at 37°C for 1 h and subsequently analyzed. Particles of 1541 (A) and 1541B (B) behave distinctly from particles of 1541D (C) and TIPT (D). TIPT samples were incubated in standard buffer at a final concentration of 1% DMSO without detergent. Particle size for 1541 and 1541B increases linearly until reaching a critical particle count. Particle count plateaus while particle size increases with increasing concentration. Particle size remains constant for 1541D and TIPT, and particle count increases linearly with concentration. Further, particles of 1541 and 1541B are significantly impacted by temperature. Note differences in y-axis scale for the different samples.

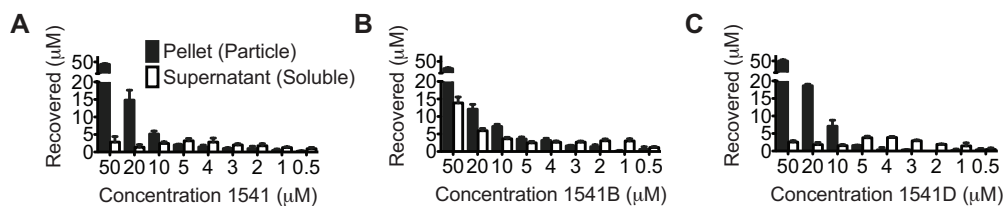


Figure 3-13. Analogs of 1541 pellet at 37°C. (A) Varying concentrations of 1541 were incubated in 1 mL of assay buffer for 1 h at 37°C with mild agitation. The samples were centrifuged. Absorbance of the supernatant was monitored at 320 nm. After removal of the remaining supernatant, 250 µL of DMSO was added and the concentration of compound in the pellet was determined. (B) Similarly, the quantity of 1541B in the pellet and the supernatant was determined after centrifugation. (C) Amounts of 1541D in the pellet and supernatant were also determined. All three compounds behaved similar to compounds pelleted immediately after compound addition.

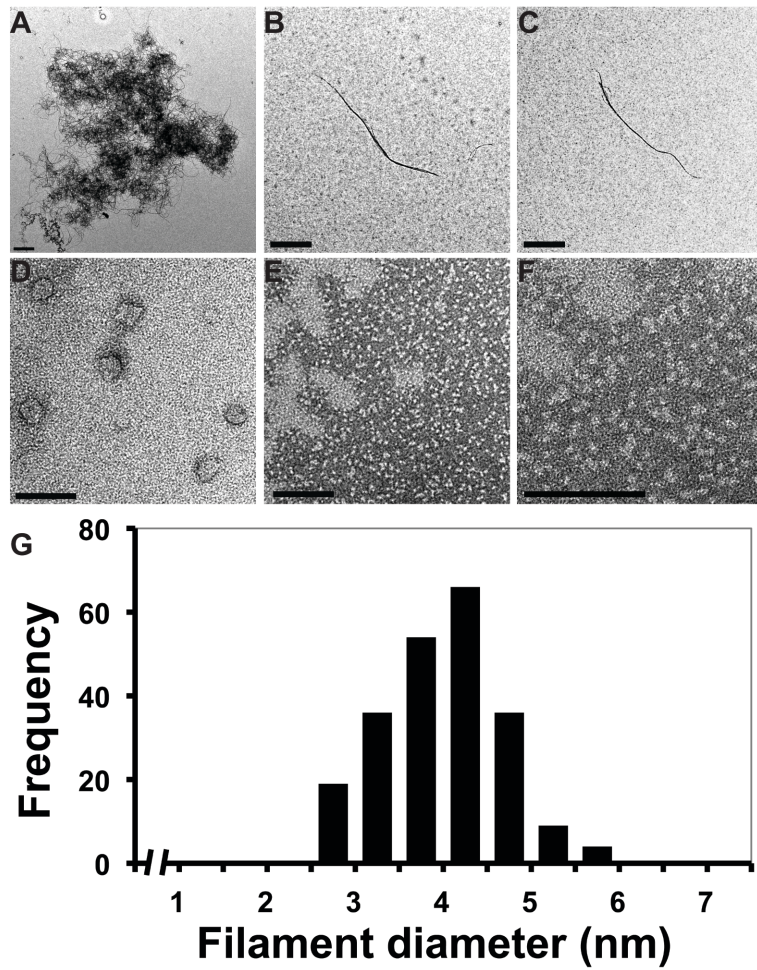


Figure 3-14. Transmission electron micrographs of fibrils, particles, and procaspase-3 (C163A). (A) Bundle of 1541 fibrils at room temperature. (B) and (C) 1541 fibrils after 1 h incubation at 37°C. (D) TIPT colloidal particles in caspase buffer. (E) and (F) Procaspase-3 (C163A) alone in caspase buffer. Magnification bars = 1 μm for (A), (B), and (C) and 100 nm for (D), (E), and (F). (G) Distribution of diameters for the smallest 1541 fibrils at 25°C. Noticeably larger fibrils were not included.

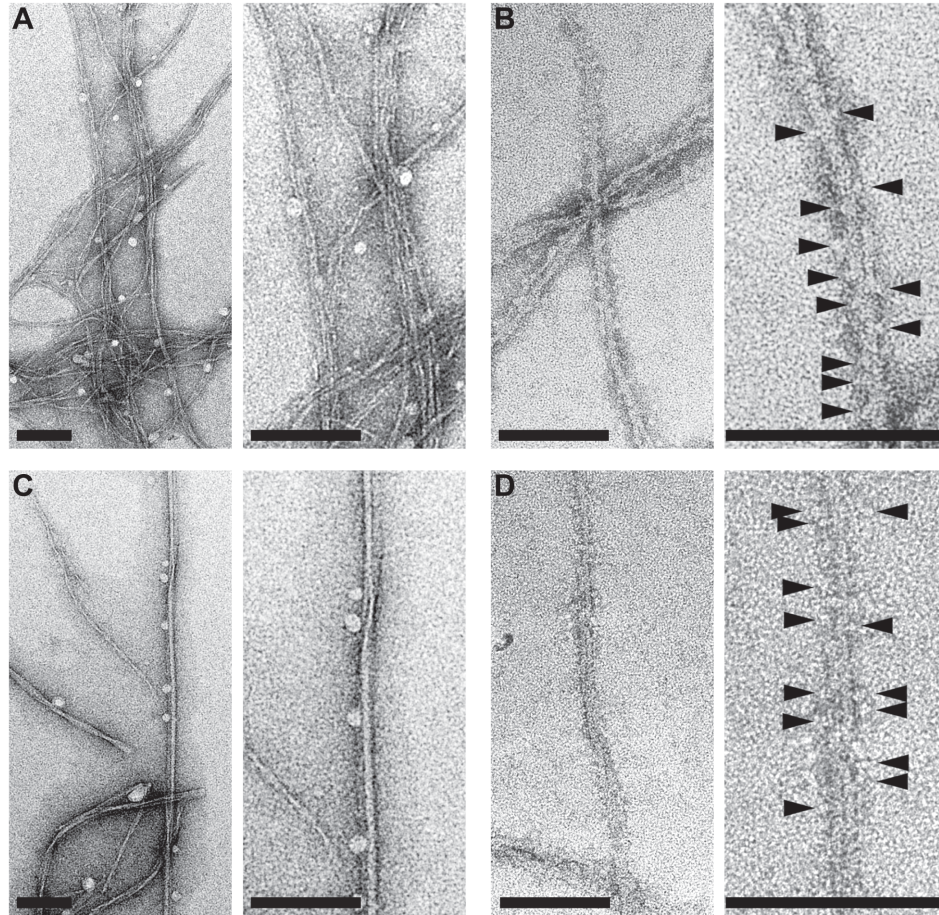


Figure 3-15. TEM images of 1541 nanofibrils with and without procaspase-3. (A) Negatively stained 1541 at 25 °C shows bundles of very thin and flexible fibrils. (B) In contrast, 1541 at 37 °C consists mainly of larger, less flexible fibrils. (C, D) 1541 fibrils decorated with procaspase-3 at (C) 25 °C and (D) 37 °C. The procaspase-3 molecules decorating the surface are indicated by arrowheads. Scale bars = 100 nm.

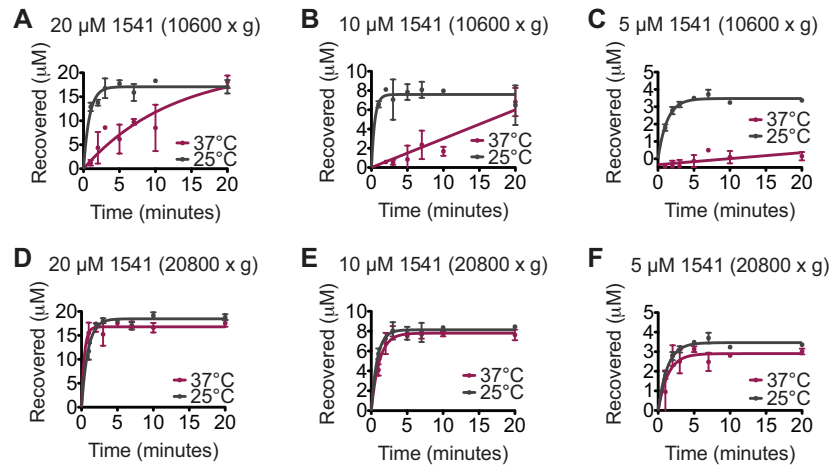


Figure 3-16. Rate of 1541 particle sedimentation by centrifugation at room temperature and at 37°C. Samples of 20 μM (A, D) 10 μM (B, E) and 5 μM 1541 (C, F) were prepared in 1 mL standard assay buffer. Samples were either centrifuged immediately at 25°C or preincubated for 1 h at 37°C followed by centrifugation at 37°C. Particles at 37°C spun down slower than particles at 25°C. Samples A, B, and C were centrifuged at 10,600xg for the indicated times. Samples D, E, and F were centrifuged at 20,800 x g. A similar rate of sedimentation was observed at the higher speed.

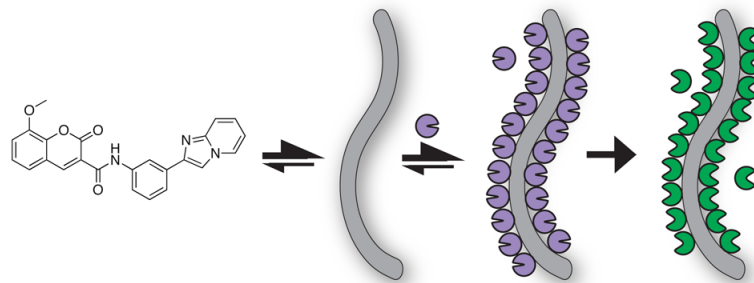


Figure 3-17. Model of procaspase-3 activation by 1541 nanofibrils. 1541 and analogues spontaneously self-assemble into nanofibrils. The fibrils bind directly to procaspase-3 to promote increased local concentration of the enzyme. Upon recruitment to the fibrils, procaspase-3 is activated to generate mature caspase-3.

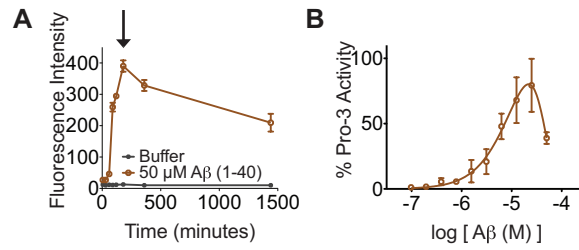


Figure 3-18. A β fibrils activate procaspase-3. (A) A β peptide (1–40) was agitated at 37 °C in a caspase activity buffer to form fibrils. Fibril formation was monitored over time by an increase in thioflavin T fluorescence. (B) A β peptide (1–40) samples were taken at 3 h (black arrow), serially diluted, and incubated with procaspase-3 for 6 h. Percent activity is shown.

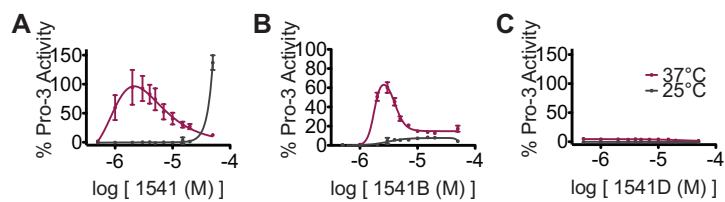


Figure 3-19. Procaspase-3 activation by 1541 and analogs at room temperature and at 37°C. 100 nM procaspase-3 was incubated with a dilution series of 1541 (A), 1541B (B), or 1541D (C) in standard assay buffer at 37°C or 25°C for 8 h. 50 μ M Ac-DEVD-AFC was added to each sample to measure activity. Percent activity was determined relative to 100% activation by the upstream protease, granzyme B. Note, at later timepoints, mild activation with 1541 is observed and full activation is observed with 1541B (data not shown).

Chapter 4:

Fibrils Colocalize Caspase-3 with Procaspase-3 to Foster Maturation

Julie A. Zorn[†], Dennis W. Wolan[†], Nicholas J. Agard[†], and James A. Wells^{†,‡}

[†]Department of Pharmaceutical Chemistry, University of California, San Francisco,
California

[‡]Department of Cellular and Molecular Pharmacology, University of California, San
Francisco, California

This work has been submitted for publication.

Abstract

Most proteases are expressed as larger inactive precursors, or zymogens, that become activated by limited proteolysis. We previously identified a small molecule, termed 1541, that dramatically promotes the maturation of the zymogen, procaspase-3, to its mature form, caspase-3. Surprisingly, compound 1541 self-assembles into nanofibrils and localization of procaspase-3 to the fibrils promotes activation. Here, we interrogate the biochemical mechanism of procaspase-3 activation on 1541 fibrils in addition to proteogenic amyloid- β (1-40) fibrils. We find no evidence that procaspase-3 alone can self-activate, consistent with its fate-determining role in executing apoptosis. In fact, the activity of procaspase-3 is >10,000,000-fold lower than mature caspase-3, making it a remarkably inactive zymogen. We show that fibril-induced colocalization of trace amounts of caspase-3 or other initiator proteases with procaspase-3 dramatically stimulates maturation of the proenzyme. Thus, similar to known cellular signaling complexes, these synthetic or natural fibrils serve as a platform to concentrate procaspase-3 for trans-activation by upstream proteases.

Introduction

Proteases catalyze the irreversible post-translational modification of amide bond hydrolysis. Thus, cellular mechanisms exist to restrict spurious activation (144). For example, cellular inhibitors can often limit the activity of a mature protease. Moreover, most proteases are expressed as inactive precursors, known as zymogens, which require an external signal to generate the active enzyme (171,172). While the biological consequences of zymogen maturation are evident, important mechanistic details remain lacking (146).

Caspases are cysteine-class aspartyl specific proteases that are expressed as such inactive precursors, known as procaspases (173). To generate the mature enzyme, procaspases require cleavage after specific aspartic acid residues to remove an N-terminal pro-domain and to form the large and small subunit, the latter processing event being critical for activation (149,174). In apoptosis, the maturation process proceeds via a signaling cascade (61). Upstream initiator procaspases-8, -9, and -10 are recruited to scaffolding complexes, such as the apoptosome or the death-inducing signaling complex (DISC), to generate active enzymes (145). Subsequently, the initiator caspases target downstream executioner procaspases-3, -6, and -7 for activation. Together these caspases can cleave >1000 downstream substrates that drive the apoptotic phenotype (175-177).

Significant efforts have been directed towards identifying small molecules that can directly activate the procaspases for use as potential chemotherapeutic agents (68,71,178). Our lab previously discovered a small molecule, termed 1541, that promotes procaspase-3 activation (**Fig. 4-1A**). Remarkably, we found that this small molecule spontaneously forms nanofibrils (4-5 nm thin and >1 μm long) that directly associate with procaspase-3 and promote activation (179). We found similar results for the natural amyloid- β peptide (residues 1-40) fibrils.

Here, we take advantage of both our synthetic 1541 nanofibrils and the amyloid- β fibrils to induce procaspase-3 activation to further understand a mechanism of zymogen maturation. We explore two possible models for activation of procaspase-3 on these platforms: enhanced processing due to induced proximity of procaspase-3 alone or from colocalization of procaspase-3 with a small population of the cleaved enzyme (180, Fig. 4-1B). Our data support a model whereby catalytic amounts of active caspase-3 or other upstream proteases are critical for procaspase activation either in the presence or absence of these fibrils. This trans-dependence for procaspase-3 activation by an upstream protease is further supported by new measurements showing it to be a remarkably inactive zymogen relative to other proteases. Thus, procaspase-3 is sensitive to activation by upstream proteases, which is dramatically accelerated when bound and concentrated on synthetic or natural fibril scaffolds.

Results

Procaspase-3 Does Not Auto-Process- We previously demonstrated using biophysical and electron microscopy techniques that procaspase-3 localization to the surface of 1541 fibrils is critical for activation (179). The maturation of procaspase-3 by 1541 to the large and small subunit of active caspase-3 occurs after a lag period of roughly 2 hours, as shown in Fig. 2A (71). However, prior studies have yet to determine the biochemical mechanism of this conversion from procaspase-3 to the mature, cleaved enzyme. We sought not only to establish the mechanism that 1541 fibrils exploit to promote procaspase-3 activation, but also to clarify the natural process for activation.

We first directly assessed if concentrating procaspase-3 alone on the fibrils is sufficient to promote trans-activation, where one proenzyme molecule cleaves another proenzyme molecule (**Fig. 4-1Bi**). To investigate this possibility, we expressed and purified an inactive mutant of procaspase-3, where the catalytic cysteine was converted to alanine (C163A). We also generated a catalytically competent, yet uncleavable procaspase-3, where the critical aspartic acid residues at the cleavage sites were mutated to alanines (62, D9A/D28A/D175A, Fig. 4-1C). The “dead” or inactive procaspase-3 was mixed with the uncleavable construct both with and without 1541. At the indicated time points, samples were quenched with LDS loading buffer, analyzed by SDS/PAGE, and visualized by silver stain (**Fig. 4-2B**). No processing was observed in the presence or absence of 1541. Furthermore, even a four-fold stoichiometric excess of the uncleavable procaspase-3 did not promote processing of the dead proenzyme (**Fig. 4-3**).

To evaluate if any trace cleavage of the inactive procaspase-3 by the uncleavable proenzyme occurred, we further visualized processing at extended times using more sensitive western blot techniques. Again, no detectable change in the amount of procaspase-3 or its cleavage products was observed with an antibody that

preferentially recognizes the large subunit of the mature caspase-3 (**Fig. 4-2C**). This indicates that 1541 fibrils do not promote trans-activation of procaspase-3 by another proenzyme molecule. Moreover, trans-activation of procaspase-3 alone is not detectable at physiologically relevant concentrations of the proenzyme (72, ~100 nM,134).

Nonetheless, we noted that incubation of wild-type procaspase-3 at high concentrations (>1 μ M) could generate the large and small subunit of the mature enzyme, even in the absence of 1541 (**Fig. 4-4**). This would suggest that the proenzyme can auto-activate; however, the above proteolytic susceptibility assay shows that intermolecular processing between two procaspase-3 molecules is restricted. Therefore, we assessed if intramolecular processing of procaspase-3 can generate a trace amount of mature caspase-3, that can then rapidly feedback to promote autocatalytic maturation of the proenzyme (**Fig. 4-1Bii**).

To evaluate this mechanism, we needed to isolate wild-type procaspase-3 activity alone and to eliminate the contribution of newly generated caspase-3 to the activation process. We used a covalent, active site inhibitor, Ac-DEVD-cmk, to preferentially label and inactivate mature caspase-3 versus procaspase-3 (**Fig. 4-5A**). Indeed, at stoichiometric concentrations the inhibitor covalently modifies mature caspase-3 to >97% by mass spectrometry, yet labels <4.0% of wild-type procaspase-3 over the same time course (**Fig. 4-5B**). Even at 100-fold excess of inhibitor relative to procaspase-3, we see only ~70% single-site modification. Thus, while procaspase-3 can bind and react with Ac-DEVD-cmk, it is much slower and less specific than labeling of the active site of mature caspase-3.

We next added stoichiometric amounts of Ac-DEVD-cmk to wild-type procaspase-3 (250 nM) with and without 1541 under our standard assay conditions. Under these conditions, no discernible change in the bands for the large and small subunit was present for up to 8 hours by silver stain (**Fig. 4-2D**). At higher wild-type

procaspase-3 concentrations (5 μ M) with sub-stoichiometric amounts of Ac-DEVD-cmk (1 μ M), processing over time was still not observed with or without 1541 by western blot analysis (**Fig. 4-2E**). Thus the proenzyme alone appears minimally capable of intramolecular auto-activation. These results in conjunction with the lack of trans-processing, argue strongly against a model whereby procaspase-3 activation occurs due to auto-proteolysis on fibrils (**Fig. 4-1Bi**).

Caspase-3 is critical for trans activation of procaspase-3- In addition to low concentrations of Ac-DEVD-cmk obliterating procaspase-3 activation, we detected trace amounts of mature caspase-3 by western blot in wild-type procaspase-3 preparations before the start of our activation assays (**Fig. 4-2E**). Together, these results suggest that this cleaved caspase-3 contaminant drives procaspase-3 processing and activation, as diagramed in **Fig. 4-1Bii**.

To further test if trace levels of caspase-3 are critical, a sub-stoichiometric amount of active caspase-3 (5%) was added to the inactive procaspase-3 (C163A). Markedly enhanced processing of the inactive proenzyme was observed in the presence of 1541 fibrils (**Fig. 4-2F**). Control experiments show that the activity of mature caspase-3 against a tetrapeptide substrate (Ac-DEVD-afc) is unaffected by 10 μ M 1541 (**Fig. 4-6**). This indicates that the nanofibrils do not further stimulate the activity of mature caspase-3 but rather promote increased cleavage of procaspase-3 when concentrated on the nanofibrils.

We further explored how trace amounts of caspase-3 affect the kinetics of wild-type procaspase-3 activation. The addition of 25 μ M 1541 to 100 nM wild-type procaspase-3 results in the familiar burst in activity after a 2-hour incubation, using cleavage of Ac-DEVD-afc as a reporter substrate (**Fig. 4-7A**). The rate of procaspase-3 activation upon inclusion of even 1% stoichiometric amount of active caspase-3

drastically shortens the lag period by 2.5-fold to approximately 40 minutes (**Fig. 4-7B**). In contrast, addition of a 1% equivalent of Ac-DEVD-cmk to wild-type procaspase-3 delayed activation to approximately 5 hours (**Fig. 4-7C**). Notably, no enhanced activation was seen in the absence of either 1541 or an upstream protease, granzyme B, for any of these conditions. In sum, these results support the model where mature caspase-3 promotes procaspase-3 processing and activation (**Fig. 4-1Bii**).

1541 fibrils increase the catalytic efficiency of upstream proteases- We further characterized this apparent change in caspase-3 catalytic efficiency against the proenzyme substrate when bound to 1541 fibrils. The catalytically inactive procaspase-3 lacking its 28 amino acid pro-domain (29-277/C163A) was used as the substrate. This construct permits evaluation of the processing rate at the critical activating cut site between the large and small subunit. In a preliminary competition assay with Ac-DEVD-afc, we found that the K_m for cleaving this zymogen substrate is greater than 100 μM (181, Fig. 4-8). Thus, we kept the proenzyme concentration at 200 nM, which is well below the K_m . Using these experimental conditions, we measured the catalytic efficiency (k_{cat}/K_m) for caspase-3 against this zymogen variant in the presence and absence of 1541 to be $4.8 \times 10^4 \text{ M}^{-1} \text{ s}^{-1}$ and $2.8 \times 10^3 \text{ M}^{-1} \text{ s}^{-1}$, respectively (181, Fig. 4-9A and Table 4-1). These data indicate the 1541 fibrils enhance the initial processing of procaspase-3 by caspase-3 by 17-fold.

We next evaluated whether this increase in activity is generalizable to other upstream proteases, such as caspase-8, granzyme-B, and the uncleavable (D9A/D28A/D175A) procaspase-3. Interestingly, the catalytic efficiency for caspase-8 cleaving the zymogen was enhanced 28-fold in the presence of 1541 compared to the absence (k_{cat}/K_m of $7.5 \times 10^5 \text{ M}^{-1} \text{ s}^{-1}$ and $2.7 \times 10^4 \text{ M}^{-1} \text{ s}^{-1}$, respectively) (**Fig. 4-9B and Table 4-1**). For granzyme-B, there was a smaller 5-fold enhancement in the presence compared to absence of 1541 ($4.1 \times 10^5 \text{ M}^{-1} \text{ s}^{-1}$ compared to $8.3 \times 10^4 \text{ M}^{-1} \text{ s}^{-1}$ to,

respectively) (**Fig. 4-9C and Table 4-1**). For the uncleavable procaspase-3 (D9A/D28A/D175A), we detected no cleavage of the simplified zymogen substrate with or without 1541 even up to 10 μ M zymogen (**Fig. 4-9D**). These results highlight the inability of procaspase-3 to auto-process, and reinforce the importance of an active, upstream protease in promoting direct activation of the zymogen.

Procaspase-3 processing by proteases that bind 1541 fibrils- The data above suggests that the activation of procaspase-3 on 1541 fibrils is due to the presence of an active protease. As such, we next evaluated using co-sedimentation assays if these upstream proteases can also associate directly with the fibrils (179, Fig. 4-10A).

Different concentrations of caspase-3 were allowed to bind a fixed concentration of 1541 fibrils. The samples were centrifuged to isolate the fibrils and the proteins bound to them. The supernatant was aspirated, and the pellet was resuspended in LDS loading buffer and analyzed by SDS/PAGE. As seen in **Fig. 4-10A**, caspase-3 binds and saturates the fibrils at roughly the same concentration as procaspase-3, albeit to a lesser extent. Caspase-8 shows slightly better binding and saturation behavior consistent with the greater enhancement in catalytic efficiency seen above. Granzyme B interacts less with the fibrils and shows the smallest change in activity in the presence of the fibrils. These studies support the notion that colocalization of an active protease with the procaspase-3 substrate is important for activation to occur.

This correlation is further established in **Fig. 4-10B**, which shows the rate of processing of the truncated, inactive procaspase-3 (29-277/C163A) by caspase-3, caspase-8, and granzyme B. As expected, very little cleavage of the zymogen was observed by caspase-3 or caspase-8 alone. However, upon the inclusion of 1541, the half-lives ($t_{1/2}$) were greatly reduced to 220 minutes and 8 minutes, respectively. The relative processing rates are consistent with the relative catalytic efficiencies of the respective enzymes. Interestingly, granzyme B has a greater intrinsic catalytic efficiency,

yet 1541 fibrils only reduced the $t_{1/2}$ 4-fold, from 77 minutes to 21 minutes. Despite the catalytic efficiency of granzyme B being greater than caspase-8, it actually cleaves procaspase-3 roughly 2-fold slower in the presence of 1541. This is consistent with colocalization being important for activation, since granzyme B does not bind to the fibrils as well as caspase-8.

We further explored the specificity for binding non-cognate proteases such as Tobacco Etch Virus (TEV) protease or thermolysin. As shown in **Fig. 4-10A**, these proteases do not interact with the 1541 fibrils to a significant degree. Correspondingly, 1541 did not stimulate them to cleave the inactive procaspase-3 (**Fig. 4-10C and 4-10D**). To enable TEV to cleave this zymogen we replaced the caspase cleavage site in the inter-subunit linker with the recognition sequence for TEV protease (D175ENLYFQ). Previous experiments showed this could be cleaved by TEV in the absence of 1541 (174). However, 1541 did not enhance the rate of cleavage of this variant by TEV (**Fig. 4-10D**). Thus, those proteases that can bind *and* colocalize to the fibrils showed dramatic enhancement in processing of procaspase-3. Those that cannot bind to the fibrils showed no enhancement in the rate at which they cleaved the procaspase-3.

Decreased Catalytic Efficiency of Resistance Mutants- In previous studies we identified point mutations in procaspase-3 (S205A or T199A) that reduced activation by 1541, but could still be cleaved and activated by granzyme B (71). We wished to test if the resistance of these constructs could result from either decreased interaction with the fibrils or from diminished catalytic efficiency relative to the wild-type enzyme.

Kinetic studies (**Table 4-2**) show that the catalytic efficiency for cleaving the preferred substrate Ac-DEVD-afc for caspase-3 (S205A) and caspase-3 (T199A) is indeed reduced 8- and 7-fold, respectively. This is mostly due to a significant decrease in the k_{cat} for both constructs. Similar results were shown for Ac-IETD-afc, a tetrapeptide substrate that mimics the cleavage site in the inter-subunit linker of procaspase-3. The

catalytic efficiency against this substrate was reduced by 4- and 14-fold for the S205A and T199A variants, respectively. These reductions in k_{cat}/K_m offset the apparent 17-fold increase in activity that results from colocalization on the fibrils. Furthermore, the procaspase-3 resistant mutants are susceptible to enhanced processing by wild-type caspase-3 in the presence of 1541, which would indicate that the mutant proenzymes still interact with the fibrils (**Fig. 4-11**). Thus, the reduction in catalytic efficiency for these variant enzymes, not binding to the fibrils, largely explains why these mutations lead to greater resistance to 1541-stimulated activation.

Procaspase-3 activation on amyloid- β (1-40) fibrils- In previous studies, we showed that the proteogenic amyloid- β (1-40) fibrils also promoted procaspase-3 activation (179). Here, we sought to determine if the activation mechanism by amyloid- β fibrils is analogous to that of 1541.

First, we wished to determine if there was direct interaction between the fibrils, procaspase-3, and caspase-3. Indeed, procaspase-3, caspase-3, as well as caspase-8 can bind and co-sediment with amyloid- β (1-40) fibrils (**Fig. 4-12A and 4-13**). Next, we sought to evaluate if this association results in increased maturation of the wild-type precursor to a large and small subunit. The amyloid- β fibrils stimulated processing of procaspase-3 as a function of time, albeit about 2 to 4-fold slower than for 1541 (**Fig. 4-12B**). The incubation period before robust procaspase-3 cleavage is more variable for the amyloid- β fibrils, depending on both the batch and the exact preparation (**Fig. 4-14**). Notably, transmission electron microscopy (TEM) studies have shown that amyloid- β (1-40) can also form small oligomers as well as longer fibrils (182,183), whereas 1541 fibrils are longer and more regular (179). This distinction between amyloid- β (1-40) and 1541 fibrils may account for the differences seen in procaspase-3 activation kinetics.

Similar to 1541, the activation of wild-type procaspase-3 on the amyloid- β fibrils is blocked by addition of sub-stoichiometric concentrations of Ac-DEVD-cmk (**Fig. 4-12C**). This is consistent with trace amounts of mature caspase-3 being necessary to drive proenzyme maturation. Furthermore, the amyloid- β (1-40) fibrils also enhance the rate of procaspase-3 (29-277/C163A) processing by exogenous caspase-3 (**Fig. 4-12D**). However, the variability in the rates of activation makes it difficult to evaluate a precise change in the catalytic efficiency of caspase-3 against the zymogen precursor.

Although caspase-8 can bind the amyloid- β (1-40) fibrils, we do not observe a significant change in procaspase-3 processing, in contrast to the 28-fold enhancement seen with 1541 fibrils (**Fig. 4-13**). A number of factors may contribute to the difference in rate and enhancement including the orientation of caspase-8 on the amyloid- β fibrils or its ability to interact with amyloid- β oligomers versus fibrils. The data show amyloid- β (1-40) can enhance processing by promoting colocalization of caspase-3 and procaspase-3, albeit more slowly than for 1541.

Procaspase-3 is an extremely inactive zymogen- Given the fact that we were unable to see any evidence for processing driven in cis or in trans by the proenzyme form, we were motivated to compare the basal activities of procaspase-3 and caspase-3. Using the standard tetrapeptide substrate, Ac-DEVD-afc, we found that mature caspase-3 has a catalytic efficiency (k_{cat}/K_m) of $7.6 \times 10^5 \text{ M}^{-1} \text{ s}^{-1}$ and a K_m of 12.0 μM , in agreement with previous reports (184,185,186, Table 4-3).

We found that the catalytic efficiency of our preparation of wild-type procaspase-3 ($4.9 \times 10^1 \text{ M}^{-1} \text{ s}^{-1}$) is roughly 15,000-fold less than the mature enzyme (**Table 4-3**). However, the K_m measured (9.8 μM) is suspiciously similar to the cleaved caspase-3 (12.0 μM). This data prompted us to determine if the procaspase-3 activity that we observed was dominated by a caspase-3 contaminant. Indeed, the addition of 1%

stoichiometric equivalent of Ac-DEVD-cmk inhibitor to 5 μM procaspase-3 reduced the activity against Ac-DEVD-afc to undetectable levels. Control studies show that the addition of 5% of Ac-DEVD-cmk to caspase-3 minimally impacted its catalytic efficiency.

To estimate the amount of caspase-3 contaminant in our wild-type procaspase-3 preparation, we took 5 μM of the proenzyme and added a dilution series of Ac-DEVD-cmk. After a 60-minute incubation with the inhibitor, 100 μM Ac-DEVD-afc was added to each sample. Activity was monitored, and initial rates were plotted versus inhibitor concentration. The initial plateau of the activity was determined to be the concentration of contaminating caspase-3 which we estimate at 10 nM cleaved caspase-3, or a 0.2% contaminant (**Fig. 4-15**).

Notably, restricting procaspase-3 processing over long incubation times required about 25-fold excess of the Ac-DEVD-cmk inhibitor over the 0.2% caspase-3 contaminant. For example, addition of 50 nM Ac-DEVD-cmk (1%) to 5 μM wild-type procaspase-3 does not completely restrict maturation of the proenzyme (**Fig. 4-16**). However, >5% Ac-DEVD-cmk does restrict any detectable processing by western blot over a 24-hour period (**Fig. 4-2E**). Excess inhibitor over the caspase-3 is important since stoichiometric concentrations of Ac-DEVD-cmk will not completely quench the mature caspase-3 (**Fig. 4-5B**), but super-stoichiometric levels will. The half-life of peptidic chloromethylketone inhibitor is less than 15 minutes under our buffer conditions (187, Fig. 4-17), which necessitated greater amounts be used because a small population of mature caspase-3 will dominate the activation process.

We next turned to the triple alanine mutant (D9A/D28A/D175A) of procaspase-3, reasoning that it should be incapable of autocatalytic maturation (62). Consistent with previous reports, we found a catalytic efficiency roughly 3,000-fold lower for the triple mutant ($2.8 \times 10^2 \text{ M}^{-1} \text{ s}^{-1}$) relative to the mature enzyme (**Table 4-3**). However, the K_m

value for the uncleavable procaspase-3 (11.2 μM) was suspiciously similar to caspase-3. Unexpectedly, we found a drastic decrease in the catalytic efficiency upon the addition of 1% Ac-DEVD-cmk to $3.0 \text{ M}^{-1} \text{ s}^{-1}$, due to a decrease in both K_m and k_{cat} . These kinetic values reduced further to $1.0 \text{ M}^{-1} \text{ s}^{-1}$ upon the inclusion of 5% Ac-DEVD-cmk (**Table 4-3**). Since such low concentrations of Ac-DEVD-cmk do not covalently modify procaspase-3 (**Fig. 4-5**), there appears to be at least two contaminant populations present in the uncleavable procaspase-3 preparations. The initial drop in activity by 90-fold suggests a population of mature caspase-3 that binds Ac-DEVD-cmk well, similar to the fully mature caspase-3. In contrast, a second population of cleaved caspase-3 appears to be present that does not bind tightly to the inhibitor, as shown by the subsequent smaller 3-fold drop in activity (see supplemental discussion and **Fig. 4-18**).

This population, which is resistant to inhibition by Ac-DEVD-cmk and retains some activity, appears to also be present in recombinant mature caspase-3 but not the inactive procaspase-3 (C163A) (**Fig. 4-18**). This indicates that the second contaminant is also a cleavage product of full-length proenzyme. There are several possible explanations for the identity of this population. First, it could simply be an alternative cleavage site in the inter-subunit linker that generates a less active enzyme. This would be consistent with previous studies on procaspase-7 (188). Second, caspase-3 and procaspase-3 are both dimers. It is possible that the less active species is the hemi-cleaved dimer. Previous reports have also described this intermediate in procaspase-7 (189,190). The kinetics of these analogous procaspase-3 cleavage products have yet to be explored.

We believe these contaminants derive from low-level proteolysis of the uncleavable procaspase-3 (D9A/D28A/D175A) during expression in *E. coli* (**Fig. 4-19 and 4-20**). To further explore this, we expressed this construct for 2.5 hours, as opposed to the typical 8-hour expression time. The catalytic efficiency of the uncleavable

procaspase-3 from the shorter expression time was roughly 80-fold lower than the uncleavable procaspase-3 described above (**Table 4-3**). Again, no activity was detectable upon the addition of 1% Ac-DEVD-cmk. Repeat batches of the uncleavable procaspase-3 yielded zymogens that were inactive up to 50 μ M of the proenzyme in the presence of 1% Ac-DEVD-cmk (**Fig. 4-21**).

We next looked at the amount of caspase-3 contaminant in 10 μ M uncleavable procaspase-3 (D9A/D28A/D175A), expressed for 2.5 hours. Again, dosing in Ac-DEVD-cmk to determine where the activity plateaued, we estimate a 40 nM contamination of caspase-3 (0.4%). Using a similar approach, we observed at least two distinct contaminants in the batch of uncleavable procaspase-3 expressed for 8 hours, consistent with the kinetic observations described (**Fig. 4-15**).

High zymogenicity of procaspase-3- Since we could largely mitigate the contribution of these cleaved contaminants to procaspase-3 activity using Ac-DEVD-cmk, we next explored the magnitude to which the proenzyme is held in an inactive state. Zymogenicity, which is the ratio of the activity of a mature enzyme to the activity of its precursor, describes the extent to which an enzyme is trapped as its inactive precursor (191,192). Larger values for the zymogenicity signify a more restrained proenzyme. Previous measurements for the zymogenicity of procaspase-3 have been estimated at >10,000 (139,180). While signifying a very inactive zymogen, our experiments would actually indicate that the proenzyme is restrained to an even greater extent with a zymogenicity >10,000,000, essentially the detection limit of the assay (**Table 4-4**).

This zymogenicity value is determined by comparing the maximum concentration of procaspase-3 (50 μ M) where we observed no activity, to the limit of detection in our catalytic efficiency assays against Ac-DEVD-afc. Since we do not observe any activity

for the proenzyme, our assessment of procaspase-3 zymogenicity includes the assumption that the K_m is similar for both the mature enzyme and its precursor. This approximation is a lower limit since our results above suggest that the K_m for procaspase-3 against Ac-DEVD-afc is actually much greater than caspase-3. We next evaluated the limit of detection by diluting caspase-3 to a concentration (5 pM) where no activity could be observed against Ac-DEVD-afc (**Fig. 4-22**). This is a conservative estimate since dilute enzymes can associate with the surface of assay plates. Even with the conservative approximations, the ratio of these two values gives us a zymogenicity > 10^7 .

Discussion

Procaspase-3 is activated by initiator proteases on synthetic and natural scaffolds- Our studies demonstrate the importance of scaffolding for colocalization of procaspase-3 with active proteases to promote explosive activation on synthetic and natural fibrils. A collection of experiments, including co-sedimentation studies with 1541 and amyloid- β (1-40) fibrils, mutational studies on procaspase-3, and thorough biochemical characterization of procaspase-3 activity, show that procaspase-3 activation does not happen to any extent here by procaspase-3 alone (**Fig. 4-1Bi**). Instead, proenzyme maturation requires a small amount of an activated caspase to bind and colocalize with the procaspase-3 on an ordered fibril scaffold (**Fig. 4-1Bii**). After a lag, activation proceeds explosively due to autocatalytic maturation of the proenzyme. This cascade is possibly enhanced by an ordered array of neighboring procaspases on the fibrils that may ignite like a fuse in a one-dimensional process down the fibril. Further work will be required to distinguish these details.

Interestingly, procaspase-3 activation by upstream proteases on 1541 nanofibrils exhibits some protease specificity. For example, the 1541 nanofibrils show the greatest enhancement and binding for the most robust initiator, caspase-8, followed by caspase-3 and granzyme-B. We show that this colocalization of procaspase-3 with active proteases results in an effective change in the catalytic efficiency of the upstream protease for processing the proenzyme. However, 1541 nanofibrils do not enhance proteolysis for some non-cognate proteases like thermolysin or TEV protease, even when presented to procaspase-3 variants containing consensus TEV protease cleavage sites in place of the natural caspase cleavage site.

The specificity of this process seems to also be at the level of the chemical composition of the fibril. Previous and unpublished studies show fibril-forming variants of 1541 can be specific for activation of individual executioner procaspases-3, -6 and -7

(71,179, unpublished results). We show here that procaspase-3 can be activated on amyloid- β (1-40) fibrils by a similar mechanism as on 1541 fibrils. Additional studies to explore the influence of different fibrillar structures on the catalytic efficiency of various upstream proteases against procaspase-3 would be instructive in identifying biologically relevant scaffolds.

Since the caspases initiate fate-determining transformations in the cells, it is intuitive that their activity would be highly restricted in the absence of a signaling event (145). Procaspases are classically recruited and activated on scaffolding complexes, such as the apoptosome, the inflammasome, and the DISC (61,145,148). The induced proximity model that describes clustering and activation of procaspase-8 and procaspase-9 upon localization to such platforms illustrates a similar model for procaspase-3 activation (180,193). Our data further suggests that procaspase-3 recruitment alone is not sufficient for auto-activation, but induced proximity to an active caspase facilitates maturation of the proenzyme.

Previous confocal microscopy studies have also illustrated a direct interaction between caspases and intracellular fibular structures. For example, caspase-9 and caspase-3 appear to colocalize with cytokeratin 18 in epithelial cells upon addition of an apoptotic inducer (164,194). Also, the Death Effector Domain (DED) motifs in the prodomain of caspase-8 can assemble into filaments in cells to promote apoptosis (195,196). Our results support that fibrils can serve as a platform for procaspase localization and maturation *in vitro*. However, further studies are necessary to understand if these mechanisms apply to the cellular activities of 1541 (71) or amyloid- β fibrils (197,198).

Previous studies demonstrate that enzymes can retain activity upon fibril formation or fibril association. Zymogens in the blood coagulation cascade are also well-

known to be activated on fibers. For example, tissue plasminogen activator (tPA) is stimulated by fibrinogen and more dramatically by fibrin (162). Remarkably, amyloid- β fibrils also enable activation of tPA (160). Furthermore, distinct aggregation states and cleavage products of the amyloid- β precursor protein have distinct impact on tPA's catalytic efficiency against its substrate plasminogen. This observation has implicated amyloid- β fibrils in the pathogenesis of hereditary cerebral hemorrhage with amyloidosis-Dutch type.

Importance of zymogenicity in the mechanism of caspase activation- Numerous structural and biochemical studies have delineated the unique mechanisms for maintaining proteases as inactive zymogens (172). Such mechanisms include an N-terminal domain that may occlude substrate from docking, a conformational change that may alter or disorder substrate binding or catalytic residues, and oligomerization or interaction with an activating partner protein or small molecule (144). In almost all cases, a proteolytic processing event is critical for activation of the proenzyme by another protease.

Interestingly, different proteases are locked in this inactive state to variable extents (180). The extent to which a zymogen is trapped in an inactive state is expressed as a ratio of the mature enzyme activity to that of its precursor (192). This ratio, also called the zymogenicity, is summarized in **Table 4-4** for some well-characterized proteases. For example, tissue plasminogen activator (t-PA) exhibits a zymogenicity between 2-10, which reflects a relatively small difference between the activity of the cleaved form and its full-length precursor (199-202). In stark contrast, trypsinogen and chymotrypsinogen are largely inactive, which is revealed by zymogenicities on the order of 10^4 to 10^6 (203,204). While the precursors for trypsin and chymotrypsin display nominal activity *in vitro*, their cellular regulation is believed to be

due to processing from upstream proteases. Other proteases have intermediate values such as Factor XIIa, which has a zymogenicity value of 4000 (205). The tremendous range in zymogenicity values likely reflects on the *in vivo* function and activation of the proteases (110).

In this study, we reassessed the zymogenicity barrier of procaspase-3. Our results suggest that procaspase-3 is at least three orders of magnitude less active than previous reports based upon the activity of the uncleavable mutant (D9A/D28A/D175A) (139,180). Key to this assessment was the unexpected discovery that active caspase-3 is present in preparations of the “uncleavable” procaspase-3 (D9A/D28A/D175A). The active product was probably generated from non-caspase proteolysis during recombinant expression. When the trace contaminants were inactivated using sub-stoichiometric amounts of the active site inhibitor, Ac-DEVD-cmk, we detected no activity. Based on the limit of detection of the assay, we estimate the activity for procaspase-3 to be >10,000,000 fold less active than mature caspase-3.

This is comparable or greater than the most inactive zymogens characterized, chymotrypsinogen and trypsinogen. This may not be surprising given the fact that caspase-3 executes the final and fate-determining stages of apoptosis. Moreover, this high zymogenicity barrier probably accounts for the lack of any evidence for procaspase-3 auto-processing, reported above. Precursors that exhibit such high zymogenicities have typically required harsh conditions *in vitro* to observe any activity. Studies with trypsinogen and chymotrypsinogen used high enzyme concentrations in the micromolar to millimolar range, low pH conditions, high ionic strength buffers, and long time courses on the orders of days to detect any processing by these precursors (143,204,206,207). In a similar vein, earlier reports demonstrate that procaspase-3 may similarly adopt an active conformation (62).

Challenges for small molecule discovery- Our results strongly suggest that auto-activation of procaspase-3 is extremely restricted or non-existent under typical cellular concentrations, ~100 nM. Activation almost certainly requires at least trace amounts of active caspase or an upstream protease to trigger processing. Based on the zymogenicity approximation here and modeling activation curves using the Michaelis-Menten equation, we estimate a small molecule activator would need to stimulate the activity of the proenzyme over 1,000-fold to generate 0.2% fractional activity to promote autocatalytic maturation of the entire procaspase-3 population within a 24 hour period. Even increasing the enzyme concentration 10-fold, to super-physiological levels (1 μ M), would only decrease this barrier to ~100-fold.

The high energetic zymogenicity barrier indicates a challenging endeavor for a small molecule to directly bind and activate procaspase-3. From our results, procaspase-3 maturation is critically dependent on the presence of active caspase. Others have reported small molecule activators of procaspase-3. In the case of PAC-1, this small molecule is proposed to function by removing an inhibitory Zn^{2+} ion (70). Clark and co-workers report another compound identified using a DOCK screen (208). This small molecule activator is proposed to bind to an allosteric site on procaspase-3 to promote activation. Additional studies will be important to elucidate if any of these compounds work by a direct activation of the proenzyme or act on the trace contaminants of mature caspase-3 to initiate the process.

The above considerations do not mean that one cannot activate a protease precursor with a small molecule. In fact, an endogenous small molecule, inositol hexaphosphate ($InsP_6$), is known to bind an allosteric site on the cysteine protease domain (CPD) of MARTX_{Vc} toxin to promote activation (52). It would be interesting to explore the zymogenicity of the CPD. Perhaps enzymes with low zymogenicity values would be better candidates for small molecule activator discovery.

Furthermore, our results suggest that increasing the activity of the mature caspase-3 or another upstream protease may also promote activation of the procaspase-3. Previous studies have demonstrated conformational flexibility of the mature caspases (63,64). As little as a two-fold change in the catalytic efficiency of caspase-3 would be enough to promote autocatalytic maturation of the proenzyme with a 0.2% contaminant. Finally, these studies also suggest that facilitating an ordered oligomerization or colocalization of procaspase-3 with the mature caspase-3 would also stimulate activation. The latter two approaches, however, depend on the cellular concentrations of both pro- and mature enzymes and are not direct activators of the proenzyme. Interestingly, successful engineering approaches have been described for both these strategies for the caspases (174,209-213).

Materials and Methods

Materials- The mature caspase-3 antibody (9664) was purchased from Cell Signaling. Thermolysin and 1,1,1,3,3,3-hexafluoro-2-propanol (HFIP) were purchased from Sigma. Amyloid- β (1-40) was purchased from AnaSpec. Ac-DEVD-afc (acetyl-Asp-Glu-Val-Asp-7-amino-4-trifluoromethylcoumarin) was purchased from SM Biochemicals LLC. Isopropyl β -D-thiogalactoside (IPTG) and Ac-DEVD-cmk (acetyl-Asp-Glu-Val-Asp-chloromethylketone) were purchased from Calbiochem. Z-VAD-fmk (Z-Val-Ala-Asp-fluoromethylketone), Ac-IETD-afc (acetyl-Ile-Glu-Thr-Asp-7-amino-4-trifluoromethylcoumarin), and AFC (7-amino-4-trifluoromethyl coumarin) were purchased from Enzo Life Sciences. The pET23b and pET15b vectors were purchased from Novagen. Granzyme B was a generous gift from Dan Hostetter and Cheryl Tajon in the Craik lab at the University of California, San Francisco (UCSF). Tobacco Etch Virus (TEV) protease was a generous gift from Charlie Morgan, and procaspase-3 (D175ENLYFQ) that has a TEV cleavage site inserted at the inter-subunit linker was a generous gift from Dan Gray in the Wells lab at UCSF. All additional reagents were purchased from Sigma, unless otherwise noted.

Constructs- Full-length human procaspase-3, -6, -7, and -9 genes were cloned into pET23b, as previously described (71,168). Truncated procaspase-8 (217-479), lacking the death effector domains, was cloned into pET15b. Truncated procaspase-3 (29-277), lacking the pro-domain, was cloned into pET23b. Quick-Change mutagenesis (Stratagene) on the above constructs was used to generate the catalytically-inactive procaspase-3 (C163A), the catalytically-inactive, truncated procaspase-3 (29-277/C163A), the uncleavable procaspase-3 (D9A/D28A/D175A), procaspase-3 (T199A), procaspase-3 (S205A), and catalytically-inactive, TEV-cleavable procaspase-3 (D175ENLYFQ/C163A).

Expression/Purification- For expression, all plasmids were transformed into the bacterial strain BL21 (DE3) pLysS. Wild type, full-length procaspase-3 was expressed and purified as previously described (71,168). Briefly, bacterial cells were grown at 37°C to an OD_{600nm} of ~0.6, and subsequent overexpression was induced with 0.2 mM IPTG at 30°C for 20 min. Cells were rapidly harvested and lysed. The clarified cell lysate was purified using a Ni-NTA affinity column, followed by anion-exchange chromatography. Purified procaspase-3 fractions were collected and stored at -80°C.

Caspase-3 was overexpressed at 30°C for 5 hours from cells transformed with the pET23b containing full-length procaspase-3. Caspase-3 (T199A) and caspase-3 (S205A) were similarly overexpressed at 30°C overnight from the respective full-length constructs. Caspase-8 was overexpressed at 12°C overnight from cells transformed with the pET15b containing procaspase-8 (217-479). Caspase-9 was overexpressed at 18°C overnight from cells transformed with the pET23b containing full-length procaspase-9. All mature caspases were purified as described for procaspase-3.

All other constructs followed the same expression and purification protocols as wild-type procaspase-3 with only the overexpression time modified as follows: catalytically-inactive procaspase-3 (C163A) – 15 hours; catalytically-inactive, truncated procaspase-3 (29-277/C163A) – 5 hours; catalytically-dead, TEV-cleavable procaspase-3 (D175ENLYFQ/C163A) – 5 hours; and uncleavable procaspase-3 (D9A/D28A/D175A) – 2 to 8 hours (exact conditions described in the text).

Synthesis of 1541- Synthesis, purification, and characterization of 1541 were performed as previously described (71).

Procaspase-3 processing assay (71)- Wild-type procaspase-3 was agitated in a caspase activity buffer (50 mM HEPES, pH 7.4, 50 mM KCl, 0.1 mM EDTA, 10 mM DTT, and 0.1% CHAPS) with 1541 or 2% DMSO alone for the indicated time intervals. Subsequent assays with procaspase-3 also included a 15-minute pre-incubation with the irreversible inhibitor, Ac-DEVD-cmk, at the specified concentrations. Samples were quenched with LDS loading buffer, and analyzed by SDS/PAGE. Protein bands were visualized by either silver stain analysis or western blot.

Procaspase-3 trans-activation assays (62,70)- The uncleavable procaspase-3 (D9A/D28A/D175A) or mature caspase-3 was agitated at 37°C with the catalytically-inactive procaspase-3 (C163A) in a caspase activity buffer (50 mM HEPES, pH 7.4, 50 mM KCl, 0.1 mM EDTA, 10 mM DTT, and 0.1% CHAPS) in the presence or absence of 1541. The irreversible inhibitor, Ac-DEVD-cmk, was added under the designated conditions to quench any cleaved caspase-3 impurity present in the uncleavable procaspase-3 expression. Samples were quenched with LDS loading buffer, and analyzed by SDS/PAGE. Protein bands were visualized by either silver stain analysis or western blot.

Procaspase-3 self-activation assays (71)- Wild-type procaspase-3 was pre-incubated for 15 minutes with DMSO alone or 1 nM Ac-DEVD-cmk in a caspase activity buffer (50 mM HEPES, pH 7.4, 50 mM KCl, 0.1 mM EDTA, 10 mM DTT, and 0.1% CHAPS). 1541 or DMSO was added to the corresponding samples and incubated at 37°C. Granzyme B (2 nM) was added to wild-type procaspase-3 to determine maximal activation levels possible. At the indicated time points, 50 μ M Ac-DEVD-afc was added to each sample, and fluorescence intensity was monitored on a SpectraMax M5 (Molecular Devices) plate reader. Initial rates were plotted at each time point using Prism v5.0c.

Caspase activity assays- The activities of procaspase-3, procaspase-3 (D9A/D28A/D175A), caspase-3, caspase-3 (S205A), and caspase-3 (T199A) were measured as previously described (59,71,138-140). Briefly, 5 μ M procaspase-3, 0.1, 10, 20, and 50 μ M procaspase-3 (D9A/D28A/D175A), 5 and 10 nM caspase-3, 5 and 10 nM caspase-3 (S205A), and 5 and 10 nM caspase-3 (T199A) were incubated in a caspase activity buffer (50 mM HEPES, pH 7.4, 50 mM KCl, 0.1 mM EDTA, 10 mM DTT, and 0.1% CHAPS). Processing of the fluorogenic substrate Ac-DEVD-afc was used to monitor activity. K_m and V_{MAX} values were determined from plots of initial rates versus substrate concentration in Prism v5.0c. Curves were fit using the standard Michaelis-Menten equation. V_{MAX} values were transformed into k_{cat} values using a linear plot of the fluorescence intensity of the AFC standard versus concentration. Sub-stoichiometric concentrations of Ac-DEVD-cmk were incorporated into subsequent assays to evaluate the impact of low levels of the cleaved caspase on procaspase activity.

Covalent modification of (pro)caspase-3- The extent of covalent modification of procaspase-3 and caspase-3 by Ac-DEVD-cmk was evaluated using an LCT-Premier LC/electrospray ionization-MS instrument (Waters) after 24 h incubation in assay buffer (50 mM HEPES, pH 7.4, 50 mM KCl, 0.1 mM EDTA, and 10 mM DTT).

Calculation of autocatalytic activation curves- To estimate autocatalytic conversion of procaspase-3 to active caspase-3, we fit our experimental data to the classic Michaelis-Menten equation:

$$v = (V_{max} * [S]) / (K_M + [S]).$$

Iterative application of this equation every minute of the reaction enabled us to estimate

the instantaneous levels of procaspase-3 and caspase-3. Additionally, we evaluated how these factors would change in response to various catalytic efficiencies and different amounts of contaminating active caspase-3. The assumptions we have input for this model are: $k_{cat} = 23.5 \text{ min}^{-1}$ for mature caspase-3, $k_{cat} = 23.5 \text{ min}^{-1} * (10^{-7})$ for procaspase-3, $K_m = 140 \text{ }\mu\text{M}$ for both caspase-3 and procaspase-3, and $[S_0] = 100 \text{ nM}$ or $1 \text{ }\mu\text{M}$ (procaspase-3). Initial levels of caspase-3 were set at 0 or 0.2% of $[S_0]$.

Co-sedimentation assays with 1541 (156,179)- 20 μL 0.5 mM 1541 or DMSO alone was added to 1 mL 0.128, 0.064, 0.032, 0.016, 0.008, 0.004, 0.002, 0.001, and 0 mg/mL procaspase-3, caspase-3, caspase-8, caspase-9, or TEV protease in a caspase assay buffer (20 mM HEPES, pH 7.4, 10 mM KCl, 1.5 mM MgCl_2 , 1 mM DTT, 1.5% Sucrose, and 0.1% CHAPS). 10 μL 0.5 mM 1541 was added to 500 μL 0.016, 0.008, 0.004, 0.002, 0.001, and 0 mg/mL granzyme B in a caspase assay buffer (50 mM HEPES, pH 7.4, 50 mM KCl, 0.1 mM EDTA, 1 mM DTT, and 0.1% CHAPS). Thermolysin was dissolved in 2.5 M NaCl and 10 mM CaCl_2 to 1.28, 0.64, 0.32, 0.16, 0.08, 0.04, 0.02, 0.01, and 0 mg/mL, and diluted 10x into a caspase assay buffer (20 mM HEPES, pH 7.4, 10 mM KCl, 1.5 mM MgCl_2 , 1 mM DTT, 1.5% Sucrose, and 0.1% CHAPS) to a final volume of 1 mL. 20 μL 0.5 mM 1541 or DMSO was next added to the thermolysin mixtures. All samples were vortexed and immediately centrifuged at 16,200xg for 15 minutes. The supernatant was aspirated, and 100 μL assay buffer was added to the pellet in each tube. Samples were diluted with 4x LDS sample buffer (Life Technologies) and analyzed by SDS/PAGE. Bands were visualized by coomassie (Bio-Rad) stain, imaged on a LI-COR Odessey Infrared Imaging System, and quantified by ImageJ. Granzyme B samples were normalized for direct comparison to other enzymes.

Rate of procaspase-3 processing by upstream proteases- 20 μ L 0.5 mM 1541 or DMSO alone was added to 1 mL 200 nM procaspase-3 (29-277/C163A) in a caspase activity buffer (20 mM HEPES, pH 7.4, 10 mM KCl, 1.5 mM MgCl₂, 1 mM DTT, 1.5% Sucrose, and 0.1% CHAPS). 2 nM caspase-8, 2 nM caspase-3, 20 nM TEV, or 200 nM TEV was subsequently added. Aliquots from each sample were taken at the indicated time points, quenched with LDS loading buffer, and analyzed by SDS/PAGE. Protein bands were visualized by silver stain and quantified by ImageJ.

Similarly, 20 μ L 0.5 mM 1541 or DMSO was added to 1 mL 200 nM procaspase-3 (29-277/C163A) in a caspase activity buffer (50 mM HEPES, pH 7.4, 50 mM KCl, 0.1 mM EDTA, 1 mM DTT, and 0.1% CHAPS), 2 nM granzyme B was added, and processing was monitored as described above.

Finally, procaspase-3 (29-277/C163A) susceptibility to processing by thermolysin was determined, as previously described (214). Briefly, thermolysin was dissolved in 2.5 M NaCl and 10 mM CaCl₂ to 0.5 mg/mL or 0.05 mg/mL. 100 μ L 10 μ M procaspase-3 (29-277/C163A) was added to 860 μ L caspase buffer. 20 μ L 2.5 mM 1541 or DMSO was subsequently added, followed by 20 μ L of the specified thermolysin stocks. Processing was monitored over time as described above except using Sypro Ruby protein gel stain (Life Technologies).

Catalytic efficiency of procaspase-3 cleavage (181,215)- 50 μ L 2 μ M procaspase-3 (29-277/C163A) followed by 10 μ L 0.5 mM 1541 or DMSO were added to 390 μ L buffer (20 mM HEPES, pH 7.4, 10 mM KCl, 1.5 mM MgCl₂, 1 mM DTT, 1.5% Sucrose, and 0.1% CHAPS) in 12 separate 1.5 mL eppendorf tubes. 50 μ L of a dilution series of an upstream protease was added last to corresponding samples to initiate the reaction. We agitated the samples at 37°C for 1 hour and quenched the reactions with LDS loading

buffer. We subsequently analyzed the samples by SDS/PAGE followed by silver stain to visualize the bands. We quantified the disappearance of the substrate with enzyme concentration and established the concentration of an upstream protease corresponding to 50% cleavage ($E_{1/2}$). Assuming pseudo-first order kinetics, the following equation gives an approximate catalytic efficiency (k_{cat}/K_m):

$$k_{cat}/K_m = \ln(2) / (E_{1/2} * t).$$

Amyloid- β (1-40) preparation- A β (1-40) fibrils were formed as previously described (170,179). Briefly, 250 μ L of a caspase activity buffer (20 mM HEPES, pH 7.4, 10 mM KCl, 1.5 mM MgCl₂, 1.5% Sucrose, 10 mM DTT, 0.1% CHAPS) was added to the lyophilized solid to 50 μ M. The peptide was agitated at 37°C for 4-6 hours. Fibril formation was confirmed by an increase in fluorescence intensity upon the addition of 15 μ L of sample to 250 μ L 5 μ M Thioflavin T (Sigma-Aldrich).

Procaspase-3 processing with A β (1-40)- 250 nM procaspase-3 was agitated in a caspase activity buffer (20 mM HEPES, pH 7.4, 10 mM KCl, 1.5 mM MgCl₂, 1.5% Sucrose, 10 mM DTT, 0.1% CHAPS) with 20 μ M A β (1-40) fibrils (4 h pre-incubation) or buffer alone for the indicated time intervals. Processing was monitored by SDS/PAGE as described above.

Trans-activation of procaspase-3 with A β (1-40)- 5 nM caspase-3 was agitated with 200 nM procaspase-3 (29-277/C163A) in a caspase activity buffer (20 mM HEPES, pH 7.4, 10 mM KCl, 1.5 mM MgCl₂, 1.5% Sucrose, 10 mM DTT, 0.1% CHAPS) with 20 μ M A β (1-40) fibrils (4 h pre-incubation) or buffer alone for the indicated time intervals. Processing was monitored by SDS/PAGE as described above.

Co-sedimentation of caspases with A β (1-40)- 50 μ M A β (1-40) peptide or buffer alone was incubated at 37°C for 6 hours. 50 μ L 1.0 mg/mL procaspase-3, caspase-3, caspase-8, caspase-9, and caspase-6 was added to 450 μ L 20 μ M A β (1-40) fibrils (6 h pre-incubation). The samples were vortexed briefly and centrifuged at 20,817xg for 20 minutes. The supernatant was aspirated, and 100 μ L assay buffer was added to the pellet in each tube. The amount of enzyme in each pellet was assessed as described for 1541 samples above.

Acknowledgements

We thank O. Julien for support and for critically reviewing the manuscript. We thank D. Hostetter and C. Tajon from the Craik lab at UCSF for providing granzyme B. We thank the Wells lab and the Small Molecule Discovery Center at UCSF for useful suggestions. This research was supported by grants from the National Institutes of Health (R01 CA136779), the National Cancer Institute (F32 CA119641-03 to D.W.W.), the National Institutes of Health (F32 AI077177 to N.J.A.), an ARCS Foundation Award (to J.A.Z.), and a Schleroderma Research Foundation Evin-Wright Fellowship (to J.A.Z.).

Footnotes

The abbreviations used are as follows: 1,1,1,3,3,3-hexafluoro-2-propanol, HFIP; Amyloid- β (1-40), A β (1-40); acetyl-Asp-Glu-Val-Asp-7-amino-4-trifluoromethylcoumarin), Ac-DEVD-afc; Isopropyl β -D-thiogalactoside, IPTG; acetyl-Asp-Glu-Val-Asp-chloromethylketone, Ac-DEVD-cmk; Z-Val-Ala-Asp-fluoromethylketone, Z-VAD-fmk; acetyl-Ile-Glu-Thr-Asp-7-amino-4-trifluoromethylcoumarin, Ac-IETD-afc; 7-amino-4-trifluoromethyl coumarin, AFC; Tobacco Etch Virus, TEV.

Protease	1541 (μM)	Time (min)	$k_{\text{cat}}/K_{\text{M}}$ ($\text{M}^{-1}\text{s}^{-1}$)	Ratio
Caspase-3	0	60	2.8×10^3	
Caspase-3	10	60	4.8×10^4	17
Caspase-8	0	20	2.7×10^4	
Caspase-8	10	20	7.5×10^5	28
Granzyme B	0	90	8.3×10^4	
Granzyme B	10	90	4.1×10^5	5

Table 4-1. 1541 fibrils increase the catalytic efficiency of upstream proteases.

Construct	K_M (μM)	kcat (s⁻¹)	kcat/K_M (M⁻¹s⁻¹)	Ratio
<i>Ac-DEVD-AFC</i>				
Wild-type	12.0 ± 0.7	9.11 ± 0.15	7.6 × 10 ⁵	1.0
T199A	16.2 ± 0.9	1.46 ± 0.02	9.1 × 10 ⁴	0.14
S205A	5.9 ± 0.3	0.63 ± 0.01	1.1 × 10 ⁵	0.12
<i>Ac-IETD-AFC</i>				
Wild-type	140 ± 10	2.25 ± 0.04	1.6 × 10 ⁴	1.0
T199A	100 ± 10	0.12 ± 0.01	1.2 × 10 ³	0.07
S205A	56 ± 3	0.25 ± 0.01	4.4 × 10 ³	0.27

Table 4-2. Decreased catalytic efficiency of caspase-3 resistance mutations.

Construct	I/E [*]	K _M (μM)	kcat (s ⁻¹)	kcat/K _M (M ⁻¹ s ⁻¹)
Caspase-3	0	12.0 ± 0.7	9.11 ± 0.15	7.6 × 10 ⁵
Caspase-3	0.05	13.3 ± 0.6	9.34 ± 0.14	7.0 × 10 ⁵
Pro-3 (D ₃ A) [¶]	0	11.2 ± 0.4	0.0031 ± (1.0 × 10 ⁻⁴)	2.8 × 10 ²
Pro-3 (D ₃ A) ^{‡, ¶}	0.01	370 ± 30	0.00098 ± (1.0 × 10 ⁻⁴)	<3.0
Pro-3 (D ₃ A) ^{‡, ¶}	0.05	890 ± 190	0.00069 ± (1.2 × 10 ⁻⁴)	<1.0
Pro-3 (WT)	0	9.8 ± 0.7	0.00048 ± (1 × 10 ⁻⁵)	4.9 × 10 ¹
Pro-3 (WT)	0.01		No activity observed.	
Pro-3 (D ₃ A) [†]	0	9.8 ± 0.6	0.00033 ± (1 × 10 ⁻⁵)	3.4 × 10 ¹
Pro-3 (D ₃ A) [†]	0.01		No activity observed.	

^{*}I/E = [Ac-DEVD-cmk] / [Enzyme]. [‡]Saturation is not reached. [¶]Expression time = 8 hours. [†]Expression time = 2.5 hours.

Table 4-3. Mature caspase-3 present with procaspase-3 dominates activity measurements.

Enzyme	Zymogenicity ^{*†}
Tissue Plasminogen Activator	2-10 ^{‡†}
Factor XII	>4000 [†]
Trypsinogen	10 ⁴ to 10 ^{6†}
Chymotrypsinogen	10 ⁴ to 10 ^{6†}
Procaspase-8	>100 [‡]
Prospase-3	>10,000 [‡]
Prospase-3 (Updated)	>10,000,000

*Zymogenicity = Mature protease activity / Zymogen activity.
[†](192), [‡](139), (180)

Table 4-4. Summary of zymogenicity values.

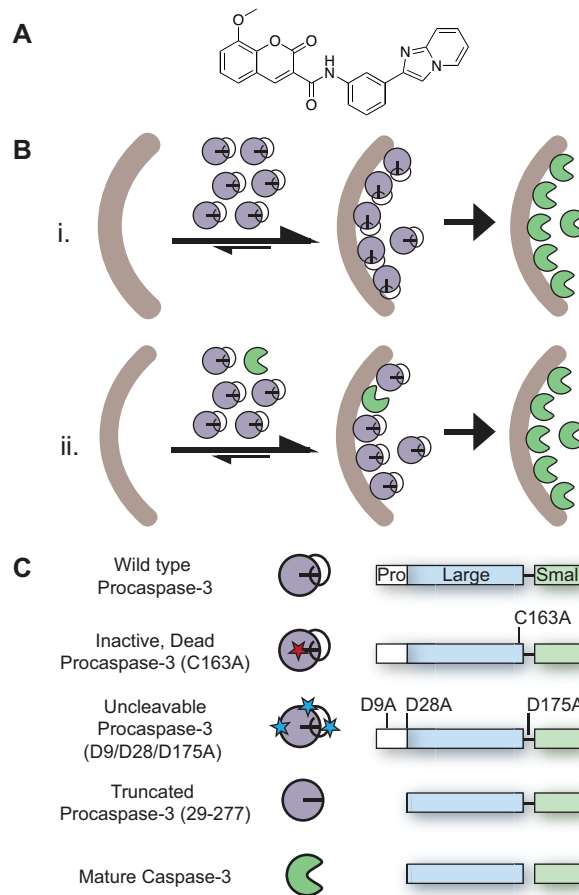


Figure 4-1. Possible models of procaspase-3 processing on 1541 fibrils. (A) Structure of compound 1541. (B) i. 1541 fibrils stimulate either cis- or trans- activation of the proenzyme alone. ii. Either trace amounts of mature caspase-3 or an exogenously added protease promotes processing and activation of procaspase-3 upon colocalization to 1541. (C) Procaspase-3 constructs used to explore potential activation mechanisms. Note, caspases are expressed as constitutive dimers, but illustrated here as monomers for simplicity.

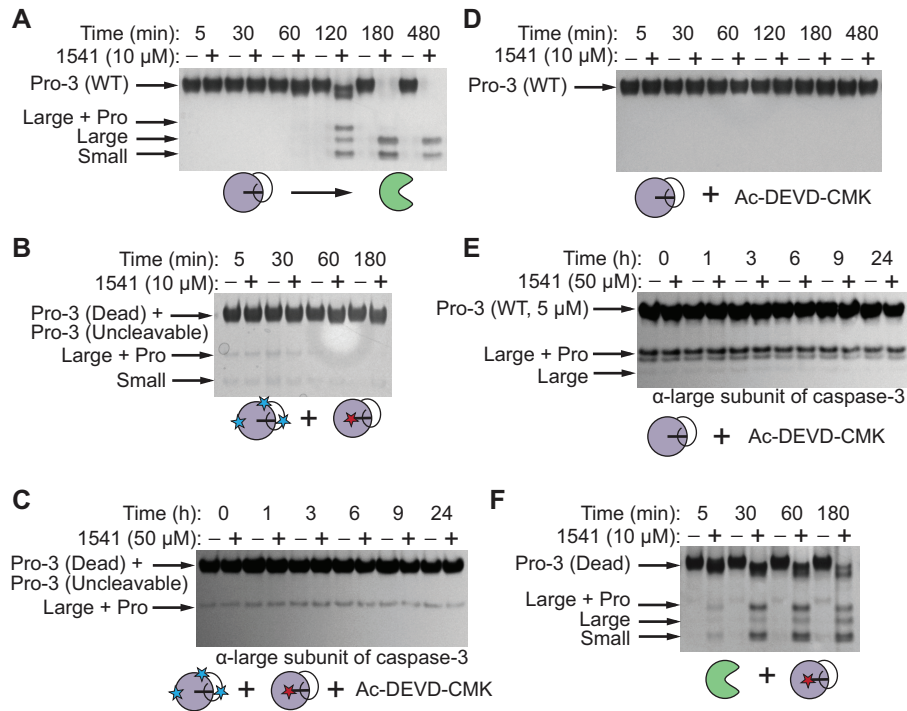


Figure 4-2. Enhanced susceptibility of procaspase-3 to processing by mature caspase-3 in the presence of 1541 fibrils. (A) Activation as a function of time for 250 nM wild-type procaspase-3 in the absence (-) or presence (+) of 10 μ M 1541. (B) Uncleavable procaspase-3 (D9A/D28A/D175A) was incubated with a catalytically inactive procaspase-3 (C163A) with (+) or without (-) 10 μ M 1541. (C) A higher concentration of uncleavable procaspase-3 (5 μ M) was added to 5 μ M dead procaspase-3 in the presence of 5% Ac-DEVD-cmk (250 nM). Processing was monitored by western blot with an antibody specific for the large subunit of cleaved caspase-3. (D) 250 nM Ac-DEVD-cmk, an irreversible inhibitor that selectively labels mature caspase-3 under the assay conditions, was added to 250 nM wild-type procaspase-3. Processing was monitored by silver stain analysis. (E) Similarly, self-activation of a higher concentration of wild-type procaspase-3 (5 μ M) in the presence of 20% (1 μ M) Ac-DEVD-cmk was monitored by western blot. (F) Processing of the inactive procaspase-3 (C163A) upon addition of mature caspase-3 (5 nM) was examined.

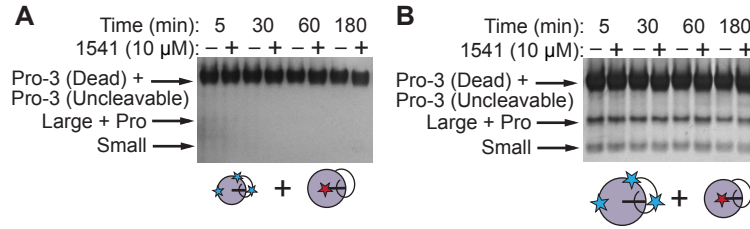


Figure 4-3. No processing of the inactive procaspase-3 (C163A) by the uncleaveable procaspase-3 (D9A/D28A/D175A). Different concentrations of the uncleaveable procaspase-3 were incubated with the inactive procaspase-3 with (+) or without (-) 10 μM 1541. The reactions were quenched with LDS loading buffer at the indicated time points, and analyzed by SDS/PAGE followed by silver stain. (A) 50 nM uncleaveable procaspase-3 added to 250 nM inactive procaspase-3. (B) 1000 nM uncleaveable procaspase-3 added to 250 nM inactive procaspase-3.

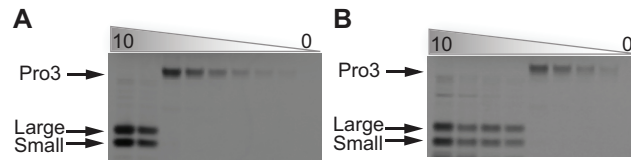


Figure 4-4. Wild-type procaspase-3 can auto-activate at high concentrations. A dilution series of wild-type procaspase-3 (starting at 10 μ M) was incubated at 37°C for (A) 4 hours or (B) 24 hours. The reactions were quenched with LDS loading buffer, analyzed by SDS/PAGE, and visualized by coomassie blue stain.

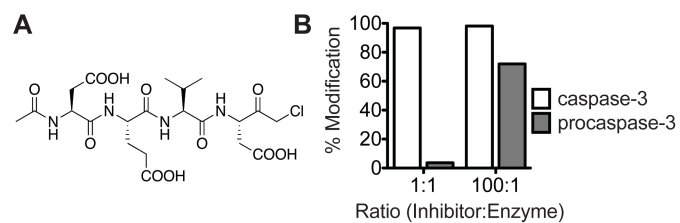


Figure 4-5. Activity-based probe for mature caspase-3. (A) Structure of Ac-DEVD-cmk. (B) 5 μ M or 500 μ M Ac-DEVD-cmk was added to 5 μ M caspase-3 or 5 μ M wild-type procaspase-3. After a 24-hour incubation at 37°C, covalent modification was evaluated by mass spectrometry.

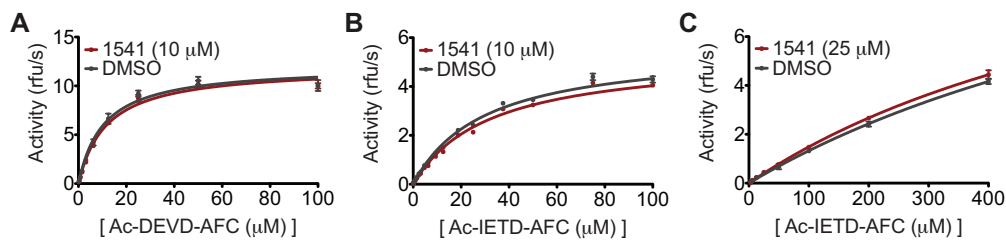


Figure 4-6. The catalytic efficiency of caspase-3, caspase-8, and granzyme B is similar with or without 1541. (A) The catalytic efficiency of caspase-3 (5 nM) against Ac-DEVD-afc was measured in the presence and absence of 10 μM 1541. (B) The catalytic efficiency of capsase-8 (20 nM) against Ac-IETD-afc was monitored with and without 10 μM 1541. Notably, we observe inhibition of caspase-3 and caspase-8 at higher concentrations of 1541 (>30 μM); however, we remained below this value to focus on activation alone. (C) Finally, the catalytic efficiency of granzyme B against Ac-IETD-afc was measured with and without 25 μM 1541.

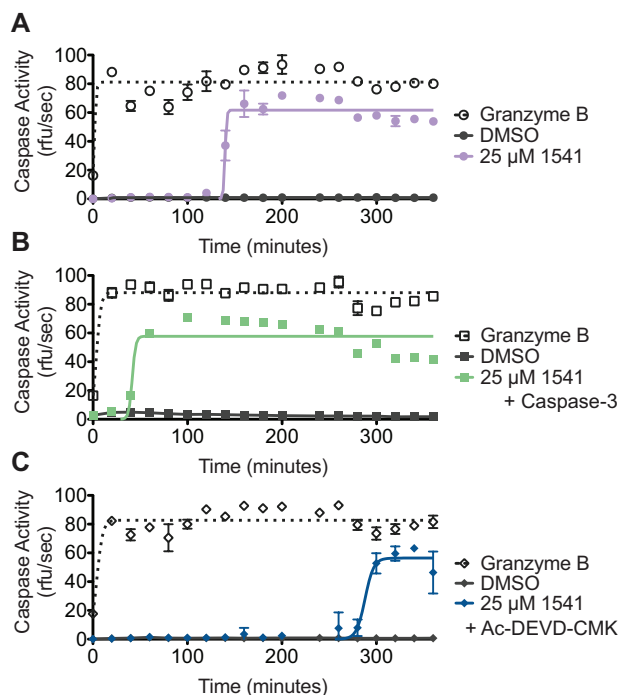


Figure 4-7. Mature caspase-3 drives activation of procaspase-3 in the presence of 1541. (A) Activation of 100 nM procaspase-3 alone (dark circles), 100 nM procaspase-3 with granzyme B (open circles), and 100 nM procaspase-3 with 25 μM 1541 (purple circles) was monitored as a function of time. (B) In the presence of 1 nM caspase-3, procaspase-3 (dark squares), procaspase-3 with granzyme B (open squares), and procaspase-3 with 25 μM 1541 (green squares) activities were monitored. (C) In the presence of 1 nM Ac-DEVD-CMK, procaspase-3 (dark diamonds), procaspase-3 with granzyme B (open diamonds), and procaspase-3 with 25 μM 1541 (blue diamonds) activities were monitored.

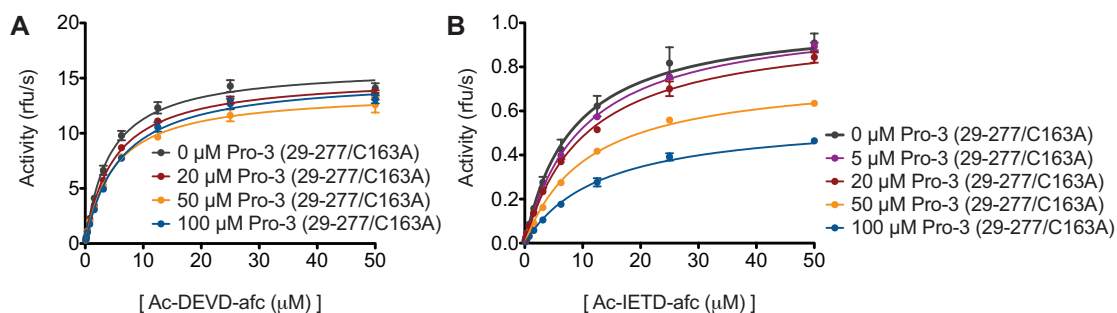


Figure 4-8. K_m approximation for caspase-3 and caspase-8 against the procaspase-3 substrate. (A) 100, 50, or 20 μM truncated, inactive procaspase-3 (29-277/C163A) was added to a dilution series of Ac-DEVD-afc (starting at 50 μM). 5 nM active caspase-3 was immediately added and processing of the tetrapeptide substrate was monitored. (B) 100, 50, 20, or 5 μM truncated, inactive procaspase-3 (29-277/C163A) was added to a dilution series of Ac-IETD-afc (starting at 50 μM). 5 nM caspase-8 was added, and processing was monitored. Once the truncated, inactive procaspase-3 becomes cleaved, it can compete for binding of the tetrapeptide substrate, which complicates a precise K_m determination. Thus, only a lower limit on the K_m can be accurately assessed using this method.

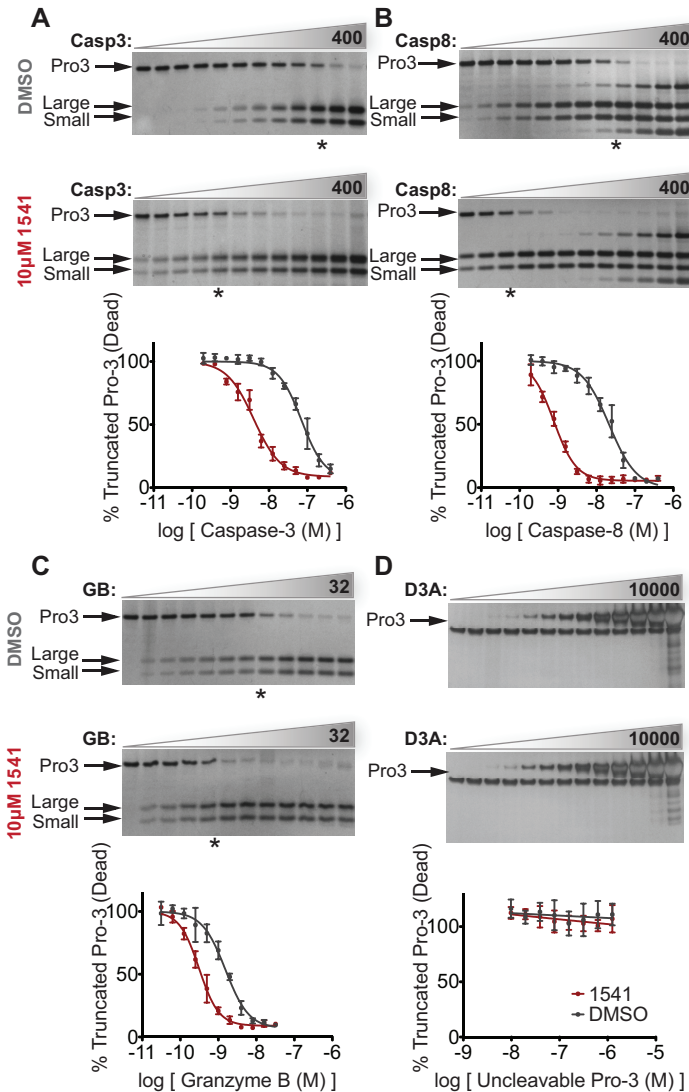


Figure 4-9. Effective change in catalytic efficiency of upstream proteases due to 1541 fibrils. (A) A dilution series of caspase-3 was added to the truncated, inactive procaspase-3 (29-277/C163A) in the absence or presence of 10 μM 1541. At 60 minutes, samples were quenched with LDS loading buffer, analyzed by SDS-PAGE, silver stained, and band intensities quantified by ImageJ. (B) Processing of the inactive procaspase-3 (C163A) by a dilution series of mature caspase-8 was assessed at 20 minutes. (C) Processing of the inactive procaspase-3 by a dilution series of granzyme B was evaluated at 90 minutes. (D) A similar analysis was performed with the uncleavable procaspase-3 (D9A/D28A/D175A) as the upstream protease after 60 minute incubation.

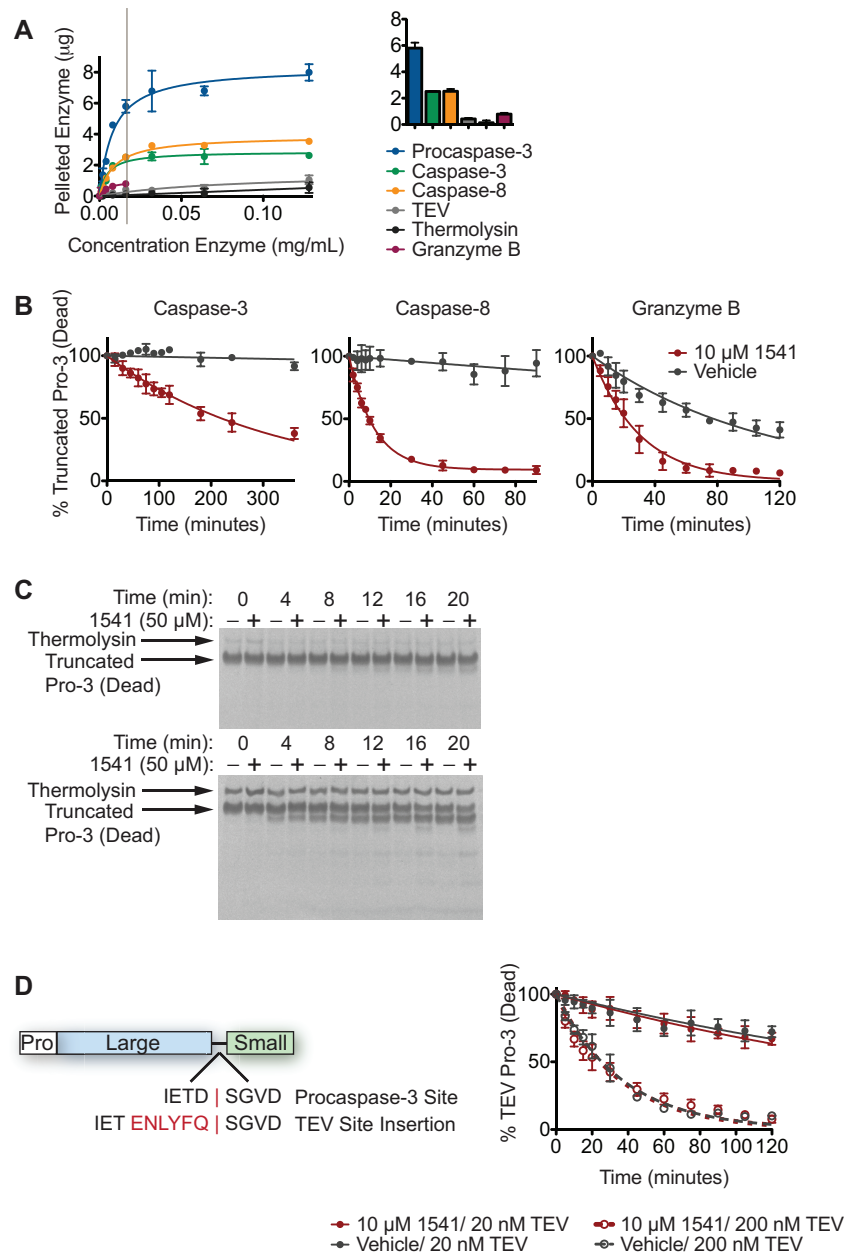


Figure 4-10. Rate of procaspase-3 cleavage by an active protease depends on its catalytic efficiency and the extent of binding to fibrils. (A) 10 μM 1541 was added to a dilution series of procaspase-3, caspase-3, caspase-8, TEV protease, thermolysin, and granzyme B, followed by centrifugation at 16,100xg for 15 minutes. The pellet was analyzed by SDS/PAGE followed by coomassie stain to determine the amount of enzyme that bound to 1541 nanofibrils. (B) 2 nM caspase-3, caspase-8, or granzyme B was added to 200 nM truncated, dead procaspase-3 (29-277/C163A) in the presence of

10 μ M 1541 or DMSO alone. Samples were collected at the indicated time points and quenched with LDS loading buffer. After analysis by SDS-PAGE and silver stain, percent cleavage of the procaspase was determined by quantifying band intensities using ImageJ. (C) Thermolysin was added to procaspase-3 (29-277/C163A) in the presence of 50 μ M 1541 or DMSO alone. Samples were quenched at the indicated time points with LDS loading buffer, and analyzed by SDS/PAGE. While minor cleavage bands in 1541 samples, distinctions are not quantifiable. (D) A TEV cleavage site was engineered into the inactive procaspase-3, rendering it susceptible to proteolysis and activation by only TEV protease. 200 nM of the inactive, TEV cleavable procaspase-3 (D175ENLYFQ/C163A) was incubated with 10 μ M 1541 or DMSO alone in the presence of 20 nM or 200 nM TEV protease. Processing was monitored as described above.

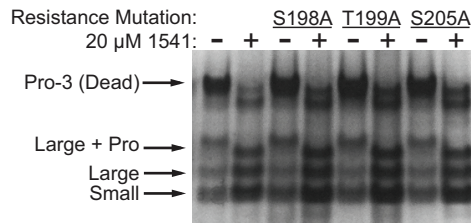


Figure 4-11. Resistance mutations in procaspase-3 are susceptible to processing by caspase-3. The inactive procaspase-3 (C163A) demonstrates increased susceptibility to processing by trace amounts (5 nM) of caspase-3 in the presence of 20 μ M 1541. Notably, resistance mutations (S198A, T199A, and S205A) were previously characterized that do not exhibit enhanced auto-activation of wild-type procaspase-3 in the presence of 1541. We generated the inactive variants for the resistance mutations of procaspase-3 (C163A/S198A, C163A/T199A, and C163A/S205A). 5 nM caspase-3 was added to 250 nM of each of the inactive, resistance mutants of procaspase-3 either with or without 20 μ M 1541. After 1 h incubation at 37°C, the samples were quenched and analyzed by SDS/PAGE followed by silver stain. These variants also show increased susceptibility to proteolysis in the presence of 1541.

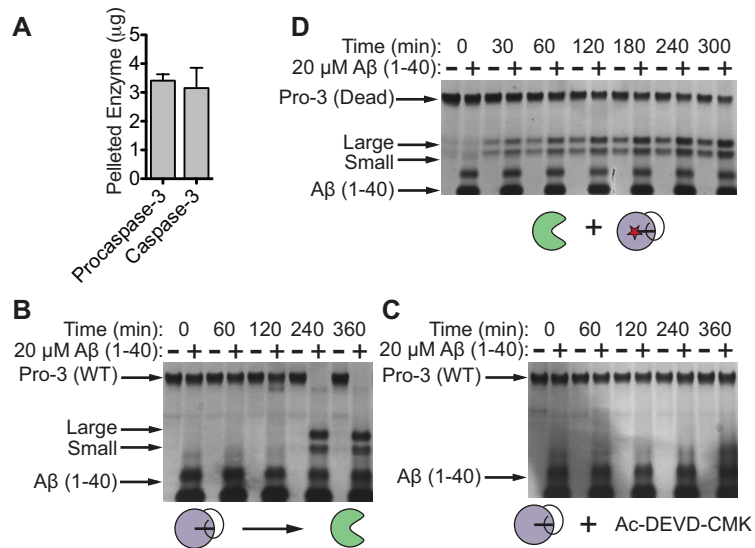


Figure 4-12. Amyloid- β (1-40) fibrils bind and enhance procaspase-3 activation. (A) 50 μ M amyloid- β (1-40) was incubated at 37°C for 6 hours to form fibrils. In 500 μ L of buffer, 20 μ M A β (1-40) fibrils and 0.1 mg/mL procaspase-3, caspase-3, or caspase-8 were added, incubated at room temperature for 5 minutes, and centrifuged at 20,800xg for 20 minutes. The pellets were analyzed for the amounts of the respective enzymes. (B) After a 4-hour incubation at 37°C, amyloid- β (1-40) or buffer alone was added to 250 nM wild-type procaspase-3. Processing was evaluated at the indicated time points. (C) Processing of 250 nM wild-type procaspase-3 with or without amyloid- β (1-40) fibrils was evaluated in the presence of 50 nM Ac-DEVD-cmk. (D) A similar preparation of amyloid- β (1-40) or buffer alone was incubated with 200 nM truncated, inactive procaspase-3 (29-277/C163A) and 5 nM caspase-3.

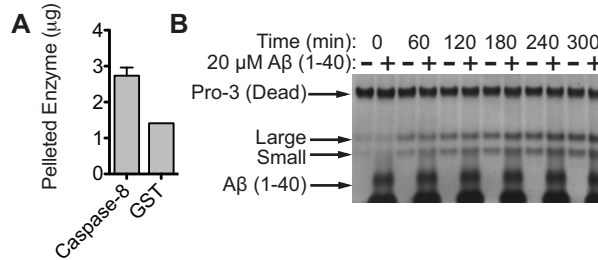


Figure 4-13. Caspase-8 binds but does not process procaspase-3 on amyloid- β (1-40) fibrils. (A) 50 μ M amyloid- β (1-40) was incubated at 37°C with agitation for 6 hours. After fibril formation, amyloid- β (1-40) was diluted to 20 μ M with 0.1-mg/mL caspase-8 or GST in a total volume of 500 μ L. Samples were incubated for 5 minutes at room temperature and centrifuged at 20,817xg for 20 minutes. The supernatant was removed, and the pellet was resuspended in LDS loading buffer. Samples were analyzed by SDS/PAGE followed by coomassie stain. (B) 50 μ M amyloid- β peptide was agitated at 37°C for 4 hours to form fibrils. 2 nM caspase-8 and 200 nM inactive procaspase-3 (C163A) were next incubated with 20 μ M amyloid- β (1-40) fibrils or in buffer alone. Aliquots were quenched with LDS loading buffer at the indicated time points and run by SDS/PAGE. Bands were visualized by silver stain analysis to assess the amount of proteolysis.

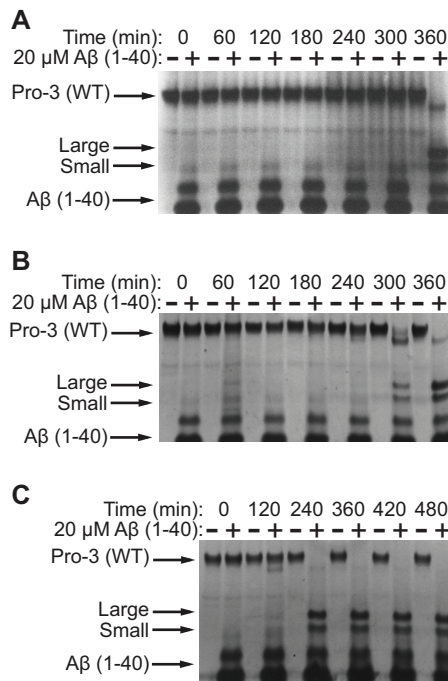


Figure 4-14. Variable times to autocatalytic maturation of wild-type procaspase-3 by different batches of amyloid- β (1-40). Different batches of 50 μ M amyloid- β (1-40) (A, B, and C) were incubated at 37°C for 4 hours. Fibril formation was assessed by increased Thioflavin T fluorescence. These amyloid- β (1-40) samples were then diluted to 20 μ M and incubated with 250 nM wild-type procaspase-3. Aliquots were quenched with LDS loading buffer at the indicated time points and run by SDS/PAGE. Bands were visualized by silver stain analysis to assess proteolysis to the large and small subunit of mature caspase-3.

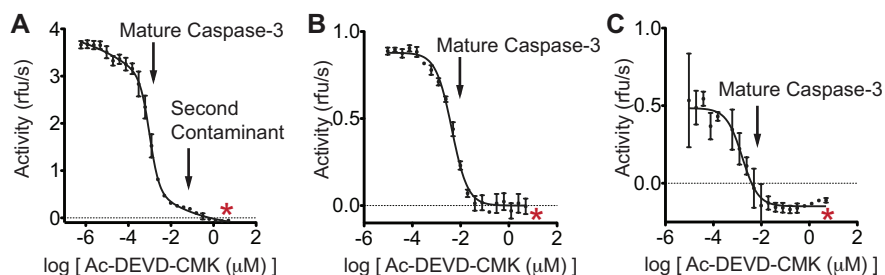


Figure 4-15. Multiple caspase-3 cleavage products identified by active site titration with Ac-DEVD-cmk. An active site titration with Ac-DEVD-cmk was performed against (A) 5 μ M uncleavable procaspase-3 (D9A/D28A/D175A) expressed for 8 hours, (B) 10 μ M uncleavable procaspase-3 expressed for 2.5 hours, or (C) wild-type procaspase-3 expressed for 20 minutes. The titration was plotted on a log scale. The red star indicates stoichiometric concentrations of Ac-DEVD-cmk. The initial drop in activity for all three procaspase preparations occurred at substoichiometric concentrations. Note the distinct levels of maximum activity for each proenzyme batch in addition to the second species detected in the uncleavable procaspase-3 expressed for 8 hours. Based on the kinetic measurements described in the text, we believe that this species weakly interacts with Ac-DEVD-cmk.

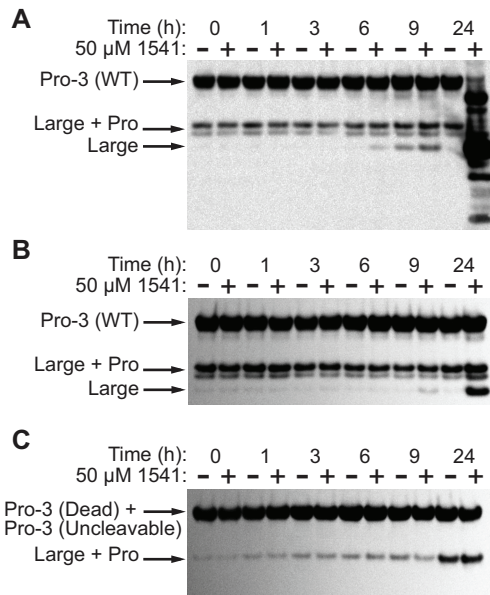


Figure 4-16. Low concentrations of Ac-DEVD-cmk do not completely quench the mature caspase-3 contaminant. (A) 50 nM Ac-DEVD-cmk was added to 5 μM wild-type procaspase-3. The proenzyme was next incubated at 37°C in the presence or absence of 50 μM 1541. Aliquots were quenched at the indicated time points. Samples were run by SDS/PAGE and analyzed by western blot using an antibody that recognizes the large subunit of caspase-3 (Cell Signaling #9442). (B) 250 nM Ac-DEVD-cmk was added to 5 μM wild-type procaspase-3. Processing was again monitored as described above. (C) 50 nM Ac-DEVD-cmk was added to 5 μM uncleavable procaspase-3 (D9A/D28A/D175A) and 5 μM inactive procaspase-3 (C163A). 50 μM 1541 or vehicle alone (DMSO) were next added to the reaction. Processing over time was again monitored.

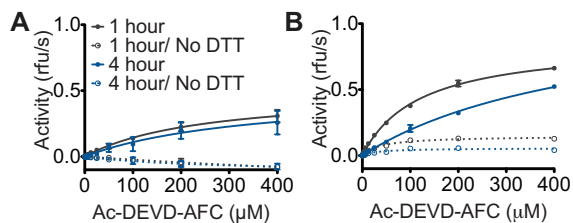


Figure 4-17. Dithiothreitol quenches Ac-DEVD-cmk at low concentrations, and Ac-VAD-fmk slowly inactivates trace caspase-3 contaminants. (A) 250 nM Ac-DEVD-cmk was added to 5 μ M uncleavable procaspase-3 (8 h expression) in buffer with (closed circles) or without (open circles) 10 mM dithiothreitol (DTT). Activity against Ac-DEVD-afc was determined after a 1-h (gray) and 4-h (blue) incubation. In cases where DTT was excluded during the incubation time, the buffer was re-adjusted to 1 mM DTT upon the addition of substrate. (B) 250 nM Z-VAD-fmk was added to 5 μ M uncleavable procaspase-3. Activity was similarly assessed for these samples.

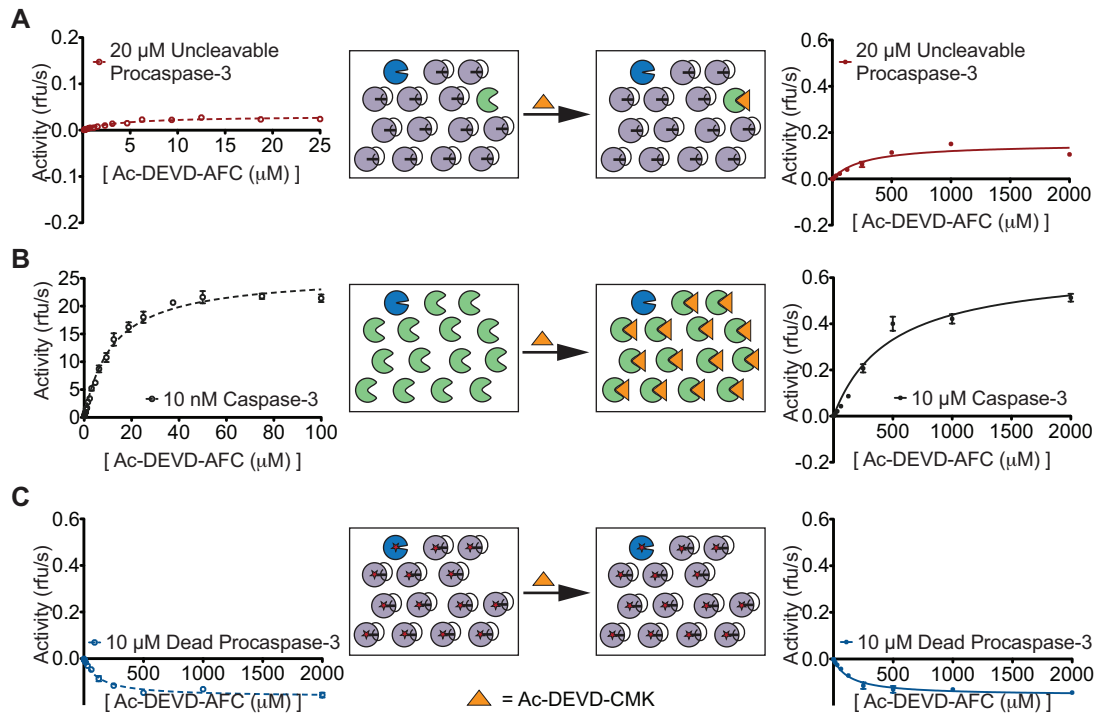


Figure 4-18. Multiple active caspase-3 variants with distinct kinetics in procaspase-3 batches. (A) The activity of 20 μM uncleavable procaspase-3 (D9A/D28A/D175A) against Ac-DEVD-afc was determined in the absence of inhibitor (open red circles). In the presence of 200 nM Ac-DEVD-cmk, the activity shifts dramatically for the uncleavable procaspase-3 (closed red circles). Interestingly, a distinct K_m is apparent. Note the different scales for substrate concentration on the x-axis. (B) The activity of 10 nM caspase-3 is monitored against Ac-DEVD-afc in the absence of inhibitor (open grey circles). 12 μM Ac-DEVD-cmk is incubated with 10 μM caspase-3 for 5 minutes. Note the 1000x increase in enzyme concentration to levels comparable to those used for the uncleavable procaspase-3. Subsequently, Ac-DEVD-afc is added to the samples and the activity is monitored (closed grey circles). (C) The activity of 10 μM of the inactive procaspase-3 variant (C163A) against Ac-DEVD-afc was assessed (open blue circles). Activity measurements were similar to values obtained for the Ac-DEVD-afc substrate in buffer alone. In the presence of 200 nM Ac-DEVD-cmk, activity measurements for the inactive procaspase-3 similarly demonstrated an inactive construct (closed blue circles).

Typical parameters on the SpectraMax M5 plate reader (Molecular Devices) include an excitation wavelength of 365 nm, an emission wavelength of 495 nm with a cutoff at 435 nm. However, at 2000 μM Ac-DEVD-afc substrate dilutions emission was monitored off peak to prevent saturation of the signal at these high substrate concentrations.

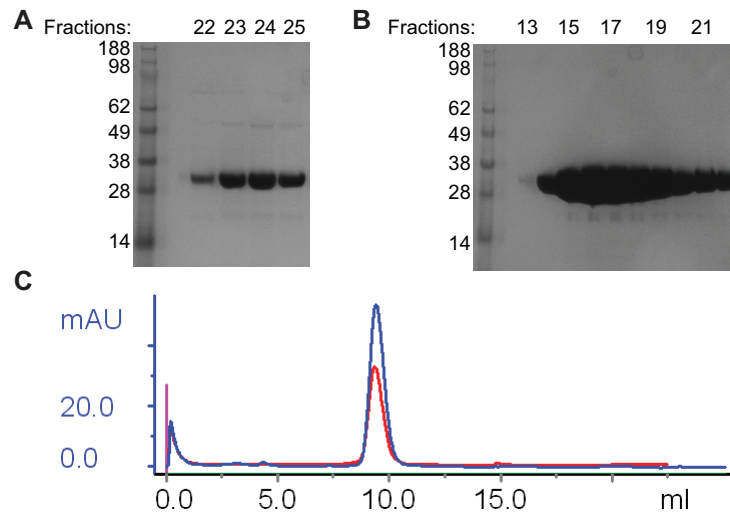


Figure 4-19. Wild-type procaspase-3 and uncleavable procaspase-3 (D9A/D28A/D175A) lack large impurities. (A) After ion exchange chromatography on wild-type procaspase-3, fractions were collected. Aliquots of each fraction were analyzed by SDS/PAGE followed by coomassie stain. (B) A similar procedure was performed on the uncleavable procaspase-3 (D9A/D28A/D175A). (C) Uncleavable procaspase-3 from batches expressed for 8 hours (red) and 2.5 hours (blue) were run on a gel filtration column. No differences or impurities were detected.

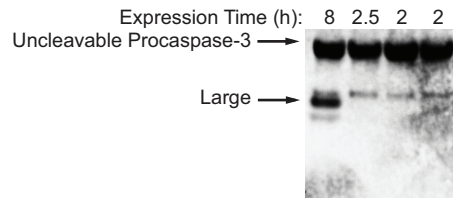


Figure 4-20. Multiple, trace caspase-3 cleavage products detected in the uncleaveable procaspase-3 (D9A/D28A/D175A). 15 μ L of 5 μ M samples of the uncleaveable procaspase-3 from different batches expressed for different times were analyzed by SDS/PAGE followed by western blot with an antibody that recognizes the C-terminus of the cleaved caspase-3 large subunit (Cell Signaling #9664). Since a large excess of the full-length procaspase-3 is loaded relative to the trace caspase-3 contaminants in each sample, the antibody non-specifically recognizes the full-length band as well.

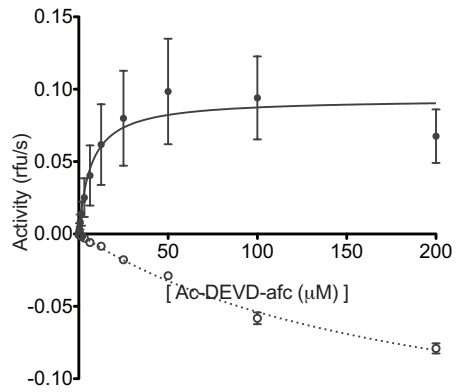


Figure 4-21. Activity of 50 μM uncleavable procaspase-3 (D9A/D28A/D175A) after thorough purification. After 3 h expression and His-affinity purification, extreme care was taken in collection of fractions from anion-exchange chromatography. The activity of 50 μM uncleavable procaspase-3 was monitored against the Ac-DEVD-afc substrate in the presence (open circles) or absence (closed circles) of 500 nM Ac-DEVD-cmk. A dilution series of 200 μM Ac-DEVD-afc Ac-DEVD-afc) was used to monitor activity. Similar results were found at higher substrate concentrations (2000 μM Ac-DEVD-afc).

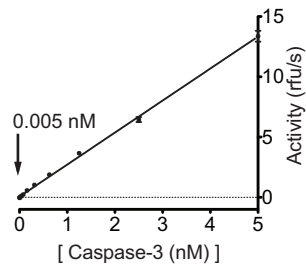


Figure 4-22. Minimum detectable concentration of mature caspase-3. 50 μ M Ac-DEVD-afc was added to a dilution series of caspase-3 (starting concentration of 5 nM). Activity was monitored and plotted. 0.005 nM caspase-3 is the minimum concentration at which activity is observed over Ac-DEVD-afc in buffer alone.

Chapter 5:

Selective Activation of Executioner Procaspases with Small Molecule Nanofibrils

Julie A. Zorn[†], Dennis W. Wolan[†], Holger Wille^{||,¶}, and James A. Wells^{†,‡}

[†]Department of Pharmaceutical Chemistry, University of California, San Francisco,
California

^{||}Institute for Neurodegenerative Disease, University of California, San Francisco,
California

[¶]Department of Neurology, University of California, San Francisco, California

[‡]Department of Cellular and Molecular Pharmacology, University of California, San
Francisco, California

Abstract

Caspases are expressed as inactive zymogens, or procaspases, that require proteolytic processing by upstream proteases to form the active protein. We previously identified a small molecule, termed 1541, that promotes activation of executioner procaspase-3 *in vitro*. Remarkably, this small molecule self-assembles into nanofibrils and acts by promoting colocalization of the procaspase with a trace amount of mature caspase. Here, we describe the synthesis of a focused library of 1541 analogues that selectively activate procaspases-3, -6, and -7. These selective procaspase activators also assemble into nanofibrils, yet display distinct interactions with each of the precursors and their respective mature enzymes. Interestingly, similar to small molecules, our nanofibrils exhibit structure activity relationships (SAR). We explore the mechanism of action of these unique particles *in vitro* for potential use as biocatalyst materials. We also show these small molecule nanofibrils identified in a screening library induce apoptosis in cancer cell lines, however our results suggest that it is unlikely due to direct procaspase activation.

Introduction

Particles, or aggregates of small molecules, have been described that inhibit enzyme activity (150). These colloidal particles are believed to sequester enzymes on the surface, resulting in local unfolding and inhibition (216). Such promiscuous enzyme inhibitors often obscure the results of high throughput screens (HTS). However, these aggregates are readily identified by several experiments designed to triage hits. These tests include detergent sensitivity, BSA sensitivity, and β -lactamase inhibition (116,135,150). Recent reports have even shown that a specific chemical class of promiscuous inhibitors can exhibit structure activity relationships (SAR) (217). While the properties of promiscuous inhibitors are carefully depicted, a similar analysis for enzyme activators has yet to be described or characterized.

Small molecule activators, in contrast to inhibitors, of enzymes are rare. Within the past decade, however, scientists have increasingly sought to promote enzyme activity rather than necessarily ablate it (147). Accordingly, screening artifacts associated with enzyme activation have only recently been reported (155). As with promiscuous enzyme inhibitors, these activators were found to be detergent sensitive. However, our small molecule activator, compound 1541, was not affected by the presence of common detergents (179). Further, 1541 self-assembled into nanofibrils, rather than the typical colloids reported for known aggregators. In this study, we show that analogues of 1541 can selectively activate highly homologous enzymes, the executioner procaspases. Similar to colloidal particles, these nanofibrils also exhibit SAR.

Procaspases are expressed as inactive precursors that require removal of an N-terminal pro-domain and an additional processing event to generate the large and small subunit of the mature caspase (149). Typically, either extracellular death ligands or intracellular stress can trigger procaspase activation via two distinct signaling networks:

the extrinsic and intrinsic pathway, respectively. In each pathway, unique scaffolding complexes are assembled that result in the recruitment of initiator procaspases, including procaspases-8, -9, and -10 (145). Upon oligomerization at these signaling complexes, initiator procaspases induce autoproteolysis to generate the active enzyme. Once processed, initiator caspases target downstream executioner procaspases-3, -6 and -7. The mature, active executioner caspases then cleave vital cellular proteins, which results in the apoptotic phenotype (175,177). Interestingly, while 1541 is a small molecule from a screening library that assembles into particles, these nanofibrils may mimic known scaffolding complexes, which promote procaspase activation. These fibrils have proven to be a useful tool for exploring procaspase activation mechanisms. Additional characterization of the interaction between these nanofibrils and the procaspases may be useful for the design of novel biocatalytic tools.

Finally, chemotherapeutic agents, such as etoposide, staurosporine, or TRAIL, do promote procaspase activation by stimulation of either the extrinsic or intrinsic pathways (125). Previous reports show that colloidal aggregates reduce this apoptotic activity of anti-cancer drugs (218). In contrast to colloidal aggregates, 1541 nanofibrils appear to be responsible for the apoptotic activity observed in cells. However, our results show that this is unlikely due to a direct mechanism of procaspase activation.

Results and Discussion

Synthesis of a Focused Library. The initial goal of our studies was to identify the core scaffold of compound 1541 required for procaspase-3 activation *in vitro* (**Fig. 5-1**). We utilized a convergent three step synthetic scheme to generate a library of 145 analogs (**Scheme 5-1**). First, we synthesized a panel of 3-carboxy-coumarin analogs by cyclization of commercially available salicylaldehydes via a Knoevenagel condensation reaction with Meldrum's acid. Meta-substituted anilines were next generated through a Suzuki coupling between 3-bromoaniline and a panel of aryl boronic acids. Lastly, the 3-carboxy-coumarins were coupled to the anilines via an amide bond formation reaction to generate the final library.

Modifications to the coumarin scaffold demonstrated that substitution at the 8-position of this moiety is essential for activity. However, only 8-hydroxy and 8-methoxy substitutions were tolerated. Bulkier groups removed any detectable procaspase-3 activity. While this substitution pattern seemed optimal, the coumarin ring can be replaced by other heterocycles. Additional modifications to the coumarin scaffold did not generate more potent compounds. In fact, in most cases, additional substituents ablated activity.

Second, meta-substitution at the central phenyl ring is not essential for activity, but affords more potent compounds. If this substitution is removed, additional modifications to the remaining scaffold are necessary. For example, a pyridinyl ring rather than the phenyl ring restores procaspase-3 activation if meta-substitution is removed. We next explored other aromatic ring substitutions at this position. The imidazo-pyridine ring persisted as the favorable substituent, however other rings were tolerated.

Distinct procaspase-3 activation profiles. Compound 1541 effectively activates procaspase-3 and -6 but not procaspase-7 (71). As indicated above, we tested our

focused library of 145 analogues of compound 1541 against procaspase-3. After a 5-hour incubation at 37°C, we added a tetrapeptide substrate, Ac-DEVD-afc, and determined initial rates. Very few analogues resulted in robust activation. Notably, compounds that did promote procaspase-3 maturation generated distinct activation profiles (**Fig. 5-2**).

These activators could be categorized into three unique classes based on their dose response curves: initial activation followed by inhibition, activation alone, or a low level of activation. Compound 1541 and compound 1541B exhibited bell-shaped curves where there was an initial burst in activity with an EC_{50} of 2.3 μ M and 1.0 μ M, respectively. As compound concentration was increased farther for 1541 and 1541B, a decrease in activity became apparent with IC_{50} 's of 91 μ M and 4.8 μ M, respectively. Some compounds displayed a high level of overall activation with a weak EC_{50} , but no inhibition. For example, compound 136 had an EC_{50} of 15 μ M with no inhibition detected. Finally, compound 161 had a potent EC_{50} (0.7 μ M), but with a very low level of activity relative to other compounds.

The analogues were next tested against recombinantly-expressed caspase-3 to determine if the inhibition seen in our procaspase-3 activation assays was due to an interaction with the fully-cleaved form of the proenzyme. Notably, the IC_{50} values determined in the procaspase-3 activation assays closely matched the IC_{50} values against the mature caspase-3 (**Fig. 5-2**). This suggests that procaspase-3 is fully matured in the presence of the compounds, but once cleaved, the active caspase-3 is inhibited.

To confirm this, we evaluated the extent of procaspase-3 processing upon the addition of a dilution series of compounds 161 and 1541 (**Fig. 5-3**). At high concentrations of these compounds, where inhibition is observed using cleavage Ac-

DEVD-afc as a readout, complete processing of procaspase-3 occurred. This supports that the compounds do not inhibit processing of the full-length proenzyme substrate, but do inhibit the mature caspase once it is formed.

Selective activation of executioner procaspases. Compound 1541 demonstrated some initial selectivity for activation of executioner procaspases-3 and -6 relative to procaspase-7 (71). Thus, we next evaluated if this selectivity profile was a general characteristic for this class of compounds.

Interestingly, we did identify compounds that preferentially activated each of the executioner procaspases (**Fig. 5-4**). Procaspase-3 selective activators, such as compound 161 and 1541B, seemed to favor the 8-hydroxy substituent on the coumarin ring and a heterocyclic substitution on the central phenyl ring. Procaspase-6 activators, such as 178 and 162, prefer the 8-methoxy group on the coumarin ring, although a clear trend for substitution at the meta-position of the central ring is unclear. Procaspase-7 activators, such as compound 53 and 74, prefer the 8-hydroxy group on the coumarin ring with alkoxy-substituted aromatic rings in the meta position of the central phenyl ring. These studies suggested that the properties of the compounds are tunable.

Active compounds self-assemble into fibrils. The SAR around our initial hit (1541) indicates a mechanism that might be independent of the particles that are formed. Thus, we further explored these additional analogs by transmission electron microscopy (TEM). As previously described, 1541 assembled into long, thin fibrils that tended to cluster into bundles (179). An initial investigation of the physical properties of a select panel of 1541 analogs indicates that while some compounds form fibrils in buffer, others appear to form standard colloidal aggregates. Interestingly, only fibril forming compounds promote procaspase activation. The additional analogues that assembled into fibrils did appear to have distinct morphologies in some cases (**Fig. 5-5**). Notably, a selective procaspase-7 activator, compound 53, and a selective procaspase-6 activator,

compound 178, produced thicker fibrils, which had a lesser tendency to bunch together. This would suggest that the structure of the fibrils dictates the selectivity for individual procaspases observed.

We also found that at higher concentrations of 1541, where inhibition is observed, 1541 still formed fibrils (data not shown). Thus, the fibrils alone are also responsible for both the activation and inhibition effects that we see in our activity assays (**Fig. 5-3**). It is possible that bunching of the fibrils at higher concentrations can disrupt productive substrate binding.

Selective procaspase-7 activation on fibrils. Previous studies delineated an activation mechanism for this class of compounds that involves colocalization of the mature caspase-3 with its procaspase-3 substrate (unpublished data). However, caspase-7 has very little intrinsic ability to cleave procaspase-7 (117). Thus, the procaspase-7 activators provided an interesting case and warranted further investigation. We chose compound 53 to further evaluate.

We first determined the ability of procaspase-7 and caspase-7 to bind to the fibrils formed by compound 53 as well as 1541 using co-sedimentation assays (156,179). For 1541, procaspase-3 and procaspase-7 interact with the fibrils to a greater extent relative to their mature forms, caspase-3 and caspase-7 (**Fig. 5-6A**). However, the mature caspase-7 interacts to a greater extent with the fibrils formed by compound 53 relative to procaspase-7 (**Fig. 5-6B**). In the case of compound 53, the specificity of the fibrils against the pro- and mature enzymes is reversed relative to 1541. This suggests that increasing the relative concentrations of active to proenzyme using a scaffold will promote procaspase-7 maturation.

We next evaluated the susceptibility of the inactive procaspase-7 (C186A) to processing by an orthogonal protease, granzyme B. Only compound 1541 appears to enhance the procaspase-7 susceptibility to a large and small subunit (**Fig. 5-6C**). This is

most likely because procaspase-7 does interact very well with 1541 fibrils, but not as well with compound 53 fibrils. As previously shown granzyme B can interact weakly with 1541 fibrils, and cleaves procaspase-7 with a high catalytic efficiency. Thus, the catalytic efficiency of the upstream protease, its affinity for the fibrils, and the affinity of its substrate procaspase for the fibrils all influence the rate of enhanced processing of the proenzyme.

Compound 1541 does not promote autocatalytic maturation of procaspase-7, but compound 53 does. In the case of self-activation, the mature caspase-7 acts as the upstream protease. Thus, we next assessed the susceptibility of the inactive procaspase-7 (C186A) to processing by mature caspase-7 in the presence of several of the compounds (**Fig. 5-6D**). While the prodomain on procaspase-7 is readily removed in most cases, only compound 53 enhances processing of procaspase-7 to a large and small subunit. In combination with the cosedimentation studies, this indicates that compound 53 appears to colocalize more caspase-7 relative to procaspase-7 to facilitate processing to the large and small subunit to promote proenzyme activation. This ability to tune the activity of the fibrils and alter natural processes further supports their utility as biocatalysts.

Distinct cellular activities. We previously characterized the apoptotic phenotype stimulated by 1541 (71). Briefly, cell death induced by 1541 is independent of both the intrinsic and extrinsic pathway, as illustrated by apoptosis observed in Bax/Bak knockout mouse embryonic fibroblasts (MEFs) and in caspase-8 deficient Jurkats, respectively. The 1541 nanofibrils appear necessary for inducing apoptosis. Centrifugation of samples to remove particulates also eliminates 1541 activity (data not shown). Previous studies have shown that colloidal aggregates sequester free molecule and reduce the potency of a chemotherapeutic drugs in cell culture (218). With 1541, the particles appear to be responsible for the cell death observed.

To understand if this mechanism was generalizable to all the particles in our library, we next examined the ability of a panel of the nanofibrils to induce caspase activity and cell death against a variety of different cell lines: HEK293, wild-type MEF, HeLa, Jurkat, and HCC1954. We first show a comparison of both caspase activity and cell viability in MEFs and HEK293 cells (**Fig. 5-7A and 5-7B**). 1541 is shown and rapidly induces cell death and caspase activity in both cell lines. However, the caspase activity levels and the toxicity of the other compounds appear more variable. This suggests that there are differences in these cells that result in divergent responses to distinct compounds. The viability of all cells after treatment for 24 hours was next compared for the panel of compounds (**Fig. 5-7C**). Again, cell line dependent effects seem apparent for individual compounds. Future work to understand the mechanism of cell death by these fibrils might identify novel chemotherapeutic targets that could exploit these differences.

Cell death is not through direct procaspase activation. Important to note is that the more selective compounds in the *in vitro* procaspase activation assays are also more selective in our cell-based assays. These results collectively hinted at a direct activation of procaspase-3 in cells by the nanofibrils. However, a direct interaction between procaspases and the fibrils in cells seems unlikely since 1541 does not promote procaspase-3 activation in lysates (data not shown). This demonstrates that other proteins compete with procaspase-3 for a direct association with the fibrils, impairing activation.

To interrogate the importance of caspase-3 catalytic activity in 1541-induced apoptosis, MCF7 cells, which lack procaspase-3, were stably transfected with either wild-type procaspase-3 or inactive procaspase-3 (C163A). A similar rate of processing of each construct was induced in both cell lines in response to 1541 (**Fig. 5-8A**). This indicates that 1541 promotes apoptosis upstream of procaspase-3.

Further, we tested 1541 against a panel of caspase knockout MEFs, including caspase-9, caspase-3, and caspase-7 (127,219). Loss of individual caspases had minimal impact on 1541 activity (**Fig. 5-8B**). Compound 178, which selectively activates procaspase-6 *in vitro*, exhibits comparable apoptosis in wild-type and caspase-6 knockout MEFs (**Fig. 5-8C**) (220). Together these results indicate a mode of apoptosis that is independent of the extrinsic and intrinsic pathways, but not through direct procaspase activation. Additional experiments are necessary to determine the exact cellular mechanism.

Conclusion

In this study, we generated a focused library of 1541 analogues. We tested this library against procaspase-3 to assess if the compounds promoted maturation and activation of the proenzyme. Notably, the compounds did display SAR, as previously described for colloidal aggregate inhibitors (218). In fact, all active compounds were found to self-assemble into nanofibrils. 1541 and the analogues described here delineate a novel class of fibril-forming molecules. While 1541 does stress a screening artifact associated with proenzyme activation, it also could be useful as a biocatalyst material.

Interestingly, unique analogues selectively activate highly homologous proenzymes, executioner procaspases-3, -6, and -7. Many analogues of 1541 were also found to be inactive. While one inactive compound was shown to form colloids, rather than fibrils, it would be interesting to explore the reason for the inactivity of the other compounds. While fibrils appear to be necessary for procaspase activation, these structures are not sufficient, as demonstrated by our selective studies. In other words, not all procaspases are activated by all fibrils. Future experiments are needed to understand the basis for this selectivity.

The fibrils not only display selectivity for activation of the procaspases, but they are also tunable. Different compounds activate procaspase-3 to different extents. Different doses of a single compound can also have distinct effects. For example, lower levels of activation are achieved at higher concentrations of 1541. Interestingly, the fibrils appear to drive both activation and inhibition. These studies highlight many different avenues that can be explored to generate useful biocatalytic tools derived from 1541. Additional studies to understand the basis for these tunable properties are warranted.

These fibrils may also highlight a novel mechanism for the regulation of procaspase activity. Only fibrils, and not colloids, were identified to activate the

procaspases. Furthermore, caspases can localize to the surface of fibrillar structures in cells, such as cytokeratin 18. It is possible that these cellular scaffolds provide a platform for procaspase activation, similar to 1541.

The 1541 nanofibrils also induce caspase activation and cell death in several different cell lines. The cellular potency of this class of compounds appears to be independent of their ability to activate the procaspases *in vitro*. However, the distinct toxicity profiles of each analogue indicate that these synthetic fibrils may be exploiting intrinsic differences in the cell lines to induce death. Future experiments to explore the cellular mechanism may identify novel chemotherapeutic targets.

Experimental Section

General Chemistry. 8-methoxy-2-oxo-2H-chromene-3-carboxylic acid was purchased from Maybridge; 3-imidazo[1,2-a]pyridin-2-yl-phenylamine was purchased from Matrix Scientific; O-(7-azabenzotriazole-1-yl)-N,N,N,N'-tetramethyluronium hexafluorophosphate was purchased from Applied Biosystems; boronic acids were purchased from Frontier Scientific, Combi-Blocks, Matrix Scientific, or Sigma-Aldrich; all other solvents and reagents were purchased from Sigma-Aldrich. ^1H and ^{13}C NMR data were collected on a Varian 400 MHz spectrometer in $\text{DMSO-}d_6$. LCMS data was acquired on a Waters Micromass ZQ in ESI+ mode, equipped with a Waters 2996 photodiode array detector and Waters Alliance 2795 separations module. The LCMS protocol consisted of sample elution through an analytical Xterra C-18 column (2.1 mm x 50 mm x 3.5 μm) at a gradient of 5-95% methanol (0.2% formic acid)/water (0.2% formic acid) over 6 minutes at a flow rate of 1.0 mL/min.

General procedure for synthesis of 2-oxo-2H-chromene-3-carboxylic acids (142). Salicylaldehydes (0.69 mmol) and Meldrum's acid (0.69 mmol) were combined in H_2O (1 mL). The solution was stirred at 75°C for 2 hours. After cooling to room temperature, the precipitate was filtered and dried at suction to give the 3-carboxy-coumarin core scaffold.

General procedure for synthesis of meta-substituted anilines (221). Commercially available boronic acids (0.693 mmol) and 3-bromoaniline (0.462 mmol) were combined in DME (2 mL) in a flame-dried, round-bottom flask. Na_2CO_3 (2M, 0.970 mmol) and $\text{Pd}(\text{PPh}_3)_4$ (0.014 mmol) were added to the stirred solution. The reaction was refluxed overnight under argon flow, and subsequently cooled to room temperature. The solvent was removed under vacuum and the resulting residue was resuspended in H_2O and extracted with CH_2Cl_2 . The organic phase was dried over MgSO_4 and concentrated

under vacuum. The crude product was purified by silica column chromatography (0-10% EtOAc/hexanes). The purification was monitored by TLC. The solvent was removed from fractions containing product.

General procedure for amide bond coupling (71). DIEA (0.27 mmol) was added to 3-carboxy-coumarins (0.24 mmol) and HATU (0.27 mmol) in 1 mL of DMF. Anilines (0.24 mmol) were then added and allowed to react overnight. If a precipitate was apparent, it was filtered and dried *in vacuo*. If a precipitate was not apparent, DMF was removed under vacuum and the reaction was resuspended in DMSO. The crude product was purified on a Parallax Flex parallel preparative reverse phase HPLC instrument (Biotage) using a solvent gradient of 10-95% ACN/H₂O with 0.05% TFA at a flow rate of 20 mL/min. UV absorbance was monitored at 254 nm and the fractions corresponding to the product peak were collected and the solvent removed under vacuum.

8-Methoxy-2-oxo-2H-chromene-3-carboxylic acid (3-imidazo[1,2-a]pyridin-2-yl-phenyl)-amide (1541). Diisopropylethylamine (DIEA, 0.044 mL, 0.25 mmol) was added to 8-methoxy-3-carboxy-coumarin (0.05 g, 0.23 mmol) and O-(7-Azabenzotriazole-1-yl)-N,N,N,N'-tetramethyluronium hexafluorophosphate (HATU, 0.096 g, 0.25 mmol) in 2 mL of dimethylformamide (DMF) with constant stirring at room temperature until a clear solution resulted. Subsequently, 3-Imidazo[1,2-a]pyridin-2-yl-phenylamine (0.048 g, 0.023 mmol) was added and allowed to react for approximately 30 minutes, when a yellow solid precipitated out of solution. The precipitate was filtered and dried under suction and then *in vacuo* to give **1541**: ¹H NMR (400 MHz, DMSO-*d*₆) δ 10.78 (s, 1H), 8.92 (s, 1H), 8.54 (d, *J* = 7.0 Hz, 1H), 8.44 (s, 1H), 8.31 (s, 1H), 7.73 (m, 2H), 7.60 (d, *J* = 9.0 Hz, 1H), 7.57 (d, *J* = 9.0 Hz, 1H), 7.44 (m, 3H), 7.26 (dd, *J* = 5.5, 6.8 Hz, 1H), 6.90 (dd, *J* = 5.5, 6.8 Hz, 1H), 3.96 (s, 3H); LCMS (ESI) *m/z* 412 (MH⁺).

8-Hydroxy-2-oxo-2H-chromene-3-carboxylic acid (3-imidazo[1,2-a]pyridin-2-yl-phenyl)-amide (1541B). 2,3-dihydroxybenzaldehyde (0.096 g, 0.69 mmol) and Meldrum's acid (0.100 g, 0.69 mmol) were combined in H₂O (1 mL). The solution was stirred at 75°C for 2h. After cooling to room temperature, the precipitate was filtered and dried at suction to give 0.123 g of 8-hydroxy-3-carboxy-coumarin in an 85% yield: LCMS (ESI) *m/z* 207 (MH⁺).

DIEA (0.046 mL, 0.27 mmol) was added to 8-hydroxy-3-carboxy-coumarin (0.050 g, 0.24 mmol) and HATU (0.101 g, 0.27 mmol) in 1 mL of dimethylformamide (DMF) with constant stirring at room temperature until a clear solution resulted. Subsequently, 3-imidazo[1,2-a]pyridin-2-yl-phenylamine (0.051 g, 0.24 mmol) was added and allowed to react overnight, when a yellow solid precipitated out of solution. The precipitate was filtered and dried under suction and then in vacuo to give 0.021 g of **1541B** in a 22% yield: LCMS (ESI) *m/z* 398 (MH⁺).

8-Methoxy-2-oxo-2H-chromene-3-carboxylic acid phenylamide (1541D). DIEA (0.044 mL, 0.25 mmol) was added to 7-methoxy-3-carboxy-coumarin (0.050 g, 0.23 mmol) and HATU (0.095 g, 0.25 mmol) in 1 mL of dimethylformamide (DMF) with constant stirring at room temperature until a clear solution resulted. Subsequently, aniline (0.021 g, 0.23 mmol) was added and allowed to react overnight, when a yellow solid precipitated out of solution. The precipitate was filtered and dried under suction and then in vacuo to give 0.055 g of **1541D** in an 82% yield: LCMS (ESI) *m/z* 296 (MH⁺).

8-Hydroxy-2-oxo-2H-chromene-3-carboxylic acid (3',4'-Dimethoxy-biphenyl-3-yl)-amide (53). DIEA (0.013 mL, 0.072 mmol) was added to 8-hydroxy-3-carboxy-coumarin (0.014 g, 0.065 mmol) and HATU (0.027 g, 0.072 mmol) in 0.36 mL of DMF with

constant stirring at room temperature until a clear solution resulted. Subsequently, 3', 4'-Dimethoxy-biphenyl-3-ylamine (0.015 g, 0.065 mmol) was added and allowed to react overnight. DMF was removed under vacuum and the reaction was resuspended in DMSO. The crude product was purified on a Parallelex Flex parallel preparative reverse phase HPLC instrument (Biotage) using a solvent gradient of 10-95% ACN/H₂O with 0.05% TFA at a flow rate of 20 mL/min. UV absorbance was monitored at 254 nm and the fractions corresponding to the product peak were collected and the solvent removed under vacuum to give 0.005 g of product in 19% yield: LCMS (ESI) *m/z* 418 (MH⁺).

8-Hydroxy-2-oxo-2H-chromene-3-carboxylic acid [3-(2,3-Dihydro-benzofuran-5-yl)-phenyl]-amide (74). 2,3-dihydrobenzofuran-5-boronic acid (0.114 g, 0.693 mmol) and 3-bromoaniline (0.05 mL, 0.462 mmol) were combined in DME (2mL) in a flame-dried, round-bottom flask. Na₂CO₃ (2M, 0.485 mL, 0.970 mmol) and Pd(PPh₃)₄ (0.017 g, 0.014 mmol) were added to the stirred solution. The reaction was refluxed overnight under argon flow, and subsequently cooled to room temperature. The solvent was removed under vacuum and the resulting residue was resuspended in H₂O and extracted with CH₂Cl₂. The organic phase was dried over MgSO₄ and concentrated under vacuum. The crude product was purified by silica column chromatography (5-20% EtOAc/hexanes). The purification was monitored by TLC. The solvent was removed under vacuum from fractions containing product, 3-(2,3-Dihydro-benzofuran-5-yl)-phenylamine, resulting in 0.0762 g in 78% yield.

DIEA (0.014 mL, 0.078 mmol) was added to 8-hydroxy-3-carboxy-coumarin (0.015 g, 0.071 mmol) and HATU (0.030 g, 0.078 mmol) in 0.36 mL of DMF with constant stirring at room temperature until a clear solution resulted. Subsequently, 3-(2,3-dihydro-benzofuran-5-yl)-phenylamine (0.015 g, 0.071 mmol) was added and allowed to react overnight when a solid precipitated out of solution. The resulting precipitate was filtered,

dried under suction, and finally dried overnight in vacuo to give 0.014 g of product in 49% yield: LCMS (ESI) m/z 400 (MH^+).

8-Methoxy-2-oxo-2H-chromene-3-carboxylic acid (3-pyrimidin-5-yl-phenyl)-amide (136). DIEA (0.012 mL, 0.071 mmol) was added to 8-methoxy-3-carboxy-coumarin (0.014 g, 0.065 mmol) and HATU (0.027 g, 0.071 mmol) in 0.5 mL of DMF with constant stirring at room temperature until a clear solution resulted. Subsequently, 3-pyrimidin-5-yl-phenylamine (0.011 g, 0.065 mmol) was added and allowed to react overnight when a solid precipitated out of solution. The resulting precipitate was filtered, dried under suction, and finally dried overnight in vacuo to give 0.015 g of product in 62% yield: LCMS (ESI) m/z 374 (MH^+).

8-Hydroxy-2-oxo-2H-chromene-3-carboxylic acid [3-(4-oxo-4H-chromen-6-yl)-phenyl]-amide (161). Chromone-6-boronic acid pinacol ester (0.237 g, 0.872 mmol) and 3-bromoaniline (0.063 mL, 0.581 mmol) were combined in dioxane (2mL) in a flame-dried, round-bottom flask. K_3PO_4 (1.27M, 0.778 mL, 0.99 mmol), PCy_3 (0.004 g, 0.014 mmol), and $Pd_2(dba)_3$ (0.005 g, 0.006 mmol) were added to the stirred solution. The reaction was refluxed overnight under argon flow, and subsequently cooled to room temperature. The solvent was removed under vacuum and the resulting residue was resuspended in CH_2Cl_2 . The organic phase was dried over $MgSO_4$, filtered, and concentrated under vacuum. The crude product was purified by flash silica column chromatography (0-100% EtOAc/hexanes). The purification was monitored by TLC. The solvent was removed under vacuum from fractions containing product, 3-(4-oxo-4H-chromen-6-yl)-phenylamine, resulting in 0.059 g in 43% yield.

DIEA (0.012 mL, 0.071 mmol) was added to 8-hydroxy-3-carboxy-coumarin (0.013 g, 0.065 mmol) and HATU (0.027 g, 0.071 mmol) in 0.5 mL of DMF with constant stirring at

room temperature until a clear solution resulted. Subsequently, 3-(4-oxo-4H-chromen-6-yl)-phenylamine (0.015 g, 0.065 mmol) was added and allowed to react overnight when a solid precipitated out of solution. The resulting precipitate was filtered, dried under suction, and finally dried overnight in vacuo to give 0.007 g of product in 27% yield: LCMS (ESI) m/z 426 (MH^+).

8-Methoxy-2-oxo-2H-chromene-3-carboxylic acid [3-(4-oxo-4H-chromen-6-yl)-phenyl]-amide (162). DIEA (0.012 mL, 0.071 mmol) was added to 8-methoxy-3-carboxy-coumarin (0.014 g, 0.065 mmol) and HATU (0.027 g, 0.071 mmol) in 0.5 mL of DMF with constant stirring at room temperature until a clear solution resulted. Subsequently, 3-(4-oxo-4H-chromen-6-yl)-phenylamine (0.015 g, 0.065 mmol) was added and allowed to react overnight when a solid precipitated out of solution. The resulting precipitate was filtered, dried under suction, and finally dried overnight in vacuo to give 0.028 g of product in 100% yield: LCMS (ESI) m/z 440 (MH^+).

8-Methoxy-2-oxo-2H-chromene-3-carboxylic acid (3', 5'-difluoro-biphenyl-3-yl)-amide (178). DIEA (0.012 mL, 0.071 mmol) was added to 8-methoxy-3-carboxy-coumarin (0.014 g, 0.065 mmol) and HATU (0.027 g, 0.071 mmol) in 0.5 mL of DMF with constant stirring at room temperature until a clear solution resulted. Subsequently, 2-(3-Amino-phenyl)-indole-1-carboxylic acid tert-butyl ester (0.013 g, 0.065 mmol) was added and allowed to react overnight when a solid precipitated out of solution. The resulting precipitate was filtered, dried under suction, and finally dried overnight in vacuo to give 0.012 g of product in 47% yield: LCMS (ESI) m/z 408 (MH^+).

Procaspase/ caspase expression and purification. Full-length human procaspase-3, -6, and -7 genes were cloned into pET23b, as previously described (71,168). Active site

cysteine residues in procaspase-3 (C163A) and procaspase-7 (C186A) were mutated to alanine by Quickchange mutagenesis (Qiagen). For expression, all plasmids were transformed into the bacterial strain BL21 (DE3) pLysS. Wild-type procaspases-3, -6, and -7, inactive procaspase-3 (C163A) and -7 (C186A), as well as caspases-3, -6 and -7 were expressed and purified as previously described (71,168).

In vitro procaspase activation assays (71). 100 nM wild-type procaspase-3, -6 or -7 was added to a caspase activity buffer (50 mM HEPES, pH 7.4, 50 mM KCl, 0.1 mM EDTA, 10 mM DTT, and 0.1% CHAPS for procaspase-3; 100 mM HEPES, pH 7.0, 5 mM CaCl₂, 1 mM DTT, and 0.1% CHAPS for procaspase-7; and 100 mM HEPES, pH 7.4, 0.1% CHAPS, and 10 mM DTT for procaspase-6). A dilution series of each compound was added and incubated at 37°C for 5 hours. Ac-DEVD-afc (acetyl-Asp-Glu-Val-Asp-7-amino-4-trifluoromethylcoumarin; SM Biochemicals LLC) was added to procaspases-3 and -7 and Ac-VEID-afc (acetyl-Val-Glu-Ile-Asp-7-amino-4-trifluoromethylcoumarin; Axxora) was added to procaspase-6 to start kinetic assays. Activity was monitored on a SpectraMax M5 (Molecular Devices) plate reader. Initial rates were plotted versus compound concentration.

Caspase activity assays. A dilution series of each compound was added to 20 nM caspase-3. Ac-DEVD-afc was added immediately to start kinetic assays. Initial rates were plotted versus compound concentration.

Wild-type procaspase processing assay. Wild-type procaspase-3 was agitated in buffer (50 mM HEPES, pH 7.4, 50 mM KCl, 0.1 mM EDTA, 1 mM DTT, and 0.1% CHAPS) with a dilution series of compound 1541 or compound 161. After a 5-hour incubation at 37°C,

samples were quenched with LDS loading buffer, analyzed by SDS/PAGE, and visualized by silver stain.

Susceptibility assays. Inactive procaspase-7 (C186A) was agitated in buffer (20 mM HEPES, pH 7.4, 10 mM KCl, 1.5 mM MgCl₂, 1.5% Sucrose, 1 mM DTT, and 0.1% CHAPS) with 25 μM of the specified compounds or DMSO alone. 20 nM active caspase-7 or 1 nM granzyme B was added to each sample. After incubation at 37°C, samples were quenched with LDS loading buffer, analyzed by SDS/PAGE, and visualized by silver stain.

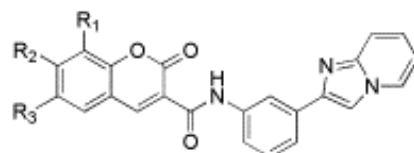
Co-sedimentation assays. Assays were performed as previously described (156,179). Briefly, 20 μL 1.25 mM compound 53, compound 1541, or DMSO alone was added to a dilution series of the inactive procaspase-7 (C186A), caspase-7, inactive procaspase-3 (C163A) or caspase-3 in 980 μL of buffer (20 mM HEPES, pH 7.4, 10 mM KCl, 1.5 mM MgCl₂, 1 mM DTT, 1.5% Sucrose, and 0.1% CHAPS). Each sample was vortexed followed by centrifugation at 16,200xg for 10 minutes. The supernatant was aspirated, and 100 μL assay buffer was added to the pellet in each tube. Samples were diluted with 4x LDS sample buffer, analyzed by SDS/PAGE, visualized by coomassie (Bio-Rad) stain, imaged on a LI-COR Odessey Infrared Imaging System, and quantified by ImageJ.

Transmission Electron Microscopy. Formvar/carbon coated 200 mesh copper grids (Ted Pella, Inc.) were glow discharged. Compound samples were generated by diluting DMSO stocks in assay buffer (50 mM HEPES, pH 7.4, 50 mM KCl, 0.1 mM EDTA, 10 mM DTT, and 0.1% CHAPS for compounds 161, 1541B and 1541D; 100 mM HEPES, pH 7.0, 5 mM CaCl₂, 1 mM DTT, and 0.1% CHAPS for compound 53; and 100 mM

HEPES, pH 7.4, 0.1% CHAPS, and 10 mM DTT for compounds 162 and 178) for a final concentration of 2% DMSO. 5 μ L of each sample was next adsorbed onto the grids followed by negative staining in 50 μ L drops (x2) of filtered 2% sodium phosphotungstate, pH 7.4. The grids were viewed in a FEI Tecnai F20 electron microscope (Eindhoven, The Netherlands) at 80 kV. A Gatan Ultrascan CCD camera recorded the images.

Cell death and caspase activation assays: 2,000 HeLa, HCC1954, MEF or HEK293 cells or 50,000 wild-type Jurkat cells were incubated with 25 μ M specified compounds (final DMSO concentration of 0.5%) for the indicated time periods in 50 μ L of media. Samples were assayed for cell viability by addition of 50 μ L of CellTiter-Glo® (Promega) and for caspase activity by the addition of 50 μ L of Caspase-Glo® 3/7 Luminescence Assay Kits.

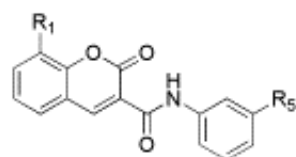
Cellular procaspase-3 processing assay in MCF7 cells: Stable cell lines expressing wild-type and inactive (C163A) procaspase-3 were previously generated (71). 1,000,000 MCF7 cells with wild-type procaspase-3 or inactive procaspase-3 (C163A) were incubated in 10 mL of media overnight in 75-cm² flask. Media was removed and replaced with media containing 10 μ M 1541. Cells were harvested at the indicated time points. Cell pellets were resuspended in PBS with 1% SDS, sonicated, and boiled for 5 minutes. Protein concentrations in lysates were quantified, and normalized. Samples were analyzed by SDS/PAGE followed by western blot with an antibody specific for the cleaved form of caspase-3 (Cell Signaling #9664). Western blots were reprobbed with GAPDH (Cell Signaling #2118).



Procaspase Activation

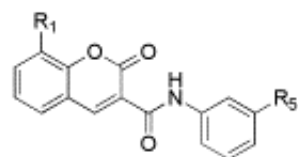
ID	R ₁	R ₂	R ₃	3	6	7
1541	-OMe	-H	-H	+++	+++	-
1541B	-OH	-H	-H	+++	-	-
1541C	-H	-H	-Br	+	+	ND
1541A	-OCF ₃	-H	-H	-	-	ND
1	-H	-OMe	-H	-	-	ND
2	-F	-H	-H	+++	+++	ND
3	-OH	-OH	-H	+	-	ND
4	-Br	-H	-H	-	-	ND
5	-OEt	-H	-H	-	-	ND
6	-H	-H	-OMe	-	-	ND
7	-H	-OH	-OH	-	-	ND
8	-OMe	-OMe	-H	-	ND	ND
9	-H	-H	-OCF ₃	-	-	ND
10	-H	-H	-I	-	-	ND
11	-H	-H	-OH	-	-	ND
12	-H	-H	-OMe	-	-	ND
13	-H	-H	-H	-	ND	ND
14		-H	-OMe	-	-	ND
1541H		-H	-OMe	-	-	ND

Table 5-1. Modifications to the substituents on the 1541 coumarin core. Procaspase activation as a result of incubation with compound for 5 hours at 37°C (+++ EC₅₀ ~ 0.5 – 10 μM; ++ EC₅₀ ~ 10 – 50 μM; + EC₅₀ ~ 50 – 200 μM; - no activation observed; ND not determined).



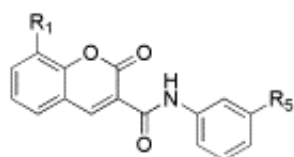
Procaspase Activation

ID	R ₁	R ₅	3	6	7
1541D	-OMe	-H	-	-	ND
15	-OH		-	-	-
1541F	-OMe		-	-	ND
16	-OH		-	-	-
1541I	-OMe		-	-	ND
17	-OH		-	-	-
18	-OMe		-	-	-
19	-OH		+++	+++	+
20	-OMe		-	-	ND
41	-OH		++	+	-
42	-OMe		-	-	-
43	-OCF ₃		-	-	-



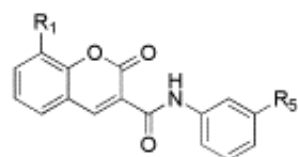
Procaspase Activation

ID	R ₁	R ₅	3	6	7
44	-OH		-	-	+++
45	-OMe		-	-	-
46	-OCF ₃		-	-	-
47	-OH		-	-	-
48	-OMe		-	-	-
49	-OCF ₃		-	-	-
50	-OH		-	-	-
51	-OMe		-	-	-
52	-OCF ₃		-	-	-
53	-OH		-	-	+++
54	-OMe		-	-	-
55	-OCF ₃		-	-	-
56	-OH		-	-	-
57	-OMe		-	-	-
58	-OCF ₃		-	-	-



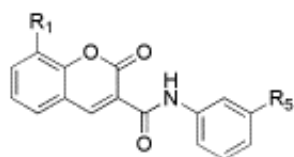
Procaspase Activation

ID	R ₁	R ₅	3	6	7
59	-OH		-	-	-
60	-OMe		-	-	-
61	-OCF ₃		-	-	-
62	-OH		-	-	++
63	-OMe		-	-	-
64	-OCF ₃		-	-	-
65	-OH		-	-	-
66	-OMe		-	-	-
67	-OCF ₃		-	-	-
68	-OH		-	-	-
69	-OMe		-	-	-
70	-OCF ₃		-	-	-
71	-OH		-	-	-
72	-OMe		-	-	-
73	-OCF ₃		-	-	-



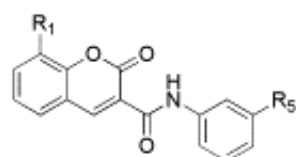
Procaspase Activation

ID	R ₁	R ₅	3	6	7
74	-OH		-	-	++
75	-OMe		-	-	-
76	-OCF ₃		-	-	-
77	-OH		-	-	+++
78	-OMe		-	-	-
79	-OCF ₃		-	-	-
80	-OH		-	-	-
81	-OMe		-	-	-
82	-OCF ₃		-	-	-
83	-OH		-	-	-
84	-OMe		-	-	-
85	-OCF ₃		-	-	-
86	-OH		-	-	-
87	-OMe		-	-	-
88	-OCF ₃		-	-	-



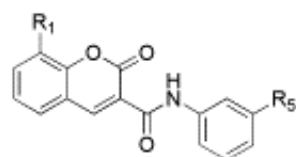
Procaspase Activation

ID	R ₁	R ₅	3	6	7
89	-OH		-	-	-
90	-OMe		-	-	-
91	-OCF ₃		-	-	-
92	-OH		-	-	-
93	-OMe		-	-	-
94	-OCF ₃		-	-	-
95	-OH		-	-	-
96	-OMe		-	-	-
97	-OCF ₃		-	-	-
98	-OH		++	-	++
99	-OMe		-	-	-
100	-OCF ₃		-	-	-



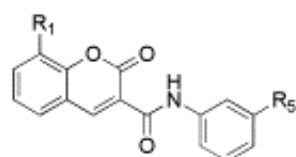
Procaspase Activation

ID	R ₁	R ₅	3	6	7
127	-OH		-	-	-
128	-OMe		-	-	-
129	-OH		-	-	-
130	-OMe		-	-	-
131	-OH		-	-	-
132	-OMe		-	-	-
133	-OH		-	-	-
134	-OMe		-	-	-
135	-OH		-	-	-
136	-OMe		+	+	-
137	-OH		-	-	-
138	-OMe		-	-	-
139	-OH		-	-	-
140	-OMe		-	-	-
141	-OH		-	-	++
142	-OMe		-	-	-



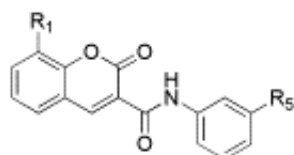
Procaspase Activation

ID	R ₁	R ₅	3	6	7
143	-OH		-	-	-
144	-OMe		-	-	-
145	-OH		-	-	-
146	-OMe		-	-	-
147	-OH		-	-	-
148	-OMe		-	-	-
149	-OH		-	-	-
150	-OMe		-	-	-
151	-OH		++	-	++
152	-OMe		-	-	-
153	-OH		++	-	++
154	-OMe		-	-	-
155	-OH		-	-	-
156	-OMe		-	-	-



Procaspase Activation

ID	R ₁	R ₅	3	6	7
157	-OH		-	-	-
158	-OMe		-	-	-
159	-OH		-	-	-
160	-OMe		-	-	-
161	-OH		+++	-	-
162	-OMe		-	+++	-
163	-OH		-	-	-
164	-OMe		-	-	-
165	-OH		-	-	-
166	-OMe		-	-	-



Procaspase Activation

ID	R ₁	R ₅	3	6	7
167	-OH		-	-	-
168	-OMe		-	-	-
169	-OH		-	-	-
170	-OMe		-	-	-
171	-OH		-	-	-
172	-OMe		-	-	-
173	-OH		-	-	-
174	-OMe		-	-	-
175	-OH		-	-	-
176	-OMe		-	-	-
177	-OH		-	-	-
178	-OMe		-	++	-

Table 5-2. Distinct meta substituents on the central ring of 1541. Procaspase activation as a result of incubation with compound for 5 hours at 37°C (+++ EC₅₀ ~ 0.5 – 10 μM; ++ EC₅₀ ~ 10 – 50 μM; + EC₅₀ ~ 50 – 200 μM; - no activation observed; ND not determined).

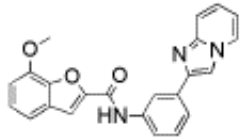
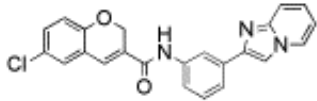
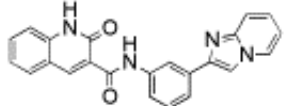
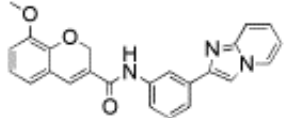
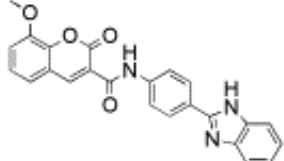
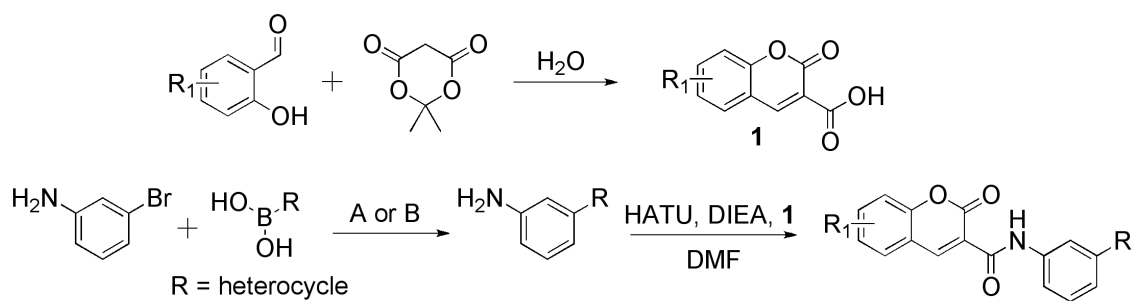
Procaspase Activation				
ID	Compound	3	6	7
179		++	++	ND
180		+	-	ND
181		++	++	ND
182		-	-	ND
183		+++	ND	ND

Table 5-3. Different heterocycles in place of the coumarin on 1541. Procaspase activation as a result of incubation with compound for 5 hours at 37°C (+++ $EC_{50} \sim 0.5 - 10 \mu\text{M}$; ++ $EC_{50} \sim 10 - 50 \mu\text{M}$; + $EC_{50} \sim 50 - 200 \mu\text{M}$; - no activation observed; ND not determined).



A. Pd(PPh₃)₄, Na₂CO₃, DME; Reflux under Ar
 B. Pd₂(dba)₃, PCy₃, K₃PO₄, dioxane; Reflux under Ar

Scheme 5-1. Synthetic route for 1541 analogues.

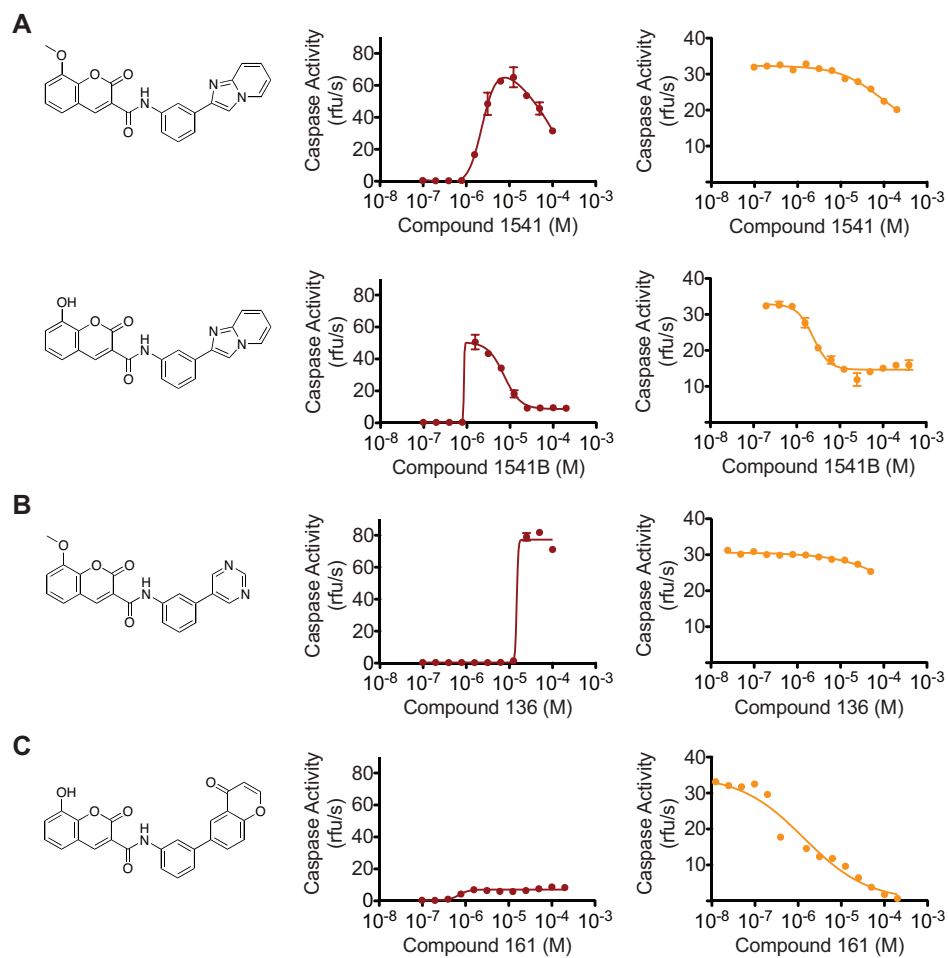


Figure 5-2. 1541 analogues exhibit unique profiles for procaspase-3 activation. (A) Compounds that show a bell-shaped curve with an initial activating event followed by inhibition. (B) Compounds that just show a high level of activation, with no inhibition. (C) Compounds that exhibit a low level of procaspase-3 activation. The inhibition curves seen in the procaspase-3 activation assays (red) match inhibition curves against recombinant caspase-3 (orange).

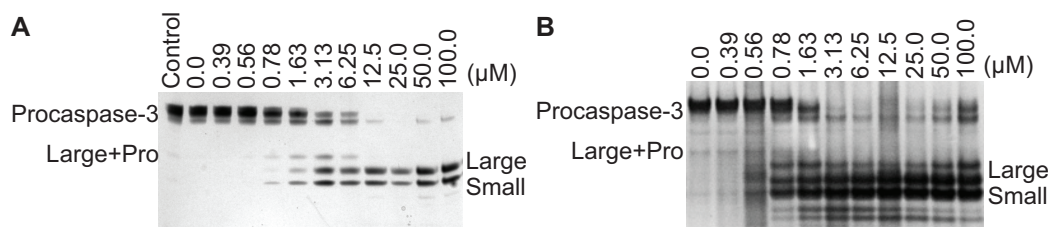


Figure 5-3. Processing of procaspase-3 by 1541 analogues. A dilution series of compound 1541 (A) or compound 161 (B) was incubated with wild-type procaspase-3 for 5 hours. Samples were quenched with LDS loading buffer, analyzed by SDS/PAGE and visualized by silver stain. Both compounds promote full processing of procaspase-3, even at concentrations where inhibition is observed against the Ac-DEVD-afc substrate.

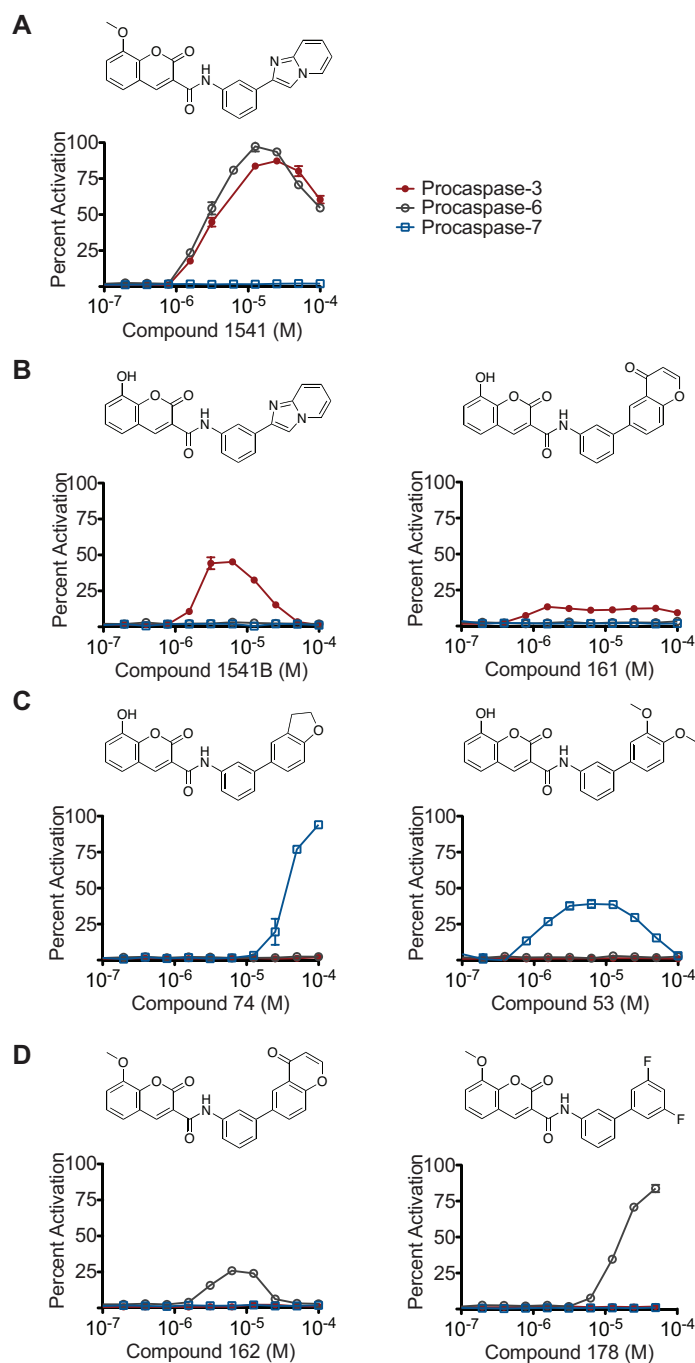


Figure 5-4. 1541 analogues show selective activation of executioner procaspases-3 (red), -6 (grey), and -7 (blue). (A) 1541 activates procaspase-3 and -6. (B) Procaspase-3 activation by select compounds. (C) Activity of compounds that preferentially activate procaspase-6. (D) Activation profiles for compounds that activate procaspase-7.

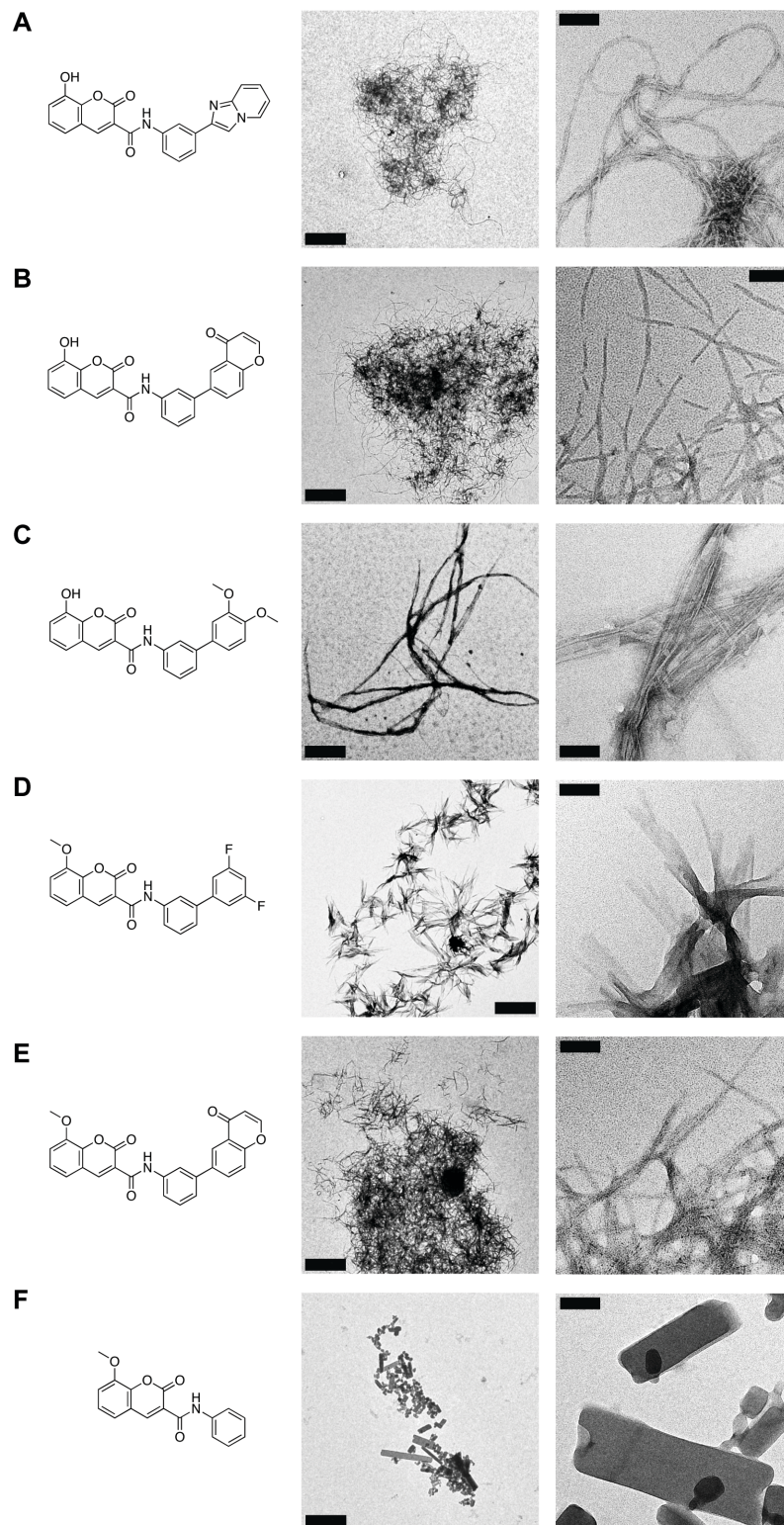


Figure 5-5. Transmission electron micrographs of 1541 analogues. Analogues of 1541 form fibrils at room temperature, as shown by negatively stained images. Samples of

compound 1541B (A), compound 161 (B), compound 53 (C), compound 178 (D), compound 162 (E), compound 1541D (F) were analyzed by TEM. Note distinctive features of individual compounds. Scale bars = 1 μm (on the left) or 100 nm (on the right).

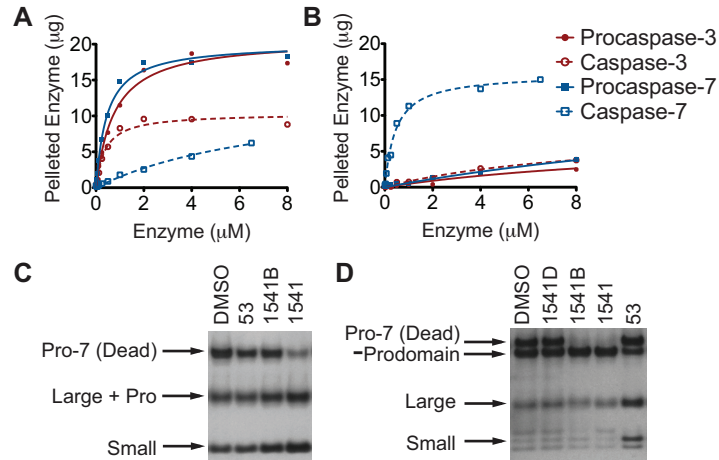


Figure 5-6. Selective activation of procaspase-7. Co-sedimentation of a dilution series of procaspase-7, procaspase-3, caspase-3, and caspase-7 with 25 μ M compound 1541 (A) or with 25 μ M compound 53 (B). (C) Susceptibility of the inactive procaspase-7 (C186A) to processing by 1 nM granzyme B in the presence of different 1541 analogues after a 60 minute incubation. (D) Susceptibility of the inactive procaspase-7 (C186A) to processing by 20 nM caspase-7 in the presence of different 1541 analogues after a 30 minute incubation.

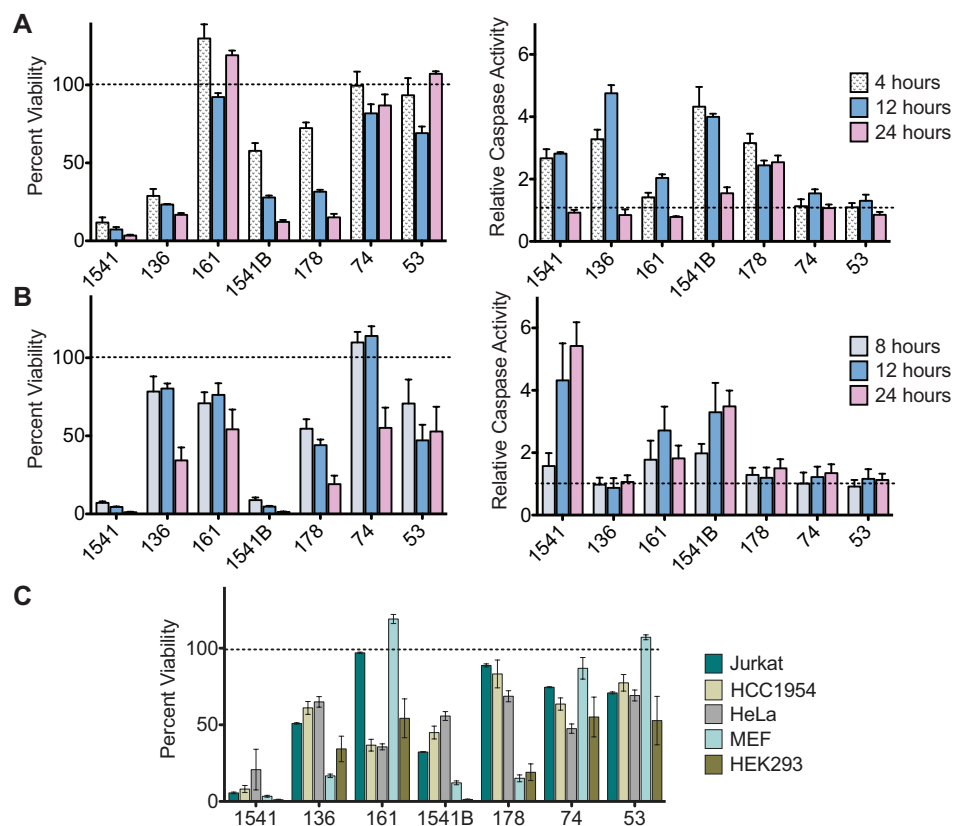


Figure 5-7. Analogues exhibit selective cell death and caspase activation profiles. (A) MEFs were treated with 25 μ M of the indicated compounds. After 4, 12, and 24 hours, cells were assayed for viability and caspase activity. Cell death was evaluated by the Cell Titer Glo (Life Technologies) assay and caspase activity by the Caspase Glo (Life Technologies) assay. (B) HEK293 cells were similarly treated with a panel of compounds and assayed for viability and caspase activity after 8, 12, and 24 hours. (C) After a 24-hour incubation with 25 μ M of the indicated compounds, Jurkat, HCC1954, HeLa, MEF, and HEK293 cells were analyzed for percent viability.

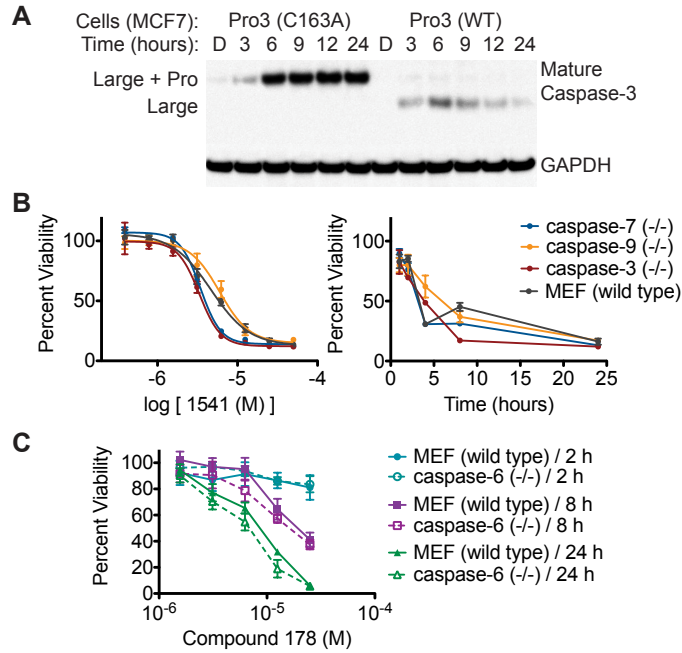


Figure 5-8. 1541 analogues induce cell death independent of direct procaspase activation. (A) MCF7 cells were stably transfected with either wild-type or inactive (C163A) procaspase-3. Similar rates of procaspase-3 processing in both cell lines treated with 1541. (B) 1541 dose response after a 24-hour incubation with wild-type or caspase knockout MEFs show overlapping EC_{50} 's. Similar rates of decreased viability in MEFs treated with 1541. (C) A dilution series of compound 178 (selective procaspase-6 activator *in vitro*) was tested against wild-type and caspase-6 knockout MEFs.

Chapter 6:
Conclusions and Future Directions

Most of the 560 human proteases are expressed as inactive precursors, or zymogens (143). These zymogens usually require external stimuli to form an active or mature enzyme (144). Caspases, which are important regulators of fate-determining cellular processes, are no exception. They are trapped as inactive precursors that become activated in response to extrinsic or intrinsic cellular signals. The known cellular mechanisms of procaspase activation upon stimulation of these pathways include localization to scaffolding complexes and processing by active, upstream proteases (61,145,148).

The goal of this thesis was to generate a better understanding of procaspase activation mechanisms as well as to reveal methods to promote zymogen maturation to the cleaved, active enzyme. Key to these studies was a detailed biochemical characterization of procaspases and the identification of a chemical tool that would facilitate procaspase activation. This chemical tool, compound 1541, was found to assemble into nanofibrils. While limited in its direct applications to cellular studies on procaspases, this tool permitted the elucidation of the natural procaspase-3 activation mechanism. Further, it suggested a novel cellular regulatory role for fibrillar structures in procaspase-3 activation. The biochemical characterization of procaspase-3 maturation on these fibrils also supports additional studies to identify small molecule activators of procaspases. Notably, these nanofibrils do induce rapid apoptosis in cells. While the cellular activity is most likely not due to direct procaspase activation, additional studies to further elucidate the mechanism of apoptosis may uncover novel chemotherapeutic targets.

Identification of a procaspase-3 activator

The mature, cleaved form of the caspases is known from structural and biochemical studies to exist in an equilibrium between an active and an inactive state.

Both conformations have been trapped with small molecules. From this evidence, procaspases were reasoned to exist in a similar equilibrium. With this rationale, compound 1541 was identified from a high-throughput screen (HTS) against procaspase-3 (71). This small molecule promoted rapid processing and activation of procaspase-3 and -6 at physiological concentrations of the proenzymes. Importantly, 1541 promoted enhanced susceptibility of procaspase-3 to proteolysis by upstream proteases. This supported the idea that the compound stabilized a more active conformation of the procaspase. Cells treated with 1541 also showed rapid caspase activation and cell death independent of signaling through both the extrinsic and intrinsic apoptotic pathways. These studies indicated a direct procaspase activation mechanism both *in vitro* and in cells.

Characterization of the activator

Initial studies on 1541 suggested that it did not assemble into promiscuous small molecule aggregates. These aggregates have been shown to act non-specifically to inhibit enzyme function and to be sensitive to detergents. 1541 and related analogues did not inhibit β -lactamase, and their activities were not affected by detergents (150). However, additional studies showed that bovine serum albumin (BSA) could restrict the activity of these small molecules, a classic test for aggregation (153). Analyses with dynamic light scattering (DLS) and particle flow cytometry demonstrated the presence of particles, but with features very distinct from previously described colloidal aggregates (156).

Transmission electron microscopy (TEM) images were invaluable in assessing the properties of these particles. Rather than colloids, 1541 and other active compounds assembled into fibrils that were roughly 4 nm in diameter and greater than 1 μ m long.

Procaspase-3 was shown to line the length of the fibrils. 1541 is a novel, self-assembling scaffold that acts as a catalyst for procaspase-3 activation. However, many properties of this class of small molecules are still unknown. Similar to known aggregators, 1541 is a fairly planar molecule, however, it does not form colloidal particles (150). Future studies to elucidate the structural features of 1541 that drive fibril assembly over colloid formation would be interesting to explore for design purposes. Furthermore, from a medicinal chemistry perspective, an ability to rationally disrupt particle formation by specific modifications to a small molecule would be a worthwhile endeavor.

Distinct analogues of 1541 also interact and activate procaspase-3 to different extents. For example, 1541B binds procaspase-3 to a greater extent compared to 1541 and activates the proenzyme much faster. Additional investigations to understand the features of this small molecule that drive these diverse interactions would be useful for bioprocessing applications. This endeavor may also permit the design of other proenzyme activators that work by a similar mechanism.

Elucidation of the *in vitro* mechanism of procaspase-3 activation

With co-sedimentation studies, procaspase-3 was shown to localize to the surface of the fibrils. This interaction was saturable, suggesting a fixed number of binding sites on 1541 nanofibrils. However, thorough biochemical characterization of procaspase-3 activity shows that the proenzyme alone does not auto-process, even in the presence of a scaffold. Maturation, and hence activation, of this proenzyme requires a small amount of an active protease. Important to this assessment was the finding that procaspase-3 contains a trace contaminant of the cleaved caspase-3 (<0.2%). Mature caspase-3 also binds to 1541 nanofibrils, suggesting that 1541 provides a scaffold for induced proximity of the active protease with its zymogen substrate to facilitate

maturation. This colocalization effect results in a 17-fold change in the catalytic efficiency of caspase-3 against its full-length proenzyme substrate.

This model for procaspase-3 activation ignores any impact of an ordered array of proenzyme activation along the length of the fibrils. In other words, it is possible that there is a cascade of activation of individual procaspase-3 molecules along the fibrils that is ignited by the trace amount of cleaved caspase-3. This model would mimic a fuse or a firecracker. Computational analyses would suggest that the 17-fold change in catalytic efficiency of caspase-3 cleaving procaspase-3 is sufficient to explain the rate enhancement in proenzyme activation. However, direct evidence is lacking. Further work will be required to distinguish these details.

Many scaffolding complexes, such as the apoptosome, the inflammasome, and the death-inducing signaling complex (DISC), are known to promote procaspase processing and activation (61,145,148). Localization or induced proximity of an active procaspase to these structures can promote trans activation: one proenzyme molecule cleaving another molecule (180). However, the results in this thesis show that in the case of procaspase-3, colocalization with an active protease, whether it is the cleaved caspase-3 or another upstream protease, is essential to facilitate maturation.

Interestingly, these analyses also reveal that a physiologically relevant fibril, amyloid- β (1-40), can bind and activate procaspase-3. This activation is less rapid than the activation observed on 1541 fibrils. The amyloid- β (1-40) fibrils induce a smaller change in caspase-3 catalytic efficiency against the procaspase-3 substrate, but the exact reason for this remains unclear. It is possible that oligomers, which are also formed upon incubation of the amyloid- β (1-40) peptide, may interact with the caspase to inhibit its activity. Additional studies will be important to evaluate this difference.

Recent reports have demonstrated localization of caspases to fibrous cellular structures, such as cytokeratin 18 or the death effector domain (DED) motifs in the prodomain of procaspase-8 (164,194-196). Future studies to evaluate the relevance of endogenous fibrils in procaspase activation may reveal a novel regulatory approach for this class of enzymes. One interesting study would be to test a panel of physiologically relevant fibrils to assess their relative impact on procaspase-3 activation.

Targeting zymogen activation

Most proteases are expressed as zymogens, yet the degree to which their activities are restricted can fluctuate. Zymogenicity describes the relative activity of a mature enzyme to its zymogen precursor. A high zymogenicity would indicate a precursor that is locked in an inactive state and requires processing for activation. A low zymogenicity indicates an active precursor, where processing is not essential for proenzyme activation. For example, processing of tissue plasminogen activator (tPA) is minimally coupled to its catalytic activity, which is signified by a low zymogenicity (2-10), whereas cleavage of trypsinogen and chymotrypsinogen is critical for activation, denoted by a high zymogenicity (10^4 - 10^6) (180,191,192).

Procaspase-3 has previously been shown to have a zymogenicity value of approximately $>10,000$ (180). This does denote a relatively inactive zymogen, however the results presented in this thesis show that earlier procaspase-3 activity measurements are dominated by a cleaved caspase-3 contaminant. If this contaminant's activity is eliminated by a sub-stoichiometric concentration of an irreversible inhibitor, the procaspase-3 zymogenicity value increases to $>10,000,000$. Similar to trypsinogen and chymotrypsinogen, the endogenous regulation of procaspase-3 is due to upstream proteases rather than auto-activation. This large value also indicates that the active conformation of procaspase-3 is highly unfavorable under physiological conditions. This

would suggest a high barrier for a small molecule to overcome to promote auto-activation of procaspase-3, and reinforces the lack of evidence for procaspase-3 auto-processing described above. However, the *in vitro* procaspase-3 characterization described above would suggest two approaches to promote procaspase-3 activation: direct activation of the mature caspase or colocalization of procaspase-3 with the mature caspase. Both of these approaches are not a direct activation of the proenzyme.

Interestingly, prior reports indicate that the initiator procaspase-8 has a lower zymogenicity of >100 (180). While these measurements could be influenced by a small amount of active caspase-8 contaminant, its relation to procaspase-3 zymogenicity is most likely consistent. This indicates a greater conformational flexibility for this proenzyme. Furthermore, cellular FLICE inhibitory protein (c-FLIP_L) has been identified as an endogenous activator of procaspase-8 (222). Activation occurs due to heterodimerization of c-FLIP_L with procaspase-8 to promote an active conformation of the proenzyme. These results combined suggest that procaspase-8 may be a better target relative to procaspase-3 for zymogen activation. In general, proenzymes with lower zymogenicities may be better pursuits for small molecule activators.

Selective activation of executioner procaspases

In this thesis, a focused library of 1541 analogues was synthesized and tested for activation of executioner procaspases-3, -6 and -7. Selective activators for each of the executioner procaspases were identified. Initial analysis of the analogues by TEM suggests that all the active compounds also assemble into fibrils, although the morphologies appear distinct. Preliminary results suggest that the fibrils exhibit selective interactions with the pro- and mature caspases-3, -6, and -7. These selective interactions could arise for several reasons: distinct substituents on 1541 analogues could interact uniquely with different proteases when displayed on the fibrils, subtle

differences in the surface charge and/or hydrophobicity of the fibrils could result in distinct interactions with different proteases, or the surface area of different fibrils could facilitate distinct interactions. Previous reports studying colloidal aggregates have also suggested that within a single structure activity relationship (SAR) series divergent modes of inhibition can exist: competitive inhibition and aggregation (217). Additional studies are necessary to distinguish these possibilities.

Interestingly, distinct activation profiles against procaspase-3 are observed for different fibril forming compounds. For example, for 1541 activation is observed at low concentrations of compound followed by inhibition observed at higher concentrations (>30 μM) (71). Other compounds show a weaker EC_{50} for activation and no inhibition. Others show a more potent EC_{50} , but only a low level of overall activation. In all cases tested, the proenzyme is completely processed, however its overall activity against a tetrapeptide substrate is impaired. The IC_{50} for inhibition in the proenzyme activation assays matches the IC_{50} for inhibition against the fully mature caspase. This suggests that while colocalization of procaspase-3 with caspase-3 leads to processing of the proenzyme, the fibrils can subsequently inhibit the activated enzyme. Further studies are necessary to understand the exact mechanism of inhibition observed.

Cellular apoptotic mechanism of fibrils

As mentioned above, 1541 induces caspase activity and cell death in a variety of cell lines. Cell death induced by 1541 is independent of both the intrinsic and extrinsic pathway, as illustrated by apoptosis observed in Bax/Bak knockout mouse embryonic fibroblasts (MEFs) and in caspase-8 deficient Jurkats, respectively (223,224).

Importantly, the fibrils appear necessary for inducing apoptosis. Centrifugation of samples to remove particulates eliminates 1541 activity. However, a direct interaction between procaspases and the fibrils in cells seems unlikely since 1541 does not

promote procaspase-3 activation in lysates. This demonstrates that other proteins compete with procaspase-3 for a direct association with the fibrils, impairing activation.

Additional studies presented in this thesis further show that a direct mechanism of procaspase-3 activation in cells is unlikely. To interrogate the importance of caspase-3 catalytic activity in 1541-induced apoptosis, MCF7 cells, which lack procaspase-3, were stably transfected with either wild-type procaspase-3 or inactive procaspase-3 (C163A) (225). A similar rate of processing of each construct was induced in both cell lines in response to 1541. This indicates that 1541 promotes apoptosis upstream of procaspase-3. Further, 1541 was tested against a panel of caspase knock-out MEFs, including caspase-9, caspase-3, and caspase-7 (219). Loss of individual caspases had minimal impact on 1541 activity. While a direct mechanism of procaspase activation seems unlikely given the above results, additional experiments are necessary to determine the exact cellular mechanism.

1541 analogues, which selectively activate procaspases-3, -6, and -7, do show more selective cytotoxicity profiles. In other words, certain compounds only induce death in certain cell lines. However, studies with caspase knock-out MEFs indicate that apoptosis induced by these compounds is not due to direct activation of the individual caspases. Further studies will be necessary to understand the differences between the selective analogues and 1541. It would also be interesting to explore the cellular activity of other fibril forming molecules, such as amyloid- β (1-40) (197).

References

1. Alaimo, P. J., Shogren-Knaak, M. A., and Shokat, K. M. (2001) *Current Opinion in Chemical Biology* **5**, 360-367
2. Cravatt, B. F., and Sorensen, E. J. (2000) *Current Opinion in Chemical Biology* **4**, 663-668
3. Stockwell, B. R. (2000) *Trends in biotechnology* **18**, 449-455
4. Cárdenas, M. L., and Cornish-Bowden, A. (1989) *The Biochemical journal* **257**, 339-345
5. Goldbeter, A., and Koshland, D. E. (1982) *Quarterly reviews of biophysics* **15**, 555-591
6. Szedlacsek, S. E., Cárdenas, M. L., and Cornish-Bowden, A. (1992) *European journal of biochemistry / FEBS* **204**, 807-813
7. Bishop, A. C., and Chen, V. L. (2009) *Journal of Chemical Biology* **2**, 1-9
8. Cárdenas, M. L., Cornish-Bowden, A., and Ureta, T. (1998) *Biochimica et biophysica acta* **1401**, 242-264
9. Matschinsky, F. (2009) *Nature reviews Drug discovery* **8**, 399-416
10. Pal, M. (2009) *Drug discovery today* **14**, 784-792
11. Matschinsky, F. M., Magnuson, M. A., Zelent, D., Jetton, T. L., Doliba, N., Han, Y., Taub, R., and Grimsby, J. (2006) *Diabetes* **55**, 1-12
12. Gidh-Jain, M., Takeda, J., Xu, L. Z., Lange, A. J., Vionnet, N., Stoffel, M., Froguel, P., Velho, G., Sun, F., and Cohen, D. (1993) *Proceedings of the National Academy of Sciences of the United States of America* **90**, 1932-1936
13. de la Iglesia, N., Veiga-da-Cunha, M., Van Schaftingen, E., Guinovart, J. J., and Ferrer, J. C. (1999) *FEBS letters* **456**, 332-338
14. Anderka, O., Boyken, J., Aschenbach, U., Batzer, A., Boscheinen, O., and Schmoll, D. (2008) *The Journal of biological chemistry* **283**, 31333-31340

15. Veiga-da-Cunha, M., and Van Schaftingen, E. (2002) *The Journal of biological chemistry* **277**, 8466-8473
16. Grimsby, J., Sarabu, R., Corbett, W. L., Haynes, N.-E., Bizzarro, F. T., Coffey, J. W., Guertin, K. R., Hilliard, D. W., Kester, R. F., Mahaney, P. E., Marcus, L., Qi, L., Spence, C. L., Tengji, J., Magnuson, M. A., Chu, C. A., Dvorozniak, M. T., Matschinsky, F. M., and Grippo, J. F. (2003) *Science (New York, NY)* **301**, 370-373
17. Ralph, E. C., Thomson, J., Almaden, J., and Sun, S. (2008) *Biochemistry* **47**, 5028-5036
18. Guertin, K. R., and Grimsby, J. (2006) *Current medicinal chemistry* **13**, 1839-1843
19. Kamata, K., Mitsuya, M., Nishimura, T., Eiki, J.-I., and Nagata, Y. (2004) *Structure (London, England : 1993)* **12**, 429-438
20. Milne, J. C., and Denu, J. M. (2008) *Current Opinion in Chemical Biology* **12**, 11-17
21. Longo, V. D., and Kennedy, B. K. (2006) *Cell* **126**, 257-268
22. Kaeberlein, M., McVey, M., and Guarente, L. (1999) *Genes & development* **13**, 2570-2580
23. Lin, S. J., Defossez, P. A., and Guarente, L. (2000) *Science (New York, NY)* **289**, 2126-2128
24. Cohen, H. Y., Miller, C., Bitterman, K. J., Wall, N. R., Hekking, B., Kessler, B., Howitz, K. T., Gorospe, M., de Cabo, R., and Sinclair, D. A. (2004) *Science (New York, NY)* **305**, 390-392
25. Lavu, S., Boss, O., Elliott, P. J., and Lambert, P. D. (2008) *Nature Reviews Drug Discovery* **7**, 841-853

26. Kaeberlein, M., Kirkland, K. T., Fields, S., and Kennedy, B. K. (2004) *PLoS Biology* **2**, E296
27. Finkel, T., Deng, C.-X., and Mostoslavsky, R. (2009) *Nature* **460**, 587-591
28. Anderson, R. M., Bitterman, K. J., Wood, J. G., Medvedik, O., and Sinclair, D. A. (2003) *Nature* **423**, 181-185
29. Kim, J.-E., Chen, J., and Lou, Z. (2008) *Nature* **451**, 583-586
30. Zhao, W., Kruse, J.-P., Tang, Y., Jung, S. Y., Qin, J., and Gu, W. (2008) *Nature* **451**, 587-590
31. Kim, E.-J., Kho, J.-H., Kang, M.-R., and Um, S.-J. (2007) *Molecular Cell* **28**, 277-290
32. Smith, B. C., Hallows, W. C., and Denu, J. M. (2008) *Chemistry & Biology* **15**, 1002-1013
33. Howitz, K. T., Bitterman, K. J., Cohen, H. Y., Lamming, D. W., Lavu, S., Wood, J. G., Zipkin, R. E., Chung, P., Kisielewski, A., Zhang, L.-L., Scherer, B., and Sinclair, D. A. (2003) *Nature* **425**, 191-196
34. Kaeberlein, M., McDonagh, T., Heltweg, B., Hixon, J., Westman, E. A., Caldwell, S. D., Napper, A., Curtis, R., DiStefano, P. S., Fields, S., Bedalov, A., and Kennedy, B. K. (2005) *The Journal of biological chemistry* **280**, 17038-17045
35. Milne, J. C., Lambert, P. D., Schenk, S., Carney, D. P., Smith, J. J., Gagne, D. J., Jin, L., Boss, O., Perni, R. B., Vu, C. B., Bemis, J. E., Xie, R., Disch, J. S., Ng, P. Y., Nunes, J. J., Lynch, A. V., Yang, H., Galonek, H., Israelian, K., Choy, W., Iffland, A., Lavu, S., Medvedik, O., Sinclair, D. A., Olefsky, J. M., Jirousek, M. R., Elliott, P. J., and Westphal, C. H. (2007) *Nature* **450**, 712-716
36. Pacholec, M., Chrnyk, B. A., Cunningham, D., Flynn, D., Griffith, D. A., Griffor, M., Loulakis, P., Pabst, B., Qiu, X., Stockman, B., Thanabal, V., Varghese, A., Ward, J., Withka, J., and Ahn, K. (2010) *The Journal of biological chemistry*

37. Frödin, M., Antal, T. L., Dümmler, B. A., Jensen, C. J., Deak, M., Gammeltoft, S., and Biondi, R. M. (2002) *The EMBO journal* **21**, 5396-5407
38. Huse, M., and Kuriyan, J. (2002) *Cell* **109**, 275-282
39. Biondi, R. M. (2004) *Trends in biochemical sciences* **29**, 136-142
40. Biondi, R. M., Komander, D., Thomas, C. C., Lizcano, J. M., Deak, M., Alessi, D. R., and van Aalten, D. M. F. (2002) *The EMBO journal* **21**, 4219-4228
41. Biondi, R. M., Cheung, P. C., Casamayor, A., Deak, M., Currie, R. A., and Alessi, D. R. (2000) *The EMBO journal* **19**, 979-988
42. Engel, M., Hindie, V., Lopez-Garcia, L. A., Stroba, A., Schaeffer, F., Adrian, I., Imig, J., Idrissova, L., Nastainczyk, W., Zeuzem, S., Alzari, P. M., Hartmann, R. W., Piiper, A., and Biondi, R. M. (2006) *The EMBO journal* **25**, 5469-5480
43. Stroba, A., Schaeffer, F., Hindie, V., Lopez-Garcia, L., Adrian, I., Fröhner, W., Hartmann, R., Biondi, R., and Engel, M. (2009) *Journal of medicinal chemistry*
44. Hindie, V., Stroba, A., Zhang, H., Lopez-Garcia, L., Idrissova, L., Zeuzem, S., Hirschberg, D., Schaeffer, F., Jørgensen, T., Engel, M., Alzari, P., and Biondi, R. (2009) *Nature Chemical Biology* **5**, 758-764
45. Biondi, R. M., Kieloch, A., Currie, R. A., Deak, M., and Alessi, D. R. (2001) *The EMBO journal* **20**, 4380-4390
46. Pellicena, P., and Kuriyan, J. (2006) *Current opinion in structural biology* **16**, 702-709
47. Tappan, E., and Chamberlin, A. R. (2008) *Chemistry & Biology* **15**, 167-174
48. Balasubramanyam, K., Swaminathan, V., Ranganathan, A., and Kundu, T. K. (2003) *The Journal of biological chemistry* **278**, 19134-19140
49. Reineke, J., Tenzer, S., Rupnik, M., Koschinski, A., Hasselmayer, O., Schratzenholz, A., Schild, H., and von Eichel-Streiber, C. (2007) *Nature* **446**, 415-419

50. Egerer, M., Giesemann, T., Jank, T., Satchell, K. J. F., and Aktories, K. (2007) *The Journal of biological chemistry* **282**, 25314-25321
51. Egerer, M., Giesemann, T., Herrmann, C., and Aktories, K. (2009) *The Journal of biological chemistry* **284**, 3389-3395
52. Lupardus, P. J., Shen, A., Bogoyo, M., and Garcia, K. C. (2008) *Science (New York, NY)* **322**, 265-268
53. Shen, A., Lupardus, P. J., Albrow, V. E., Guzzetta, A., Powers, J. C., Garcia, K. C., and Bogoyo, M. (2009) *Nature Chemical Biology* **5**, 469-478
54. Prochazkova, K., and Satchell, K. J. F. (2008) *The Journal of biological chemistry* **283**, 23656-23664
55. Prochazkova, K., Shuvalova, L. A., Minasov, G., Voburka, Z., Anderson, W. F., and Satchell, K. J. F. (2009) *Journal of Biological Chemistry* **284**, 26557-26568
56. Pop, C., and Salvesen, G. S. (2009) *The Journal of biological chemistry* **284**, 21777-21781
57. Creagh, E. M., Conroy, H., and Martin, S. J. (2003) *Immunological reviews* **193**, 10-21
58. Yi, C. H., and Yuan, J. (2009) *Developmental cell* **16**, 21-34
59. Stennicke, H. R., and Salvesen, G. S. (1998) *Biochimica et biophysica acta* **1387**, 17-31
60. Earnshaw, W. C., Martins, L. M., and Kaufmann, S. H. (1999) *Annual review of biochemistry* **68**, 383-424
61. Salvesen, G. S., and Riedl, S. J. (2008) *Advances in experimental medicine and biology* **615**, 13-23
62. Roy, S., Bayly, C. I., Gareau, Y., Houtzager, V. M., Kargman, S., Keen, S. L., Rowland, K., Seiden, I. M., Thornberry, N. A., and Nicholson, D. W. (2001)

- Proceedings of the National Academy of Sciences of the United States of America* **98**, 6132-6137
63. Hardy, J. A., Lam, J., Nguyen, J. T., O'Brien, T., and Wells, J. A. (2004) *Proceedings of the National Academy of Sciences of the United States of America* **101**, 12461-12466
 64. Scheer, J. M., Romanowski, M. J., and Wells, J. A. (2006) *Proceedings of the National Academy of Sciences of the United States of America* **103**, 7595-7600
 65. Gao, J., Sidhu, S. S., and Wells, J. A. (2009) *Proceedings of the National Academy of Sciences of the United States of America* **106**, 3071-3076
 66. Chai, J., Wu, Q., Shiozaki, E., Srinivasula, S. M., Alnemri, E. S., and Shi, Y. (2001) *Cell* **107**, 399-407
 67. Riedl, S. J., Fuentes-Prior, P., Renatus, M., Kairies, N., Krapp, S., Huber, R., Salvesen, G. S., and Bode, W. (2001) *Proceedings of the National Academy of Sciences of the United States of America* **98**, 14790-14795
 68. Putt, K. S., Chen, G. W., Pearson, J. M., Sandhorst, J. S., Hoagland, M. S., Kwon, J.-T., Hwang, S.-K., Jin, H., Churchwell, M. I., Cho, M.-H., Doerge, D. R., Helferich, W. G., and Hergenrother, P. J. (2006) *Nature Chemical Biology* **2**, 543-550
 69. Denault, J.-B., Drag, M., Salvesen, G. S., Alves, J., Heidt, A. B., Deveraux, Q., and Harris, J. L. (2007) *Nature Chemical Biology* **3**, 519; author reply 520
 70. Peterson, Q. P., Goode, D. R., West, D. C., Ramsey, K. N., Lee, J. J. Y., and Hergenrother, P. J. (2009) *Journal of molecular biology* **388**, 144-158
 71. Wolan, D. W., Zorn, J. A., Gray, D. C., and Wells, J. A. (2009) *Science (New York, NY)* **326**, 853-858
 72. Svingen, P. A., Loegering, D., Rodriguez, J., Meng, X. W., Mesner, P. W., Holbeck, S., Monks, A., Krajewski, S., Scudiero, D. A., Sausville, E. A., Reed, J.

- C., Lazebnik, Y. A., and Kaufmann, S. H. (2004) *Clinical cancer research : an official journal of the American Association for Cancer Research* **10**, 6807-6820
73. Zhang, B. B., Zhou, G., and Li, C. (2009) *Cell metabolism* **9**, 407-416
74. Hardie, D. G. (2003) *Endocrinology* **144**, 5179-5183
75. Hardie, D. G. (2007) *Annual review of pharmacology and toxicology* **47**, 185-210
76. Amodeo, G. A., Rudolph, M. J., and Tong, L. (2007) *Nature* **449**, 492-495
77. Crute, B. E., Seefeld, K., Gamble, J., Kemp, B. E., and Witters, L. A. (1998) *The Journal of biological chemistry* **273**, 35347-35354
78. Chen, L., Jiao, Z.-H., Zheng, L.-S., Zhang, Y.-Y., Xie, S.-T., Wang, Z.-X., and Wu, J.-W. (2009) *Nature* **459**, 1146-1149
79. Xiao, B., Heath, R., Saiu, P., Leiper, F. C., Leone, P., Jing, C., Walker, P. A., Haire, L., Eccleston, J. F., Davis, C. T., Martin, S. R., Carling, D., and Gamblin, S. J. (2007) *Nature* **449**, 496-500
80. Townley, R., and Shapiro, L. (2007) *Science (New York, NY)* **315**, 1726-1729
81. Kahn, B. B., Alquier, T., Carling, D., and Hardie, D. G. (2005) *Cell metabolism* **1**, 15-25
82. Sabina, R. L., Holmes, E. W., and Becker, M. A. (1984) *Science (New York, NY)* **223**, 1193-1195
83. Corton, J. M., Gillespie, J. G., Hawley, S. A., and Hardie, D. G. (1995) *European journal of biochemistry / FEBS* **229**, 558-565
84. Cool, B., Zinker, B., Chiou, W., Kifle, L., Cao, N., Perham, M., Dickinson, R., Adler, A., Gagne, G., Iyengar, R., Zhao, G., Marsh, K., Kym, P., Jung, P., Camp, H. S., and Frevert, E. (2006) *Cell metabolism* **3**, 403-416
85. Göransson, O., McBride, A., Hawley, S. A., Ross, F. A., Shpiro, N., Foretz, M., Viollet, B., Hardie, D. G., and Sakamoto, K. (2007) *The Journal of biological chemistry* **282**, 32549-32560

86. Scott, J. W., van Denderen, B. J. W., Jorgensen, S. B., Honeyman, J. E., Steinberg, G. R., Oakhill, J. S., Iseli, T. J., Koay, A., Gooley, P. R., Stapleton, D., and Kemp, B. E. (2008) *Chemistry & Biology* **15**, 1220-1230
87. Sanders, M. J., Ali, Z. S., Hegarty, B. D., Heath, R., Snowden, M. A., and Carling, D. (2007) *The Journal of biological chemistry* **282**, 32539-32548
88. Zhao, G., Iyengar, R. R., Judd, A. S., Cool, B., Chiou, W., Kifle, L., Frevert, E., Sham, H., and Kym, P. R. (2007) *Bioorganic & Medicinal Chemistry Letters* **17**, 3254-3257
89. Pang, T., Zhang, Z.-S., Gu, M., Qiu, B.-Y., Yu, L.-F., Cao, P.-R., Shao, W., Su, M.-B., Li, J.-Y., Nan, F.-J., and Li, J. (2008) *The Journal of biological chemistry* **283**, 16051-16060
90. Kim, C., Cheng, C. Y., Saldanha, S. A., and Taylor, S. S. (2007) *Cell* **130**, 1032-1043
91. Taylor, S. S., Kim, C., Cheng, C. Y., Brown, S. H. J., Wu, J., and Kannan, N. (2008) *Biochimica et biophysica acta* **1784**, 16-26
92. Yang, J., Kennedy, E. J., Wu, J., Deal, M. S., Pennypacker, J., Ghosh, G., and Taylor, S. S. (2009) *The Journal of biological chemistry* **284**, 6241-6248
93. Saldanha, S. A., Kaler, G., Cottam, H. B., Abagyan, R., and Taylor, S. S. (2006) *Analytical chemistry* **78**, 8265-8272
94. Budas, G. R., Koyanagi, T., Churchill, E. N., and Mochly-Rosen, D. (2007) *Biochemical Society transactions* **35**, 1021-1026
95. Csukai, M., and Mochly-Rosen, D. (1999) *Pharmacological research : the official journal of the Italian Pharmacological Society* **39**, 253-259
96. Churchill, E. N., Qvit, N., and Mochly-Rosen, D. (2009) *Trends in endocrinology and metabolism: TEM* **20**, 25-33
97. Silverman, R. H. (2003) *Biochemistry* **42**, 1805-1812

98. Wreschner, D. H., McCauley, J. W., Skehel, J. J., and Kerr, I. M. (1981) *Nature* **289**, 414-417
99. Tanaka, N., Nakanishi, M., Kusakabe, Y., Goto, Y., Kitade, Y., and Nakamura, K. T. (2004) *The EMBO journal* **23**, 3929-3938
100. Tanaka, N., Nakanishi, M., Kusakabe, Y., Goto, Y., Kitade, Y., and Nakamura, K. T. (2005) *Nucleic acids symposium series (2004)*, 323-324
101. Nakanishi, M., Goto, Y., and Kitade, Y. (2005) *Proteins* **60**, 131-138
102. Nakanishi, M., Tanaka, N., Mizutani, Y., Mochizuki, M., Ueno, Y., Nakamura, K. T., and Kitade, Y. (2005) *The Journal of biological chemistry* **280**, 41694-41699
103. Thakur, C. S., Jha, B. K., Dong, B., Das Gupta, J., Silverman, K. M., Mao, H., Sawai, H., Nakamura, A. O., Banerjee, A. K., Gudkov, A., and Silverman, R. H. (2007) *Proceedings of the National Academy of Sciences of the United States of America* **104**, 9585-9590
104. Papa, F. R., Zhang, C., Shokat, K., and Walter, P. (2003) *Science (New York, NY)* **302**, 1533-1537
105. McPherson, J. D., Marra, M., Hillier, L., Waterston, R. H., Chinwalla, A., Wallis, J., Sekhon, M., Wylie, K., Mardis, E. R., Wilson, R. K., Fulton, R., Kucaba, T. A., Wagner-McPherson, C., Barbazuk, W. B., Gregory, S. G., Humphray, S. J., French, L., Evans, R. S., Bethel, G., Whittaker, A., Holden, J. L., McCann, O. T., Dunham, A., Soderlund, C., Scott, C. E., Bentley, D. R., Schuler, G., Chen, H. C., Jang, W., Green, E. D., Idol, J. R., Maduro, V. V., Montgomery, K. T., Lee, E., Miller, A., Emerling, S., Kucherlapati, Gibbs, R., Scherer, S., Gorrell, J. H., Sodergren, E., Clerc-Blankenburg, K., Tabor, P., Naylor, S., Garcia, D., de Jong, P. J., Catanese, J. J., Nowak, N., Osoegawa, K., Qin, S., Rowen, L., Madan, A., Dors, M., Hood, L., Trask, B., Friedman, C., Massa, H., Cheung, V. G., Kirsch, I. R., Reid, T., Yonescu, R., Weissenbach, J., Bruls, T., Heilig, R., Branscomb, E.,

Olsen, A., Doggett, N., Cheng, J. F., Hawkins, T., Myers, R. M., Shang, J., Ramirez, L., Schmutz, J., Velasquez, O., Dixon, K., Stone, N. E., Cox, D. R., Haussler, D., Kent, W. J., Furey, T., Rogic, S., Kennedy, S., Jones, S., Rosenthal, A., Wen, G., Schilhabel, M., Gloeckner, G., Nyakatura, G., Siebert, R., Schlegelberger, B., Korenberg, J., Chen, X. N., Fujiyama, A., Hattori, M., Toyoda, A., Yada, T., Park, H. S., Sakaki, Y., Shimizu, N., Asakawa, S., Kawasaki, K., Sasaki, T., Shintani, A., Shimizu, A., Shibuya, K., Kudoh, J., Minoshima, S., Ramser, J., Seranski, P., Hoff, C., Poustka, A., Reinhardt, R., Lehrach, H., and Consortium, I. H. G. M. (2001) *Nature* **409**, 934-941

106. Venter, J. C., Adams, M. D., Myers, E. W., Li, P. W., Mural, R. J., Sutton, G. G., Smith, H. O., Yandell, M., Evans, C. A., Holt, R. A., Gocayne, J. D., Amanatides, P., Ballew, R. M., Huson, D. H., Wortman, J. R., Zhang, Q., Kodira, C. D., Zheng, X. H., Chen, L., Skupski, M., Subramanian, G., Thomas, P. D., Zhang, J., Gabor Miklos, G. L., Nelson, C., Broder, S., Clark, A. G., Nadeau, J., McKusick, V. A., Zinder, N., Levine, A. J., Roberts, R. J., Simon, M., Slayman, C., Hunkapiller, M., Bolanos, R., Delcher, A., Dew, I., Fasulo, D., Flanigan, M., Florea, L., Halpern, A., Hannenhalli, S., Kravitz, S., Levy, S., Mobarry, C., Reinert, K., Remington, K., Abu-Threideh, J., Beasley, E., Biddick, K., Bonazzi, V., Brandon, R., Cargill, M., Chandramouliswaran, I., Charlab, R., Chaturvedi, K., Deng, Z., Di Francesco, V., Dunn, P., Eilbeck, K., Evangelista, C., Gabrielian, A. E., Gan, W., Ge, W., Gong, F., Gu, Z., Guan, P., Heiman, T. J., Higgins, M. E., Ji, R. R., Ke, Z., Ketchum, K. A., Lai, Z., Lei, Y., Li, Z., Li, J., Liang, Y., Lin, X., Lu, F., Merkulov, G. V., Milshina, N., Moore, H. M., Naik, A. K., Narayan, V. A., Neelam, B., Nusskern, D., Rusch, D. B., Salzberg, S., Shao, W., Shue, B., Sun, J., Wang, Z., Wang, A., Wang, X., Wang, J., Wei, M., Wides, R., Xiao, C., Yan, C., Yao, A., Ye, J., Zhan, M., Zhang, W., Zhang, H., Zhao, Q., Zheng, L., Zhong, F., Zhong, W., Zhu, S.,

Zhao, S., Gilbert, D., Baumhueter, S., Spier, G., Carter, C., Cravchik, A., Woodage, T., Ali, F., An, H., Awe, A., Baldwin, D., Baden, H., Barnstead, M., Barrow, I., Beeson, K., Busam, D., Carver, A., Center, A., Cheng, M. L., Curry, L., Danaher, S., Davenport, L., Desilets, R., Dietz, S., Dodson, K., Doup, L., Ferriera, S., Garg, N., Gluecksmann, A., Hart, B., Haynes, J., Haynes, C., Heiner, C., Hladun, S., Hostin, D., Houck, J., Howland, T., Ibegwam, C., Johnson, J., Kalush, F., Kline, L., Koduru, S., Love, A., Mann, F., May, D., McCawley, S., McIntosh, T., McMullen, I., Moy, M., Moy, L., Murphy, B., Nelson, K., Pfannkoch, C., Pratts, E., Puri, V., Qureshi, H., Reardon, M., Rodriguez, R., Rogers, Y. H., Romblad, D., Ruhfel, B., Scott, R., Sitter, C., Smallwood, M., Stewart, E., Strong, R., Suh, E., Thomas, R., Tint, N. N., Tse, S., Vech, C., Wang, G., Wetter, J., Williams, S., Williams, M., Windsor, S., Winn-Deen, E., Wolfe, K., Zaveri, J., Zaveri, K., Abril, J. F., Guigó, R., Campbell, M. J., Sjolander, K. V., Karlak, B., Kejariwal, A., Mi, H., Lazareva, B., Hatton, T., Narechania, A., Diemer, K., Muruganujan, A., Guo, N., Sato, S., Bafna, V., Istrail, S., Lippert, R., Schwartz, R., Walenz, B., Yooseph, S., Allen, D., Basu, A., Baxendale, J., Blick, L., Caminha, M., Carnes-Stine, J., Caulk, P., Chiang, Y. H., Coyne, M., Dahlke, C., Mays, A., Dombroski, M., Donnelly, M., Ely, D., Esparham, S., Fosler, C., Gire, H., Glanowski, S., Glasser, K., Glodek, A., Gorokhov, M., Graham, K., Gropman, B., Harris, M., Heil, J., Henderson, S., Hoover, J., Jennings, D., Jordan, C., Jordan, J., Kasha, J., Kagan, L., Kraft, C., Levitsky, A., Lewis, M., Liu, X., Lopez, J., Ma, D., Majoros, W., McDaniel, J., Murphy, S., Newman, M., Nguyen, T., Nguyen, N., Nodell, M., Pan, S., Peck, J., Peterson, M., Rowe, W., Sanders, R., Scott, J., Simpson, M., Smith, T., Sprague, A., Stockwell, T., Turner, R., Venter, E., Wang, M., Wen, M., Wu, D., Wu, M., Xia, A., Zandieh, A., and Zhu, X. (2001) *Science (New York, NY)* **291**, 1304-1351

107. Chen, C.-H., Budas, G. R., Churchill, E. N., Disatnik, M.-H., Hurley, T. D., and Mochly-Rosen, D. (2008) *Science (New York, NY)* **321**, 1493-1495
108. Okuzumi, T., Fiedler, D., Zhang, C., Gray, D. C., Aizenstein, B., Hoffman, R., and Shokat, K. M. (2009) *Nature Chemical Biology* **5**, 484-493
109. Sergina, N. V., Rausch, M., Wang, D., Blair, J., Hann, B., Shokat, K. M., and Moasser, M. M. (2007) *Nature* **445**, 437-441
110. Neurath, H., and Walsh, K. A. (1976) *Proceedings of the National Academy of Sciences of the United States of America* **73**, 3825-3832
111. Stack, M. S., and Pizzo, S. V. (1993) *The Journal of biological chemistry* **268**, 18924-18928
112. Abdul-Ghani, M., and Megeney, L. A. (2008) *Cell stem cell* **2**, 515-516
113. Boatright, K. M., and Salvesen, G. S. (2003) *Current Opinion in Cell Biology* **15**, 725-731
114. Shi, Y. (2002) *Molecular Cell* **9**, 459-470
115. Wei, Y., Fox, T., Chambers, S. P., Sintchak, J., Coll, J. T., Golec, J. M., Swenson, L., Wilson, K. P., and Charifson, P. S. (2000) *Chemistry & Biology* **7**, 423-432
116. Feng, B. Y., Simeonov, A., Jadhav, A., Babaoglu, K., Inglese, J., Shoichet, B. K., and Austin, C. P. (2007) *Journal of medicinal chemistry* **50**, 2385-2390
117. Van de Craen, M., Declercq, W., Van den brande, I., Fiers, W., and Vandenameele, P. (1999) *Cell Death and Differentiation* **6**, 1117-1124
118. Fernandes-Alnemri, T., Armstrong, R. C., Krebs, J., Srinivasula, S. M., Wang, L., Bullrich, F., Fritz, L. C., Trapani, J. A., Tomaselli, K. J., Litwack, G., and Alnemri, E. S. (1996) *Proceedings of the National Academy of Sciences of the United States of America* **93**, 7464-7469

119. Srinivasula, S. M., Fernandes-Alnemri, T., Zangrilli, J., Robertson, N., Armstrong, R. C., Wang, L., Trapani, J. A., Tomaselli, K. J., Litwack, G., and Alnemri, E. S. (1996) *The Journal of biological chemistry* **271**, 27099-27106
120. Asbóth, B., Stokum, E., Khan, I. U., and Polgar, L. (1985) *Biochemistry* **24**, 606-609
121. Hedstrom, L. (2002) *Chemical reviews* **102**, 4501-4524
122. Rominger, C. M., Schaber, M. D., Yang, J., Gontarek, R. R., Weaver, K. L., Broderick, T., Carter, L., Copeland, R. A., and May, E. W. (2007) *Archives of biochemistry and biophysics* **464**, 130-137
123. Bertrand, R., Solary, E., O'Connor, P., Kohn, K. W., and Pommier, Y. (1994) *Experimental Cell Research* **211**, 314-321
124. Kaufmann, S. H. (1989) *Cancer Research* **49**, 5870-5878
125. Kaufmann, S. H., and Earnshaw, W. C. (2000) *Experimental Cell Research* **256**, 42-49
126. Walker, P. R., Smith, C., Youdale, T., Leblanc, J., Whitfield, J. F., and Sikorska, M. (1991) *Cancer Research* **51**, 1078-1085
127. Lakhani, S. A., Masud, A., Kuida, K., Porter, G. A., Booth, C. J., Mehal, W. Z., Inayat, I., and Flavell, R. A. (2006) *Science (New York, NY)* **311**, 847-851
128. Juo, P., Kuo, C. J., Yuan, J., and Blenis, J. (1998) *Current biology : CB* **8**, 1001-1008
129. Wei, M. C., Zong, W. X., Cheng, E. H., Lindsten, T., Panoutsakopoulou, V., Ross, A. J., Roth, K. A., MacGregor, G. R., Thompson, C. B., and Korsmeyer, S. J. (2001) *Science (New York, NY)* **292**, 727-730
130. Wei, M. C., Lindsten, T., Mootha, V. K., Weiler, S., Gross, A., Ashiya, M., Thompson, C. B., and Korsmeyer, S. J. (2000) *Genes & development* **14**, 2060-2071

131. Jänicke, R. U., Sprengart, M. L., Wati, M. R., and Porter, A. G. (1998) *The Journal of biological chemistry* **273**, 9357-9360
132. Blanc, C., Deveraux, Q. L., Krajewski, S., Jänicke, R. U., Porter, A. G., Reed, J. C., Jaggi, R., and Marti, A. (2000) *Cancer Research* **60**, 4386-4390
133. Edelhoch, H. (1967) *Biochemistry* **6**, 1948-1954
134. Pop, C., Chen, Y. R., Smith, B., Bose, K., Bobay, B., Tripathy, A., Franzen, S., and Clark, A. C. (2001) *Biochemistry* **40**, 14224-14235
135. Feng, B. Y., and Shoichet, B. K. (2006) *Nature Protocols* **1**, 550-553
136. McGovern, S. L., Caselli, E., Grigorieff, N., and Shoichet, B. K. (2002) *Journal of medicinal chemistry* **45**, 1712-1722
137. Garcia-Calvo, M., Peterson, E. P., Rasper, D. M., Vaillancourt, J. P., Zamboni, R., Nicholson, D. W., and Thornberry, N. A. (1999) *Cell Death and Differentiation* **6**, 362-369
138. Stennicke, H. R., and Salvesen, G. S. (1997) *The Journal of biological chemistry* **272**, 25719-25723
139. Stennicke, H. R., and Salvesen, G. S. (1999) *Cell Death and Differentiation* **6**, 1054-1059
140. Pop, C., Pop, C., Timmer, J., Timmer, J., Sperandio, S., Sperandio, S., Salvesen, G. S., and Salvesen, G. S. (2006) *Molecular Cell* **22**, 269-275
141. Shiozaki, E. N., Chai, J., and Shi, Y. (2002) *Proceedings of the National Academy of Sciences of the United States of America* **99**, 4197-4202
142. Deshmukh, M. N., Burud, R., Baldino, C., Chan, P., and Liu, J. (2003) *Synthetic Communications* **33**, 3299-3303
143. Kassell, B., and Kay, J. (1973) *Science (New York, NY)* **180**, 1022-1027
144. Turk, B. (2006) *Nature reviews Drug discovery* **5**, 785-799
145. Li, J., and Yuan, J. (2008) *Oncogene* **27**, 6194-6206

146. Shen, A. (2010) *Molecular bioSystems* **6**, 1431-1443
147. Zorn, J. A., and Wells, J. A. (2010) *Nature Chemical Biology* **6**, 179-188
148. Schroder, K., and Tschopp, J. (2010) *Cell* **140**, 821-832
149. Stennicke, H. R., and Salvesen, G. S. (2000) *Biochimica et biophysica acta* **1477**, 299-306
150. McGovern, S. L., Helfand, B. T., Feng, B., and Shoichet, B. K. (2003) *Journal of medicinal chemistry* **46**, 4265-4272
151. Ryan, A. J., Gray, N. M., Lowe, P. N., and Chung, C.-w. (2003) *Journal of medicinal chemistry* **46**, 3448-3451
152. Reddie, K., Roberts, D., and Dore, T. (2006) *Journal of medicinal chemistry* **49**, 4857-4860
153. Coan, K. E. D., and Shoichet, B. K. (2007) *Molecular bioSystems* **3**, 208-213
154. Seidler, J., McGovern, S. L., Doman, T. N., and Shoichet, B. K. (2003) *Journal of medicinal chemistry* **46**, 4477-4486
155. Goode, D. R., Totten, R. K., Heeres, J. T., and Hergenrother, P. J. (2008) *Journal of medicinal chemistry* **51**, 2346-2349
156. Coan, K. E. D., and Shoichet, B. K. (2008) *Journal of the American Chemical Society* **130**, 9606-9612
157. Doak, A. K., Wille, H., Prusiner, S. B., and Shoichet, B. K. (2010) *Journal of medicinal chemistry* **53**, 4259-4265
158. Yuan, S., Yu, X., Asara, J. M., Heuser, J. E., Ludtke, S. J., and Akey, C. W. (2011) *Structure (London, England : 1993)* **19**, 1084-1096
159. Shibayama, Y., Joseph, K., Nakazawa, Y., Ghebrehiwet, B., Peerschke, E. I., and Kaplan, A. P. (1999) *Clinical immunology (Orlando, Fla)* **90**, 89-99
160. Kingston, I. B., Castro, M. J., and Anderson, S. (1995) *Nature Medicine* **1**, 138-142

161. Fowler, D. M., Koulov, A. V., Alory-Jost, C., Marks, M. S., Balch, W. E., and Kelly, J. W. (2006) *PLoS Biology* **4**, e6
162. Kranenburg, O., Bouma, B., Kroon-Batenburg, L. M. J., Reijerkerk, A., Wu, Y.-P., Voest, E. E., and Gebbink, M. F. B. G. (2002) *Current biology : CB* **12**, 1833-1839
163. Fowler, D. M., Koulov, A. V., Balch, W. E., and Kelly, J. W. (2007) *Trends in biochemical sciences* **32**, 217-224
164. Dinsdale, D., Lee, J. C., Dewson, G., Cohen, G. M., and Peter, M. E. (2004) *The American journal of pathology* **164**, 395-407
165. Wellington, C. L., and Hayden, M. R. (2000) *Clinical genetics* **57**, 1-10
166. Kim, J., Grate, J., and Wang, P. (2006) *Chemical Engineering Science* **61**, 1017
167. Ge, J., Lu, D., Liu, Z., and Liu, Z. (2009) *Biochemical Engineering Journal* **44**, 53
168. Denault, J.-B., and Salvesen, G. S. (2003) *Current protocols in protein science / editorial board, John E Coligan [et al]* **Chapter 21**, Unit 21.13
169. Coan, K., and Shoichet, B. (2008) *Journal of the American Chemical Society* **130**, 9606-9612
170. Smith, T. J., Stains, C. I., Meyer, S. C., and Ghosh, I. (2006) *Journal of the American Chemical Society* **128**, 14456-14457
171. Khan, A. R., and James, M. N. (1998) *Protein science : a publication of the Protein Society* **7**, 815-836
172. Stroud, R. M., Kossiakoff, A. A., and Chambers, J. L. (1977) *Annual review of biophysics and bioengineering* **6**, 177-193
173. Donepudi, M., and Grütter, M. G. (2002) *Biophysical chemistry* **101-102**, 145-153
174. Gray, D. C., Mahrus, S., and Wells, J. A. (2010) *Cell* **142**, 637-646
175. Mahrus, S., Trinidad, J. C., Barkan, D. T., Sali, A., Burlingame, A. L., and Wells, J. A. (2008) *Cell* **134**, 866-876

176. Dix, M. M., Simon, G. M., and Cravatt, B. F. (2008) *Cell* **134**, 679-691
177. Lüthi, A. U., and Martin, S. J. (2007) *Cell Death and Differentiation* **14**, 641-650
178. Schipper, J. L., MacKenzie, S. H., Sharma, A., and Clark, A. C. (2011) *Biophysical chemistry* **159**, 100-109
179. Zorn, J. A., Wille, H., Wolan, D. W., and Wells, J. A. (2011) *Journal of the American Chemical Society* **133**, 19630-19633
180. Salvesen, G. S., and Dixit, V. M. (1999) *Proceedings of the National Academy of Sciences of the United States of America* **96**, 10964-10967
181. Timmer, J. C., Zhu, W., Pop, C., Regan, T., Snipas, S. J., Eroshkin, A. M., Riedl, S. J., and Salvesen, G. S. (2009) *Nature Structural and Molecular Biology* **16**, 1101-1108
182. Lee, J., Culyba, E. K., Powers, E. T., and Kelly, J. W. (2011) *Nature Chemical Biology* **7**, 602-609
183. Stine, W. B., Jungbauer, L., Yu, C., and LaDu, M. J. (2011) *Methods in molecular biology (Clifton, NJ)* **670**, 13-32
184. Pop, C., Feeney, B., Tripathy, A., and Clark, A. C. (2003) *Biochemistry* **42**, 12311-12320
185. Ganesan, R., Mittl, P. R. E., Jelakovic, S., and Grütter, M. G. (2006) *Journal of molecular biology* **359**, 1378-1388
186. Karki, P., Lee, J., Shin, S. Y., Cho, B., and Park, I.-S. (2005) *Archives of biochemistry and biophysics* **442**, 125-132
187. Graybill, T. L., Dolle, R. E., Helaszek, C. T., Ator, M. A., and Strasters, J. (1995) *Bioorg Med Chem Lett* **5**, 1197-1202
188. Zhou, Q., and Salvesen, G. S. (1997) *The Biochemical journal* **324 (Pt 2)**, 361-364

189. Denault, J.-B., Denault, J.-B., Békés, M., Békés, M., Scott, F. L., Scott, F. L., Sexton, K. M. B., Sexton, K. M. B., Bogyo, M., Bogyo, M., Salvesen, G. S., and Salvesen, G. S. (2006) *Molecular Cell* **23**, 523-533
190. Berger, A. B., Witte, M. D., Denault, J.-B., Sadaghiani, A. M., Sexton, K. M. B., Salvesen, G. S., and Bogyo, M. (2006) *Molecular Cell* **23**, 509-521
191. Tachias, K., and Madison, E. L. (1997) *The Journal of biological chemistry* **272**, 28-31
192. Tachias, K., and Madison, E. L. (1996) *The Journal of biological chemistry* **271**, 28749-28752
193. Srinivasula, S. M., Ahmad, M., Fernandes-Alnemri, T., and Alnemri, E. S. (1998) *Molecular Cell* **1**, 949-957
194. Lee, J. C., Schickling, O., Stegh, A. H., Oshima, R. G., Dinsdale, D., Cohen, G. M., and Peter, M. E. (2002) *The Journal of Cell Biology* **158**, 1051-1066
195. Yuan, R. T., Young, S., Liang, J., Schmid, M. C., Mielgo, A., and Stupack, D. G. (2012) *Apoptosis : an international journal on programmed cell death* **17**, 229-235
196. Siegel, R. M., Martin, D. A., Zheng, L., Ng, S. Y., Bertin, J., Cohen, J., and Lenardo, M. J. (1998) *The Journal of Cell Biology* **141**, 1243-1253
197. Umeda, T., Tomiyama, T., Sakama, N., Tanaka, S., Lambert, M. P., Klein, W. L., and Mori, H. (2011) *Journal of neuroscience research* **89**, 1031-1042
198. Bucciantini, M., Calloni, G., Chiti, F., Formigli, L., Nosi, D., Dobson, C. M., and Stefani, M. (2004) *The Journal of biological chemistry* **279**, 31374-31382
199. Boose, J. A., Kuismanen, E., Gerard, R., Sambrook, J., and Gething, M. J. (1989) *Biochemistry* **28**, 635-643
200. Tate, K. M., Higgins, D. L., Holmes, W. E., Winkler, M. E., Heyneker, H. L., and Vehar, G. A. (1987) *Biochemistry* **26**, 338-343

201. Madison, E. L., Kobe, A., Gething, M. J., Sambrook, J. F., and Goldsmith, E. J. (1993) *Science (New York, NY)* **262**, 419-421
202. Madison, E. L., and Sambrook, J. E. (1993) *Methods in enzymology* **223**, 249-271
203. Robinson, N. C., Neurath, H., and Walsh, K. A. (1973) *Biochemistry* **12**, 420-426
204. Gertler, A., Walsh, K. A., and Neurath, H. (1974) *Biochemistry* **13**, 1302-1310
205. Silverberg, M., and Kaplan, A. P. (1982) *Blood* **60**, 64-70
206. Lonsdale-Eccles, J. D., Neurath, H., and Walsh, K. A. (1978) *Biochemistry* **17**, 2805-2809
207. Kay, J., and Kassell, B. (1971) *The Journal of biological chemistry* **246**, 6661-6665
208. Schipper, J. L., MacKenzie, S. H., Sharma, A., and Clark, A. C. (2011) *Biophysical chemistry* **159**, 100-109
209. MacCorkle, R. A., Freeman, K. W., and Spencer, D. M. (1998) *Proceedings of the National Academy of Sciences of the United States of America* **95**, 3655-3660
210. Tse, E., and Rabbitts, T. H. (2000) *Proceedings of the National Academy of Sciences of the United States of America* **97**, 12266-12271
211. Oberst, A., Pop, C., Tremblay, A. G., Blais, V., Denault, J.-B., Salvesen, G. S., and Green, D. R. (2010) *Journal of Biological Chemistry* **285**, 16632-16642
212. Chang, D. W., Xing, Z., Capacio, V. L., Peter, M. E., and Yang, X. (2003) *The EMBO journal* **22**, 4132-4142
213. Muzio, M., Stockwell, B. R., Stennicke, H. R., Salvesen, G. S., and Dixit, V. M. (1998) *The Journal of biological chemistry* **273**, 2926-2930
214. Park, C., and Marqusee, S. (2005) *Nature methods* **2**, 207-212

215. Pop, C., Salvesen, G. S., and Scott, F. L. (2008) *Methods in enzymology* **446**, 351-367
216. Coan, K. E. D., Maltby, D. A., Burlingame, A. L., and Shoichet, B. K. (2009) *Journal of medicinal chemistry* **52**, 2067-2075
217. Ferreira, R. S., Bryant, C., Ang, K. K. H., McKerrow, J. H., Shoichet, B. K., and Renslo, A. R. (2009) *Journal of medicinal chemistry* **52**, 5005-5008
218. Owen, S. C., Doak, A. K., Wassam, P., Shoichet, M. S., and Shoichet, B. K. (2012) *ACS chemical biology* DOI: 10.1021/cb300189b
219. Zheng, T. S., Hunot, S., Kuida, K., and Flavell, R. A. (1999) *Cell Death and Differentiation* **6**, 1043-1053
220. Graham, R. K., Ehrnhoefer, D. E., and Hayden, M. R. (2011) *Trends in neurosciences* **34**, 646-656
221. Monsieurs, K., Rombouts, G., Tapolcsányi, P., Mátyus, P., and Maes, B. (2006) *Synlett* **2006**, 3225-3230
222. Yu, J. W., Jeffrey, P. D., and Shi, Y. (2009) *Proceedings of the National Academy of Sciences* **106**, 8169-8174
223. Oakes, S. A., Scorrano, L., Opferman, J. T., Bassik, M. C., Nishino, M., Pozzan, T., and Korsmeyer, S. J. (2005) *Proceedings of the National Academy of Sciences of the United States of America* **102**, 105-110
224. Wesselborg, S., Engels, I. H., Rossmann, E., Los, M., and Schulze-Osthoff, K. (1999) *Blood* **93**, 3053-3063
225. Walsh, J. G., Cullen, S. P., Sheridan, C., Lüthi, A. U., Gerner, C., and Martin, S. J. (2008) *Proceedings of the National Academy of Sciences of the United States of America* **105**, 12815-12819

Appendix A:
Library Release Form

Publishing Agreement

It is the policy of the University to encourage the distribution of all theses, dissertations, and manuscripts. Copies of all UCSF theses, dissertations, and manuscripts will be routed to the library via the Graduate Division. The library will make all theses, dissertations, and manuscripts accessible to the public and will preserve these to the best of their abilities, in perpetuity.

I hereby grant permission to the Graduate Division of the University of California, San Francisco to release copies of my thesis, dissertation, or manuscript to the Campus Library to provide access and preservation, in whole or in part, in perpetuity.



Author Signature

June 14, 2012

Date